IDENTIFICATION AND CHARACTERISATION OF ASPARAGINYL ENDOPEPTIDASE EXPRESSION AND FUNCTION IN T REGULATORY CELLS

Chaido Stathopoulou

Thesis submitted for the degree of Doctor of Philosophy

Institute of Cellular Medicine

Newcastle University

September 2019

Abstract

The cysteine protease asparaginyl endopeptidase (AEP) is expressed in antigen presenting cells (APCs) and is involved in activation of proteolytic enzymes and antigen processing. Mice with a global deletion of AEP (*Lgmn*$^{-/-}$) develop a lysosomal disorder characterised by the accumulation of cathepsins but otherwise do not exhibit an immune phenotype. However, an increased frequency of regulatory T cells (Treg) in the periphery has been reported suggesting that AEP expression regulates Treg cell stability through Foxp3 degradation. To study the induction of AEP expression in mouse Treg cells, naïve and $CD4^+CD25^+$ T cells were cultured under Treg-inducing (iTreg) conditions which include TGF-β1. Freshly isolated $CD4^+$ T cells did not express any AEP while cells cultured under iTreg conditions expressed the highest levels of AEP. To test the function of AEP in activated peripheral Treg cells, a mouse model of melanoma was used. *Lgmn*$^{-/-}$ mice with melanoma showed an increased frequency of tumour infiltrating Treg cells compared to controls although tumour growth was similar between the two groups. Next, the expression profile of AEP in human T cells was investigated as the mechanisms regulating AEP expression and function in these cells remain unclear. To study the induction of AEP expression in human Treg cells, naïve and $CD4^+CD25^+$ T cells were cultured under iTreg conditions. AEP was expressed in freshly isolated populations. Also, cells cultured under iTreg conditions expressed the highest levels of AEP. Blocking TGF-β1 signalling with a TGFBR-I inhibitor led to a decrease in active AEP expression within the cells. Stimuli that could block AEP activity were also tested. In keeping with previously published work, blockade of PD-1 led to an increase of AEP activity levels in human lymphocytes. These findings demonstrate that AEP expression is inversely regulated by TGF-β1 and PD-1 signalling in human T cells with implications for immunotherapy.

Declaration

I declare that no work presented in this thesis has been submitted elsewhere for the award of any other degrees or qualifications. Work presented here has been carried out by myself unless otherwise stated and all sources of information have been acknowledged by reference.

Acknowledgements

I would like to thank Newcastle University for funding my Ph.D. through the Research Excellence Academy award and my supervisor Dr. Shoba Amarnath for her guidance throughout this project as well as her contribution to the mouse studies. Specifically, I would like to thank her for performing the mouse phenotyping, the data of which I analysed and presented in my thesis. Also, I would like to thank her for processing the B16 melanoma cell line and for performing the intraperitoneal mouse injections during the *in vivo* experiment. My contribution was data analysis, managing and monitoring the mice, recording tumour sizes and harvesting and processing the tumours in preparation for flow cytometry.

I would also like to thank Dr. Arian Laurence for his expert advice, Professor Andrew Mellor for his constructive feedback on the final thesis and Professor Collin Watts for providing the *Lgmn*$^{-/-}$ mouse strain. I would also like to thank my colleague Miss Grace Mallet for her technical support during the first year of my Ph.D. Special thanks to Mr. Jonathan Scott from Professor John Simpson's group at Newcastle University for providing all the blood samples from healthy volunteers which I used for the purpose of isolating human lymphocytes. Also, thank you to Dr. Amy Anderson and Dr. Fiona Cooke from Newcastle University for providing me with cultured human dendritic cells which I processed and used in my western blot and enzyme activity experiments.

Last but not least, massive thanks to my dad for his advice, encouragement and mental support throughout my Ph.D.

Table of Contents

List of Figures

List of Abbreviations

Activation peptide	AP
AEP inhibitor	AEPi
Alzheimer’s disease	AD
Antibody	Ab
Antigen	Ag
Antigen presenting cell	APC
Asparaginyl endopeptidase	AEP
Asparaginyl-specific mono-carboxypeptidase	ACP
Autoimmune gastritis	AIG
Autoimmune regulator	AIRE
Azacytidine	Aza
Bicinchoninic acid	BCA
Bone marrow	BM
Bovine serum albumin	BSA
Chromatin immunoprecipitation	ChIP
Common mediator SMAD4	Co-SMAD4
Conventional T cell	Tconv
Cortical thymic epithelial cell	cTEC
Cycloheximide	CHX
Dendritic cell	DC
Dimethyl sulfoxide	DMSO
DNA methyltransferase 1	DNMT1
Dulbecco Modified Eagle Media	DMEM
Endoplasmic reticulum	ER
Enzymatic chemiluminescence	ECL
Ethylenediaminetetraacetic acid	EDTA
Experimental autoimmune encephalomyelitis	EAE
Fetal bovine serum	FBS
Fluorescence minus one	FMO
Fluorescence-activated cell sorting	FACS
Forkhead box	FOX
Forkhead box protein 3	FOXP3

Forward scatter	FSC
Graft versus host disease	GvHD
Granulocyte-macrophage colony-stimulating factor	GM-CSF
Histone acetyltransferase	HAT
Histone deacetylase	HDAC
Human Tissue Act	HTA
IkB kinase complex	IKK
Individually ventilated	IV
Induced Treg	iTreg
Interleukin 2 receptor subunit beta	IL2Rβ
Intracellular	IC
Knock out	KO
Legumain	LGMN
Legumain stabilisation and activity modulation	LSAM
Lipopolysaccharide	LPS
Lymph node	LN
Major histocompatibility complex	MHC
Mean fluorescence intensity	MFI
Medullary thymic epithelial cell	mTEC
Mesenteric lymph node	MLN
MicroRNA	miRNA
Natural Treg	nTreg
Neuropilin-1	Nrp-1
n-octyl-beta-D-glycopyranoside	n-octyl
Non-coding DNA sequence	CNS
Nuclear export sequence	NES
Nuclear factor of activated T cell	NFAT
Nuclear localisation sequence	NLS
Ovalbumin	OVA
PBS-HEPES	PBS-H
Peripheral blood mononuclear cells	PBMCs
Peripheral Treg	pTreg
Permeabilization	Perm

Peroxisome proliferator-activated receptor gamma	PPAR-γ
Phenylmethylsulfonyl fluoride	PMSF
Phosphate-buffered saline	PBS
Phosphorylated SMAD	pSMAD
Phytohemagglutinin	PHA
Protein phosphatase 2 A	PP2Ai
Radioimmunoprecipitation assay	RIPA
Radioimmunoprecipitation assay buffer	RIPA
Receptor-regulated SMAD	R-SMAD
Recombinant human	rh
Recombinant mouse	rm
Red blood cell	RBC
Retinoic acid	RA
Roswell Park Memorial Institute	RPMI
Side scatter	SSC
Signal peptide	SP
Signal transducer and activator of transcription	STAT
Specific pathogen free	SPF
T cell receptor	TCR
T cytotoxic cell	Tc
T helper cell	Th
T regulatory cell	Treg
Tetanus toxin C-terminal fragment	TTCF
Thymic Treg	tTreg
Toll-like receptor	TLR
Transcription factor	TF
Treg-specific demethylated region	TSDR
Tumour associated macrophage	TAM
Visceral adipose tissue	VAT
Wild type	WT

Chapter 1. Introduction

1.1 The Immune System

The immune system is imperative for protecting the host against deleterious pathogens and damaged cells. Although the ability of the immune system to recognise nonself was initially introduced as the main driver of immune responses, this failed to explain why immune responses are not induced in certain circumstances such as following vaccinations with foreign antigens or why the immune system is unable to clear tumours that express neoantigens (Matzinger, 2002). Therefore, in 1994, a new model, namely, the 'danger model' was introduced which stated that the immune system prioritises damage signals rather than just foreign material which can often be non-pathogenic (Matzinger, 1994; Matzinger, 2002). These alarm signals are released or produced by damaged or stressed cells such as necrotic cells under non-physiological conditions which then activate antigen presenting cells thus driving immune responses (Matzinger, 2002). Various factors namely, the type of pathogen together with the type of tissue can determine the type of immune response that is needed (Matzinger, 2002).

The immune system consists of two arms, namely the innate and the adaptive immune systems. Innate immunity constitutes the first line of defence activated when a danger signal is detected (Freeman, 2000). In contrast, the adaptive immune system provides long-term immunity against pathogens such as bacteria, viruses, fungi and parasitic helminths due to its ability to adapt and generate immune memory (Paul and Seder, 1994). The adaptive immune system is constituted of T cells and B cells whereby T cells elicit cell-mediated immunity and B cells impart humoral immunity mediated by antibodies (Germain, 2002).

T cells are comprised of two main sub-types namely $CD8^+$ cytotoxic T cells and $CD4^+$ T helper cells which are generated in the thymus (Miller, 1961; Nishizuka and Sakakura, 1969; Germain, 2002). As the name suggests, $CD8^+$ cytotoxic T cells (Tc) have the capacity to kill infected and tumour cells. $CD8^+$ T cells require $CD4^+$ T helper cells (Th) for initial priming, sustained activation and function (O'Shea and Paul, 2010). Therefore, $CD4^+$

T helper cells are comprised of numerous sub-types in order to efficiently co-ordinate immune responses for specific pathogenic organisms efficiently (Mosmann and Coffman, 1989).

1.2 The Regulatory T cell

In addition to effector subtypes, $CD4^+$ T helper cells also consist of a regulatory population called T regulatory (Treg) cells (Sakaguchi *et al.*, 1995). Regulatory T cells are immunosuppressive cells that form part of the adaptive immune system and are essential for immune tolerance and homeostasis (Sakaguchi, 2004).

The first indication that T cells possess immunosuppressive function came in the 1970s when thymocytes were shown to regulate antigenic responses in thymectomised, irradiated mice that were reconstituted with bone marrow transplants containing thymocytes and immunised with sheep red blood cells (Gershon and Kondo, 1970). In 1971 it was shown that transfer of immunocompetent cells from immunised mice to naïve hosts downregulated immune responses to the same antigenic challenge (Gershon and Kondo, 1971). Although failure to identify specific cell markers for this 'suppressor cell' led to a decrease in the popularity of this concept during the 1980s and 1990s, in 1981, removal of the thymus during weeks 2-4 in mice led to autoimmunity characterised by tissue infiltration by T cells further reinforcing the idea of T cells as suppressors (Kojima and Prehn, 1981). In 1982 it was shown that syngeneic transfer of $CD4^+CD8^-$ thymocytes protected these mice from autoimmunity (Sakaguchi *et al.*, 1982). In addition, subsequent experiments showed that depletion of $CD25^{high}CD4^+$ T cells from the injected cell population abrogated the observed protective effect (Sakaguchi *et al.*, 1985). Finally, in 2001, the discovery of Foxp3 as a specific cell marker of this suppressor T cell in mice provided the final proof for the existence and importance of the Treg cell in immune tolerance (Brunkow *et al.*, 2001).

However, it should be noted that Treg cell function is not the only mechanism organisms use to maintain peripheral tolerance. Additional mechanisms include T cell exhaustion due to prolonged T cell exposure to antigens and prolonged activation (Crespo *et al.*, 2013; Saeidi *et al.*, 2018).

On the other hand, insufficient stimulatory signals where the T cell receptor is activated in the absence of co-stimulatory signals (cytokine signalling and co-receptor signalling) can lead to T cell anergy (Crespo *et al.*, 2013; Saeidi *et al.*, 2018). In addition to T cells non-responsiveness, another example of a suppressive mechanism is the function of tolerogenic antigen presenting cells which can enhance the generation of Treg cells through the secretion of retinoic acid and the cytokine TGF-β (Takenaka and Quintana, 2017). Also, stimulation of these cells via TLR9, a receptor recognising foreign DNA from bacteria and viruses, can drive the induction of indoleamine 2,3-dioxygenase (IDO) - an enzyme that catalyses tryptophan which results in amino acid depletion and cell cycle arrest at the G1 phase thus downregulating T cell proliferation (Mellor *et al.*, 2002; Brandacher *et al.*, 2008). Finally, they are involved in the negative selection of autoreactive T cells in the thymus (Takenaka and Quintana, 2017).

1.2.1 *Regulatory T cell development in the thymus*

Treg cells are generated in the thymus and in the periphery and are characterised by the expression of a master transcription factor called Forkhead box protein 3 (Foxp3) (Hori and Sakaguchi, 2004). Foxp3 plays an important role in Treg cell development and function and its expression is associated with Treg cell lineage commitment (Hori and Sakaguchi, 2004).

Both CD8 and CD4 T cells arise from a common lymphoid progenitor (CLP) that enters the thymus from the bone marrow (Starr *et al.*, 2003; Shah and Zuniga-Pflucker, 2014). There, it goes through different stages of maturation as it progresses though the different thymic compartments (Starr *et al.*, 2003; Shah and Zuniga-Pflucker, 2014). First, CLP enters the cortex where it goes through CD4 and CD8 double negative stages (DN) (Starr *et al.*, 2003; Shah and Zuniga-Pflucker, 2014). During this process, the thymocyte assembles the T cell receptor (TCR) complex and upon successful expression of the complex, the co-expression of the CD4 and CD8 co-receptors is initiated (Starr *et al.*, 2003; Shah and Zuniga-Pflucker, 2014). The result is a double positive cell (DP) which interacts with antigen-presenting cortical thymic epithelial cells (cTEC) and dendritic cells (DCs) (Starr *et al.*, 2003; Shah and Zuniga-Pflucker, 2014). Low affinity for the

antigens or inability of the TCR to recognise the presented antigens and transmit signals of sufficient magnitude induces cell apoptosis – a process called ‘death by neglect’ (Starr *et al.*, 2003; Shah and Zuniga-Pflucker, 2014). Successful interaction with the antigen results in the loss of expression of either the CD4 or CD8 co-receptor resulting in a single positive cell (SP) (Starr *et al.*, 2003; Shah and Zuniga-Pflucker, 2014). The decision between CD4 or CD8 expression depends on the chance interaction with either MHC II or MHC I molecules presented on cTECs and DCs (Starr *et al.*, 2003; Shah and Zuniga-Pflucker, 2014). SP cells migrate to the medulla where they undergo the final step of T cell maturation called negative selection (Starr *et al.*, 2003; Shah and Zuniga-Pflucker, 2014). During this step, any cells that interact with self-antigens presented by medullary thymic epithelial cells (mTEC) and thymic dendritic cells (DCs) undergo apoptosis (Starr *et al.*, 2003; Shah and Zuniga-Pflucker, 2014).

The first evidence for Treg cell development in the thymus was provided by a study which demonstrated that subjecting mice to thymectomy at day 3 resulted in the development of autoimmune pathology while this observation did not hold true when neonates were subjected to thymectomy at day 7 (Sakaguchi *et al.*, 1995). This study provided an initial proof of concept which suggested that Treg cells could be developed in the thymus. In support of this argument, it has been shown that thymic Treg cells generated in the early stages of perinatal development during day 0 – 10, are critical for immunotolerance and that they form a functionally distinct Treg cell subset that remains stable in numbers throughout life (Yang *et al.*, 2015). Contrary to adult Treg cells, these perinatal Treg cells were the only ones able to rescue autoimmunity in Treg cell-depleted and/or autoimmune regulator (AIRE) knock out mice after adoptive transfer indicating the importance of AIRE, a protein involved in peripheral tissue antigen presentation in medullary thymic epithelial cells (mTECs), in early Treg cell development (Guerau-de-Arellano *et al.*, 2009; Yang *et al.*, 2015). Following this observation that Treg cells develop in the thymus, numerous reports have described various stimuli that drive Treg cell development. First and foremost, expression of a TCR specific for self-antigens was critical for Treg cell differentiation in the thymus, forming the current paradigm that Treg cell

development occurs when TCR avidity for a self-antigen is between the avidities that drive positive and negative selection (Maloy and Powrie, 2001) (figure 1.1). However, studies on Treg cell biology have suggested that the activation of the AKT/mTOR pathway downstream of TCR signalling can inhibit Treg cell differentiation by degrading FOXO proteins (Haxhinasto *et al.*, 2008; Ouyang *et al.*, 2010). FOXO proteins are transcription factors that are required for Treg cell development (Ouyang *et al.*, 2010). Specifically, the overexpression of retrovirally-introduced AKT in naïve cells led to a decrease in Foxp3 expression *in vitro* and failure of immature Foxp3$^-$ thymocytes to differentiate into Treg cells *in vivo* (Haxhinasto *et al.*, 2008). It should be noted that natural Treg cells already expressing Foxp3 were not affected by that intervention. Restoration of both Foxp3 expression and treatment with Rapamycin (both downstream targets of AKT) did not rescue the phenotype completely (Haxhinasto *et al.*, 2008). This suggested a direct effect of AKT early in Treg cell differentiation prior to Foxp3 expression. Hence, the current paradigm is that TCR signalling activates the NF-κB pathway, which is critical for Treg cell development (Sauer *et al.*, 2008). Over-expression of IKKb by-passed the need for TCR signalling in Treg cell development and resulted in Treg cell development in the thymus of RAG-deficient TCR-transgenic mice (expressing either the MHC class II-restricted OT-II TCR or the MHC class I-restricted P14TCR), which does not normally generate Treg cells (Long *et al.*, 2009). In addition to a TCR signal, Treg cells also require co-stimulatory signals for their development (Tai *et al.*, 2005). In particular CD28 signal is critical for Treg cell development, with 80% reduction in Treg cell development in CD28 deficient mice (Tai *et al.*, 2005). In addition to CD28, another co-stimulatory molecule, CD40 which binds to CD154 on activated T cells is also important for expansion, but not selection of Treg cell populations (Grewal and Flavell, 1998).

Cytokines are implicated in the development of Treg cells, with IL-2 efficiently inducing Treg cell development and to a lesser extent IL-15, which is also involved in this process (Burchill *et al.*, 2008). TGF-β is implicated in directly inducing Foxp3 during thymic Treg cell development, however, the role of TGF-β in development is still controversial (Liu *et al.*, 2008a). In fact, a study by Konkel et al., showed that TGF-β released in the thymus by

apoptotic cells may play a role in Treg cell differentiation (Konkel *et al.*, 2014).

Lastly, antigen presenting cell (APC) populations are also key to Treg cell development in the thymus. In addition to the level of MHC I and II expression determining the frequencies of $CD4^+$ and $CD8^+$ T cells, the level of antigen presentation on APCs has also an impact on the number of Treg cells generated in the thymus (Hsieh *et al.*, 2012). Reduction of MHC II expression on mTECs leads to increased Treg cell differentiation in mice and this is proposed to be due to a reduction in TCR avidity (overall strength of TCR signalling) (Hsieh *et al.*, 2012). TCR avidity is also determined by the number of APCs expressing the same self-Ag and therefore the probability that the developing T cell will encounter the self-Ag (Hsieh *et al.*, 2012). Low Ag encounter is thought to promote Foxp3 expression and Treg cell differentiation (Hsieh *et al.*, 2012). Also, it is possible that stochastic expression of different types of antigens between mTECs and DCs may regulate thymic Treg cell development (Hsieh *et al.*, 2012). This may also be partly due to thymic- and cell-type specific expression of proteases involved in antigen processing generating distinct repertoires of antigens presented on MHC molecules (Collado *et al.*, 2013).

In summary, two models are proposed for Treg cell development in the thymus, namely, the instructive and stochastic model (figure 1.1) (Hsieh *et al.*, 2012). In the instructive model, high affinity of the TCR for the self-Ag leads to negative selection in the medulla, low affinity leads to the development of conventional naïve T cells while intermediate levels of affinity lead to the generation of Treg cells (Hsieh *et al.*, 2012). In the stochastic model, early TCR signalling (depending on TCR avidity level) may confer resistance to negative selection (Hsieh *et al.*, 2012). In addition, TCR signalling events during the DN stage is proposed to lead to remodelling of the *Foxp3* locus generating a $Foxp3^-$ Treg cell precursor which then can express Foxp3 in response to IL-2 or IL-15 stimulation (Hsieh *et al.*, 2012). However, since the frequency of $Foxp3^+$ DP cells is less than 1%, APCs of the cortex are thought to play a minor role in Treg cell development compared to mTECs (Bensinger *et al.*, 2001; Aschenbrenner *et al.*, 2007; Lee and Hsieh, 2009; Hsieh *et al.*, 2012).

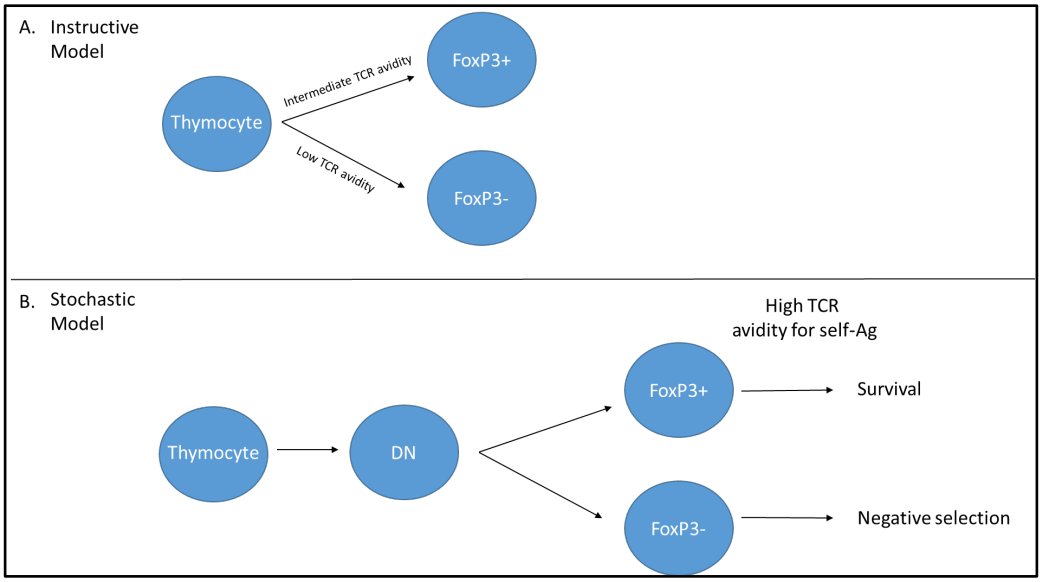

Figure 1.1 Two models of thymic development of regulatory T cells. **A.** In the instructive model, cells expressing TCRs with sufficient avidity for self-antigens express Foxp3. **B.** The stochastic model supports the idea of the random generation of single positive cells irrespective of the strength of TCR signalling. These autoreactive cells escape negative selection in the medulla and form the thymic Treg cell population. Figure adapted from (Hsieh *et al.*, 2012).

1.2.2 *Regulatory T cell development in the periphery*

In addition to the thymic Treg cell population, there is also a peripheral Treg cell population induced from naïve $CD4^+$ T cells that exit the thymus. Naïve $CD4^+$ T cells differentiate into different subsets - including Treg cells - depending on particular cues from the microenvironment (Freeman, 2000). In response to damage or infections, dendritic cells (DCs) process antigens and present them on two distinct classes of membrane proteins called major histocompatibility complexes (MHC) (Germain, 1994). These are recognised by the CD4 and CD8 co-receptors present on T cells, which results in T cell activation (Swain, 1983). When DCs process and present nonameric antigenic peptides through MHC-Class I, it is $CD8^+$ T cells that get activated whereas in the case of $CD4^+$ T cells, DCs present larger peptides through MHC-Class II (Sette *et al.*, 1989). For instance, in the case of viral antigens, DCs will present antigenic peptides on their MHC-Class I and II while also secreting inflammatory cytokines such as IL-12 (Kaplan *et al.*, 1996).

Numerous T helper cell subsets with distinct phenotypic and functional characteristics have been identified in the periphery (figure 1.2). Similar to thymic Treg cells, peripherally-derived Treg cells were identified as a type of immunosuppressive cell expressing the master transcription factor Foxp3 (Wu *et al.*, 2006; Ramsdell and Ziegler, 2014).

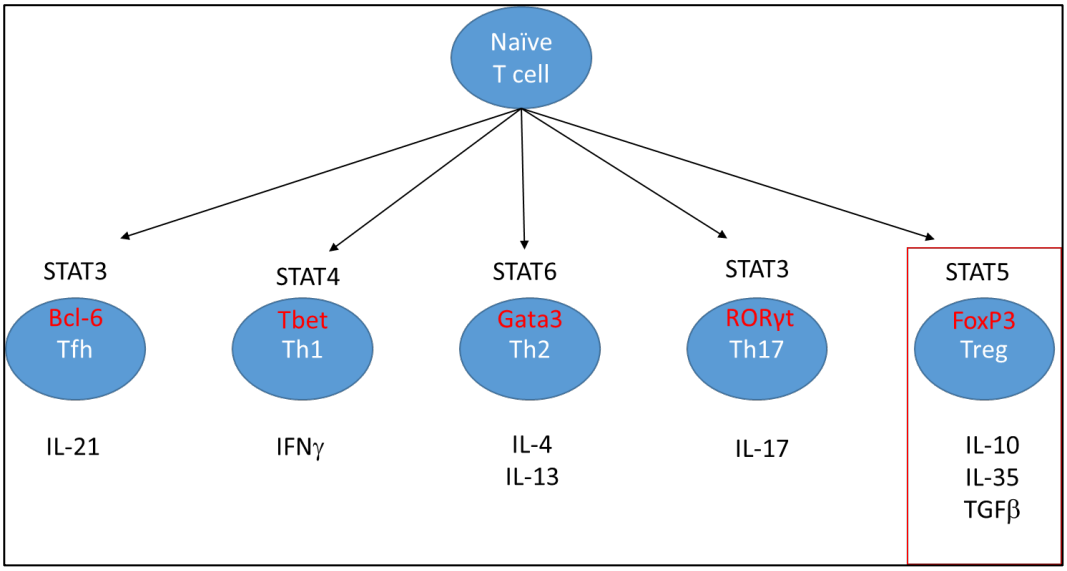

Figure 1.2 CD4⁺ T helper subsets and their associated master transcription factors. This figure summarises the major CD4⁺ T cell subsets identified by the cytokines they express and the transcription factors regulating their differentiation. Figure adapted from (O'Shea and Paul, 2010).

There is currently increasing evidence of T helper cells exhibiting plasticity in terms of cytokine production and master transcription factor expression that blurs the boundaries between T helper cell subsets and makes their classification into distinct cell lineages challenging (O'Shea and Paul, 2010).

For instance, it has been demonstrated that Th1 cells can express Foxp3 as well as Tbet leading to the identification of Tbet⁺FoxP3⁺ double positive cells (Koch *et al.*, 2009). Thus, it is proposed that T helper cell subsets are not fully determined and that they do maintain some functional plasticity even after their initial differentiation in response to cytokines.

1.3 Characterisation and Nomenclature of Regulatory T Cell Subsets

Treg cells can be subdivided into peripheral (pTreg) and thymic-derived natural (tTreg) Treg cells and it is hypothesised that the two subsets exhibit distinct levels of plasticity regarding their immunosuppressive activity

(Shevach and Thornton, 2014). For the purposes of this study and in accordance with the current nomenclature, thymic Treg cells are referred to as tTreg cells and Treg cells induced in the periphery as pTreg cells - both contained within the earlier 'natural Treg cell' nomenclature (nTreg) (Abbas *et al.*, 2013). *In vitro* induced Treg cells are referred to as iTreg cells. It should be noted that pTreg cells should not be confused with the total peripheral pool of Treg cells, a heterogeneous population consisting of both pTreg, tTreg and in certain cases induced Treg (iTreg) cells.

As Treg cell subsets can exhibit different suppression mechanisms and have different implications on disease management, various studies have attempted to differentiate tTreg from pTreg cells by studying their phenotypic and functional profiles. Although the expression of Foxp3 remains the main phenotypic characteristic of Treg cells, it is not a suitable marker for distinguishing Treg cell subsets as it is found in both tTreg and pTreg cells. Treg cells are mainly identified by their expression of CD4 and CD25 along with Foxp3 but they are also known to express other markers such as CTLA-4, ICOS, GITR, PD-1, CD62L and CD103 which are all general activation markers expressed on activated $CD4^+$ T cells (Singh *et al.*, 2015). Apart from Foxp3, there are no other mouse Treg-specific markers while in humans FOXP3 can also be found in activated T cells.

1.3.1 *tTreg cells*

Thymic Treg cells constitute the majority of Treg cells found in the mouse (90%) while a smaller percentage are pTreg cells (Shevach and Thornton, 2014). These percentages however, are less clear in humans. In both humans and mice, nTreg cells comprise 5-10% of total $CD4^+$ T cells and 1-2% of cells circulating in the peripheral blood (Halim *et al.*, 2017). The development of polyclonal tTreg cells is thought to be the main mechanism by which central tolerance is established. tTreg cells are also known for their distinct TCR repertoire for self-antigens which is only partially overlapping with that of naïve $CD4^+$ T cells (Pacholczyk *et al.*, 2006). In contrast, pTreg cells are derived from naïve $CD4^+$ T cells in the peripheral lymph nodes (LN) after exposure to self and non-self antigens (Hori and Sakaguchi, 2004). These are involved in feto-maternal tolerance where the production of

allogeneic pTreg cell specific for the fetus is important (Aluvihare *et al.*, 2004).

1.3.2 *pTreg cells*

Contrary to tTreg cells that depend primarily on IL-2 for their development in the thymus (Malek, 2008), pTreg cells depend on TGF-β for their differentiation from $CD4^+$ $CD25^-$ conventional T cells (Tconv) (Chen *et al.*, 2003). TGF-β activates SMAD3, which induces Foxp3 by interacting with the CNS1 enhancer region on its promoter (Zheng *et al.*, 2010). IL-2 on the other hand, activates the transcription factor STAT5 which induces *foxp3* expression and Foxp3 in turn induces the expression of the IL-2 receptor in a positive feedback loop (Gavin *et al.*, 2007). Both tTreg and pTreg cells depend on TCR and co-stimulatory signalling which results in NF-κB activation and subsequent *foxp3* gene expression (Sauer *et al.*, 2008). However, the methylation status of *foxp3* differs between tTreg and pTreg cells. tTreg cells possess a highly demethylated CNS2 region which is associated with lineage stability (Zheng *et al.*, 2010).

1.3.3 *Heterogeneity within Treg cell subsets*

In addition to the differences observed between tTreg and pTreg cells, functional and phenotypic heterogeneity is also observed within both subsets resulting in Treg cell subpopulations with distinct repertoires of chemokine receptors expressed on their surface. For example, Treg cells acquire CD62L and CCR7 expression in the thymus which are required for their migration to secondary lymph nodes (Lee *et al.*, 2007). There, CCR7 and CD62L are downregulated and depending on the antigens present, cells express chemokine receptors required for their migration to non-lymphoid tissues (Lee *et al.*, 2007). One example of that is the expression of CCR4, which is required for migration to the skin (Sather *et al.*, 2007).

There is also evidence that Treg cells can form distinct Treg cell populations with tissue-dependent functions/suppressive programs (Yuan *et al.*, 2014). For example, Treg cells residing in visceral adipose tissue (VAT Treg cells) can be distinguished from spleen and LN Treg cells in terms of gene expression and their TCR and chemokine receptor repertoires (Feuerer *et al.*, 2009). Specifically, they express molecules involved in lipid metabolism

such as the nuclear peroxisome proliferator-activated receptor gamma (PPAR-γ) involved in adipocyte differentiation (Tontonoz and Spiegelman, 2008; Cipolletta *et al.*, 2012). Studies in knock-out mice have demonstrated that PPAR-γ is responsible for establishing and maintaining VAT Treg cell numbers as PPAR-γ knock out Treg cells expressed less KLRG1, CD69 and GATA3 and were also less able to accumulate in the gut (Cipolletta *et al.*, 2012). PPAR-γ deletion however, did not affect the numbers or the phenotypes of Treg cells in the lymph nodes (Cipolletta *et al.*, 2012).

Treg cells can also be subdivided into effector and memory subtypes. Although Treg cells are highly activated cells expressing activation markers, there are also memory Treg cells. These are responsible for maintaining long-term immune tolerance in tissues, as they are able to persist in the absence of their specific antigen and limit the severity of autoimmune reactions mediated by the re-encounter of self-antigens (Rosenblum *et al.*, 2011). This was demonstrated in a study by Rosenblum et al. in 2011 where mice expressing the self-antigen ovalbumin (OVA) in the skin experienced a milder autoimmune reaction and were able to recover more rapidly from autoimmune dermatitis (caused by skin-specific expression of OVA) after the re-induction of OVA with doxycycline (Rosenblum *et al.*, 2011). This was largely attributed to OVA-specific tTreg cells as the majority of DOII (OVA-specific) T cells found in the skin were $Foxp3^+$ (Rosenblum *et al.*, 2011). Depletion of the cell population via anti-CD25 antibody treatment prior to re-induction of OVA led to autoimmunity equivalent to that of a primary immune response (Rosenblum *et al.*, 2011). Taken together, these data suggest that thymically derived, OVA-specific Treg cells are the major contributors to long-term, tissue-specific immune tolerance in the periphery (Rosenblum *et al.*, 2011).

Attempts to distinguish tTreg from pTreg cells had limited success. Some of the factors that need to be considered when characterising Treg cells and their subsets include their environment, whether they are active or anergic, the amount and stability of Foxp3 expression and whether they are polyclonal, monoclonal or antigen-specific (Shevach and Thornton, 2014).

One of the limitations in understanding Treg cells is the discrepancies that exist between the animal models and humans. In humans, FOXP3 is expressed in both conventional and regulatory human T cells after stimulation of their TCR (Walker *et al.*, 2003). Induced Treg cells from human naïve cells, although they do express FOXP3, they fail to suppress the proliferation of naïve T cells and are able to produce effector cytokines such as IL-2 and IFN-γ (Tran *et al.*, 2007). Different isoforms of FOXP3 have also been identified in humans specific to Treg cells (Allan *et al.*, 2005). Taken together, these data could suggest a difference in the way human Treg cells respond to TGF-β stimulation and may indicate an alternative pathway of Treg cell lineage commitment in humans (Shevach and Thornton, 2014).

1.4 Foxp3

Foxp3 plays a central role in Treg cell biology as its expression is essential for Treg cell function and stability while its deletion results in autoimmunity both in humans and mice (Gavin *et al.*, 2007). In mice, Foxp3 is expressed in Treg cells but in humans it can also be found in activated epithelial and naïve T cells where it is transiently expressed and does not confer suppressive function (Mailer, 2018).

1.4.1 *Discovery and nomenclature*

Foxp3 is a member of the forkhead box (FOX) family of transcription factors. This family of transcription factors is characterised by a conserved DNA-binding sequence of 100 residues called the Fox domain (Hannenhalli and Kaestner, 2009). This domain was first characterised in 1989 in *Drosophila melanogaster* after mutations in this domain led to developmental defects of the head (Weigel *et al.*, 1989). The Fox family of proteins are involved in a variety of developmental processes and consist of 40 members which are subdivided in different subclasses such as the FoxO and FoxP class (Hannenhalli and Kaestner, 2009). For instance, FoxO family members regulate glucose homeostasis whereas FoxP family members such as FoxP2 are involved in speech development (Hannenhalli and Kaestner, 2009). In 2000 the Fox nomenclature committee proposed that human Fox proteins will be named in capital letters (e.g. FOXP3) whereas mouse proteins would be written only with the first letter in capitals (Foxp3)

(Kaestner *et al.*, 2000). Proteins from other vertebrates would be referred to with the first letter and the subclass letter in capitals (FoxP3) (Kaestner *et al.*, 2000). In this study, this nomenclature is used interchangeably where reference to both mouse Foxp3 and human FOXP3 is made.

1.4.2 *Gene structure*

The human *FOXP3* gene is located on the short arm of the X chromosome (Xp11.23) while the mouse homolog is found at the XA1.1;X3.41 cM region of the X chromosome. The two homologs are 87% identical in nucleotide sequence and consist of 11 coding exons (figure 1.3) (Ziegler, 2006).

1.4.3 *Protein structure*

Mouse Foxp3 and human FOXP3 are approximately 47-kDa in size and share 86.5% similarity in amino acid sequence. However, human FOXP3 consists of 431 amino acids whereas the mouse Foxp3 is 429 amino acids long. Both have a half-life of less than 30 minutes (Lee *et al.*, 2008).

The Foxp3 protein has four domains that are important for its function namely, the repressor domain, the zinc finger domain, the leucine zipper domain and the forkhead domain (figure 1.3) (Lopes *et al.*, 2006). The repressor domain of Foxp3 differs from other members of the FoxP subclass such as FOXP1, -2 and -4 in that it is a proline-rich region as opposed to a glutamine-rich region (Deng *et al.*, 2012). It is located near the N-terminus and its function is to inhibit Foxp3 binding to the DNA unless the protein dimerises (Mailer, 2018). It also contains part of a nuclear export sequence (NES1) (Magg *et al.*, 2012). The zinc finger domain is involved in the dimerization of the protein, its structural stability and its ability to interact with its binding partners and DNA (Coffer and Burgering, 2004). The zipper domain is a leucine-rich domain and is also important for the homodimerisation and heterodimerisation of the protein (Coffer and Burgering, 2004). This domain also contains a second nuclear export sequence (NES2) (Magg *et al.*, 2012). Finally, Foxp3 differs from other members of its subclass in the position of its forkhead domain which is located near the carboxyl-terminus of the protein (Coffer and Burgering, 2004). It is responsible for the DNA-binding specificity of Foxp3 to GTAAACA motifs via its winged helix and consists of 3 alpha helixes, 2 β

strands and 2 loops (figure 1.4) (Kaestner *et al.*, 2000; Coffer and Burgering, 2004; Chen *et al.*, 2015).

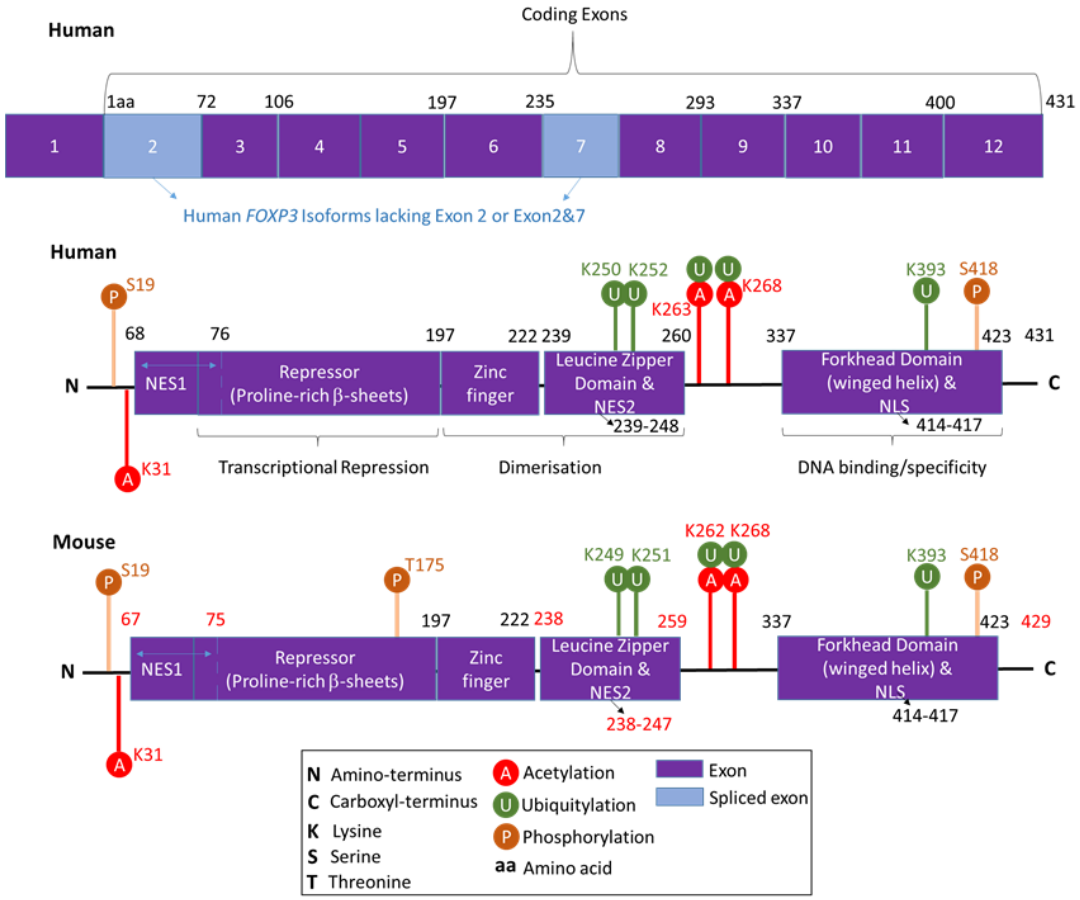

Figure 1.3 Structure of Foxp3. Structure of the human *FOXP3* gene and the human FOXP3 and mouse Foxp3 protein with its functional domains and post-translational modifications. Post-translational modifications regulate the transcriptional activity of Foxp3 and include phosphorylation at serine and threonine residues as well as ubiquitylation and acetylation at lysine residues. Ubiquitylation targets the protein for proteasomal degradation while acetylation prevents degradation by the proteasome. Phosphorylation can also protect the protein from degradation but it can also repress DNA binding and nuclear localisation (Deng *et al.*, 2019).

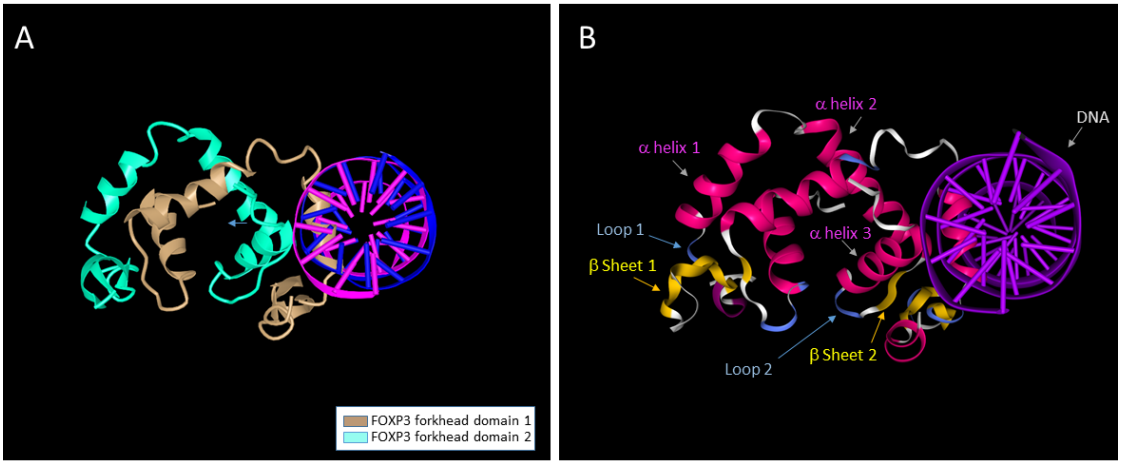

Figure 1.4 Structure of the FOXP3 dimer. 3D structure of the FOXP3 homodimer. **A.** One peptide of the homodimer is coloured in light green and the other in light brown. The FOXP3 homodimer is bound to double stranded DNA coloured in blue and pink via its forkhead domain. **B.** Each FOXP3 peptide consists of 3 alpha helixes, 2 β strands and 2 loops (Chen *et al.*, 2015). Image taken from the Protein Data Bank (ID: 4WK8).

1.4.4 *Human FOXP3 isoforms*

FOXP3 can act both as a transcriptional repressor and activator (Lopes *et al.*, 2006; Bandukwala *et al.*, 2011). It was first identified in mice exhibiting the scurfy phenotype (Ramsdell, 2003; Ramsdell and Ziegler, 2014). This was an X-linked syndrome that spontaneously arose in mice after exposure to irradiation which resulted in a 2bp insertion in the 8th exon of the *foxp3* gene resulting in a protein that lacks its forkhead domain (Brunkow *et al.*, 2001). These mice were characterised by scaly skin, reddened eyes and enlarged spleen and lymph nodes which ultimately causes death three weeks after birth (Ramsdell and Ziegler, 2014). This is similar to CTLA-4 KO mice which also die at 3-4 weeks after birth due to the development of a lymphoproliferative disease characterised by increased peripheral T cell activation and lethal organ infiltration by lymphocytes (Tivol *et al.*, 1995). Since scurfy mice also showed increased proliferation of $CD4^+$ T cells, this indicated the involvement of Foxp3 in immunoregulation (Brunkow *et al.*, 2001). The identification of IPEX in humans, an X-linked condition caused by FOXP3 mutations affecting its ability to homodimerize and exert its functions, reinforced the idea that FOXP3 is a unique association marker of

Treg cells (Bennett *et al.*, 2001; Brunkow *et al.*, 2001; Ziegler, 2006). Clinical symptoms of patients with IPEX include chronic dermatitis, diabetes, thyroiditis, autoimmune endocrinopathy, severe diarrhoea and hemocytopenia (Otsubo *et al.*, 2011).

Contrary to mice, humans can express multiple isoforms of FOXP3. These can lack the second coding exon or the second and seventh exons together (Mailer, 2018). However, the function of these isoforms have not been fully elucidated. It is estimated that 20-30% of total FOXP3 in human Treg cells is full length, 1-3% of the total FOXP3 mRNA lacks both exon 2 and 7 (Mailer *et al.*, 2015) while it is unknown what percentage lacks the second exon only.

The isoform lacking the second coding exon is 4 kDa smaller than the full length protein and Jurkat T cells transduced with this isoform had higher proliferation rates compared to those expressing the full length protein (Allan *et al.*, 2005). Strong TCR activation was proposed to increase levels of this isoform compared to the full length one which was preferentially increased after weak TCR activation (Chen *et al.*, 2013). This isoform is found primarily in the nucleus but cannot promote its own transcription while in IPEX patients, mutations in this exon did not impair Treg cell development (Otsubo *et al.*, 2011).

The isoform lacking both the second and seventh exons is found only in the nucleus as it lacks both NES1 and NES2 and it is not functional as its ability to dimerise is affected (Li *et al.*, 2007). Also, it has been demonstrated that lack of both exons is associated with an increase in IL-2 and IL-17 levels in colon biopsies of Crohn's patients (Mailer *et al.*, 2015). The FOXP3 protein sequence encoded by the second exon can interact with RORγt therefore it was hypothesised that the lack of this isoform could promote Th17 differentiation but *in vitro* studies failed to prove that (Mailer *et al.*, 2015). The function of these isoforms remains unclear but it is hypothesised that they compete for cofactors with the full length FOXP3 (Magg *et al.*, 2012).

1.4.5 *Localisation*

Retention of FOXP3 in the nucleus is essential for the maintenance of the Treg cell phenotype (Magg *et al.*, 2012). Activation of human naïve T cells

leads to the translocation of FOXP3 to the cytoplasm whereas in activated human Treg cells, FOXP3 is maintained in the nucleus (Magg *et al.*, 2012). Site directed mutagenesis experiments led to the identification of NES1 and NES2 regions in FOXP3 which are conserved between mouse and human apart from a single amino acid substitution - L74V in NES1 (Magg *et al.*, 2012). These mutants showed decreased translocation to the cytoplasm compared to the full length FOXP3 protein but they did not differ in their suppressive capacity when compared to each other (Magg *et al.*, 2012). However, only the full length protein can induce the PIM-2 kinase so distinct functions of the isoforms are possible (Basu *et al.*, 2008).

In addition to the nuclear export sequences, studies have identified potential regions that may be involved in nuclear localisation (NLS) though these studies remain controversial. Two amino acid changes within the $_{414}$RKKR$_{417}$ sequence near the carboxyl terminus of the forkhead domain of FOXP3 resulted in the inability of the protein to translocate into the nucleus in transfected HEK293 cells (Lopes *et al.*, 2006).

Other studies performed in mice identified additional regions as NLS. Specifically, Hancock et al. demonstrated that three different regions are involved in nuclear localisation of mouse Foxp3 (Hancock and Ozkaynak, 2009). The first is a 12 amino acid sequence at the carboxyl terminus of the protein (NLS1) (Hancock and Ozkaynak, 2009). This was identified after mutations of the previously identified $_{414}$RKKR$_{417}$ motif failed to inhibit Foxp3 translocation into the nucleus but did so after deletion of that 12 amino acid sequence (Hancock and Ozkaynak, 2009). Despite the removal of NLS1, some Foxp3 was still able to localise in the nucleus (Hancock and Ozkaynak, 2009). Further mutational experiments led to the identification of NLS2 – two HNM repeats adjacent to the forkhead domain of Foxp3 towards the N terminus (Hancock and Ozkaynak, 2009). In addition to NLS1 and NLS2, a third sequence was identified as deletion of 51 amino acids at the N terminus (NLS3) which inhibited translocation of Foxp3 into the nucleus (Hancock and Ozkaynak, 2009).

However, it is worth noting that human FOXP3 and mouse Foxp3 are not 100% identical therefore the same changes can have a different effect on

their function. Also, the use of GFP-Foxp3 fusion constructs is known to disrupt its function (Bettini *et al.*, 2012). Finally, mutations can alter the secondary structure of the protein which can affect its function and subsequently its ability to localise in the nucleus therefore it does not necessarily mean that they lie within a nuclear localisation sequence.

1.4.6 *Transcriptional regulation of Foxp3*

Regulation of Foxp3 and its role in signalling has been studied extensively. Expression of Foxp3 can be induced *in vitro* by stimulating naïve T cells with TGF-β and IL-2 (Chen *et al.*, 2003) and can confer an immunosuppressive phenotype to $CD4^+CD25^-$ Tconv cells (Hori *et al.*, 2003). According to a study by Hill et al., Foxp3 alone does not result in a complete Treg cell signature suggesting that Treg cell lineage determination occurs at an early stage of Treg cell differentiation prior to the induction of Foxp3 expression and is Foxp3 independent (Hill *et al.*, 2007).

Despite that, Foxp3 is consistently expressed in Treg cells and its expression is associated with the downregulation of IL-2 and IL-4 and upregulation of the Treg cell markers CD25 and CTLA-4 (Hori *et al.*, 2003). The stability of Foxp3 expression can determine lineage commitment and functional stability in Treg cells. This is apparent in Treg cell subsets, which can exhibit variability in Foxp3 expression. For instance, TGF-β-induced Treg cells such as pTreg and iTreg cells depend on the continued presence of TGF-β for Foxp3 expression contrary to tTreg cells (Floess *et al.*, 2007; Polansky *et al.*, 2008). Epigenetic modifications are largely implicated in this process and studying the transcriptional and translational regulation of Foxp3 will lead to a more complete understanding of Treg cell stability.

The methylation of the Treg cell-specific demethylated region (TSDR) is important in regulating Foxp3 expression on a transcriptional level (Polansky *et al.*, 2008). This is a DNA region upstream of the first exon of the *foxp3* gene that regulates the expression of the gene and its methylation status is considered an indicator of Treg cell differentiation and stability. Continuous expression of Foxp3 is associated with functional stability in Treg cells (Floess *et al.*, 2007).

The stability of Treg cells was first demonstrated in a study where CFSE-labelled Treg cells were injected into mice and the frequency of Foxp3$^+$ cells was measured 14 days later using flow cytometry (Floess *et al.*, 2007). These cells were able to retain Foxp3 expression which suggested an epigenetic mechanism underlying Foxp3 stability. CpG regions of sorted Treg cells were compared to those of Tconv which demonstrated that demethylation occurred specifically in Treg cells in a non-random way as all epigenetic modifications were limited to a specific region upstream of exon 1 of the *foxp3* locus. It also demonstrated that the region was critical for successful transcription of Foxp3 as only vectors harbouring the insert upstream of the promoter were able to show luciferase activity. Consistent with these data was the fact that Treg cells correlated with acetylated histone modifications - indicative of open chromatin accessible to the transcriptional machinery. This study also showed that Foxp3 expression and CpG demethylation first occurs in developing thymocytes at the SP stage and that iTreg cells exhibit partial CpG demethylation resulting in unstable Foxp3 expression even after prolonged/continuous stimulation with TGF-β (Fontenot *et al.*, 2005; Floess *et al.*, 2007).

In vitro cell culture of naïve T cells in the presence of TGF-β and subsequent restimulation of sorted Foxp3$^+$ iTreg cells in the presence of Azacytidine (Aza) led to an increased number of Foxp3$^+$ iTreg cells present in the media after several days of culture (Polansky *et al.*, 2008). This indicated a stable Foxp3 expression mechanism and a TGF-β independent mechanism of *de novo* Foxp3 induction (Polansky *et al.*, 2008). This is associated with demethylation of TSDR as Azacytidine are nucleoside analogues with the ability to incorporate into DNA and RNA and inhibit DNA methyltransferase 1 (DNMT1)(Creusot *et al.*, 1982). In addition, reporter assays using vectors with methylated TSDR sequences in CD4$^+$ T cells showed that luciferase activity was significantly lower than those with the demethylated construct suggesting that transcription was decreased due to methylation (Polansky *et al.*, 2008). When comparing the methylation status of TSDR of sorted Foxp3$^+$ and Foxp3$^-$ cells, only the Aza-treated Foxp3$^+$ cells had a completely demethylated TSDR region. They were also the only ones with Foxp3 mRNAs supporting the theory that methylation of TSDR regulated Foxp3

expression in the transcriptional level. In further support of this theory, *in vivo* induced Treg cells that were expanded *in vitro* exhibited stable Foxp3 expression which correlated with demethylation of TSDR. These experiments demonstrated that the methylation of TSDR controls Treg cell stability through the maintenance of Foxp3 expression and that nTreg cells are more stable than iTreg cells (Floess *et al.*, 2007).

A variety of transcription factors can bind to TSDR affecting Treg cell numbers and stability (Zheng *et al.*, 2010). Some of them are the NF-κB TF cRel, Runx1, SMAD3, NFAT, Ap-1, STAT5 and CREB (Kanamori *et al.*, 2016) (figure 1.5). They can regulate Foxp3 expression by binding to different regions of the TSDR called the conserved non-coding DNA sequence elements (CNS) namely CNS1, CNS2 and CNS3. It is thought that initial TCR activation together with co-receptor signalling results in open chromatin which allows the recruitment/binding of the NF-κB transcription factor cRel to CNS3 which is important for early tTreg cell development in the thymus (Rao *et al.*, 2003). Reportedly, CNS3 knock out mice show significant decrease in frequencies of $Foxp3^+$ $CD4^+$ SP cells (tTreg cells) and deletion of cRel in mice was found to have a similar effect (Zheng *et al.*, 2010). CNS1 on the other hand, can interact with SMAD3 and NFAT complexes in response to TGF-β stimulation and is important for iTreg cell generation *in vitro* and pTreg cell differentiation *in vivo* as CNS1 knock out mice show decreased numbers of $Foxp3^+$ cells present in mesenteric lymph nodes (MLNs) and gut-associated lymphoid tissues (GALT)(Zheng *et al.*, 2010). Also, pTreg cell numbers were abnormally low in aged mice (6 months old). Lastly, CNS2 can interact with CREB and STAT5 (Kim and Leonard, 2007) and is involved in the propagation of Foxp3 expression in daughter cells affecting Treg cell lineage stability as Foxp3 can bind on its CNS2 region promoting its own expression (Zheng *et al.*, 2010). It was shown that CNS2 is demethylated in tTreg but not in pTreg cells or naïve cells. Specifically, it was found that DNMT1 and histone deacetylases (HDACs) are released form the region upon TCR stimulation in the presence of IL-2 allowing transcription factors such as STAT5 to bind to the enhancer and initiate Foxp3 transcription (Burchill *et al.*, 2007).

These studies have demonstrated that TSDR methylation plays an important role in regulating Foxp3 expression, which can differ among Treg cell subsets such as tTreg, pTreg and iTreg cells indicating differences in their differentiation process and function.

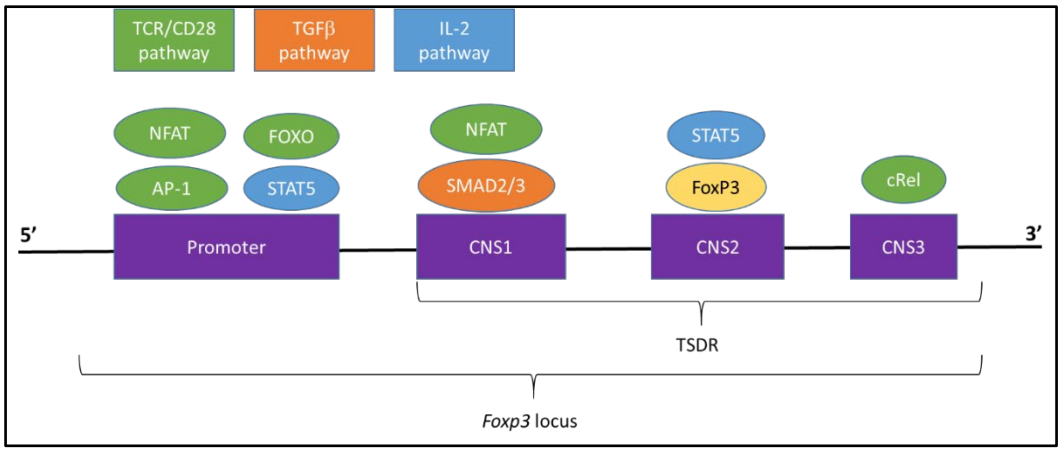

Figure 1.5 Transcription factors regulating Foxp3 expression. Schematic shows the TSDR locus annotated for its enhancer regions; CNS1, CNS2 and CNS3 together with their associated transcriptional regulators. Figure adapted from (Kanamori *et al.*, 2016).

1.4.7 *Cytokine signalling*

The signalling pathways involved in Foxp3 regulation play a central role in Treg cell development, differentiation and functional stability. TCR activation is required for *de novo* Foxp3 expression and Treg cell-mediated suppression. There are three major signalling pathways involved in Treg cell biology namely the IL-2 receptor-mediated JAK/STAT pathway, the TGF-β receptor-mediated SMAD pathway and the TCR/co-receptor-mediated MAP kinase pathway (figure 1.6). T cells can acquire and maintain Foxp3 expression after stimulation with IL-2 in the presence of TGF-β and TGF-β can activate SMAD3, which in turn activates Foxp3 transcription. TCR stimulation activates NFAT, which in turn activates the NF-κB family of transcription factors such as cRel - important for Treg cell differentiation in the thymus. Also, Foxp3 expression is reinforced through STAT5 – a downstream signalling molecule of the IL-2 receptor. Understanding these

mechanisms and how they are regulated will help understand Treg cell function.

1.4.8 *TGF-β and SMAD2/3 signalling*

TGF-β-mediated signalling is a highly complex process involved in nearly all aspects of T cell biology. There are three types of TGF-β namely TGF-β1, 2 and 3 and all of them are important for T cell survival and homeostasis. Knock out mice for TGF-β2 and 3 fail to develop at the embryonic stage

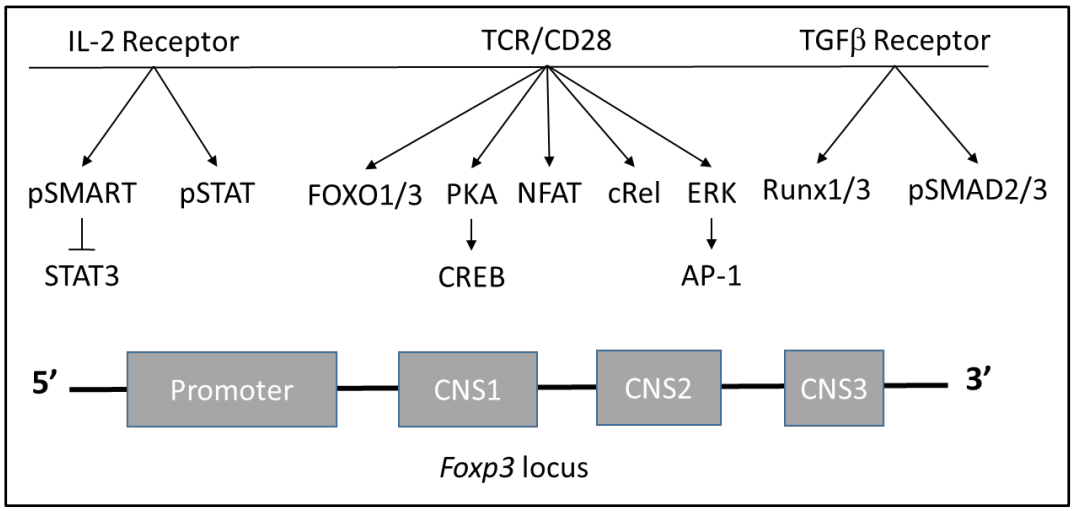

Figure 1.6 The three major signalling pathways involved in Treg cell development, function and maintenance. Signalling cascades regulating Foxp3 expression in Treg cells: IL-2 receptor signalling through STATs, TCR/co-receptor signalling through JAK/STAT and MAPK and finally TGF-β receptor signalling through SMADs. Figure adapted from (Nie *et al.*, 2015).

while TGF-β1 deletion also leads to embryonic lethality and severe systemic inflammation in new-born mice (Shull *et al.*, 1992; Proetzel *et al.*, 1995; Sanford *et al.*, 1997; Letterio and Roberts, 1998). TGF-β acts by binding to its receptor - a serine threonine kinase receptor - leading to the formation of a complex consisting of four receptor molecules: two type I and two type II receptors. The type II receptor phosphorylates type I which in turn catalyses ATP into ADP and phosphorylates/activates receptor-regulated SMADs (R-SMADs) that are attached to its cytoplasmic region via accessory proteins. This releases the phosphorylated SMAD (pSMAD) which then associates with the common mediator SMAD4 (Co-SMAD4). This guides the complex into the nucleus where it acts as a transcription factor to activate gene expression (Attisano and Wrana, 1996). Reportedly, TGF-β has an anti-apoptotic and anti-proliferative effect on cells and it inhibits T cell

differentiation promoting pluripotency and a central memory phenotype (Brabletz *et al.*, 1993; Genestier *et al.*, 1999; Gorelik *et al.*, 2000; Gorelik and Flavell, 2002). In support of that, Th1 cells induced in the presence of TGF-β maintain IL-2 expression (Gorelik and Flavell, 2002).

One of the earliest studies that looked at the role of TGF-β in Treg cells demonstrated that TGF-β could inhibit naïve T cell proliferation *in vitro* and that naïve cells stimulated with anti-CD3 and APCs in the presence of TGF-β resulted in decreased proliferation (Chen *et al.*, 2003). The addition of IL-2 in the media was able to partly rescue the phenotype but TGF-β was still able to inhibit the differentiation of naive T cells into Th1 or Th2 effector cells. Additionally, culture of naive T cells in the presence of TGF-β led to a higher frequency of $CD25^+$ cells in the media than when it was absent and these cells also expressed Foxp3 suggesting a role of TGF-β in iTreg cell induction. Most importantly, these TGF-β-induced iTreg cells could prevent asthmatic reactions in mice, which proved that iTreg cells could maintain their function *in vivo* (Chen *et al.*, 2003).

In support of this, another study demonstrated that the frequency of pTreg cells in young *TGF-β1*$^{-/-}$ mice was significantly lower than that of wild type mice whereas tTreg cell frequencies were the same in both groups (Marie *et al.*, 2005). In addition to this, intracellular staining of *TGF-β1*$^{-/-}$ Treg cells showed decreased expression of Foxp3 compared to wild type Treg cells which correlated with impaired suppressive function. However, this could probably be because the mice had more effector T cells than Treg cells due to lack of TGF-β. It should be noted that TGF-β produced by APCs in *in vitro* suppression assays was able to compensate for loss of function of *TGF-β1*$^{-/-}$ Treg cells and suppress proliferation of wild type naïve T cells. This might be due to both TGF-β and IL-2 being released in the media which could have induced wild type iTreg cells which were able to suppress proliferation. It has been shown that TGF-β can be directly released by apoptotic cells as well as macrophages in response to signals released by other apoptotic cells which can often confound results (Fadok *et al.*, 2000; Chen *et al.*, 2001).

TGF-β-SMAD signalling is particularly important in T cell biology as SMADs can regulate cell proliferation and lineage determination. SMADs are recruited to open chromatin regions that have been previously modified by T-cell lineage master transcription factors (Mullen *et al.*, 2011). There, they form oligomers and associate with other transcription factors to form complexes in order to initiate transcription. Thus, SMAD complexes can form part of the cell's molecular signature and be indicative of a specific cell lineage and activation state. There are three types of SMADs namely the R-SMADs, Co-SMAD and I-SMADs (Derynck and Zhang, 2003). SMAD2/3 belong to the first category and they are of particular interest as they are implicated in Treg cell differentiation (Xu *et al.*, 2010). After T cell activation, NFAT and SMAD3 can bind to the CNS1 region of the *foxp3* locus and induce Foxp3 expression (Tone *et al.*, 2008). It is thought that binding of SMAD3 on the enhancer occurs at an early stage soon after stimulation with TGF-β and acts by accelerating the acetylation of histones which opens the chromatin. Subsequent binding of NFAT on the enhancer region occurs after the binding of SMAD3 and its role is to maintain Foxp3 expression (Tone *et al.*, 2008). In support of this, retinoic acid (RA) has been found to promote SMAD3 activation (pSMAD3) and binding to CNS1 (Xiao *et al.*, 2008). It has been reported that the receptors of RA can bind to both the promoter and enhancer region of *foxp3* and that the recruited RA can increase histone acetylation thus augmenting pSMAD3 binding to the enhancer (Xu *et al.*, 2010). Deletion of those binding sites in luciferase reporter assays led to complete loss of luciferase activity even after stimulation of cells with TGF-β and RA. Besides pSMAD3, RA and NFAT which are all positive regulators of Foxp3 expression, there are other molecules that can have an inhibitory effect on Foxp3 transcription. For instance IL-27 can activate STAT3 (pSTAT3) which binds to a region downstream of the *foxp3* enhancer displacing pSMAD3 thus acting as a silencer (Xu *et al.*, 2010). This is further supported by a study in STAT3 knock out mice where IL-27-mediated inhibition of Foxp3 expression was decreased (Xu *et al.*, 2010). It should be noted that IL-27 also signals through STAT1, which can render IL-27 effective in suppressing Foxp3 even in the absence of STAT3. In addition, it has been reported that SMAD2 can

also regulate STAT3 phosphorylation thus affecting Foxp3 expression (Martinez *et al.*, 2010).

In summary, these data have demonstrated the importance of TGF-β in Treg cell differentiation through its downstream signalling molecules most notably SMAD2 and SMAD3.

1.4.9 *IL-2 and JAK/STAT signalling*

Another important signalling pathway involved in Treg cell development and function is the IL-2 receptor-mediated responses. The IL-2 receptor is a type 1 transmembrane cytokine receptor which transmits signals by recruiting JAK tyrosine kinases upon interaction with its ligand IL-2. This results in the phosphorylation of downstream molecules such as PI13K, Erk and the transcription factor STAT5 (Burchill *et al.*, 2007). The IL-2 receptor plays an important role in Treg cell differentiation and is one of the main markers used to distinguish Treg cells as it is overexpressed on their cell surface after activation. It signals through STATs most importantly STAT3 and STAT5. Briefly, IL-2 induces STAT5 which then binds to the promoter of *foxp3* which induces Foxp3 transcription. Foxp3 then induces the expression of IL-2 receptor in a positive feedback loop. In accordance with this, it has been demonstrated that interleukin 2 receptor subunit beta (IL2Rβ) knock out mice show reduced number of tTreg and pTreg cells (Burchill *et al.*, 2007). Also, transgenic expression of Foxp3 in *IL2Rβ*$^{-/-}$ cells can impart regulatory function as observed in *in vitro* suppression assays and *in vivo* where numbers of Foxp3^{+} cells in the thymus were restored (Burchill *et al.*, 2007). This indicated the importance of downstream IL2Rβ signalling in Treg cell development. This was further supported by a chromatin immunoprecipitation (ChIP) analysis using an antibody (Ab) for STAT5 which demonstrated that STAT5 can bind to the promoter region of *foxp3* regulating its expression. Reportedly, disruption of the STAT5 gene leads to a significant decrease in tTreg and pTreg cell numbers in a manner analogous to IL2Rβ deletion further supporting the theory that STAT5 is important for Treg cell development (Burchill *et al.*, 2007). It should be noted that STAT5 can bind to multiple regions in the *foxp3* locus one of which overlaps with a STAT3 binding site (Xu *et al.*, 2010).

STATs can coordinate immune responses depending on the microenvironment and the cytokines present. STAT3 in particular, is associated with Th17-mediated responses as it can upregulate the master transcription factor of Th17 cells RORγt in response to IL-6 stimulation (Veldhoen *et al.*, 2006). As mentioned before, STAT3 can negatively regulate Foxp3 expression which is further supported by the fact that IL-6 failed to suppress Foxp3 expression in the absence of STAT3 *in vitro* (Laurence *et al.*, 2012). In addition, IL-27 signalling through STAT1 was able to suppress Foxp3 expression despite the absence of STAT3 (Laurence *et al.*, 2012). However, STAT3 is also required for Treg cell-mediated suppression of Th17 cells. Reportedly, STAT3 deletion in mice led to intestinal inflammation and loss of Treg cell-mediated suppression of Th17 responses (Chaudhry *et al.*, 2009). ChIP analysis for Foxp3 showed an association between Foxp3 and pSTAT3 suggesting a mechanism of action whereby STAT3 facilitates the recruitment of Foxp3 to Th17-response elements such as the IL-6 and TGF-β1 promoter regions thus regulating Th17 functions.

As mentioned before, the CNS2 region has been shown to play an important role in maintaining Foxp3 stability and lineage stability in Treg cells. This region, while largely demethylated in Treg cells, it can become remethylated upon Treg cell division, which in turn leads to loss of Foxp3 expression (Feng *et al.*, 2014). This is thought to be due to decreased IL-2 signalling and decreased pSTAT5 binding to the CNS2 region during this process (Feng *et al.*, 2014). In support of this, overexpression of pSTAT5 in CNS2-deficient Treg cells was able to rescue Foxp3 expression in a similar way to stimulation with a high amount of IL-2 (Feng *et al.*, 2014). This is thought to be due to the existence of multiple binding sites of STAT5 on the *foxp3* locus including on the promoter, which could compensate for the loss of CNS2 (Feng *et al.*, 2014). STAT5 is activated by IL-2 signalling therefore it was proposed that sufficient IL-2 signalling could partially compensate for CNS2 function in maintaining Foxp3 expression (Feng *et al.*, 2014). Although IL-2 improved cell viability of both wild type and CNS2-deficient Treg cells, it failed to stabilise Foxp3 expression in the CNS2-deficient Treg cells (Feng *et al.*, 2014). Therefore, it was proposed that CNS2 could partially

compensate for decreased IL-2 signalling whereas increased STAT5 activation could compensate for the absence of CNS2 (Feng *et al.*, 2014). Indeed, increased IL-2 signalling correlated with increased phosphorylation of STAT5 and Foxp3 expression in CNS2-deficient Treg cells *in vitro*. Furthermore, when CNS2-deficient and wild type Treg cells were stimulated with IL-2 in the presence or absence of the pro-inflammatory cytokine IL-4, ChIP-qPCR analysis showed an overlap of STAT5 and STAT6 binding sites on CNS2 (Feng *et al.*, 2014). STAT6 is associated primarily with the Th2 cell lineage and competitive binding of the two STATs for sites on CNS2 could influence T cell lineage commitment. In support of this, STAT6 has been shown to recruit DNMT1, which can methylate CpG islands found in that region thus repressing Foxp3 expression (Feng *et al.*, 2014). *In vivo*, CNS2 was important for the propagation of the Treg cell lineage as irradiated mice that were injected with CNS2-deficient Treg cells showed a significant decline in the frequency of that population after five weeks (Feng *et al.*, 2014). In addition to this, all CNS2-deficient Treg cells that were injected in mice with experimental autoimmune encephalomyelitis (EAE), lost Foxp3 expression whereas a third of the wild type Treg cells were able to maintain it (Feng *et al.*, 2014). Taken together, these results suggest CNS2 is critical for the maintenance of Foxp3 expression and Treg cell lineage commitment in both inflammatory and resting states.

In summary, these data demonstrate that STAT-mediated signalling in response to TCR signalling and the IL-2 receptor is a highly complex process that depends on surrounding signals from the microenvironment and can affect gene expression therefore regulating cell lineage commitment and function.

1.5 Post-translational regulation of Foxp3 - proteolytic cleavage by asparaginyl endopeptidase

Post-translational regulation of Foxp3 expression has been recently shown to regulate Foxp3 expression in Treg cells as it determines the amount and stability of the transcription factor present in the cell thus affecting the duration/strength of Foxp3-mediated signalling and ultimately Treg cell stability and function (Deng *et al.*, 2019).

1.5.1 *Discovery and nomenclature*

Proteolytic degradation mediated by proteases in lysosomes plays an important role in post-translational regulation of Foxp3. An example of such a protease is the cysteine protease asparaginyl endopeptidase (AEP). This protein was first discovered in 1980 in the bean plant *Phaseolus vulgaris* and its expression has since been confirmed in other plants, trematodes, ticks and mammals but is absent from bacteria (Dall and Brandstetter, 2016). Its expression in humans was confirmed in 1996 (Tanaka *et al.*, 1996). Since its discovery, it has been given a variety of names influenced by the localisation and function of the enzyme in these organisms. Some of the names include haemoglobinase, endopeptidase B, vacuolar processing enzyme, nucellain, PRSC1, asparaginyl carboxypeptidase, asparaginyl endopeptidase and legumain (LGMN) – the last one being the most commonly used (Dall and Brandstetter, 2016).

1.5.2 *Gene structure*

In humans, AEP is found on the long part of chromosome 14 at position 14q.32.12 and it consists of 18 exons. In mice, it is found on chromosome 12 at position 12.12E and it consists of 15 exons. Both mouse and human express three isoforms of the protease but only one of them is currently known to be functional. Both organisms also carry a pseudogene of legumain. In humans the pseudogene is located on chromosome 13 at position 13q21.31 while in mouse it is found on chromosome 5 at position 5.5F. The above information was obtained from the UniProt and NCBI online databases (UniProt human identifier code: Q99538 & mouse identifier O89017 code, NCBI human gene ID 5641 & mouse gene ID 19141).

1.5.3 *Protein structure and activation*

Human AEP is 433 amino acids long and it is 83% identical in sequence to the mouse which is 435 amino acids long. LGMN can exist in two forms: the inactive and active form depending on the pH of the environment (Li *et al.*, 2003). The inactive form is called ‘prolegumain zymogen’ and it is the 56 kDa full-length protein normally found in endosomes (Li *et al.*, 2003). It consists of four domains namely the signal peptide (SP), the catalytic domain (LGMN), the activation peptide (AP) and the legumain stabilisation and activity modulation domain (LSAM) (Dall and Brandstetter, 2013). The

N-terminal SP domain is involved in protein trafficking from the ER into the Golgi apparatus whereas the AP domain loops around and links the catalytic domain to that of LSAM (Dall and Brandstetter, 2016). This way LSAM serves as a blocking substrate for AEP in an autoinhibitory fashion (figure 1.7) (Dall and Brandstetter, 2016). This form of the protein is stable at neutral pH (Li *et al.*, 2003). As endosomes mature into lysosomes, the pH drops which triggers prolegumain to undergo autoactivation (figure 1.8) (Li *et al.*, 2003). During this process, it is cleaved at the Asn323 residue located on the C-terminus at pH 5.5 and at the Asp21 and Asp25 on the N-terminus at a lower pH (Li *et al.*, 2003). Depending on the pH, autocatalytic cleavage can result in the formation of either AEP (46 kDa) or asparaginyl-specific mono-carboxypeptidase (ACP) (47 kDa) with endopeptidase and exopeptidase activities respectively (Dall and Brandstetter, 2016)). Each of these substrates is active at different pH levels with AEP being active at acidic pH whereas ACP at higher pH levels (Dall and Brandstetter, 2016). AEP is unstable at neutral pH unless ubiquitinated at the Asn323 residue or complexed with other molecules such as integrins and cystatin inhibitors (Dall and Brandstetter, 2016). In addition to its endo- and exo-peptidase activity, LGMN can acquire a carboxypeptidase activity during activation in endosomes that is stable at neutral pH (Dall and Brandstetter, 2013).

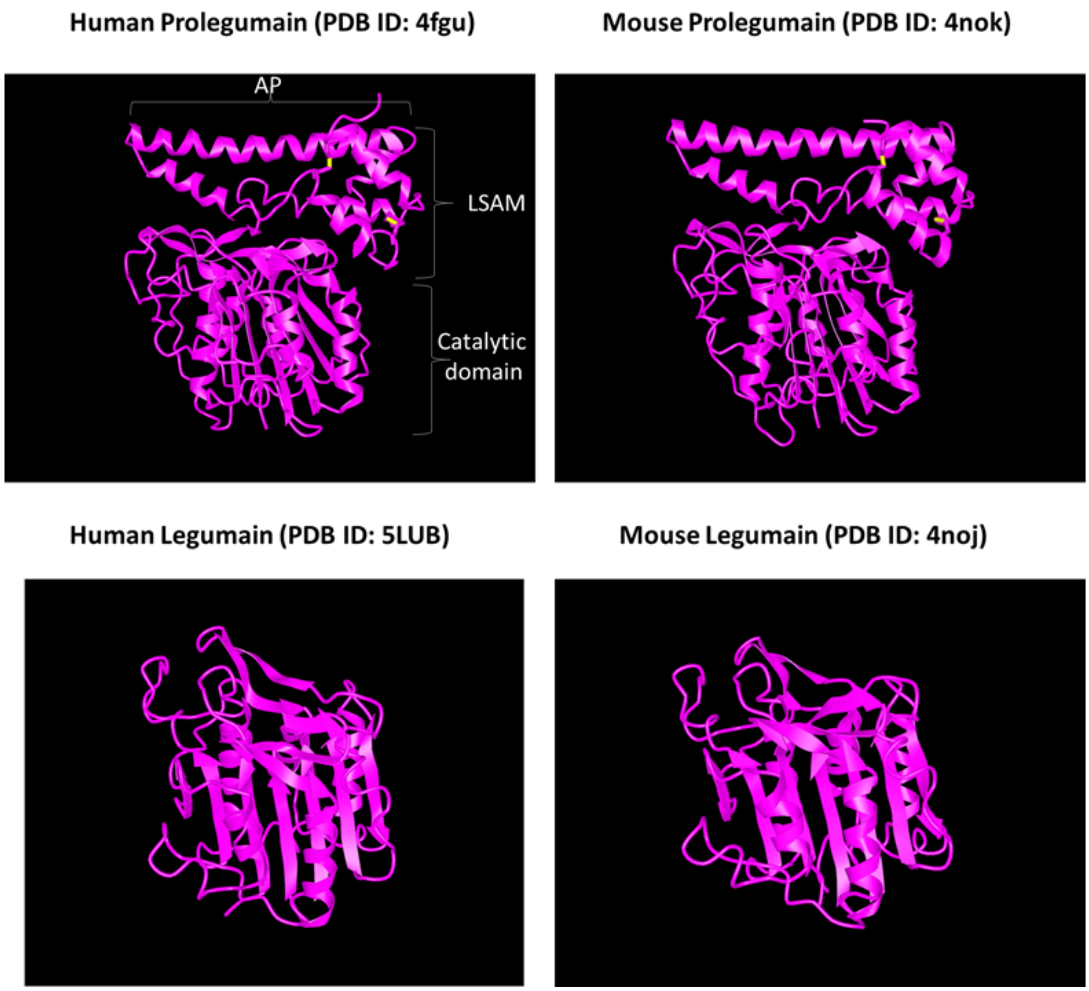

Figure 1.7 Protein structure of LGMN. 3D illustration of the homology of human and mouse inactive and active LGMN. Inactive LGMN/prolegumain (top row) consists of four domains: the signal peptide (SP, not shown), the catalytic domain, the activation peptide (AP) and the legumain stabilisation and activity modulation domain (LSAM). The AP domain loops around and links the catalytic domain to that of LSAM. This way LSAM serves as a blocking substrate for AEP in an autoinhibitory fashion. Drop in pH triggers prolegumain to undergo autoactivation (Dall and Brandstetter, 2016). The active form (bottom row) consists of the catalytic domain only. Images taken from the Protein Data Bank (PDB ID: 4fgu, 4nok, 5lub, 4noj).

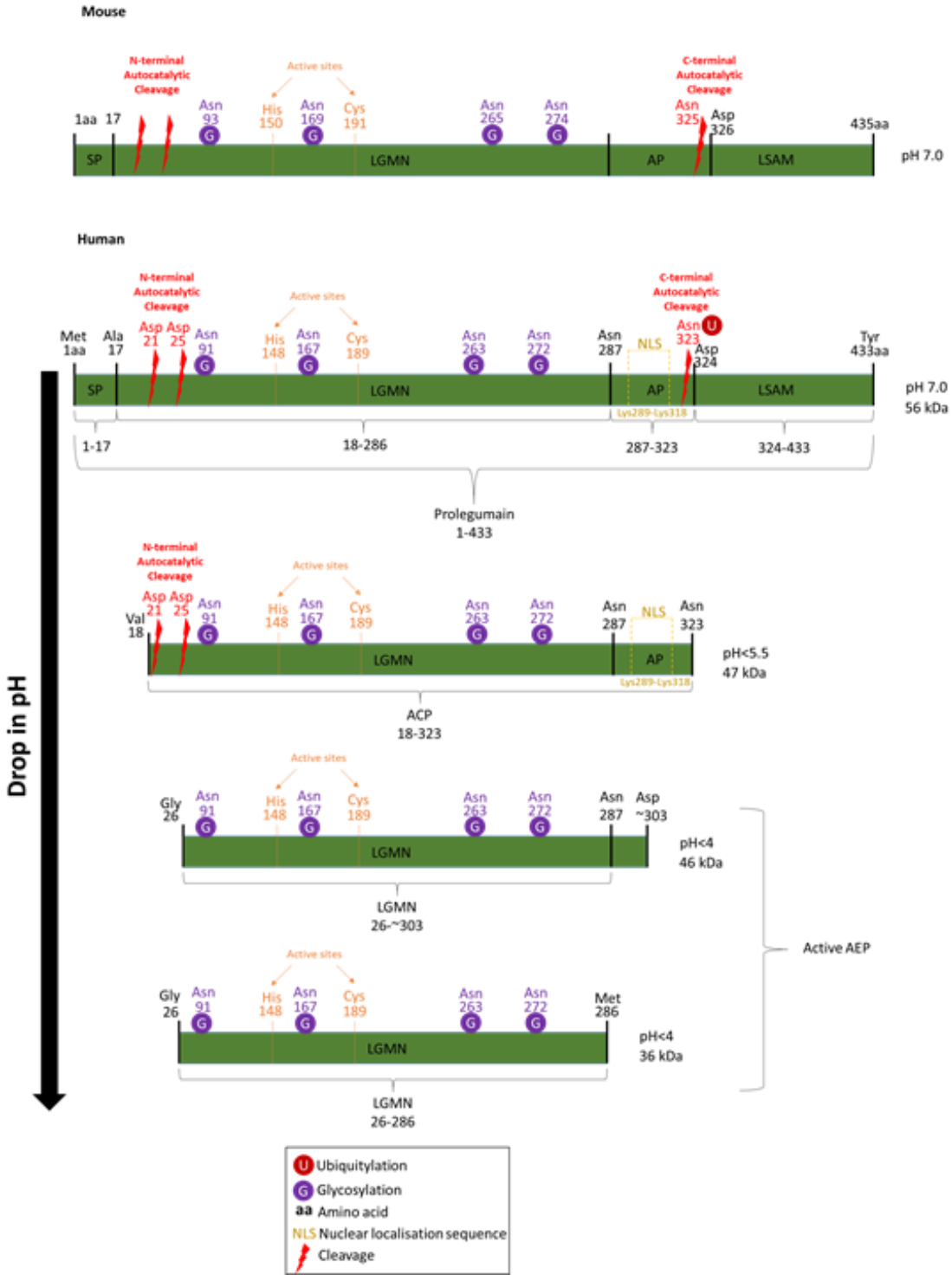

Figure 1.8 Activation of human LGMN. pH-dependent activation of human LGMN annotated with its domains, active sites and post-translational modifications including its glycosylation (important for protein structure stability and function) and ubiquitination sites (that target protein for proteasomal degradation). Prolegumain consists of four domains: the signal peptide (SP, important for protein trafficking from the ER to the Golgi apparatus), the catalytic domain (LGMN), the activation peptide (AP) and the legumain stabilisation and activity modulation domain (LSAM). N and C terminal processing occurs during protein activation. Peptide sizes ≤ 46 kDa are considered enzymatically active. Image adapted from (Dall and Brandstetter, 2016).

1.5.4 *Localisation and function*

The localisation of the protein often provides insight into its function and LGMN has been found to be expressed primarily in kidneys and in APCs mainly in endosomes and lysosomes and occasionally in the nucleus owing to its NLS (Dall and Brandstetter, 2016). This is further supported by studies in mice deficient for LGMN (Shirahama-Noda *et al.*, 2003). These knock out mice accumulate unprocessed pro-cathepsins in abnormally large lysosomes in kidney cells suggestive of a lysosomal storage disorder (Shirahama-Noda *et al.*, 2003). Specifically, western blotting detected increased levels of unprocessed single-chain cathepsins in the knock out mice compared to the wild type mice, which was also reflected in protease activity assays showing a 50% decrease in cathepsin H activity (Shirahama-Noda *et al.*, 2003). Due to this accumulation of inactive proteases, results from experiments involving AEP inhibitors should be interpreted with caution as blocking AEP may have an indirect effect on the activity of other proteases (which are its substrates) and therefore the observed effect might be due to the suboptimal activity of these proteases rather than AEP. An example of an indirect effect is that AEP-mediated activation of cathepsin L enhances Th1 responses in humans while in mice it represses Th17 cell differentiation (Hou *et al.*, 2015; Freeley *et al.*, 2018).

In addition to the *Lgmn*$^{-/-}$ mice generated by Shirahama-Noda et al., the same strain was also generated by Matthews et al. which exhibited the same phenotype and was used throughout this project (Matthews *et al.*, 2010). The strain was generated by deletion of part of exon 3 and intron 2 via homologous recombination in HM1 mouse embryonic stem cells which were then injected into mouse blastocytes of a C57BL/6 background (Matthews *et al.*, 2010). These chimeras produced heterozygous offspring which were then backcrossed for more than 10 generations in order to eliminate any WT cells that may have been propagated from chimeric blastocytes (Matthews *et al.*, 2010). However, it should be noted that during homologous recombination other genes that are in proximity to LGMN may have also been affected during homologous recombination. Such genes include those encoding for the Ras and Rab interactor 3 protein which is a GTP binding protein involved in the exchange of GDP for GTP and a gene

encoding for the Golgi subfamily A member 5 protein which is involved in the maintaining of Golgi structure (data obtained from browsing the chromosomal region of LGMN in the Ensembl online database, human ID: ENSG00000100600, mouse ID: ENSMUSG00000021190).

Some of LGMN's substrates that have been identified include prolegumain (autoactivation), self-antigens, other cysteine proteases such as cathepsins, cystatin inhibitors and Toll-like receptors (TLRs) (Dall and Brandstetter, 2016). All these contain asparagine residues that AEP specifically recognises and cleaves (Ishii, 1993). It has been shown that LGMN is involved in MHC II peptide loading as stimulation of mouse peripheral blood mononuclear cells (PBMCs) with the tetanus toxin C-terminal fragment (TTCF) Ag in the presence of the AEP inhibitor AENK inhibited the presentation of the Ag on MHC molecules (Manoury *et al.*, 1998). In contrast, cells stimulated with the Ag in the absence of AENK expressed MHC molecules on their surface within an hour of stimulation (Manoury *et al.*, 1998). In support of that, when the TTCF Ag was pre-digested with AEP, MHC presentation of the Ag occurred more rapidly - within half an hour of stimulation - even in the presence of the inhibitor. Interestingly, AEP fails to recognise and cleave N-glycosylated proteins, which can result in a preference for cleavage of microbial Ags that lack posttranslational modifications (Manoury *et al.*, 1998).

AEP has been previously shown to be involved in the initial steps of MHC II processing through the removal of the invariant chain Ii in human B cells and DCs (Maehr *et al.*, 2005). In mice however, no differences were observed in the maturation of MHC II in APCs from *Lgmn*$^{-/-}$ APCs compared to WT. Also, Ag presentation in these cells was just as efficient which was also reflected in the numbers of $CD4^+$ T cells which were normal (Maehr *et al.*, 2005). Instead, cathepsin S was found to play an important role as its absence resulted in the accumulation of Ii intermediates (Maehr *et al.*, 2005).

Furthermore, AEP has been associated with the destruction of the immunological epitope found in myelin basic protein (MBP) in human B cells leading to the development of multiple sclerosis (Manoury *et al.*, 2002).

However, subsequent studies have demonstrated that the serine protease cathepsin G is responsible for the destruction of this epitope. Specifically, MBP incubation with B cell lysosomal extracts failed to produce AEP-specific cleaved peptides while mutated MBP at the AEP cleavage site still resulted in the degradation of the protein (Burster *et al.*, 2004). Also, MBP fragments were still present following selective inhibition of AEP while B cell lysosomes expressed low amounts of AEP protein (Burster *et al.*, 2004). Endocytosed cathepsin G on the other hand, destroyed the immunogenic epitope of MBP and this process was blocked by treatment with PMSF which is an inhibitor of serine proteases (Burster *et al.*, 2004).

Collectively, these data indicate that proteases such as AEP can be highly selective in terms of their substrates and that they are important players in regulating immune responses through their role in Ag processing and presentation.

Other functions of AEP include cleavage-mediated TLR activation and degradation of DNase inhibitors (Sepulveda *et al.*, 2009; Basurto-Islas *et al.*, 2013). In fact, it has been shown that activated TLR9 translocates into lysosomes where it is cleaved by AEP at Asn466 (Sepulveda *et al.*, 2009). This enables it to recognise foreign RNA and induce the production of inflammatory signals such as IL-6 and IL-12 (Sepulveda *et al.*, 2009). Incubation of radiolabelled TLR9 with proteases and protease inhibitors resulted in degradation of the receptor (Sepulveda *et al.*, 2009). However, when the AEP inhibitor MV026630 (Loak *et al.*, 2003) was used, TLR9 was not cleaved supporting the role of AEP in TLR9 activation. Furthermore, no TLR9 signalling was detected in high pH conditions while transfection of *TLR9*$^{-/-}$ dendritic cells with the active, cleaved form of TLR9 restored cytokine production (Sepulveda *et al.*, 2009). Site-directed mutagenesis of Asn466 also abrogated TLR9-mediated signalling (Sepulveda *et al.*, 2009). Taken together, these data suggest a direct involvement of AEP in TLR9 signalling in mouse DCs which has wider implications in DC-mediated immune responses (Sepulveda *et al.*, 2009). IL-10 stimulation has been shown to increase the pH of APC endosomes whereas IL-6 has the opposite effect (Fiebiger *et al.*, 2001). This is thought to affect Ag presentation and TCR signalling therefore it is hypothesised that LGMN could be implicated

in the modulation of immune responses. This is further supported by the fact that MHC II presentation and maturation of DCs is thought to be regulated by the expression of cysteine protease inhibitors called cystatins (Pierre and Mellman, 1998). Additionally, LGMN can facilitate the recruitment of apoptosomes and inflammasomes via its death domain located in the C terminus that facilitates the assembly of oligomers (Martinon *et al.*, 2002; Yuan *et al.*, 2010).

In pathophysiological conditions, due to the abnormal conditions of the microenvironment, AEP can be found in a variety of subcellular fractions including the cytosol, nucleus, the cell surface and even in the extracellular compartment (Dall and Brandstetter, 2016). For instance, one of the causes of Alzheimer's disease (AD) is the truncation and hyperphosphorylation of the tau protein, which disrupts the cell microtubules thus forming intracellular toxic neurofibrillary aggregations (Zhang *et al.*, 2014). AEP is thought to play a role in this as it can directly cleave tau on N255 and N368 residues independently of phosphorylation (Zhang *et al.*, 2014). This was demonstrated after incubation of AEP with tau, which resulted in two tau fragments only under optimum pH conditions (pH 6). Furthermore, treatment of cells with the anti-AEP Ab prevented tau fragmentation while truncation of the protein was also avoided when cells were incubated with the AEP inhibitor AENK (Zhang *et al.*, 2014). Mutations of the AEP cleavage sites also had the same effect. In contrast, mutation of other protease-specific cleavage sites did not affect AEP-mediated cleavage. This suggests that AEP cleaves tau independently of other proteases in a highly specific manner. Furthermore, tau phosphorylation did not affect tau fragmentation by AEP as treatment of cells with the inhibitor of the protein phosphatase 2 A (PP2Ai) had no effect on tau fragmentation (Zhang *et al.*, 2014). However, it has been shown that AEP can also activate PP2Ai thus enhancing the phosphorylation of tau (Basurto-Islas *et al.*, 2013). Finally, incubation of tubulin with His-tagged tau fragments resulted in the formation of tau neurofibrillary tangles as opposed to incubation with the full-length protein (Zhang *et al.*, 2014). This supported the idea of tau fragments being the cause of tangle formation. *In vivo*, *Lgmn*$^{-/-}$ mice with tauopathy showed improved cognitive function and reduced levels of phosphorylated tau

similar to mice expressing a mutated AEP-resistant tau (Zhang *et al.*, 2014). LGMN has also been associated with neuronal apoptosis caused by the degradation of DNase inhibitors such as SET, which results in increased DNA damage (Liu *et al.*, 2008b). Taken together, these data highlight the role of AEP in the pathogenicity of AD and suggest AEP as a potential drug target.

Cancer is another disease where AEP is deregulated. LGMN has been found to be expressed extracellularly and on the cell surface of a wide variety of tumour cells such as tumour associated macrophages (TAMs) (Luo *et al.*, 2006). A study by Haugen et al. also demonstrated the expression of proteolytically active LGMN in the nucleus of human colorectal cancer cell lines (Haugen *et al.*, 2013). It was also demonstrated that different cell lines could vary in terms of the amount of active and inactive LGMN expression as well as the distribution of these forms within the cell (Haugen *et al.*, 2013). For example, it was shown that active forms of the enzyme can be found in the nucleus where it can degrade histone 3 (H3.1) in a dose dependent manner (Haugen *et al.*, 2013).

Collectively, these data suggest that LGMN is involved in immune responses, immune tolerance, signalling, apoptosis and even gene transcription (nuclear localisation) therefore it could be a potential target for the treatment of a variety of diseases including cancer and autoimmune diseases such as Alzheimer's.

1.5.5 *Regulation of AEP*

Understanding the signalling mechanisms that regulate AEP could give further insight into how AEP can be targeted for therapeutic purposes. Whether the same signalling mechanisms that are currently being targeted and used as immunotherapy in the clinic, are also implicated in AEP expression remains unknown. Examples of such co-receptors include CTLA-4 and PD-1 which are both associated with the Treg cell lineage (being Treg cell markers) and regulate Treg cell function thus regulating peripheral tolerance and anti-tumour immunity.

CTLA-4 (CD152) is a negative co-receptor homologous to CD28 and is expressed on T cells upon initial activation while it is constitutively

expressed on Treg cells (Walunas *et al.*, 1994). High dosage of anti-CTLA-4 mAb results in autoimmune gastritis in normal mice while CTLA-4 blockade *in vitro* inhibits Treg cell-mediated suppression of naïve T cells in a dose-dependent manner (Takahashi *et al.*, 2000). Treg cell-specific depletion of CTLA-4 promotes anti-tumour immunity through the increased differentiation of naïve T cells into the Th1 and Th2 effector subtypes in wild type (WT) mice receiving splenocytes from *CTLA-4*$^{-/-}$ mice in addition to leukaemia cells (Wing *et al.*, 2008). It is worth noting that although the tTreg cell frequency was not altered in the conditional knock out mouse, there was an increased frequency of pTreg cells in the lymph nodes and spleen demonstrating the inefficiency of *CTLA-4*$^{-/-}$ Treg cells in suppressing T cell proliferation in the periphery (Wing *et al.*, 2008). In contrast, CTLA-4 activation induces tolerance and reduces graft rejection in mice receiving islet xenografts (Lenschow *et al.*, 1992). Despite the inhibitory effect of CTLA-4 on effector T cells, CTLA-4 enhances Treg cell activity. Treg cell-specific deletion of the gene leads to lack of suppressive activity through the inhibited production of TGF-β (Chen *et al.*, 1998; Wing *et al.*, 2008). Interestingly, the stronger the affinity of the TCR for its antigen, the more CTLA-4 is expressed on the cell surface (Pardoll, 2012). *CTLA-4*$^{-/-}$ Treg cells - although they develop normally, they fail to downregulate the expression of CD80/CD86 on APCs in mixed lymphocyte reaction cultures which leads to the activation and proliferation of responder cells *in vitro* (Wing *et al.*, 2008). CTLA-4 competes with CD28 for CD80 and inhibits downstream TCR signalling (Linsley *et al.*, 1994). This interaction can induce APCs to activate indoleamine 2,3-dioxygenase (IDO) - an enzyme that catalyses tryptophan (Mellor *et al.*, 2002) which results in amino acid depletion and downregulation of APC-mediated T cell proliferation (Munn *et al.*, 1999). However, the exact mechanisms of CTLA-4 function remain unclear as a different set of studies have suggested that CTLA-4, which is found constitutively expressed on Treg cells, exerts its function by interacting with its ligands on the surface of APCs and inducing their endocytosis and proteolytic degradation (Sansom, 2015). Whether AEP is involved in this process remains unknown although substrate overload as a result of

increased endocytosis has been shown to trigger an increase in AEP mRNA levels in mouse embryonic fibroblasts (Martinez-Fabregas *et al.*, 2018).

As for PD-1, it is a 288 amino acid negative co-receptor expressed on a variety of cells including myeloid derived and B and T cells (Riley, 2009). It interacts with its ligands PDL-1 and PDL-2 inducing peripheral tolerance (Riley, 2009). It downregulates TCR signalling and limits the activity of effector T cells by inhibiting activation of PI3K, CD3ζ, ZAP70, PKCθ and Erk (Parry *et al.*, 2005; Keir *et al.*, 2008). PD-1 activation has been shown to promote iTreg cell generation by downregulating mTOR and activating PI3K antagonists such as the phosphatase and tension homolog PTEN (Francisco *et al.*, 2009). Contrary to CTLA-4, PD-1 is required for the long-term survival of Treg cells as only blockade of PD-L1 in antigen-specific tolerised T cells failed to protect mice from autoimmunity (Fife *et al.*, 2009).

In support of this, PDL-1-treated iTreg cells exhibit enhanced Foxp3 expression and stability both *in vitro* and *in vivo* (Francisco *et al.*, 2009). Specifically, *PDL-1*$^{-/-}$ APCs were unable to induce iTreg cells *in vitro* whereas culture of naïve cells with PDL-1-coated beads was able to induce iTreg cells even in the absence of TGF-β (Francisco *et al.*, 2009). PDL-1 treated iTreg cells were more potent suppressors of proliferation than control iTreg cells (Francisco *et al.*, 2009). In addition, adoptive transfer of naïve T cells into *PDL-1*$^{-/-}$ *Rag*$^{-/-}$ mice resulted in a 10-fold decrease in the frequency of Foxp3^{+} T cells than in *Rag*$^{-/-}$ mice and they died from immune hyperactivation (Francisco *et al.*, 2009). All these data along with the fact that PDL-1-treated iTreg cell cultures exhibited reduced levels of pPKB, pmTOR, pERK2 and increased levels of PI3K antagonists such as PTEN, support the idea of PDL-1 positively regulating Treg cell development and function while having the opposite effect on naïve and T effector cells (Francisco *et al.*, 2009). This suggests that PDL-1 can positively regulate Foxp3 expression in the periphery while also maintaining Treg cell function.

More importantly, recent experiments performed by Dr. Shoba Amarnath have demonstrated that PDL-1-treated Tbet^{+}iTreg cells were more efficient at protecting mice from colitis and graft versus host disease (GvHD) which also correlated with the downregulation of AEP mRNA expression in these

cells compared to Tbet^{+}iTreg cells (appendix D). Collectively, this indicates that there is a link between PD-1 signalling, AEP expression and Treg cell function and stability.

A comprehensive understanding of protease activity and co-receptor signalling in Treg cells will facilitate the use of Treg cells as therapeutic agents or targets for the treatment of autoimmune diseases and cancer.

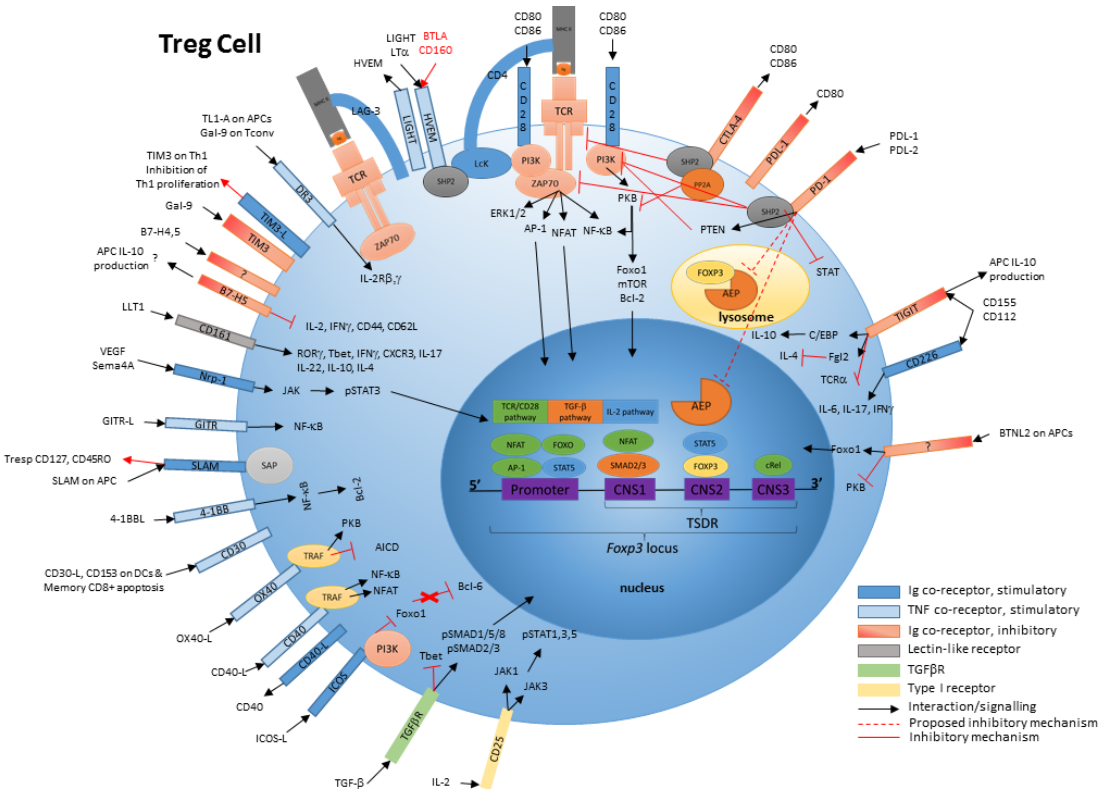

Figure 1.9 Signalling in a regulatory T cell. Image illustrating the complexity of Treg cell signalling. Co-receptor signalling regulates Treg cell activity and stability by delivering positive and negative signals.

1.6 Hypothesis

Previous work performed by Dr Shoba Amarnath has demonstrated that in mouse models of colitis and GvHD, treatment of mice with PDL-1-treated Tbet^{+}iTreg cells led to improved survival rates and clinical scores compared to cohorts that received Tbet^{+}iTreg cells (figure 1 in appendix D). To elucidate the mechanism behind the effect of PDL-1 stimulation on enhancing Treg cell function, a microarray analysis was performed by Dr Shoba Amarnath to determine which genes were deferentially expressed between the Tbet^{+}iTreg and PDL-1-treated Tbet^{+}iTreg cell populations. This analysis showed the significant downregulation (~16-fold, $p=1*10^{-6}$) of the gene encoding for AEP in the PDL-1-treated population (figure 2 in appendix D). This, in addition to the role of PDL-1 signalling in enhancing Treg cell differentiation and function (Francisco *et al.*, 2009), proposed a model whereby Foxp3 and subsequently Treg cell function and stability may be regulated by AEP in a PD-1 dependent manner. This knowledge could potentially be used to inform medical practices. Specifically, PDL-1 stimulation combined with AEP inhibition could be integrated into Treg cell expansion regimes in clinical trials that aim to generate and use 'enhanced' Treg cells as cell therapy for the treatment of GvHD and autoimmune disorders. Similarly, based on the hypothesis that PD-1 signalling has a negative effect on AEP expression (therefore enhancing Treg cell stability), AEP could be used as a prognostic biomarker in tumour biopsies to predict whether the patient would benefit from PD-1/PDL-1 blockade treatment.

Lending support to the argument of AEP modulating T cell function, studies have demonstrated that in addition to APCs, AEP is also expressed in mouse and human T cells where it plays a role in CD4^{+} helper T cell function (Probst-Kepper *et al.*, 2009; Aschenbrenner *et al.*, 2018; Freeley *et al.*, 2018). However, apart from the proposed role of PD-1 signalling in downregulating AEP, little else is known about the signalling mechanisms that regulate AEP expression in Treg cells in either mice or humans.

Based on all the above, it is here hypothesised that AEP plays a role in the Treg cell signature and that additional co-stimulatory and/or co-inhibitory signalling mechanisms can regulate AEP expression in mouse and human Treg cells thus affecting Treg cell stability and function. Specifically,

signalling mechanisms involved in establishing the Treg cell lineage - such as TGF-β1 and IL-2-mediated signalling - are hypothesised to play a role in AEP protein expression.

Further exploration of the signalling mechanisms modulating AEP expression in human Treg cells would provide valuable insight into the manipulation of these cells for therapeutic purposes in an autoimmune setting whereby inhibition of AEP could elicit powerful immunosuppressive responses.

1.7 Aims

This study aims to:

- determine the function of AEP in natural and induced Treg cells in mice
- determine signals that modulate AEP expression in mice
- determine AEP expression in human T cells
- determine signals that modulate AEP expression in human T cells.

Chapter 2. Materials & Methods

2.1 Mice

Wild type (WT) and CD45.1^{+} congenic, female mice on a C57BL/6 background were purchased at 7 weeks of age from Charles River, UK and were bred and maintained at Newcastle University. The CD45.1^{+} mice were used for cell cultures presented in figures 3.6-9. Female and male *Lgmn*$^{-/-}$ mice on a C57BL/6 background were kindly provided by Professor Colin Watts from the University of Dundee. Female and male *Lgmn*$^{-/-}$ mice were used to provide cells for the Foxp3 degradation assays. Only female *Lgmn*$^{-/-}$ mice were used for phenotypic characterisation and *in vivo* experiments. All mice were housed in specific pathogen free (SPF) conditions in individually ventilated (IV) cages. Experiments were carried out on mice that were 8 to 10 weeks old. All animal experiments were carried out in accordance with Newcastle University animal health and safety guidelines. The use of animals for this research was approved by the Comparative Biology Centre and the Newcastle Ethical Review committee and performed under a UK Home Office approved Project Licence (PPL:7008838) held by Dr. Shoba Amarnath. Personal licence was held by Chaido Stathopoulou (PIL:I33145B3D). All experimental procedures carried out at Newcastle University incorporated the NC3R guidelines for animal research and the data are presented according to the ARRIVE guidelines.

2.2 Reagents

2.2.1 *Cell culture reagents*

Mouse and human cells were cultured in complete, sterile media supplemented with 10% fetal bovine serum (FBS) (Labtech, Sussex, UK) that had been previously inactivated by incubation in a water bath at 56^{o}C for 90 min. FBS is isolated from the circulating blood of bovine foetuses and provides growth factors for cells cultured *in vitro*. Heating FBS is done in order to inactivate complement components and growth inhibitors that may interfere with immunological assays and T cell cultures. For the mouse experiments, Dulbecco Modified Eagle Media-1640 (DMEM) (Lonza, Surrey, UK) was used whereas for the human studies Roswell Park Memorial Institute media (RPMI) (Sigma, MO, USA) was used. The difference between the two types of media is that DMEM contains a higher

concentration of nutrients while RPMI is more suitable for human T lymphocytes. For both mouse and human experiments, complete media were supplemented with 10% FBS, glutamine (Gibco, Loughborough, UK; 1mM), non-essential amino acids (Sigma, MO, USA; 0.1mM), 2-β-mercaptoethanol (Sigma, MO, USA; 50μM), sodium pyruvate (Sigma, MO, USA; 1mM), penicillin and streptomycin (Sigma, MO, USA; 50U/ml). 2-β-mercaptoethanol was added as an antioxidant to lower the levels of oxygen radicals produced by cell metabolic processes thus reducing oxidative stress. The antibiotics penicillin and streptomycin were included to prevent the growth of bacteria in the media.

For the cryopreservation of cells, freezing media made up of 90% sterile FBS (heat inactivated) and 10% dimethyl sulfoxide (DMSO) (Sigma, MO, USA) was used. DMSO was used to prevent formation of ice crystals during freezing that would otherwise kill the cells.

For cell sorting, a buffer (Miltenyi buffer recipe) made up of phosphate-buffered saline (PBS) (Sigma, MO, USA), 0.5% bovine serum albumin (BSA) (Cell Signaling, MA, USA) and 2 mM ethylenediaminetetraacetic acid (EDTA) (Sigma, MO, USA) was used. EDTA was used to prevent formation of cell aggregates that would interfere with the sorting process and the purity of the sorted populations.

Cell lysis buffer was made up of a protease inhibitor cocktail tablet (Roche, Basel, Switzerland) dissolved in 10 ml of radioimmunoprecipitation assay buffer (RIPA) (Sigma, MO, UK) with the addition of the phosphatase inhibitor cocktails 2 and 3 (Sigma, MO, UK, 0.01%) to preserve the phosphorylation status of proteins and protect them from degradation. The final pH of this buffer was 7.5.

Alternatively, a less harsh lysis buffer containing Triton X-100 was used. In contrast to RIPA buffer which contains a powerful denaturing ionic detergent – SDS, Triton X-100 is a non-ionic detergent and better at maintaining protein structure. Here, the cells were lysed with HEPES buffer suitable for maintaining pH levels (Sigma, MO, USA; 100 mM) supplemented with sodium chloride (Sigma, MO, USA; 300 mM) to preserve protein structure and prevent nonspecific protein interactions. The lysis buffer was also

supplemented with the phosphoseryl and phosphothreonyl phosphatase inhibitor sodium fluoride (Sigma, MO, USA; 40 mM), triton X-100 (Sigma, MO, USA; 1% v/v), the protease inhibitor phenylmethylsulfonyl fluoride (PMSF) (Sigma, MO, USA; 1 mM), EDTA (Sigma, MO, USA; 4 mM) and the phosphatase inhibitor cocktails 2 and 3 (Sigma, MO, UK, 0.01%). EDTA prevented protein interactions and inhibited protease function. The final pH of this buffer was 7.5.

2.2.2 *Flow cytometry reagents*

Fluorescence-activated cell sorting (FACS) buffer was used for cell staining and it was made up of 0.5% BSA (Cell Signaling, MA, USA), and 0.01% of sodium azide (Sigma, MO, USA) diluted in PBS. Sodium azide is an inhibitor of aerobic metabolism but here it was used as a chemical preservative for the fluorescent antibodies used for cell staining while BSA was added to minimise nonspecific binding of staining antibodies.

2.2.3 *Western blot reagents*

Cell lysates were stained with sample reducing agent containing dithiothreitol (Thermo Fisher Scientific, MA, UK; 1x) and LDS sample buffer (Thermo Fisher Scientific, MA, UK; 1x) to reduce and denature proteins in preparation for gel electrophoresis.

TBST buffer was used for washing western blot nitrocellulose membranes and preparing solutions of primary and secondary antibodies. It was made up in water and contained 20 mM Tris HCl and 150 mM NaCl with pH levels adjusted to 7.4-7.6. The buffer also contained the non-ionic detergent Tween 20 (Sigma, MO, USA; 0.1%) to reduce non-specific antibody binding.

Stripping buffer was used to remove any membrane-bound antibodies in preparation for membrane reprobing. Since this technique relied on low pH, the buffer was made up of water, glycine (Sigma, MO, USA; 0.1M), sodium chloride (Sigma, MO, USA; 0.1M) and hydrochloric acid (Sigma, MO, USA; 0.06N) and the pH adjusted to 2.5.

2.2.4 *AEP enzyme activity assay reagents*

Assay buffer was made up with the pH buffering agent MES (Sigma, MO, USA; 50mM) and NaCl (Sigma, MO, USA; 250mM) which was used to

preserve protein structure and keep proteins soluble. Components were diluted in purified water with the final pH adjusted to 5.

Activation buffer was used to activate AEP present in cell lysates. It was made up with purified water containing the pH buffering agent sodium acetate (Sigma, MO, USA; 50 mM) and NaCl (Sigma, MO, USA; 100 mM) at pH 4.0 (optimal for AEP activation).

A special lysis buffer was used to extract cell protein and maintain AEP protein structure. The buffer was made up with water containing sodium citrate (Sigma, MO, USA; 100 mM), EDTA (Sigma, MO, USA; 1 mM) and 1% of the non-ionic detergent n-octyl-beta-D-glycopyranoside (n-octyl) (Merck Millipore, MA, USA) that is capable of preserving enzymes in their native state during cell lysis. Buffer pH was adjusted to 5.8 which maintains AEP function but prevents further autocatalytic activation (Li *et al.*, 2003).

2.3 Cell Counting

Viable cells were counted using a dye exclusion procedure whereby only dead cells with disrupted cell membranes were able to take up the dye. The cells were stained with 0.4% sterile trypan blue (Sigma, MO, USA) at either 1:1 or 1:10 dilution and counted using a haemocytometer grid.

2.4 Cryopreservation of Mouse Cells

Mouse cells were washed once with sterile PBS and resuspended in FBS (heat-inactivated), supplemented with 10% DMSO. Cells were stored in -80^{o}C for 24hrs and then transferred to liquid nitrogen.

2.5 Cryopreservation of Human Peripheral Blood Mononuclear Cells (PBMCs)

Human PBMCs were centrifuged at 300xg for 10 min at room temperature in sterile PBS and resuspended in half of the desired volume of freezing media. The other half - containing 20% DMSO - was added slowly drop by drop to the tube while mixing gently. Cells were stored at 20-30 x 10^6 cells/ml in a cryovial. Samples were kept at -80^{o}C for 24hrs prior to transferring to liquid nitrogen.

Thawing of PBMCs was performed by dipping the cryovial in a 37^{o}C water bath for a maximum of two minutes. Then, 10 ml of pre-warmed RPMI was

added to the cells (1:10 dilution). The thawed cells were centrifuged at 300xg for 10 min at room temperature and the pellet resuspended in RPMI media and the cell number was determined.

2.6 Mouse Tissue Harvest

2.6.1 *Splenocyte isolation*

To phenotypically characterise mouse strains and obtain lymphocytes for the *in vitro* experiments, mice were culled using schedule 1 and the spleens were dissected out. Excess fat and surrounding tissue was removed and the tissue was stored in ice cold, sterile, complete DMEM. Under sterile conditions, the spleen was washed with 5 ml of sterile, cold DMEM and smashed using the back of a plunger from a 5ml syringe. The suspension was passed through a 70 μm filter to ensure a single cell suspension and the filter was washed with an additional 5 ml of cold DMEM media to ensure maximum yield of approximately 100 x 10^6 cells per spleen. The suspension was centrifuged at 600xg for 5 minutes at 4°C and the pellet was resuspended in 3 ml of red blood cell lysis buffer (RBC) (BioLegend, CA, USA). RBC lysis was performed over 2 min on ice. 10 ml of media was added to deactivate the RBC lysis buffer and the cells were centrifuged at 600xg for 5 minutes at 4°C and then washed with 10 ml of media. This washing step was performed twice. The cells were counted and the cell concentration was brought down to 10 x 10^6 cells per ml with complete media.

2.6.2 *Bone marrow isolation*

Mouse bone marrow (BM) cells were isolated from WT mice and used as positive controls for AEP expression on western blots. To obtain the cells, WT mice underwent schedule 1 sacrifice and both hind legs were removed at the hip and skinned. The legs were stored in ice cold PBS containing 1% HEPES buffer. To isolate the bone marrow, the legs were stripped of all muscle tissue and tibia snapped above the ankle and below the knee joint using a pair of forceps. The femurs were also snapped above the knee and just below the hip joint. Each bone was flushed through with PBS-HEPES buffer using a 20ml syringe until it run clear. After flushing the bones, the harvested bone marrow was resuspended with a syringe and filtered through a 70 μm filter into a 50ml falcon tube and then centrifuged at 600xg

for 5 minutes at 4°C. The pellet was resuspended in PBS-HEPES buffer and the cells were counted and the concentration brought to 1 x 10^6 cells/ml with complete DMEM media supplemented with recombinant mouse granulocyte-macrophage colony-stimulating factor (rm-GM-CSF) (Miltenyi Biotec, Bergisch Gladbach, Germany; 20 ng/ml) and rm-IL4 (R&D systems, MN, USA; 40 ng/ml). This was done to induce differentiation of monocytes into dendritic cells. The bone marrow-derived cells were cultured in a flask and incubated overnight at 37°C, CO_2 5%, humidity 95%. On day 2, 50% of the media contained in the flask was replaced with fresh media and the cells incubated for an additional 3 days. 24hrs before harvest, the cells were stimulated with *E.coli*-derived lipopolysaccharide (LPS) (Sigma, MO, USA; 1 μg/ml) to enhance AEP expression. To harvest the cells, the bottom of the flask was scraped using a cell scraper.

2.7 Mouse T Cell Isolation

Naïve T cells ($CD4^+CD25^-$) and natural Treg cells ($CD4^+CD25^+$) were isolated using the MACS Miltenyi Biotec $CD4^+CD25^+$ Regulatory T cell isolation kit (Miltenyi Biotec, Bergisch Gladbach, Germany) according to manufacturer's instructions. Splenocytes were suspended in Miltenyi buffer and labelled with a biotin-antibody (Ab) cocktail containing Abs against CD8a, CD11b, CD45R, CD49b, and Ter-119. Splenocytes were then labelled with monoclonal CD25-PE antibodies and anti-biotin antibodies conjugated to microbeads (Miltenyi Biotec, Bergisch Gladbach, Germany). Magnetic separation was then performed using an LD column (Miltenyi Biotec, Bergisch Gladbach, Germany) to collect all the unlabelled $CD4^+$ cells via negative selection. Lastly, the eluted $CD4^+$ cells were labelled with microbeads conjugated to monoclonal anti-PE Abs and run through an MS column (Miltenyi Biotec, Bergisch Gladbach, Germany). The collected $CD4^+CD25^-$ (naïve) T cells were then tested for purity by flow cytometry prior to phenotyping and cell culture. This method yielded purity of at least 80%.

For the collection of $CD4^+CD25^+$ (nTreg) T cells, cells that remained in the MACS MS column were flushed through using a plunger and 1 ml of Miltenyi buffer (positive collection).

2.8 Mouse T Cell Culture

Following isolation, naïve and nTreg cells were cultured at $1x10^6$ cells/ml in 24-well plates for 72hrs at 37ºC, CO_2 5%, humidity 95%. In order to identify signals that induce AEP expression *in vitro*, naïve and nTreg cells were cultured under iTreg inducing conditions with or without the presence of PDL-1 (see below for product details). At the end of the culture, cells were characterised for Foxp3 expression by flow cytometry and cell lysates were obtained for AEP protein analysis by western blotting.

In preparation for cell culture, plates were coated with anti-CD3 (BD Pharmingen, CA, USA; clone:145-2C11; 5µg/ml) and in certain experiments with recombinant mouse PDL-1 (R&D systems, MN, USA; 5µg/ml) for 3hrs at 37ºC. Following coating, the wells were washed three times with PBS to remove any floating Abs. Removal of these Abs minimised the risk of unwanted cross-reactivity between the Fc region of the floating anti-CD3 or PDL-1 Abs with the Fc receptors expressed on the T cell surface. Culture media was then supplemented with soluble anti-CD28 (BD Pharmingen, CA, USA; clone:37.51;2µg/ml) and rhIL-2 (Peprotech, London, UK, 80ng/ml) to induce T cell activation and expansion. Anti-IL4 (BioXCell, OX, UK; clone:11B11;10µg/ml) and anti-IFNγ (BioXCell, OX, UK; clone:11B11;10µg/ml) Abs as well as rhTGF-β1 (R&D systems, MN, USA; 2 or 5 ng/ml) were used in certain culture conditions for inducing iTreg cells.

2.9 Staining Mouse Splenocytes for Flow Cytometry

Single cell suspensions of splenocytes were characterised for surface and intracellular (IC flow) markers using flow cytometry both before and after culture. Splenocytes were stained for CD4, CD8, Nrp-1, Helios, CD62L, CD25, Foxp3, CD127, CD44, PD-1, PDL-1, IL-17A, IL-4, IFNγ and IL-10. Flow cytometry staining antibodies for CD4 (clone: RM4-5), CD8 (clone: 53-6.7), Nrp-1 (clone: 3E12), Helios (clone: 22F6), PD-1 (clone: RPM1-30), PDL-1 (clone: 10F.9G2), CD62L (clone: MEL-14), CD127 (clone: A7R34) and IL-4 (clone:11B11) were purchased from BioLegend, CA, USA. Fluorescent Abs for CD25 (clone; PC61) and CD44 (clone: IM7) were obtained from BD Biosciences, CA, USA whereas Abs for Foxp3 (clone: FJK-16s), IL-10 (clone:JES5-16E3), IFN-γ (clone: XMG1.2) and IL-17A (clone: eBio17B7) were purchased from Thermo Fisher Scientific, MA, UK.

Splenocytes were first centrifuged at 600xg for 5 minutes at 4°C and re-suspended in FACS buffer. Cell surface antibodies were diluted at 1:20 dilution in FACS buffer and then 5 μl of the diluted antibody was added to 100 μl of sample. Final concentration for all antibodies in the sample was 2.5 μg/ml. Neat anti-CD16/CD32 (FC block) (Thermo Fisher Scientific, MA, UK; clone 93Fc; 2.5 μg/ml) was added to prevent any non-specific binding of staining antibodies to cell Fc receptors thus reducing background staining. The samples were then incubated at 4°C for 30 minutes in the dark. Splenocytes were washed twice by centrifugation at 600xg for 5 minutes at 4°C in FACS buffer and then the pellet was re-suspended in 200 μl of fixing buffer (BD Biosciences, CA, USA) and incubated in the dark at 4°C for 20 minutes. 2 ml of permeabilisation (perm) buffer (BD Biosciences, CA, USA) was then added to allow staining for intracellular markers. Splenocytes were centrifuged twice at 600xg for 5 minutes at 4°C in perm buffer and intracellular antibodies were added at a final concentration of 2.5 μg/ml. Whenever Foxp3 was included in the panel, the Foxp3 Transcription Factor Staining Buffer Kit (Thermo Fisher Scientific, MA, UK) was used according to the manufacturer's instructions. The fixed splenocytes were incubated overnight at 4°C in the dark and then centrifuged twice at 600xg for 5 minutes at 4°C in perm buffer and then centrifuged again at 600xg for 5 minutes at 4°C and the pellet resuspended in 500 μl FACS buffer in preparation for flow cytometry.

For cytokine profiling, mouse splenocytes were stimulated with phorbol 12-myristate 13-acetate (PMA) (Sigma, MO, USA; 10μg/ml) and ionomycin (Sigma, MO, USA; 1μg/ml) for two hours at 37°C. To inhibit protein transport from the Golgi apparatus to the cell membrane and prevent any loss of cytokine content, splenocytes were treated with brefeldin (BioLegend, CA, USA; 5 μg/ml) and monensin A (BioLegend, CA, USA; 2μM) for another two hours at 37°C. Splenocytes were then characterised for CD4, IFN-γ, IL-10, IL-17A and IL-4 expression by flow cytometry.

Phenotypic characterisation and cytokine profiling of WT and *Lgmn*$^{-/-}$ mice that is presented in figure 3.1 was performed by Dr. Shoba Amarnath as described above.

2.10 Preparation of Compensation Beads and Cells

Cells were preferably used whenever possible for the purpose of setting up compensation voltages as they constituted a more accurate representation of the samples of interest in terms of size, granularity and expression levels of markers. Cellular single stains were treated the same way as cell samples except they were stained with a single fluorescent Ab in addition to an Fc block. An unstained cell sample treated with an Fc block only was also included in order to allow separation of the negative from the positive cell population during the compensation process.

Beads were sometimes used for compensation purposes (Thermo Fisher Scientific, MA, UK) as single colour controls to correct for any overlap in emission wavelengths of the fluorochromes used. The beads were stained with the same antibodies used to stain the cell samples. Approximately half an hour before running the samples through the flow cytometer, one drop (10 μl) of beads was added to 100 μl of FACS buffer followed by 0.5 μl of fluorescent antibody stock (final concentration 5 μg/ml). The beads were then incubated for 20 min at 4^{o}C in the dark, topped up with 400 μl with FACS buffer and then run through the cytometer and the voltages were set up. Unstained beads were not needed as the purchased product originally contained both stainable (beads that react with the light chain of antibodies of mouse, rat and rabbit origin) and unstainable beads (internal negative control).

2.11 Flow Cytometry Data Acquisition

Data were acquired using either a FACS CANTO II or Fortessa X20 machine. Cells were characterised based on their size, granularity and the fluorescent markers they express. Cell size was determined by forward scatter (FSC) and cell granularity by side scatter (SSC). FSC and SSC are determined by the light diffraction index detected by a light detector. The FSC detector is positioned opposite the FSC laser whereas the SSC detector is positioned at a 90^{o} angle from SSC laser. The voltages for FSC and SSC remained constant throughout the experiment in order to maintain gating consistency.

In order to compensate for spectral overlap of fluorochromes with similar emission wavelengths and minimise fluorescent bleeding into adjacent detectors, either beads or cells stained with a single colour were run first through the machine. Then, cell samples containing all the fluorochrome-conjugated antibodies except for one (fluorescence minus one or FMO) were used to determine and eliminate any background staining. The FSC and SSC voltages were re-adjusted for cells whenever beads were used for compensation. The cell samples were run after the adjustment of voltages which were kept constant throughout any individual experiments. Equal number of events (number of cells detected by the cytometer) were recorded for the single cell or $CD4^+$ gate.

2.12 Flow Cytometry Data Analysis

Exclusion of cell debris and impurities from the analysis was achieved by gating live lymphocytes based on FSC and SSC. Doublets were also gated out prior to the identification and gating of lymphocytes based on CD4 expression. Data were analysed using FCS Express version 6 (De Novo Software, USA).

2.13 Foxp3 Degradation Assay

In order to determine differences in Foxp3 turnover between WT and *Lgmn*$^{-/-}$ iTreg cells, a Foxp3 degradation assay was performed.

To optimise the assay, $CD4^+CD25^-$ T cells from WT splenocytes were isolated using the Miltenyi kit. Cells were cultured *in vitro* at 1 x 10^6 cells/ml for 3 days (72 hrs) in complete DMEM media as described in section 2.8. On day 3, cell culture media was supplemented with fresh rhIL-2 (80 ng/ml) and cells incubated for 24 more hours at 37^{o}C, CO_2 5%, humidity 95%. On day 4, cells were treated with either the protein synthesis inhibitor cycloheximide (CHX) (Sigma, MO, USA; 100 μg/ml) or 0.1% vehicle control (DMSO) for 30 min, 2hrs, 4hrs, 6hrs and 24hrs and harvested using RIPA lysis buffer at different time points in preparation for protein analysis via western blotting.

Following optimisation, $CD4^+CD25^-$ T cells from WT and *Lgmn*$^{-/-}$ mice were cultured under iTreg conditions in 24-well plates as described in section 2.8. After 72hrs of culture, the cells were counted and stimulated with rhIL-2

(Peprotech, London, UK; 80ng/ml) for 24hrs to rest. On day 4, the cells were stimulated with 100μg/ml CHX for 30 min, 2hrs, 6hrs and 24hrs. Cell lysates were obtained and Foxp3 expression levels were analysed by western blotting.

2.14 B16F10 melanoma mouse model

B16F10 melanoma cells were kindly provided by Dr. Pawel Muranski and Prof. Nick Restifo from NCI, NIH and processed by Dr. Shoba Amarnath in preparation for the *in vivo* experiment. Specifically, melanoma cells were thawed from liquid nitrogen and added to a flask containing 50 ml of complete DMEM media. Cells were cultured overnight at 37^{o}C, CO_2 5%, humidity 95%. Media was then aspirated and replaced with 50 ml of fresh media in order to remove any toxic DMSO contained in the freezing media. Cells were expanded *in vitro* until the desired number of cells for the *in vivo* study was reached. Expanding melanoma cells were split at 1:3 or 1:5 ratio to maintain 70% confluence. To harvest the cells, culture media was aspirated, and cells washed with 30 ml of pre-warmed sterile PBS. This was done to completely remove any residual media that could deactivate trypsin. Following the PBS wash, 20 ml of 1x trypsin (Lonza, Surrey, UK) was added and cells were incubated at 37^{o}C, CO_2 5%, humidity 95% for 5-7 minutes. 20 ml DMEM media was then added to terminate trypsinisation and prevent cell cytotoxicity. Cells in suspension were transferred to a Falcon tube and centrifuged at 600xg for 5 minutes at 4^{o}C and re-suspended in 10 ml of media. Cells were centrifuged again at 600xg for 5 minutes at 4^{o}C and the pellet resuspended in sterile PBS at a concentration of 300,000 cells per ml (60,000 per 200μl).

For the *in vivo* experiment, WT and *Lgmn*$^{-/-}$ mice were subcutaneously injected with 0.3 x 10^6 mouse B16F10 melanoma cells. Tumours were left to grow for 11 days and mouse weight and tumour size was monitored throughout the experiment. Mouse weight was measured everyday while tumour size was measured every day from day 5. Mouse cohorts received intraperitoneal injections of either rat IgG2b isotype (BioXCell, OX, UK; clone:LTF-2; 1.25μg/μl) or PDL-1-blocking antibody (BioXCell, OX, UK; clone:10F.9G2; 1.25μg/μl) (250 μg in 200 μl of sterile PBS per mouse) on days 5, 7 and 9 by Dr. Shoba Amarnath. Mice were euthanised and tumours

were harvested on day 11 and digested into single cell suspensions. The frequencies of Treg cells within the tumours were then determined by flow cytometry by Dr. Shoba Amarnath.

To obtain single cell suspensions, whole tumours were harvested into complete DMEM media and stored on ice. Tumours were rinsed with PBS and incubated at 37^{o}C for 30 min in FBS-free DMEM media containing DNAse (Sigma, MO, USA; DNAse 0.5mg/ml) and Liberase (Sigma, MO, USA; 0.25 mg/ml). The digested tissue was then filtered through a 100 μm filter into 5 ml of FBS and the suspension was topped up to 25 ml with DMEM media. Cells were centrifuged at 600xg for 5 min at 4^{o}C and the pellet was resuspended in 10 ml DMEM media. Cell suspension was then layered on top of 5 ml lymphocyte separation media (PromoCell, Heidelberg, Germany) and centrifuged at 400xg for 20 min at RT with the brakes off. Separated lymphocytes were transferred into a fresh tube and washed twice with 10 ml of DMEM media at 600rpm for 5 min at 4^{o}C. Lymphocytes were then resuspended in 2 ml DMEM media and stained for flow cytometry as outlined in section 2.9.

2.15 Human Donors

PBMCs or whole blood from healthy donors aged 18 and above from both males and females was kindly provided by Professor John Simpson's group from Newcastle University as part of "The role of inflammation in human immunity" study after informed consent was taken. Samples were stored according to Human Tissue Act (HTA) guidelines.

2.16 Lymphocyte Separation

Human blood was diluted with sterile PBS at 1:1 ratio and layered on lymphocyte separation media (PromoCell, Heidelberg, Germany) at 2:1 ratio. Then, it was centrifuged at 600xg for 30 min at room temperature without any deceleration. The PBMCs were transferred into a new tube and centrifuged at 600xg for 10 min at room temperature. The pellet was then washed twice with 20 ml of sterile PBS; once at 600xg for 10 min and once at 300xg for 10 min. The PBMCs were counted and diluted to the appropriate concentration in preparation for the next experimental procedure.

2.17 Human Miltenyi T cell Isolation

Human naïve T cells ($CD4^+CD25^-$) and $CD4^+CD25^+$ T cells were obtained using the MACS Miltenyi Biotec $CD4^+CD25^+$ Regulatory T cell isolation kit (Miltenyi Biotec, Bergisch Gladbach, Germany) according to the manufacturer's instructions. Lymphocytes were suspended in Miltenyi buffer and labelled with a biotin-antibody cocktail containing Abs against CD8, CD14, CD15, CD16, CD19, CD36, CD56, CD123, TCRγ/δ, and CD235a. Lymphocytes were then labelled with microbeads conjugated to anti-biotin antibodies. Magnetic separation was then performed using an LD column to collect all the unlabelled $CD4^+$ cells via negative selection. The collected $CD4^+$ T cells were directly labelled with microbeads conjugated to anti-CD25 antibodies and run through an MS column. This allowed the collection of $CD4^+CD25^-$ T cells which were then tested for purity by flow cytometry prior to phenotyping and cell culture. This method yielded purity of at least 80%.

For the collection of $CD4^+CD25^+$ T cells, cells that remained in the MACS MS column were flushed through using a plunger and 1 ml of Miltenyi buffer (positive collection). Purity tests were not performed due to poor cell yield.

2.18 Human T cell Sorting

To increase purity of the isolated populations prior to cell culture, human T cells were sorted using the FACS Fusion sorter (BD Biosciences, NJ, USA). Following the isolation of lymphocytes from blood, PBMCs were centrifuged for 10 min at 300xg and the pellet resuspended in 1 ml Miltenyi buffer. 5 μl of anti-human Trustain Fc block (BioLegend, CA, USA: 5 μg/ml) were added to limit background staining and the sample incubated for 10 min at room temperature. Then, lymphocytes were stained with 5 μl of neat antibody for CD4 (BioLegend, CA, USA; clone A161A1: 5 μg/ml), CD25 (BioLegend, CA, USA; clone BC96: 2.5 μg/ml), CD127 (BioLegend, CA, USA; clone A019D5: 7.5 μg/ml) and CD45RA (BioLegend, CA, USA; clone HI100: 0.6 μg/ml) for 15 min at 4°C in the dark. Following staining, the cells were counted and washed once with 10 ml Miltenyi buffer. Cells were brought to a concentration of 10 x 10^6 cells/ml in Miltenyi buffer and filtered through a moistened 40 μm filter into a sterile FACS tube to obtain a single-cell

suspension. DAPI was added last (Invitrogen, CA, USA; 5 μg/ml) to stain dead cells. Naïve T cells were characterised as $CD4^+CD25^-CD127^{high}CD45RA^+$ cells. Human Treg cells were sorted based on CD4 positivity, low levels of CD127 and high levels of CD25 expression. The collected naïve T cells were tested for purity by flow cytometry immediately after cell sorting. This method yielded purity of 95% and above. The collected $CD4^+CD25^{high}CD127^-$ T cells were not tested for purity due to limited cell numbers acquired per donor.

2.19 Human T cell Culture

Following isolation either using the Miltenyi kit or the cell sorter, naïve and Treg cells were cultured at $1x10^6$ cells/ml in 96-well plates for 5 days at 37°C, CO_2 5%, humidity 95%. In order to identify signals that induce AEP expression *in vitro*, naïve and Treg cells were cultured under iTreg inducing conditions (αCD3, αCD28, rhIL-2, rhTGF-β1). The cells were then expanded for an additional 7 days at 37°C, CO_2 5%, humidity 95% with rhIL-2 added every two days (on day 5, 7, 9 and 11). On day 12 the cells were characterised for FOXP3 expression by flow cytometry and cell lysates were obtained for AEP protein analysis by western blotting (figure 2.1).

Cell culture was performed as following: 96-well, round-bottom plates were coated with anti-CD3 (BioLegend, CA, USA; clone:OKT3;5μg/m) for 3hrs at 37°C and the wells were washed three times with PBS to remove any floating Abs. Removal of these Abs minimised the risk of unwanted cross-reactivity between the Fc region of the floating anti-CD3 Abs with the Fc receptors expressed on the T cell surface. Culture media was then supplemented with soluble anti-CD28 (BioLegend, CA, USA; clone:CD28.2;2μg/ml) and rhIL-2 (Peprotech, London, UK; 100ng/ml) to induce T cell activation and expansion. Anti-IL4 (BioLegend, CA, USA; clone:MP4-25D2;10μg/ml) and anti-IFNγ (BioLegend, CA, USA; clone:B27;10μg/ml) Abs as well as rhTGF-β1 (R&D systems; MN, USA; 5ng/ml) were used in certain culture conditions for inducing iTreg cells (figure 2.1).

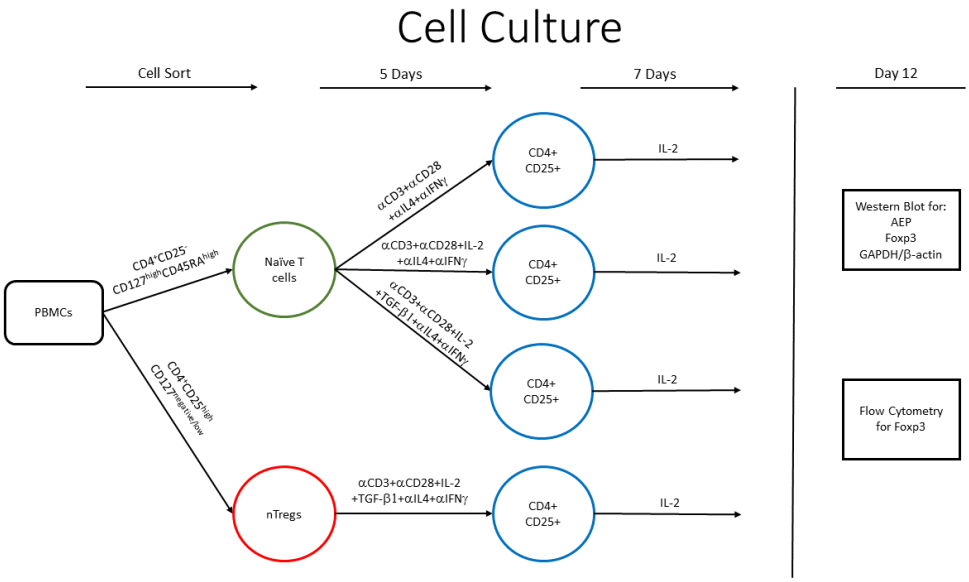

Figure 2.1 Schematic diagram of human T cell culture. T cell culture conditions of sorted human naïve and nTreg cells.

2.20 Characterisation of Human PBMCs Using Flow Cytometry

In order to phenotypically characterise human lymphocytes, PBMCs were stained for CD4 (BioLegend, CA, USA; clone A161A1: 0.5 μg/ml), CD25 (BioLegend, CA, USA; clone BC96: 1 μg/ml), CD127 (BioLegend, CA, USA; clone A019D5: 0.75 μg/ml), Nrp-1 (BioLegend, CA, USA; clone 12C2: 0.15 μg/ml), Helios (BioLegend, CA, USA; clone 22F6: 0.15 μg/ml), FOXP3 (BioLegend, CA, USA; clone 259D: 3.6 μg/ml), PD-1 (BioLegend, CA, USA; clone EH12.2H7: 1 μg/ml) and anti-human Trustain Fc block (BioLegend, CA, USA: 3 μg/ml). The Foxp3 Transcription Factor Staining Buffer Kit was used for FOXP3 staining. The same staining methodology was used as described in 2.9. Data were acquired and analysed as described in 2.11-12.

2.21 Protein Extraction

To obtain cell lysates for AEP protein analysis, cells were lysed using sonication (SANYO, MSE UK LTD) following chemically-induced cell lysis (either RIPA- or Triton X-100-containing lysis buffer). The cells were centrifuged at 300xg for 10 minutes in 1 ml of PBS and the pellet resuspended in the desired volume of lysis buffer prior to sonication for 10 sec at power setting 8 and frequency 23 kHz. The cell lysates were then

centrifuged at maximum speed of 14,800xg for 5 minutes at 4°C and the supernatant transferred to a fresh tube prior to storage at -80°C.

Alternatively, cells were lysed with lysis buffer containing HEPES. Sonication was not used when cells were lysed with this buffer. Cells were centrifuged at 300xg for 10 minutes in 1 ml of PBS and the pellet resuspended in the desired volume of HEPES lysis buffer (PMSF was added to the lysis buffer fresh each time, 30 minutes before lysis in order to ensure its stability in the aqueous solution). The samples were then vortexed for 15 seconds and incubated on ice for 10 minutes. After that, the cells were centrifuged at the maximum speed of 14,800xg for 5 minutes at 4°C and the supernatants were stored at -80°C.

Cells lysates were occasionally obtained by snap freezing the cells in dry ice. The cells were centrifuged at 300xg for 10 minutes in 1 ml of PBS and the pellet resuspended in 20 μl of lysis buffer. Samples were incubated on dry ice for 5 min and then stored at -80°C.

2.22 Protein Quantification

Protein was measured using the Pierce™ bicinchoninic acid assay (BCA assay) kit (Thermo Fisher Scientific, MA, UK) and the Bradford assay according to the manufacturer's instructions. Absorbance was measured at 562 nm using the VersaMax™ Microplate Reader and the SoftMax® Pro Software (Molecular Devices LLC).

2.23 Concentrating Protein from Small Pellets

Lysates with low protein concentrations (no AEP bands) were acetone precipitated. Undiluted cold acetone (Sigma, MO, UK) was added to the protein solution in 4:1 ratio and the sample incubated at -20°C for 1 hr. Samples were then centrifuged at 14,000xg for 10min at 4°C and the pellet was allowed to air dry. The acetone-free pellet was resuspended in reducing buffer overnight in a thermoshaker at 4°C. The reducing buffer consisted of 20% 10x reducing agent, 50% 4x LDS, 10% β-mercaptoethanol (Sigma, MO, UK) and 20% lysis buffer solution (either RIPA or HEPES depending on what was used for the initial cell lysis).

2.24 Western Blotting

In order to detect and quantify protein expression within samples, the semi-quantitative technique of western blotting was used. All lysates were brought to equal concentrations following protein quantification with the BCA assay. Then, the lysates were stained with reducing agent and LDS and boiled for 5 min at 95^{o}C. Samples were cooled on ice prior to gel loading. Human DCs (kindly provided by Dr. Amy Anderson and Dr. Fiona Cooke from ICM, Newcastle University) and mouse bone marrow-derived DCs and as well as human CD4^{-} APC-enriched lymphocytes were used as positive controls. Lysates were run under reducing conditions on precast 4-12% Bis-Tris, 10-20% SDS-PAGE gradient gels (Thermo Fisher Scientific, MA, UK) at 130V for 70 minutes in 500 ml SDS running buffer (Thermo Fisher Scientific, MA, UK) supplemented with 0.5 ml antioxidant to maintain reducing conditions (Thermo Fisher Scientific, MA, UK) and transferred onto 0.45μm nitrocellulose membrane (Thermo Fisher Scientific, MA, UK) at 110V for 90 minutes in transfer buffer (Thermo Fisher Scientific, MA, UK). Membranes were blocked with 5% fat-free semi-skimmed milk in TBST buffer and incubated overnight at 4^{o}C with primary antibodies to human AEP (R&D systems, MN, USA, polyclonal; 0.1 μg/ml), FOXP3 (Cell Signaling, MA, USA; clone D608C, D25D4), GAPDH (Cell Signaling, MA, USA), β-tubulin (Cell Signaling, MA, USA; clone 9F3) and β-actin (Cell Signaling, MA, USA) in TBST containing either 5% milk or BSA (Cell Signaling, MA, USA). β-tubulin, β-actin and GAPDH were used as internal controls.

For the mouse studies, primary antibodies to mouse AEP (R&D systems, MN, USA; clone 301417, monoclonal), Foxp3 (Cell Signaling, MA, USA; clone D608R), β-tubulin and GAPDH were used as appropriate.

The recommended antibody concentrations were used (except for the antibody for human AEP). Immunoreactivity was detected by sequential incubation with HRP-conjugated secondary Ab and enzymatic chemiluminescence (ECL) (Millipore Immobilon Western Chemiluminescant HRP Substrate, MA, USA). All secondary antibodies were obtained from R&D systems, MN, USA.

Images were obtained using either the LICOR Odyssey Fc Imager (LI-COR Biosciences) or an X-ray film developer (Photon Imaging Systems, NY, USA). Images were analysed using ImageJ (BSD-2, public domain). For the human studies, the 56 (inactive) and 37 kDa (active) AEP band sizes were analysed.

Where membranes were stained for more than one protein, the membranes were stripped of any bound Abs and then re-probed with another primary Ab. In order to do that, the membranes were washed twice with 20 ml TBST for 15 minutes and then they were incubated at room temperature for 10-20 minutes in stripping buffer. Following stripping, the membranes were washed twice with 20 ml water for 15 minutes and then once with 20 ml TBST for 15 minutes. Finally, the membranes were blocked in 5% milk for 1 hr at 4^{o}C in preparation for staining with the primary Ab.

2.25 Optimisation of Human AEP Detection

In order to optimise the band signal intensity of human AEP detected during X-ray film development, a series of primary and secondary Ab dilutions were tested along with different exposure times to ECL reagents. 16 μg of sorted human APC-enriched lymphocyte lysates were used for this purpose. The optimum conditions were determined at 2 minutes of exposure to ECL reagents when 0.1 μg/ml primary Ab and a 1:1000 dilution of the secondary Ab were used.

2.26 AEP Enzyme Activity Assay

2.26.1 *Standard curve optimisation*

In order to determine AEP activity in human T cell lysates, an enzyme activity assay was performed (figure 2.2). A series of 7-Amino-4-methylcoumarin-Chromophore (AMC) (Sigma, MO, USA) standards were prepared and tested using a fluorimeter (POLARstar Omega, BMG LABTECH, UK). The concentrations ranged from 50 mM to 0.012 μM in a total of 100 μl assay buffer per well. AMC was excited at 355 nm and the emitted signal was detected at 460 nm (top read). The standards were read in 4 replicates in a black, Corning, 96-well, flat-bottom plate (Scientific Laboratory Supplies, Nottingham, UK) at 37^{o}C. The entire plate was read in

kinetic mode 6 times (6 cycles, 1 min/cycle) and each individual well was read 20 times/cycle (0.4 sec/well).

In order to amplify the signal emitted from the lower AMC concentrations and make sure that the signal intensities emitted from these standards stay within the detection range limits of the machine, the gain value was adjusted for each plate at the beginning of each experiment. This was done by selecting the standard with the highest AMC concentration and setting it to 75% of total signal detected by the plate reader. This also minimised the risk of the detection filter getting saturated which would otherwise lead to inaccurate measurements of higher intensity signals.

Blank controls containing only assay buffer were included in the plate to determine background noise levels. Readouts for every single standard were averaged and normalised to blank. The log2 values of the normalised fluorescent intensity (FI) values were plotted against the log2 values of the standard concentrations (μM) to produce a standard curve. The linearity of the regression model was tested using the R^2 value which was > 0.97.

2.26.2 *Sample optimisation and substrate specificity*

Positive controls were tested for optimisation purposes. Fresh lysates of human DCs that were kindly provided by Dr. Fiona Cooke from ICM, Newcastle University were lysed with a lysis buffer optimal for maintaining AEP activity (n-octyl lysis buffer) and tested. Specifically, 0.5 x 10^6 DCs were washed with 1 ml PBS at 300xg at 4°C for 10 min and lysed by adding 100 μl lysis buffer and incubating the samples for 10 min on ice. The lysate was centrifuged at maximum speed of 14,800xg at 4°C for 5 min and the protein concentration determined using a BCA assay. The sample was then diluted to 1:1 ratio with activation buffer and incubated for 2 hours at 37°C. 10 μg of lysate was loaded in each well followed by the addition of the AEP-specific substrate Z-Ala-Ala-Asn-AMC (Bachem, Bubendorf, Switzerland) at a final concentration of 100 μM in a total of 100 μl reaction. The plate was read straight after addition of substrate and at 10 min intervals up to 120 min of total incubation time. Plate readings were also taken the following day at 24 hrs after addition of substrate to determine the optimum incubation

time with the substrate. Controls containing only substrate were included for normalisation purposes.

Optimum conditions for 10 μg of DC lysate were determined at 90 min after addition of substrate at 100 μM final concentration in a total of 100 μl reaction mixture per well.

To assess the specificity of the substrate, human dendritic cells were lysed using n-octyl lysis buffer and 10 μg of protein lysate was diluted with activation buffer at 1:1 ratio and incubated for 2 hrs at 37°C to activate AEP with the addition of 5 μM pepstatin A (Sigma, MO, USA). The reaction mixture was topped up to 100 μl with assay buffer and AEP-specific substrate to a final concentration of 100 μM. A blank control containing 100 μM substrate in assay buffer was included. Readouts were taken at regular intervals and activity levels were normalised to the blank control.

Following the optimisation of the positive controls, samples were screened for AEP activity using the same method whereby following the addition of the substrate at 100 μM final concentration, the plate was incubated for at least 90 min at 37°C in the dark prior to reading. AEP activity is presented as μmoles of substrate released per min of substrate incubation time per mg of lysate protein contained in the well.

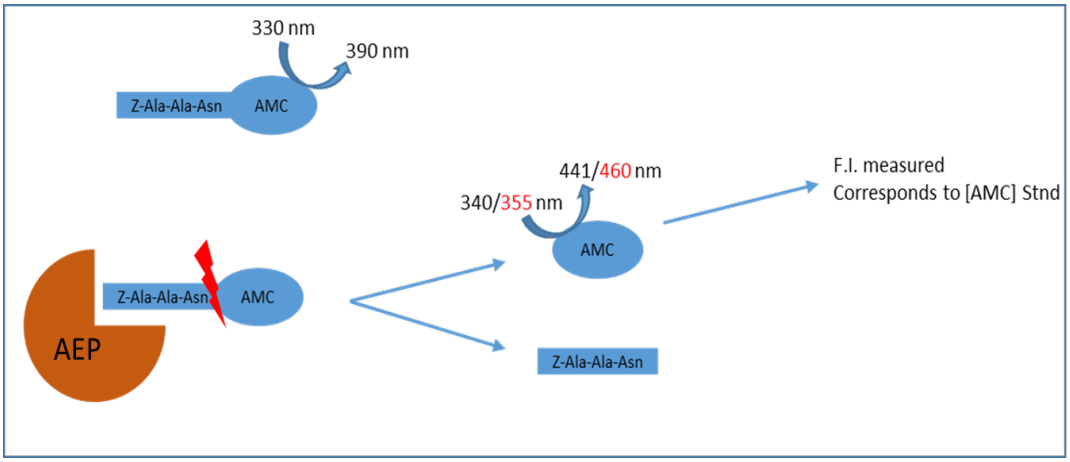

Figure 2.2 AEP enzyme activity assay. Schematic diagram outlining the principle of the AEP enzyme activity assay.

2.26.3 *PHA lymphocyte expansion*

PBMCs were cultured in 48- or 24-well plates at 1 x 10^6 cells per ml in complete RPMI media. The cells were stimulated with 2 μg/ml of

phytohemagglutinin-M (PHA) (Sigma, MO, USA) and expanded for 5 days at 37°C, CO_2 5%, humidity 95%. 1 x 10^6 cells were taken on day 0 and day 5 and stained with CD3 APC (BioLegend, CA, USA; clone OKT3: 0.8 μg/ml), CD4 Percpcy5.5 (5 μg/ml), CD8 PE (BioLegend, CA, USA; clone HIT8a: 0.6 μg/ml) and Fc block (5 μg/ml) as described in 2.20. Cells from day 0 and day 5 were harvested using n-octyl lysis buffer in preparation for the enzyme activity assay.

In addition to PHA, in certain experiments, PBMCs were also treated with: 10, 1 or 0.5 μM of TGFBR-I inhibitor (TOCRIS, OX, UK; SB431542) or 100 μM of STAT3 inhibitor (Sigma, MO, USA; S3I-201) or soluble PD-1 blocking Ab (BioLegend, CA, USA; clone EH12.2H7, 10 μg/ml) that was added to the culture on day 0. DMSO- or IgG2a (BioXCell, OX, UK; clone: C1.18.4; 10μg/ml) isotype-treated PBMCs were used as controls as appropriate. Cells were harvested on day 5 and AEP activity measured.

2.27 Public Data Mining

Microarray datasets publicly available in the Gene Expression Omnibus (GEO) repository at the National Centre for Biotechnology Information were analysed using the provided online GEO2R tool. Individual samples/cell populations were manually assigned into groups and AEP mRNA levels were compared between these groups. Normalisation of data was not necessary as only normalised data are uploaded in the database. Also, the GEO2R tool automatically performs log2 transformations where appropriate. The Benjamin & Hochberg false discovery rate method was applied (default) to limit false positives rates. Output AEP mRNA expression levels are presented in bar graphs (figure 4.3, figure 5.8, figure 5.4). In figure 5.4, AEP mRNA levels are expressed as log2 fold change values (Log2Fc) as the initial data available for analysis were provided as normalised Log2 values only. Specifically, the Log2Fc values for the 'IL-6 stimulation + TGFBR-I inhibitor' condition were normalised to the equivalent 'IL-6 stimulation only' condition (figure 5.4).

2.28 Statistical Analysis

Statistical analysis was determined using GraphPad Prism (GraphPad Software, Inc). The Shapiro-Wilk normality test was used to confirm normal

distribution of data. For normal distributions where two groups were compared, a two-tailed Student's t test was performed. For non-normal distributions, the nonparametric Wilcoxon (paired) or Mann-Whitney (unpaired) test was used. For comparison of three or more groups (normal distribution), a One Way ANOVA was performed followed by appropriate multiple comparison tests. For non-normal distributions, the nonparametric Kruskal-Wallis test was used. Unless stated otherwise, histogram columns represent the mean values for each experiment and error bars indicate the standard error of the mean (±SEM). P values less than 0.05 were defined as statistically significant (*p≤0.05, **p≤0.01, ***p≤0.001 and ****p≤0.0001).

2.29 Reagents Table

REAGENT or RESOURCE	SOURCE	IDENTIFIER
Antibodies		
PE/Cy5 anti-mouse CD4 (RM4-5)	Biolegend	Cat# 100409
PE/Cy7 anti-mouse CD279 (PD-1)(RPM1-30)	Biolegend	Cat# 109109
Brilliant Violet 711™ anti-mouse CD274 (B7-H1, PD-L1)(10F.9G2)	Biolegend	Cat# 124319
FITC anti-mouse CD62L (MEL-14)	Biolegend	Cat# 104405
Brilliant Violet 510™ anti-mouse CD127 (IL-7Rα)(A7R34)	Biolegend	Cat# 135033
PE Anti-Mouse CD44 (IM7)	BD Biosciences	Cat# 553134
APC Anti-Mouse Foxp3 (FJK-16s)	Thermo Fisher Scientific	Cat# 17-5773-82
PE Anti-Mouse Foxp3 (FJK-16s)	Thermo Fisher Scientific	Cat# 12-5773-82
Anti-Mouse IL-4 (11B11)	Biolegend	Cat# 16-7041-81
APC Anti-Mouse IL-10 (JES5-16E3)	Thermo Fisher Scientific	Cat# 17-7101-81
APC Anti Mouse IL-17A (eBio17B7)	Thermo Fisher Scientific	Cat# 17-7177-81
PE/Cy7 Anti-Mouse IFNγ (XMG1.2)	Thermo Fisher Scientific	Cat# 25-7311-82
PE Anti-Mouse CD25 (PC61)	Biolegend	Cat# 102007
Brilliant Violet 711™ anti-mouse CD8a Antibody	Biolegend	Cat# 100759
PerCP/Cy5.5 anti-mouse CD304 (Neuropilin-1) Antibody	Biolegend	Cat# 145207

CD16/CD32 Monoclonal Antibody (93)	Thermo Fisher Scientific	Cat# 14-0161-82
FITC anti-human CD4 (A161A1)	Biolegend	Cat# 357405
PerCP/Cy5.5 anti-human CD4 (A161A1)	Biolegend	Cat# 357414
APC anti-human CD3 (OKT3)	Biolegend	Cat#317317
APC anti-human CD25 (BC96)	Biolegend	Cat# 302609
FITC anti-human CD25 (BC96)	Biolegend	Cat# 302603
Brilliant Violet 421™ anti-human CD25 (BC96)	Biolegend	Cat# 302629
PE/Cy7 anti-human CD127 (IL-7Rα)(A019D5)	Biolegend	Cat# 351319
PE anti-human CD45RA (HI100)	Biolegend	Cat# 304108
PE anti-human CD8a (HIT8a)	Biolegend	Cat#300907
FITC anti-human CD304 (Neuropilin-1)(12C2)	Biolegend	Cat# 354511
PE anti-mouse/human Helios (22F6)	Biolegend	Cat# 137206
APC/Cy7 anti-human CD279 (PD-1)(EH12.2H7)	Biolegend	Cat# 329922
Human TruStain FcX™	Biolegend	Cat# 422302
Alexa Fluor 647 anti-human FoxP3 (259D)	Biolegend	Cat# 320213
Alexa Fluor 488 anti-mouse/human T-bet (4B10)	Biolegend	Cat# 644830
APC anti-human IFN-γ Pricing & Availability Clone (4S.B3)	Biolegend	Cat# 502511
Mouse Anti-CD3 (145.2C11)	BD Pharmingen	Cat# 5533057
Mouse Anti-CD3 (145.2C11)	BioXCell	Cat# BP0001-1
Mouse Anti-CD28 (37.51)	BD Pharmingen	Cat# 553294
Mouse Anti-CD28 (37.51)	BioXCell	Cat# BE0015-1
Mouse Anti-IL4 (11B11)	BioXCell	Cat# BE0045
Mouse Anti-IFNγ (11B11)	BioXCell	Cat# BE0055
Human Anti-CD3 (OKT3)	Biolegend	Cat# 317304
Human Anti-CD28 (CD28.2)	Biolegend	Cat# 302914
Human Anti-IFNγ (B27)	Biolegend	Cat# 506513
Human Anti-IL4 (MP4-25D2)	Biolegend	Cat#500815
Human Anti-PD-1 (EH12.2H7)	Biolegend	Cat#329912
Mouse IgG2a, k (C1.18.4)	BioXCell	Cat#BE0085

Anti-mouse PDL-1 (10F.9G2) (*in vivo*)	BioXCell	Cat#BP0101
Rat IgG2b (LTF-2) (*in vivo*, isotype)	BioXCell	Cat#BP0090
Anti-goat IgG HRP	Vector Laboratories	Cat# PI-9500
Anti-goat IgG HRP	R&D Systems	Cat# HAF109
Anti-human Legumain	R&D Systems	Cat# AF2199
Anti-human FOXP3 (D608C)	Cell Signal	Cat# 12632S
Anti-human FOXP3 (D25D4)	Cell Signal	Cat# 5298S
GAPDH	Cell Signal	Cat# 5174
β-actin	Cell Signal	Cat# 4967
Anti-Rat IgG HRP	R&D Systems	Cat# HAF005
Anti-Rabbit IgG HRP	R&D Systems	Cat# AF008
Anti-Rabbit IgG HRP	Vector Laboratories	Cat# PI-1000
β-tubulin (9F3)	Cell Signal	Cat# 2128S
Anti-mouse Legumain (301417)	R&D Systems	Cat# MAB2058
Anti-mouse Foxp3 (D608R)	Cell Signal	Cat# 12653S
Mouse Strains and Cell Lines		
C57BL/6	Charles River	Cat#632
C57BL/6 *Lgmn*$^{-/-}$	Prof. Colin Watts, Dundee, UK	N/A
C57BL/6 CD45.1	Jax Mice	Cat#002014
B16F10 melanoma	Dr. Pawel Muranski and Dr. Nick Restifo, NCI, NIH	N/A
Human DCs	Dr Amy Anderson, Dr Fiona Cooke, ICM, Newcastle University, UK	N/A
Chemicals, Peptides and Recombinant Proteins		
DMEM-1640	Lonza	Cat# 12-604F
PBS	Sigma	Cat# D8537
RBC lysis buffer	Biolegend	Cat# 420301
One Comp Beads	Thermo Fisher Scientific	Cat# 01-1111-42
Lymphocyte separation media	Promocell	Cat# C-44010
RPMI-1640	Sigma	Cat# R8758-500ML

Fetal Bovine Serum	Labtech	Cat# FCS-SA/500-41213
DMSO	Sigma	Cat# D2650
Glutamine	Gibco	Cat# 25-030-081
Non-essential Amino Acids	Sigma	Cat# M7145-100ml
2-β-mercaptoethanol	Sigma	Cat# M6250-10ML
Sodium Pyruvate	Sigma	Cat# S8636-100ml
Penicillin-Streptomycin	Sigma	Cat# P4333-100ML
rmIL-4	R&D Systems	Cat# 404-ML-010
rmPD-L1 Fc	R&D Systems	Cat# 1019-B7-100
rm-GM-CSF	Miltenyi Biotec	Cat# 130-094-043
LPS	Sigma	Cat# L2630-10mg
rhIL-2	Peprotech	Cat# 200-02
rhTGF-β1	R&D Systems	Cat#240-B
Radioimmunoprecipitation Assay Buffer (RIPA)	Sigma	Cat# R0278
Leupeptin	Sigma	Cat#E18
Pepstatin A	Sigma	Cat#EI10
Phytohemagglutinin-M (PHA)	Sigma	Cat#11082132001
TGFBR-I inhibitor (SB431542)	TOCRIS	Cat#1614
STAT3 inhibitor (S3I-201)	Sigma	Cat#SML0330-5MG
Protease Inhibitor Cocktail Tablets	Roche	Cat# 11 836 153 001
Phosphatase Inhibitor Cocktails 3	Sigma	Cat# P0044-1ML
Phosphatase Inhibitor Cocktails 2	Sigma	Cat# P5726-1ML
HEPES Buffer	Sigma	Cat# H0887-100ml
Sodium Azide	Sigma	Cat# S2002
Glycine	Sigma	Cat# 410225-50G
Hydrochloric Acid	Sigma	Cat# 2104-50ML
Sodium Chloride	Sigma	Cat# S7653
Sodium Fluoride	Sigma	Cat# S7920
Cycloheximide	Sigma	Cat# C4859-1ML

Triton X-100	Sigma	Cat# X100
Tween 20	Sigma	Cat# P1379-500ML
Trypsin	Lonza	Cat# BE02-007E
PMSF	Sigma	Cat# 93482-50ml-F
EDTA	Sigma	Cat# E7889-100ML
NuPAGE MES SDS Running Buffer 20x	Thermo Fisher Scientific	Cat# NP0002
NuPAGE transfer buffer	Thermo Fisher Scientific	Cat# NP00061
NuPAGE Antioxidant	Thermo Fisher Scientific	Cat# NP0005
4-12% Bis-Tris, 10-20% SDS-PAGE Gels	Thermo Fisher Scientific	Cat# NP0322BOX
Nitrocellulose Membrane 0.45uM	Thermo Fisher Scientific	Cat# 88025
Reducing Agent 10x	Thermo Fisher Scientific	Cat# B0004
LDS 4x	Thermo Fisher Scientific	Cat# NP0008
Acetone	Sigma	Cat# 270725
Trypan Blue	Sigma	Cat# T8154
BSA	Cell Signaling	Cat# 9998s
Phorbol 12-myristate 13-acetate (PMA)	Sigma	Cat# P8139
Ionomycin	Sigma	Cat# I0634
Brefeldin	Biolegend	Cat# 420601
Monensin	Biolegend	Cat# 420701
7-Amino-4-methylcoumarin-Chromophore	Sigma	Cat# A9891
MES	Sigma	Cat# M3671
n-Octyl-β-dglucopyranoside	Merck-Milipore	Cat# 494459-1GM
Sodium Citrate	Sigma	Cat# S4641
Z-Ala-Ala-Asn-AMC	Bachem	Cat# I-1865.0050
Sodium Acetate	Sigma	Cat# S2889
Dnase I Grade II	Sigma	Cat# 10104159001
Liberase tL	Sigma	Cat# 5401020001
DAPI	Invitrogen	Cat# D1306
Critical Commercial Assays		
Foxp3 Transcription Factor Staining Buffer Kit	Thermo Fisher Scientific	Cat# A25866A

BD Cytofix/Cytoperm™ Fixation/ Permeabilization Solution Kit	BD Pharmingen	Cat# 554714
Bicinchoninic Acid Assay (BCA assay)	Thermoscientific	Cat# 10678484
Millipore Immobilon	Merck Millipore	Cat# WBKLS0500
MS Columns	Miltenyi Biotec	Cat# 130-042-201
LD Columns	Miltenyi Biotec	Cat# 130-042-901
Mouse Regulatory T cell isolation kit	Miltenyi Biotec	Cat# 130-091-041
Human Regulatory T cell isolation kit	Miltenyi Biotec	Cat# 130-091-301
Equipment, Software and Algorithms		
BD FACS CANTO II	BD Biosciences	N/A
BD LS Fortessa X20	BD Biosciences	N/A
BD FACSAria™ Fusion Cell Sorter	BD Biosciences	N/A
FCS Express version 6	De Novo Software	N/A
GraphPad Prism	GraphPad Software, Inc	N/A
SoftMax Pro Software	Molecular Devices LLC	N/A
VersaMax™ Microplate Reader	Molecular Devices LLC	N/A
Image Studio Lite version 5.2	LI-COR Biosciences	N/A
LICOR Odyssey Fc Imager	LI-COR Biosciences	N/A
X ray film developer	Photon Imaging Systems	Cat# 9992305500
Adobe Illustrator CC 2015	Adobe Systems	N/A
ImageJ	BSD-2, public domain	N/A
Soniprep 150 Sonicator	SANYO MSE UK LTD	N/A
GE Healthcare Amersham Hypercassette-AutoradiographyCassette (18 x 24cm)	Amersham GE healthcare	Cat# 10499404
GE Healthcare Amersham Hyperfilm ECL	Amersham GE healthcare	Cat# 10607665
POLARstar Omega	BMG LABTECH	N/A
Corning 96 Well Black Flat Bottom Not Treated Microplate	Scientific Laboratory Supplies	Cat# CLS3915

Chapter 3. AEP Expression in Mouse T Cells

3.1 Introduction

AEP is implicated in antigen processing and presentation in mouse APCs (Antoniou *et al.*, 2000). Specifically, processing of TTCF by AEP has been shown to confer a kinetic advantage to mouse DCs as *Lgmn*$^{-/-}$ DCs were less efficient at processing TTCF *in vitro* (Matthews *et al.*, 2010). Also, *Lgmn*$^{-/-}$ mice have been shown to exhibit a lysosomal disorder characterised by the accumulation of lysosomal proteases, demonstrating AEP's involvement in the activation of other proteolytic enzymes such as cathepsins H and L with further implications in mouse immune responses (Shirahama-Noda *et al.*, 2003).

In addition to APCs however, AEP has been shown to exhibit a T cell lineage-specific expression pattern which suggests a role in T cell lineage determination and function (Hou *et al.*, 2015). The idea of proteolytic enzymes regulating T cell immune responses in mice has been previously explored by other groups. A notable example is cathepsin L which in its single-chain form can promote CD4^{+} naïve T cell differentiation into the Th17 lineage (Hou *et al.*, 2015). Inhibition of cathepsin L by serpinB1 negatively regulates Th17 cell differentiation (Hou *et al.*, 2015). AEP has a similar inhibitory effect on Th17 cell differentiation through its ability to process cathepsin L into its two-chain form (Hou *et al.*, 2015). WT and *serpinb1*$^{-/-}$ CD4^{+} naïve T cells cultured under Th17-inducing conditions in the presence of the AEP-specific inhibitor LI-1 led to an increase in Th17 cell differentiation in a LI-1-dose-dependent manner (Hou *et al.*, 2015). In addition, AEP expression was shown to be strongly induced in Th17 and Treg cells, but not in Th1 or Th2 cells (Hou *et al.*, 2015). Interestingly, TGF-β stimulation is important for the differentiation of both Th17 and Treg cells but not for Th1 or Th2. Therefore, it is hypothesised that it may play a role in the induction of AEP expression.

Previous work performed by the group has demonstrated the downregulation of AEP mRNA in PDL-1-treated Tbet^{+}iTreg cells compared to Tbet^{+}iTreg cells and that these cells (Tbet^{+}iTregPDL1) were also better at preventing/alleviating GvHD and colitis in mice (appendix D)

(Stathopoulou *et al.*, 2018). This, in addition to the fact that AEP expression was observed in mouse iTreg and Tbet$^+$iTreg cells but not in Tbet$^+$Th1 cells, further highlights the importance of AEP in mouse Treg cell differentiation and function (Stathopoulou *et al.*, 2018). Therefore, it is here hypothesised that signalling mechanisms involved in establishing the Treg cell lineage - such as TGF-β1 and IL-2-mediated signalling - may play a role in inducing AEP protein expression. Understanding those mechanisms will provide valuable insight into the manipulation of Treg cells for therapeutic purposes.

3.2 Aims

The aim of this chapter is to study the function of AEP in mouse Treg cells and identify signals that regulate AEP expression in these cells. Therefore, AEP expression was studied in:

- iTreg and expanded Treg cells
- tumour infiltrating nTreg cells (TILs) (consisting of both tTreg and pTreg cells) in an *in vivo* mouse model of melanoma.

3.3 Results

3.3.1 *Characterisation of WT and Lgmn$^{-/-}$ mice*

AEP can degrade Foxp3 protein but whether it modulates the phenotype of Treg cells by altering their phenotypic profile is unknown. Also, as AEP is a proteolytic enzyme, in addition to Foxp3 it may modulate effector cytokine secretion in Treg cells. Differential cytokine expression between WT and *Lgmn$^{-/-}$* Treg cells would indicate a new regulatory role for AEP in modulating cytokine phenotype in Treg cells. To address the hypothesis, multi-parametric flow cytometry to characterise CD4$^+$ T cells and CD4$^+$Foxp3$^+$ Treg cells (nTreg cells) was performed in WT and *Lgmn$^{-/-}$* mice.

Splenocytes from WT and *Lgmn$^{-/-}$* mice were characterised for cell surface markers and cytokine expression by flow cytometry by Dr. Shoba Amarnath (figure 3.1). With wild type splenocytes for controls, *Lgmn$^{-/-}$* T cells were characterised for CD4, CD8, CD44, CD62L, CD25, Foxp3, CD127, Nrp-1 and Helios expression. Splenocytes were also stimulated with PMA (10µg/ml) and ionomycin (1µg/ml) for two hours at 37^{o}C to stimulate cytokine production and then, treated with brefeldin (5 µg/ml) and monensin A (2µM) for another two hours at 37^{o}C to inhibit exocytosis and therefore

prevent loss of these cytokines prior to flow cytometry. Splenocytes were then characterised for CD4, IFN-γ, IL-10, IL-17A and IL-4 expression.

Experiments showed that *Lgmn*$^{-/-}$ mice had normal frequencies of CD4^{+} (10-13%) and CD8^{+} (7-8%) T cells as well as T effector (CD44^{high}CD62L^{low}) (17-22%) and central memory T cells (CD44^{low}CD62L^{high}) (46-50%) (figure 3.1A-B). In addition, no changes in cytokine expression of T cells were observed (figure 3.1A-B, E-G). However, *Lgmn*$^{-/-}$ mice had a significantly increased frequency ($p=0.008$) of CD4^{+}Foxp3^{+} Treg cells (16.3%) present in the spleen compared to WT mice (12%) (figure 3.1C-D). Also, these Treg cells had significantly increased ($p=0.004$) protein expression levels of Foxp3 per cell (MFI 8.5) compared to wild type Treg cells (MFI ~6.5) as indicated by MFI (figure 3.1D). Finally, the fact that *Lgmn*$^{-/-}$ mice exhibited similar frequencies of thymic Treg cells (CD4^{+}Foxp3^{+}Nrp-1^{+} and CD4^{+}Foxp3^{+}Helios^{+}) as WT mice (~80%) (figure 3.1E-F), suggests that the increased frequencies of CD4^{+}Foxp3^{+} Treg cells (figure 3.1D) are due to increased frequencies of peripheral Treg cells.

In summary, although AEP deficiency did not alter the cytokine profile of CD4^{+} T cells, increased frequencies of regulatory T cells in the periphery were observed in mice with a global deletion of AEP as well as increased Foxp3 expression within these Treg cells. This suggests that AEP can modulate mouse Treg cells and that AEP expression may have a role in regulating Foxp3 expression in these cells.

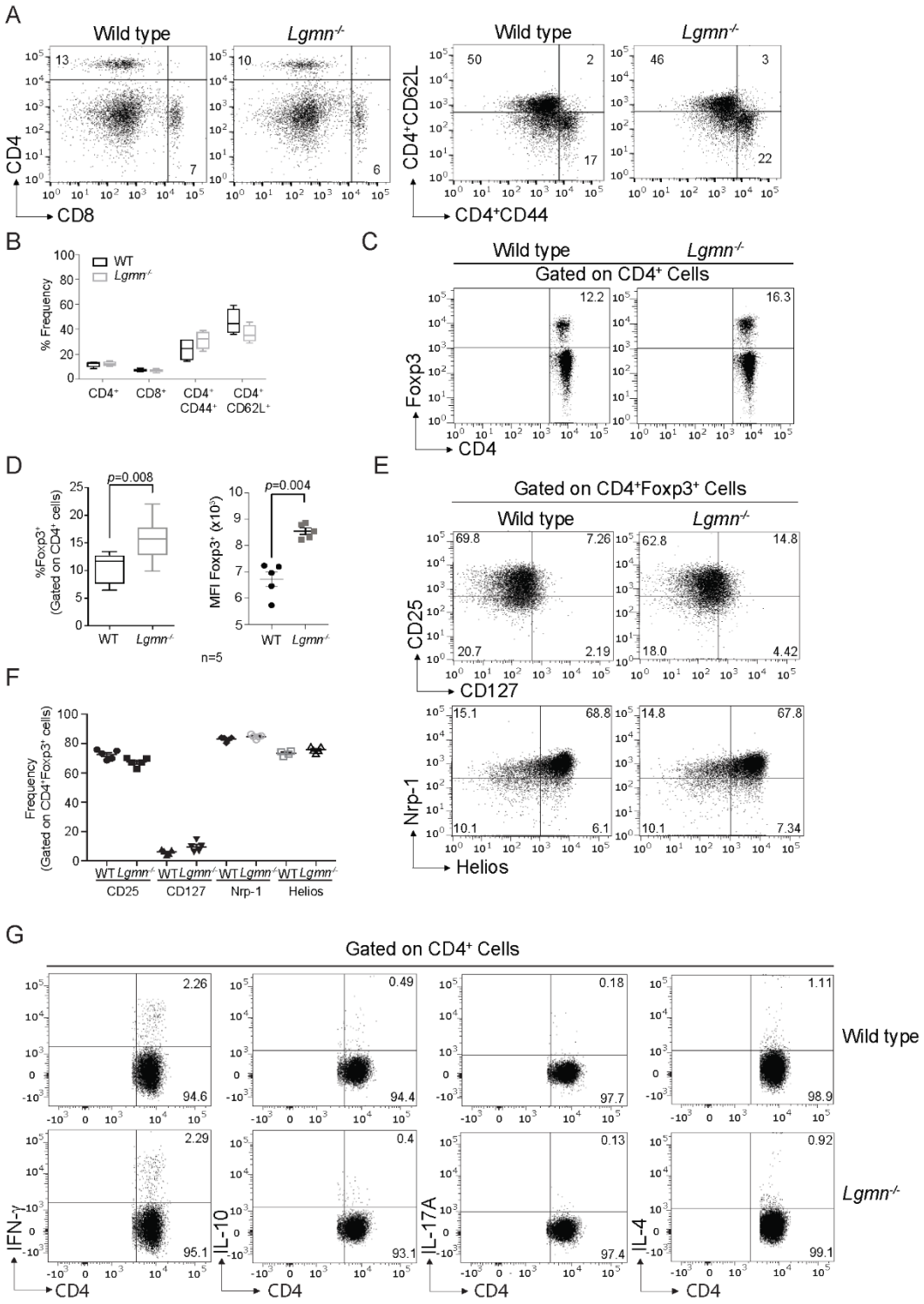
A
Wild type
Lgmn-/-
CD4
CD8
CD4+CD62L
CD4+CD44
B
WT
Lgmn-/-
% Frequency
CD4+
CD8+
CD4+ CD44+
CD4+ CD62L+
C
Gated on CD4+ Cells
Foxp3
CD4
D
p=0.008
%Foxp3+ (Gated on CD4+ cells)
p=0.004
MFI Foxp3+ (x10³)
n=5
E
Gated on CD4+Foxp3+ Cells
CD25
CD127
Nrp-1
Helios
F
Frequency (Gated on CD4+Foxp3+ cells)
CD25
CD127
Nrp-1
Helios
G
Gated on CD4+ Cells
Wild type
Lgmn-/-
IFN-γ
IL-10
IL-17A
IL-4
CD4

Figure 3.1 Phenotypic characterisation and cytokine profiling of wild type and *Lgmn*$^{-/-}$ mice. Splenocytes from B6 wild type and *Lgmn*$^{-/-}$ mice were characterised for CD4, CD8, CD44, CD62L, CD25, Foxp3, CD127, Nrp-1 and Helios expression. Splenocytes were also stimulated with PMA (10µg/ml) and ionomycin (1µg/ml) for two hours at 37ºC and then, treated with brefeldin (5 µg/ml) and monensin A (2µM) for another two hours at 37ºC. Cells were then characterised for CD4, IFN-γ, IL-10, IL-17A and IL-4 expression. **A.** Flow plots illustrating the frequency of CD4^{+} and CD8^{+} T cells within the single cells gate (left) as well as effector (CD44^{high}CD62L^{low}) and central memory (CD44^{low}CD26L^{high}) T cells within the CD4 gate (right). N=4. **B.** Summarising graph showing percentage frequencies of CD4^{+}, CD8^{+}, CD4^{+}CD44^{+} and CD4^{+}CD26L^{+} T cells. N=4. **C.** Flow plots illustrating the frequency of CD4^{+}Foxp3^{+} (nTreg) T cells in wild type and *Lgmn*$^{-/-}$ mice. N=5. **D.** Summary graphs showing the frequency of nTreg cells as well as the mean fluorescence intensity (MFI) of Foxp3 expression in nTreg cells in the spleens of WT and *Lgmn*$^{-/-}$ mice. Cells were gated on CD4^{+} T cells. N=5. **E.** Phenotypic characterisation of nTreg cells for CD25, CD127, Nrp-1 and Helios expression in WT and *Lgmn*$^{-/-}$ mice. N=5. **F.** Summary graph showing percentage frequency of nTreg cells that express CD25, CD127, Nrp-1 and Helios. N=5. **G.** Flow plots illustrating expression of IFN-γ, IL-10, IL-17A and IL-4 within the CD4 gate in stimulated WT and *Lgmn*$^{-/-}$ cells. N=1. The Shapiro-Wilk normality test was used to confirm normal distribution of data and an unpaired, Student's t test was used for variance analysis. P values ≤0.05 were defined as statistically significant. Experiments were performed by Dr. Shoba Amarnath.

3.3.2 *Foxp3 turnover in WT and Lgmn*$^{-/-}$ *iTreg cells*

Since AEP is a protease and has been shown to degrade Foxp3 in Tbet^{+}iTreg cells, the question of whether a similar mechanism exists in iTreg (Tbet^{-}) cells was addressed (Stathopoulou *et al.*, 2018). For this purpose, a protein turnover assay was developed and optimised.

CD4^{+}CD25^{-} T cells from WT splenocytes were isolated using the Miltenyi kit. This kit uses magnetic beads for the negative selection of naïve CD4^{+}CD25^{-} T cells from a pre-enriched CD4^{+} T cell population. Pre-enrichment occurs after depletion of platelets, erythrocytes, monocytes, granulocytes, epithelial cells, fibroblasts and activated lymphocytes and NK cells from the spleen sample. The unwanted populations are stained with biotin-conjugated Abs for cell-specific markers and magnetic microbeads conjugated to anti-biotin Abs. Stained cells are captured and retained in the magnetic column allowing only the population of interest (CD4^{+}) to pass through and get eluted. The eluted cells are labelled with CD25-PE Abs and

anti-PE Abs conjugated to microbeads and then run through a separate column. Naïve $CD4^+CD25^-$ cells are eluted while $CD4^+CD25^+$ cells are retained in the column. The latter can be manually flushed through to collect the $CD4^+CD25^+$ Treg cell population.

Here, naïve T cells were cultured *in vitro* at 1 million cells/ml for 72 hrs in complete DMEM media in αCD3-coated plates (5 μg/ml) with the addition of αCD28 (2 μg/ml), rhIL-2 (80 ng/ml) and rhTGF-β1 (5 ng/ml) to differentiate them into iTreg cells. Cells were cultured with or without αIL-4 (10 μg/ml) and αIFN-γ (10 μg/ml) and on day 3, cell culture media was supplemented with fresh rhIL-2 (80 ng/ml) and cells incubated for 24 more hours. On day 4, cells were treated with either the protein synthesis inhibitor cycloheximide (CHX) (100 μg/ml) or DMSO (0.1%) and harvested using RIPA lysis buffer at different time points in preparation for analysis of Foxp3 expression via western blotting.

This experiment showed that inhibition of protein turnover with CHX led to a progressive reduction in Foxp3 abundance relative to GAPDH, reflecting Foxp3 degradation compared to DMSO controls (figure 3.2). In addition, inclusion of αIL-4 and αIFN-γ neutralising antibodies in culture media did not alter Foxp3 expression levels or degradation rates in iTreg cells so these antibodies were not included in the degradation assay experiments that followed (figure 3.2).

Following optimisation, Foxp3 turnover experiments were then performed to determine whether AEP can regulate Foxp3 expression in iTreg cells and whether this effect is maintained over time (figure 3.3). The same methodology was used as described in the optimisation experiment except that $CD4^+CD25^-$ T cells from both WT and *Lgmn*$^{-/-}$ splenocytes were used. Although saturation/overexposure of the GAPDH labels in the first experiment prevented any band quantification, raw data indicate that *Lgmn*$^{-/-}$ iTreg cells show increased Foxp3 protein levels at 0hr compared to WT iTreg cells and that this difference is maintained over time for at least up to 24 hrs *in vitro* (figure 3.3 A-C). The decreased Foxp3 protein turnover in CHX-treated *Lgmn*$^{-/-}$ iTreg cells indicates that AEP regulates Foxp3 expression at a posttranslational level. This is in accordance with the

hypothesis that AEP regulates Treg cells through regulating Foxp3 protein expression.

However, it should be noted that more time points and a nuclear internal control could be used in future experiments to validate these results. This would give further insight into the half-life of Foxp3 in the *Lgmn*$^{-/-}$ iTreg cells relative to the WT controls while the bands of a nuclear housekeeping gene would be less likely to get saturated due to the lower expression levels of the nuclear marker compared to the cytoplasmic marker. Also, phenotypic characterisation of the iTreg cell population and a functional assay on day three would help eliminate the possibility of culture contamination which could have skewed the results. Although a Treg cell suppression assay was attempted to assess the quality of the purified Treg cells (appendix C), low iTreg cell numbers from the *in vitro* cultures did not permit flow cytometry and suppression assays to be performed.

A

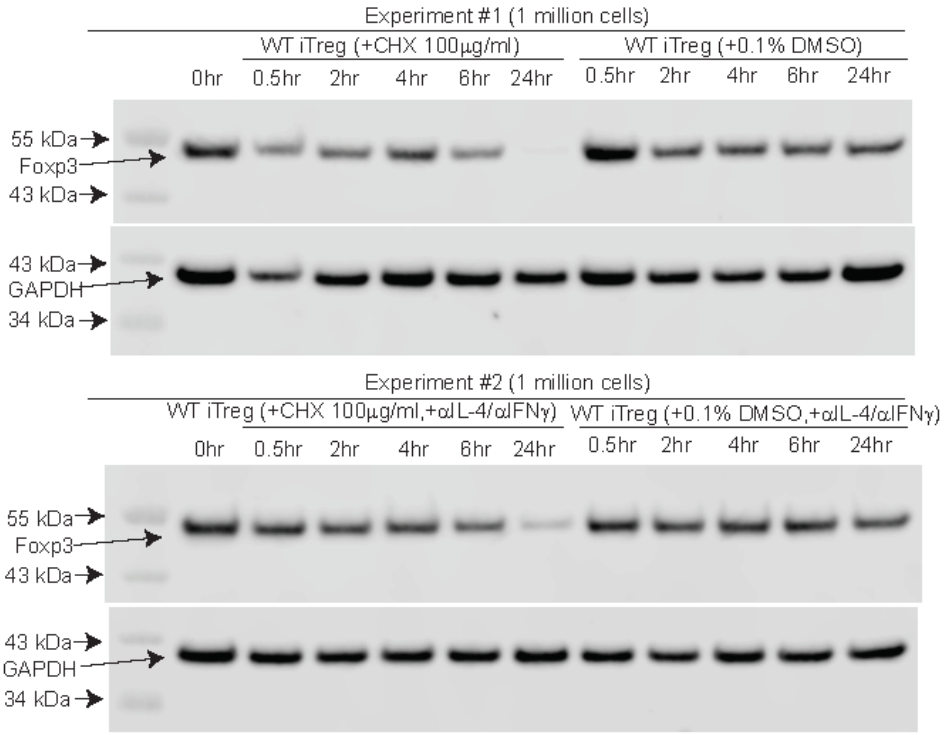
Experiment #1 (1 million cells)
WT iTreg (+CHX 100µg/ml)
WT iTreg (+0.1% DMSO)
0hr 0.5hr 2hr 4hr 6hr 24hr
0.5hr 2hr 4hr 6hr 24hr
55 kDa
Foxp3
43 kDa
43 kDa
GAPDH
34 kDa
Experiment #2 (1 million cells)
WT iTreg (+CHX 100µg/ml,+αIL-4/αIFNγ)
WT iTreg (+0.1% DMSO,+αIL-4/αIFNγ)
0hr 0.5hr 2hr 4hr 6hr 24hr
0.5hr 2hr 4hr 6hr 24hr
55 kDa
Foxp3
43 kDa
43 kDa
GAPDH
34 kDa

B

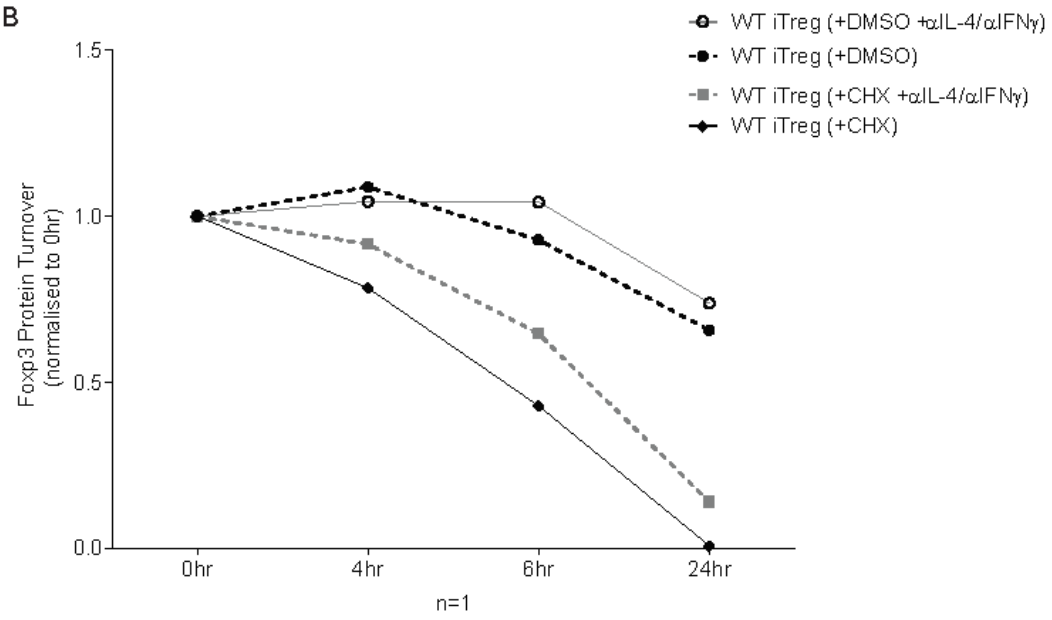
WT iTreg (+DMSO +αIL-4/αIFNγ)
WT iTreg (+DMSO)
WT iTreg (+CHX +αIL-4/αIFNγ)
WT iTreg (+CHX)
Foxp3 Protein Turnover (normalised to 0hr)
1.5
1.0
0.5
0.0
0hr
4hr
6hr
24hr
n=1

Figure 3.2 Foxp3 turnover in WT iTreg cells optimisation. $CD4^+CD25^-$ T cells from WT splenocytes were isolated using the Miltenyi kit. Cells were cultured *in vitro* at 1 million cells/ml for 3 days (72 hrs) in complete DMEM media in αCD3-coated plates (5 μg/ml) with the addition of αCD28 (2 μg/ml), rhIL-2 (80 ng/ml) and rhTGF-β1 (5 ng/ml). Cells were cultured with or without αIL-4 (10 μg/ml) and αIFN-γ (10 μg/ml). On day 3, cell culture media was supplemented with fresh rhIL-2 (80 ng/ml) and cells incubated for 24 more hours. On day 4, cells were treated with either CHX (100 μg/ml) or DMSO (0.1%) and harvested using RIPA lysis buffer at different time points. Lysates were reduced and boiled and run under reducing conditions on a precast, 4-12% Bis-Tris gradient gel. **A.** Western blot images showing Foxp3 expression in each time point. Membranes were stripped and re-probed for GAPDH. **B.** Graph showing Foxp3 protein turnover over time. Bands were normalised to GAPDH and the 0hr condition. Foxp3 bands were quantified using ImageJ and normalised to GAPDH. N=1

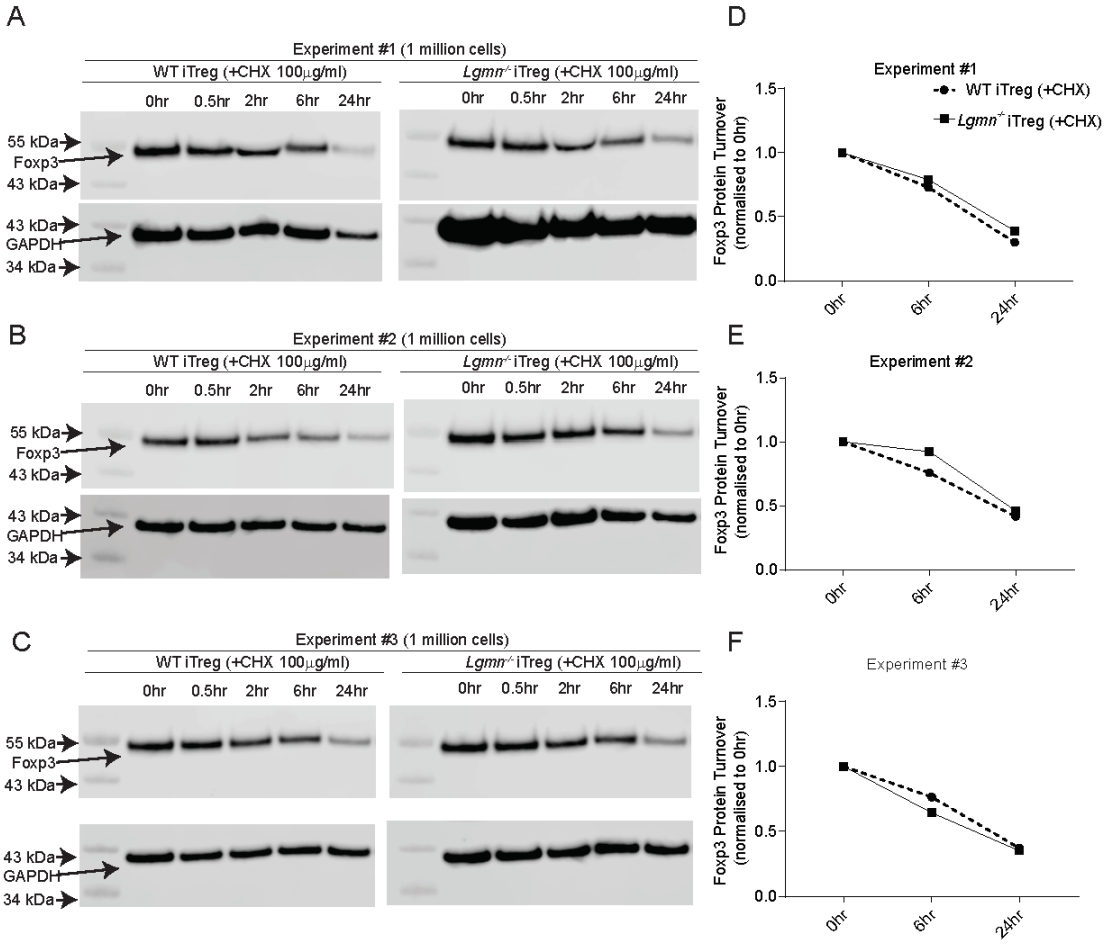

Figure 3.3 Foxp3 turnover in WT and *Lgmn*$^{-/-}$ iTreg cells. CD4^{+}CD25^{-} T cells from WT and *Lgmn*$^{-/-}$ splenocytes were isolated using the Miltenyi kit. Cells were cultured *in vitro* at 1 million cells/ml for 3 days (72 hrs) in complete DMEM media in αCD3-coated plates (5 μg/ml) with the addition of αCD28 (2 μg/ml), rhIL-2 (80 ng/ml) and rhTGF-β1 (5 ng/ml). On day 3, cell culture media was supplemented with fresh rhIL-2 (80 ng/ml) and cells incubated for 24 more hours. On day 4, cells were treated with CHX (100 μg/ml) and harvested using RIPA lysis buffer at different time points in preparation for protein analysis via western blotting. Lysates were reduced and boiled and run under reducing conditions on a precast, 4-12% Bis-Tris gradient gel. **A-C.** Western blot images showing Foxp3 expression in each time point. Membranes were stripped and re-probed for GAPDH. **D-F.** Graphs showing Foxp3 protein turnover over time. Bands were normalised to GAPDH and the 0hr condition. Foxp3 bands were quantified using ImageJ and normalised to GAPDH. N=3

3.3.3 *Induction of AEP expression in iTreg cells*

A trend towards decreased Foxp3 turnover was noted in *Lgmn*$^{-/-}$ iTreg cells indicating that AEP regulates Foxp3 expression. Therefore, signals that could induce AEP expression in WT iTreg cells were next investigated. Signalling mechanisms involved in establishing the Treg cell lineage - such as TGF-β1 and IL-2-mediated signalling – are hypothesised to play a role in inducing AEP protein expression. For this purpose, AEP expression was studied in expanded naïve and Treg (iTreg and nTreg) cells from wild type mice. $CD4^+CD25^-$ (naïve) and $CD4^+CD25^+$ (nTreg) T cells were sorted from mouse splenocytes using the Miltenyi kit as described in chapter 2.7 and 3.3.2 and cultured for 3 days in αCD3-coated plates (5 μg/ml) in the presence of αIL-4 (10 μg/ml) and αIFN-γ (10 μg/ml) with the addition of αCD28 (2 μg/ml), rhIL-2 (80 ng/ml) and rhTGF-β1 (2 or 5 ng/ml) where appropriate. Cells were then harvested using a RIPA-based lysis buffer and AEP expression determined using western blotting.

The experiment was repeated twice. To validate the culture conditions, Foxp3 expression in each condition was assessed using flow cytometry. In the first experiment, more than 70% of cells cultured under iTreg conditions (αCD3, αCD28, rhIL-2, rhTGF-β1) expressed Foxp3 indicating the successful differentiation and expansion of iTreg and nTreg cells *in vitro* (figure 3.4B-C). Using a higher concentration of TGF-β1 did not alter the frequency of $Foxp3^+$ T cells at the end of the culture within the iTreg condition (figure 3.4C). This indicates that 2 ng/ml of rhTGF-β1 is sufficient for inducing Treg cells. In addition, TCR stimulation with or without rhIL-2 was also able to induce Foxp3 expression in naïve T cells (46-52%) (figure 3.C). Specifically, TCR stimulation alone seemed to be inducing higher Foxp3 expression (52 & 48.8%) than TCR stimulation in combination with rhIL-2 (46.3%). Increased cell proliferation of activated naïve T cells - especially in the absence of survival signals delivered by IL-2 - may have led to the depletion of nutrients in the media thus causing increased cell apoptosis and the subsequent release of TGF-β1 in the media. Considering that activated naïve T cells also produce IL-2, the presence of both IL-2 and TGF-β1 in the media could have induced Foxp3 expression. In contrast, supplementing media with rhIL-2 at the start of the culture may have limited

cell apoptosis which could account for the lower frequencies of Foxp3$^+$ T cells in this condition (46.3%). Nevertheless, the frequency of Foxp3$^+$ T cells in these populations remained lower than those cultured under iTreg conditions where rhTGF-β1 was included in the culture from day 0 (>74%).

Following T cell differentiation and expansion, western blotting showed that AEP expression could be detected in all conditions, in activated naïve T cells as well as iTreg cells (figure 3.5). AEP expression was highest in cells cultured in the presence of TGF-β1 i.e. under iTreg conditions (figure 3.5B). In addition, naïve T cells stimulated with αCD3 and αCD28 showed higher AEP levels compared to those that were also stimulated with rhIL-2. Although the potential role of TCR signalling in AEP activation could not be determined as all conditions included αCD3, these data seem to coordinate with the Foxp3$^+$ T cell frequencies (figure 3.4). This along with the fact that AEP expression was also induced in nTreg cells expanded under iTreg conditions indicates that AEP expression coordinates with Foxp3 expression and that TGF-β1 plays an important role in inducing the highest level of AEP expression in mouse Treg cells. Collectively, these data suggest that AEP expression is associated with the Treg cell lineage. Additional studies that would further confirm this include studying Foxp3 and AEP expression using fluorescently-labelled probes and confocal microscopy. Finally, stimulation of nTreg cells with TGF-β1 alone in the absence of TCR stimulation would also help to further validate these results.

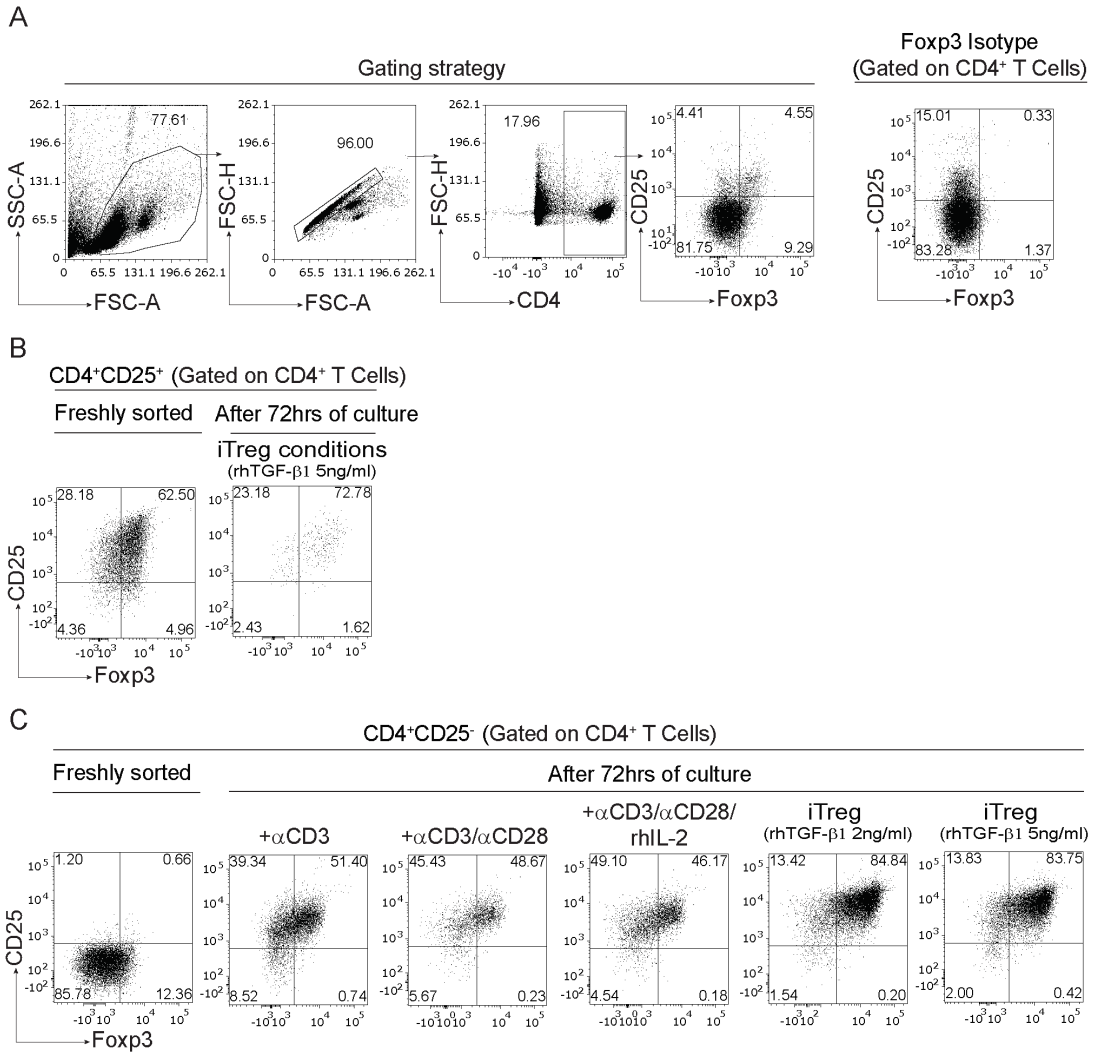

Figure 3.4 iTreg cell expansion and characterisation – mouse 1. $CD4^+CD25^-$ and $CD4^+CD25^+$ T cells from WT splenocytes were isolated using the Miltenyi kit. Cells were cultured *in vitro* at 1 million cells/ml for 72 hrs in complete DMEM media in αCD3-coated plates (5 μg/ml) in the presence of αIL-4 (10 μg/ml) and αIFN-γ (10 μg/ml) with the addition of αCD28 (2 μg/ml), rhIL-2 (80 ng/ml) and rhTGF-β1 (2 and 5 ng/ml) where appropriate. iTreg conditions included αCD3, αCD28, rhIL-2 and rhTGF-β1. Cells from each condition were characterised for CD4 and Foxp3 expression. The rest were harvested using RIPA lysis buffer in preparation for protein analysis via western blotting. **A.** Splenocyte characterisation on day 0 illustrating the gating strategy for identifying nTreg cells. **B.** Flow plots showing the frequency of $CD25^+Foxp3^+$ cells in sorted $CD4^+CD25^+$ T cells that were cultured under iTreg conditions. **C.** Flow plots showing the frequency of $CD25^+Foxp3^+$ cells in sorted $CD4^+CD25^-$ T cells that were cultured under different conditions. N=1

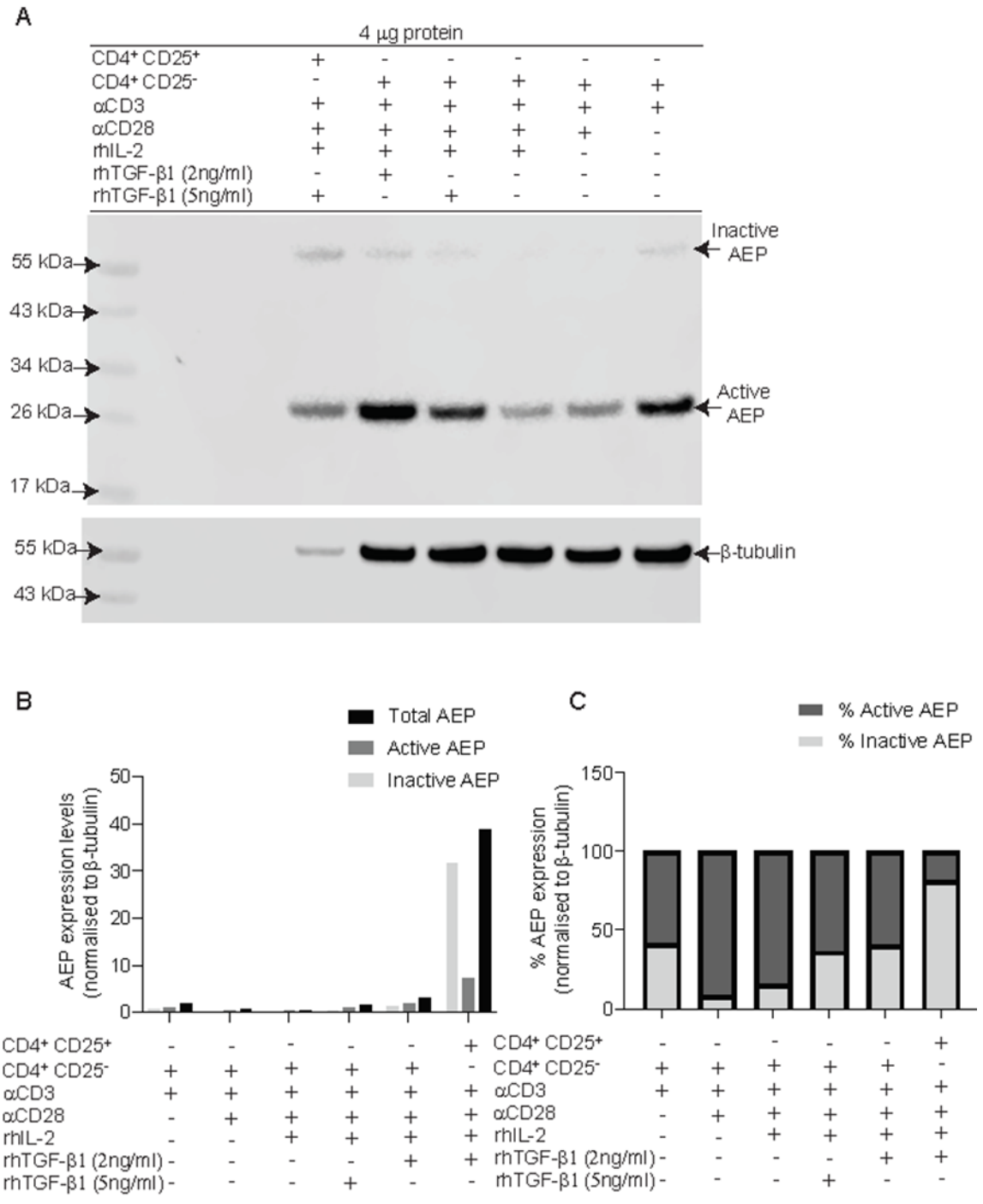
A
4 µg protein
CD4+ CD25+ + - - - - -
CD4+ CD25- - + + + + +
αCD3 + + + + + +
αCD28 + + + + + -
rhIL-2 + + + + - -
rhTGF-β1 (2ng/ml) - + - - - -
rhTGF-β1 (5ng/ml) + - + - - -
55 kDa
43 kDa
34 kDa
26 kDa
17 kDa
Inactive AEP
Active AEP
55 kDa
43 kDa
β-tubulin
B
Total AEP
Active AEP
Inactive AEP
AEP expression levels (normalised to β-tubulin)
50
40
30
20
10
0
CD4+ CD25+ - - - - - +
CD4+ CD25- + + + + + -
αCD3 + + + + + +
αCD28 - + + + + +
rhIL-2 - - + + + +
rhTGF-β1 (2ng/ml) - - - - + +
rhTGF-β1 (5ng/ml) - - - + - -
C
% Active AEP
% Inactive AEP
% AEP expression (normalised to β-tubulin)
150
100
50
0
CD4+ CD25+ - - - - - +
CD4+ CD25- + + + + + -
αCD3 + + + + + +
αCD28 - + + + + +
rhIL-2 - - + + + +
rhTGF-β1 (2ng/ml) - - - - + +
rhTGF-β1 (5ng/ml) - - - + - -

Figure 3.5 AEP expression in expanded murine iTreg cells – mouse 1. $CD4^+CD25^-$ and $CD4^+CD25^+$ T cells from WT splenocytes were isolated using the Miltenyi kit. Cells were cultured *in vitro* at 1 million cells/ml for 72 hrs in complete DMEM media in αCD3-coated plates (5 μg/ml) in the presence of αIL-4 (10 μg/ml) and αIFN-γ (10 μg/ml) with the addition of αCD28 (2 μg/ml), rhIL-2 (80 ng/ml) and rhTGF-β1 (2 and 5 ng/ml) where appropriate. Cells from each condition were harvested using RIPA lysis buffer in preparation for protein analysis via western blotting. Lysates were reduced and boiled and run under reducing conditions on a precast, 4-12% Bis-Tris gradient gel. **A.** Western blot image showing AEP expression in each of the culture conditions. Stripped and re-probed western blot membrane was imaged for β-tubulin. **B.** Bar graph showing the expression levels of active, inactive and total AEP in each of the conditions. Bands were normalised to β-tubulin. **C.** Bar graph showing the percentage ratio of active and inactive AEP expressed in each of the culture conditions. AEP bands were quantified using ImageJ. The active and inactive AEP bands were normalised to β-tubulin and the normalised values were divided by the total AEP and then multiplied by 100. N=1

When the experiment was repeated a second time, more than 50% of cells cultured under iTreg conditions expressed Foxp3 indicating the successful differentiation and expansion of iTreg and nTreg cells *in vitro* (figure 3.6B-C). Although TCR stimulation with or without rhIL-2 was able to induce Foxp3 expression in naïve T cells (1.3 - 3.7%) (figure 3.6C), the frequencies of $Foxp3^+$ T cells were considerably lower than those observed in the first experiment (46 - 52%) (figure 3.4C). As in the first experiment, TCR stimulation (αCD3 and αCD28) induced higher Foxp3 expression (3.7%) than TCR stimulation in combination with rhIL-2 (1.3%). Also, the frequency of $Foxp3^+$ T cells in these populations remained lower than those cultured under iTreg conditions (>54%).

Western blotting revealed a similar pattern of AEP expression as AEP could be detected in activated naïve T cells as well as iTreg cells (figure 3.7). AEP expression was highest in cells cultured under iTreg conditions (figure 3.7B). In addition, naïve T cells stimulated with both αCD3 and αCD28 showed higher AEP levels compared to those that were also stimulated with rhIL-2. These data seem to coordinate with the $Foxp3^+$ T cell frequencies (figure 3.6C). Similarly to the first experiment, AEP expression was induced in nTreg cells expanded under iTreg conditions although quantification of this band was not possible due to the absence of the house keeping gene (figure 3.7).

Issues with the band intensity of the β-tubulin housekeeping have been observed in multiple blots, specifically in the freshly isolated Treg ($CD4^+CD25^+$) cell population that had been cultured under iTreg cell conditions (figure 3.5, 3.7 and 3.9). This may be due to membrane overstripping which could have removed the protein from the nitrocellulose membrane. However, that does not explain why the rest of the tubulin bands remained unaffected. Therefore, it is possible that this is a cell-specific and/or culture condition-specific effect. It has been reported in the literature that TGF-β can have an impact on the levels of housekeeping genes such as β-actin and β-tubulin (Lomri and Marie, 1990). Furthermore, cell confluency during cell culture can also affect expression levels of housekeeping genes even though an equal amount of protein has been loaded on the gel (Samantha Greer *et al.*, 2010). Specifically, changes in the confluency of cultured NIH3T3 fibroblasts has been shown to affect the levels of α-tubulin and GAPDH but it did not affect the levels of β-actin (Samantha Greer *et al.*, 2010). Also, this may be a cell-specific effect as human DCs were shown to express low levels of GAPDH (figure 4.19) but high levels of β-actin, even though an equal amount of protein was loaded on the gel in both cases (5 μg) (figure 4.21). More validation experiments of the housekeeping genes need to be performed to account for internal control variation in each experimental context. Alternatively, more accurate approaches of protein normalisation could be used in future experiments such as total protein staining.

Collectively, these data are in agreement with the first experiment and support the hypothesis that TGF-β1 plays an important role in inducing AEP expression in mouse Treg cells.

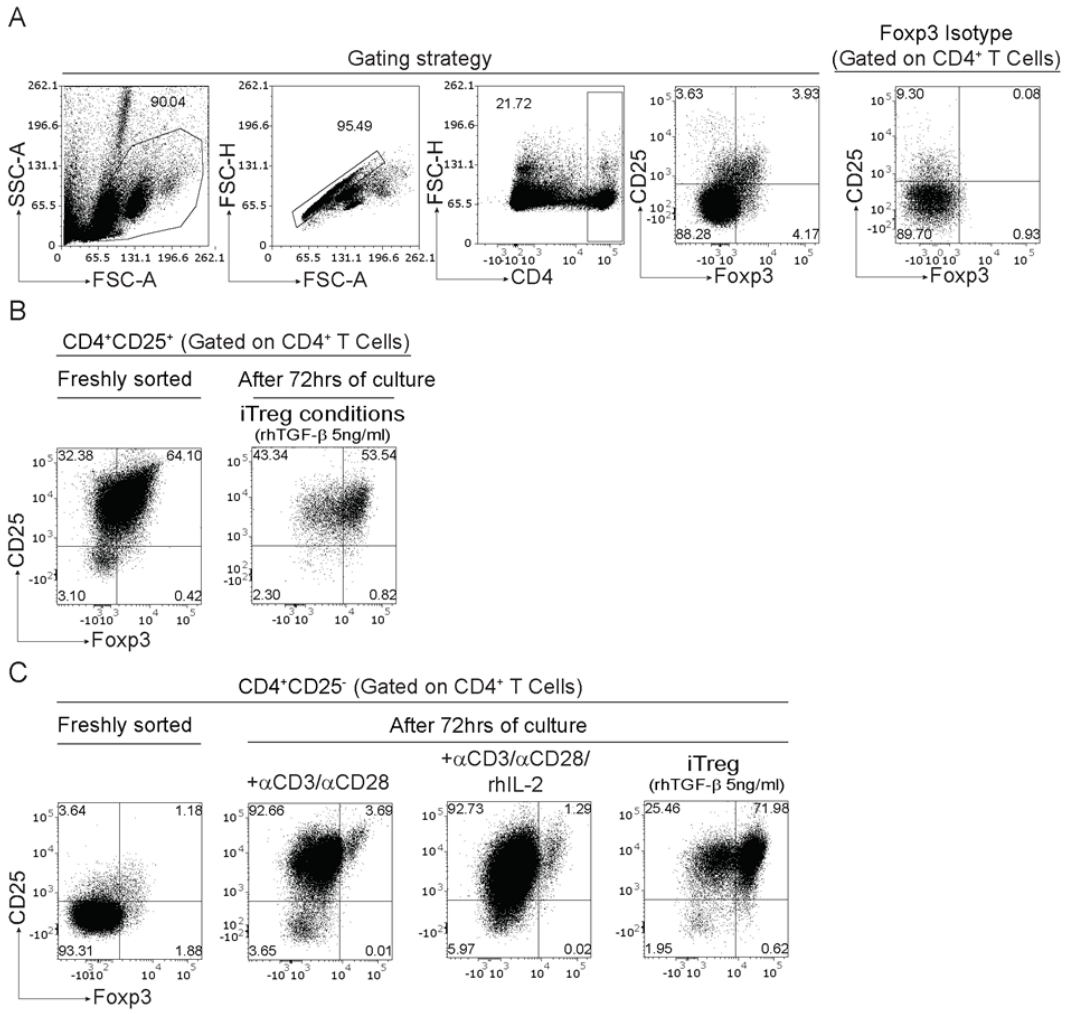

Figure 3.6 iTreg cell expansion and characterisation – mouse 2. $CD4^+CD25^-$ and $CD4^+CD25^+$ T cells from WT splenocytes were isolated using the Miltenyi kit. Cells were cultured *in vitro* at 1 million cells/ml for 72 hrs in complete DMEM media in αCD3-coated plates (5 μg/ml) in the presence of αIL-4 (10 μg/ml) and αIFN-γ (10 μg/ml) with the addition of αCD28 (2 μg/ml), rhIL-2 (80 ng/ml) and rhTGF-β1 (5 ng/ml) where appropriate. Cells from each condition were characterised for CD4 and Foxp3 expression. The rest were harvested using RIPA lysis buffer in preparation for protein analysis via western blotting. **A.** Splenocyte characterisation on day 0 illustrating the gating strategy for identifying nTreg cells. **B.** Flow plots showing the frequency of $CD25^+Foxp3^+$ cells in sorted $CD4^+CD25^+$ T cells that were cultured under iTreg conditions. **C.** Flow plots showing the frequency of $CD25^+Foxp3^+$ cells in sorted $CD4^+CD25^-$ T cells that were cultured under different conditions. N=1

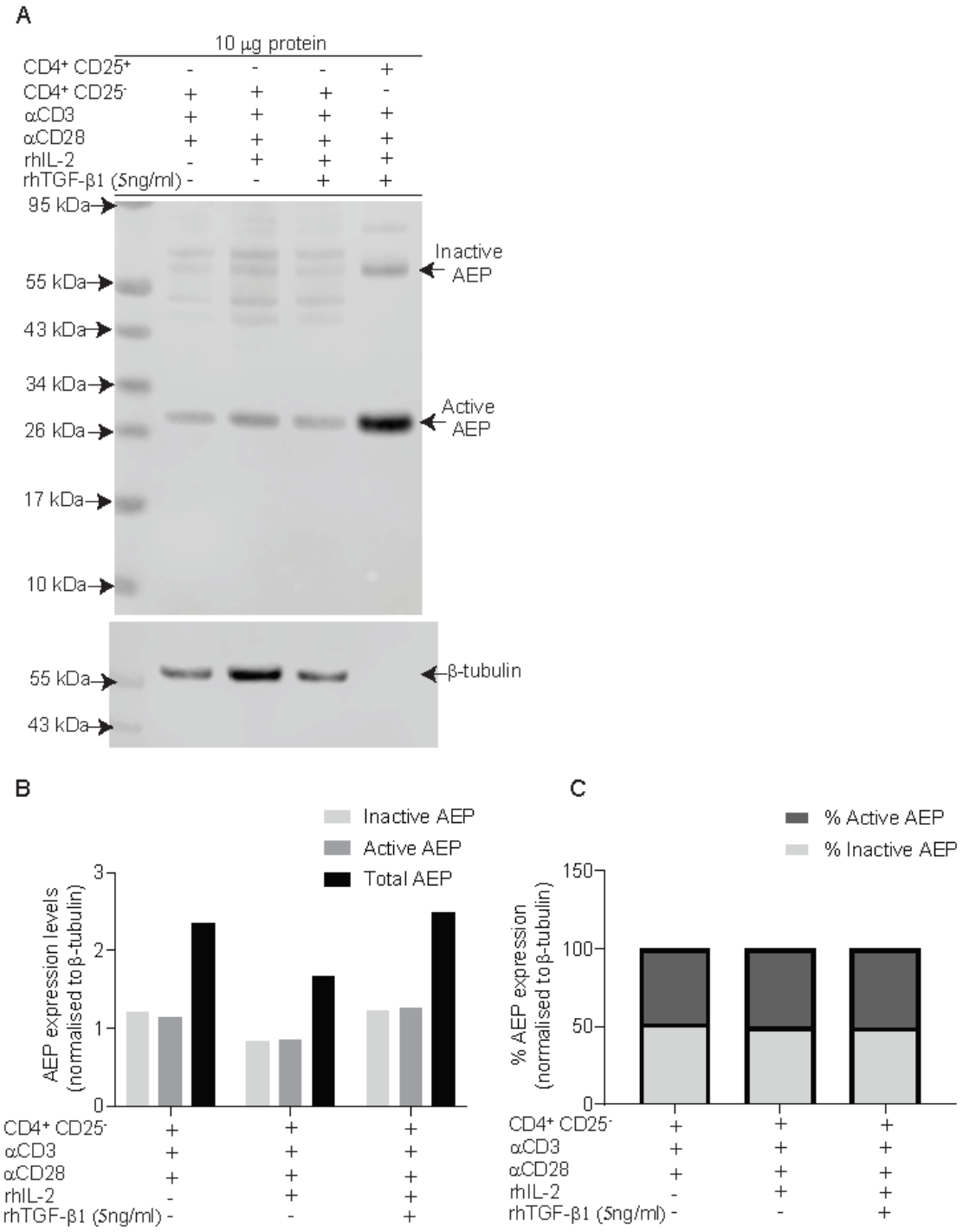
A
10 μg protein
CD4+ CD25+ - - - +
CD4+ CD25- + + + -
αCD3 + + + +
αCD28 + + + +
rhIL-2 - + + +
rhTGF-β1 (5ng/ml) - - + +
95 kDa
55 kDa
43 kDa
34 kDa
26 kDa
17 kDa
10 kDa
Inactive AEP
Active AEP
55 kDa
43 kDa
β-tubulin
B
Inactive AEP
Active AEP
Total AEP
AEP expression levels (normalised to β-tubulin)
0
1
2
3
CD4+ CD25- + + +
αCD3 + + +
αCD28 + + +
rhIL-2 - + +
rhTGF-β1 (5ng/ml) - - +
C
% Active AEP
% Inactive AEP
% AEP expression (normalised to β-tubulin)
0
50
100
150
CD4+ CD25- + + +
αCD3 + + +
αCD28 + + +
rhIL-2 - + +
rhTGF-β1 (5ng/ml) - - +

Figure 3.7 AEP expression in expanded murine iTreg cells– mouse 2. $CD4^+CD25^-$ and $CD4^+CD25^+$ T cells from WT splenocytes were isolated using the Miltenyi kit. Cells were cultured *in vitro* at 1 million cells/ml for 72 hrs in complete DMEM media in αCD3-coated plates (5 μg/ml) in the presence of αIL-4 (10 μg/ml) and αIFN-γ (10 μg/ml) with the addition of αCD28 (2 μg/ml), rhIL-2 (80 ng/ml) and rhTGF-β1 (5 ng/ml) where appropriate. Cells from each condition were harvested using RIPA lysis buffer in preparation for protein analysis via western blotting. Lysates were reduced and boiled and run under reducing conditions on a precast, 4-12% Bis-Tris gradient gel. **A.** Western blot image showing AEP expression in each of the culture conditions. Stripped and re-probed western blot membrane was imaged for β-tubulin. **B.** Bar graph showing the expression levels of active, inactive and total AEP in each of the conditions. Bands were normalised to β-tubulin. **C.** Bar graph showing the percentage ratio of active and inactive AEP expressed in each of the culture conditions. AEP bands were quantified using ImageJ. The active and inactive AEP bands were normalised to β-tubulin and the normalised values were divided by the total AEP and then multiplied by 100. N=1

3.3.4 *PDL-1 downregulates AEP in murine iTreg and expanded Treg cells*

In addition to signals that can induce AEP expression, signals that downregulate AEP were next investigated. PDL-1, has been shown to downregulate AEP expression in $Tbet^+$iTreg and iTreg cells generated *in vitro* (Stathopoulou *et al.*, 2018). In order to determine whether a similar mechanism exists in nTreg cells, AEP expression was studied in both mouse iTreg and nTreg cells that were expanded under iTreg conditions in the presence of a PDL-1 stimulatory antibody (figure 3.8, 3.9).

$CD4^+CD25^-$ (naïve) and $CD4^+CD25^+$ (nTreg) T cells were sorted from WT mouse splenocytes using the Miltenyi kit (method described in sections 2.7, 3.3.2) and cultured for 3 days in αCD3-coated plates (5 μg/ml) in the presence of αIL-4 (10 μg/ml) and αIFN-γ (10 μg/ml) with the addition of αCD28 (2 μg/ml), rhIL-2 (80 ng/ml) and rhTGF-β1 (2 or 5 ng/ml) where appropriate. In certain conditions, plates were also coated with PDL-1 (5 μg/ml). Cells were then harvested using a RIPA-based lysis buffer and AEP expression determined using western blotting.

In this experiment, more than 70% of cells cultured under iTreg conditions expressed Foxp3 (figure 3.8). In agreement with data presented in figure 3.4, using a higher concentration of TGF-β1 did not significantly alter the

frequency of Foxp3$^+$ T cells at the end of the culture (74 – 82%) (figure 3.8B). A similar pattern of Foxp3 and AEP expression was observed as in figures 3.4-3.7. Specifically, TCR stimulation in combination with rhIL-2 was able to induce Foxp3 expression in naïve T cells (45.5%) (figure 3.8B). Although the frequency of Foxp3$^+$ T cells in this population was higher than that observed in previous experiments, it remained lower than those cultured under iTreg conditions (>70%) (figure 3.8).

Western blotting revealed a similar pattern of AEP expression as AEP could be detected in activated naïve T cells stimulated with rhIL-2 as well as in iTreg and expanded nTreg cells (figure 3.9). However, similar levels of AEP expression were observed in the rhIL-2 and the iTreg conditions. These data seem to coordinate with the Foxp3$^+$ T cell frequencies as higher Foxp3 expression within the IL-2 condition correlated with higher AEP expression. In support of this, there was no significant increase in AEP expression levels in iTreg cells induced with either 2 or 5 ng/ml of TGF-β1 which is in accordance with the flow cytometry data on Foxp3 expression (figure 3.8-9).

Collectively, these data are in agreement with the previous experiments (figure 3.4-3.7) and support the hypothesis that TGF-β1 plays an important role in inducing AEP expression in mouse Treg cells.

In addition, downregulation of AEP expression was observed in all PDL-1-stimulated populations (iTreg and expanded nTreg cells) which supports previous data showing PDL-1 downregulating AEP in murine Tbet$^+$iTreg and iTreg cells (figure 3.9) (Stathopoulou *et al.*, 2018).

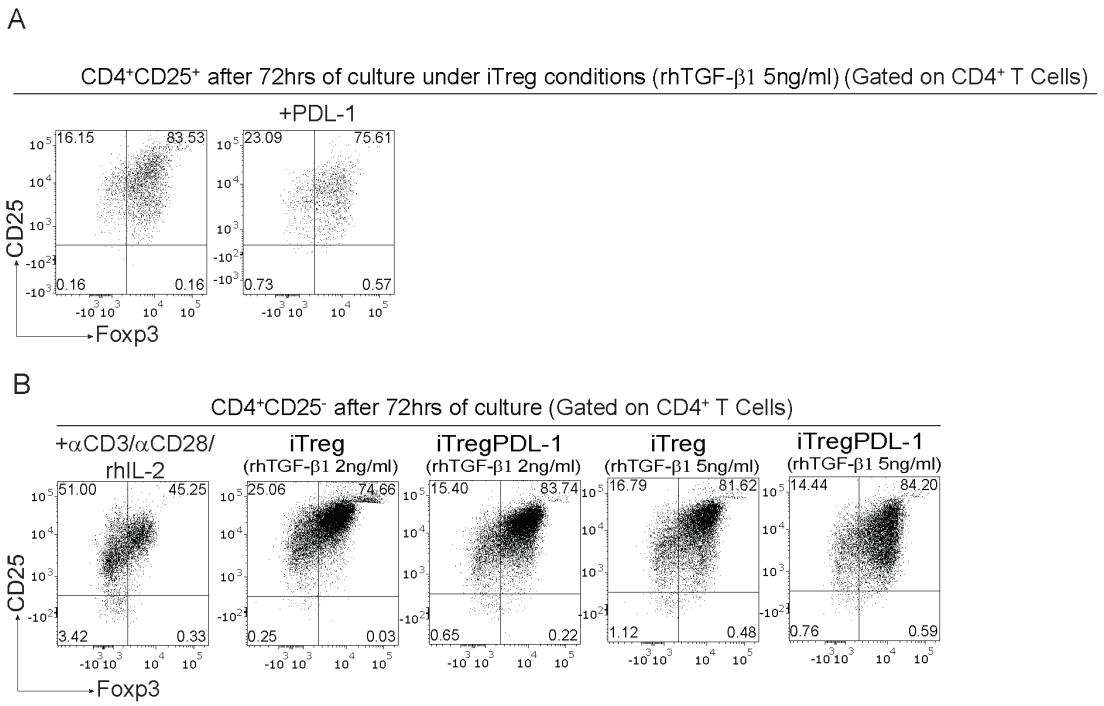

Figure 3.8 iTreg cell expansion and characterisation – mouse 3. $CD4^+CD25^-$ and $CD4^+CD25^+$ T cells from WT splenocytes were isolated using the Miltenyi kit. Cells were cultured *in vitro* at 1 million cells/ml for 72 hrs in complete DMEM media in αCD3-coated plates (5 μg/ml) in the presence of αIL-4 (10 μg/ml) and αIFN-γ (10 μg/ml) with the addition of αCD28 (2 μg/ml), rhIL-2 (80 ng/ml) rhTGF-β1 (2 or 5 ng/ml) and PDL-1 (5 μg/ml, coated wells) where appropriate. Cells from each condition were characterised for CD4 and Foxp3 expression. The rest were harvested using RIPA lysis buffer in preparation for protein analysis via western blotting. **A.** Flow plots showing the frequency of $CD25^+Foxp3^+$ cells in sorted $CD4^+CD25^+$ T cells that were cultured under iTreg conditions with or without PDL-1. **B.** Flow plots showing the frequency of $CD25^+Foxp3^+$ cells in sorted $CD4^+CD25^-$ T cells that were cultured under different conditions. N=1

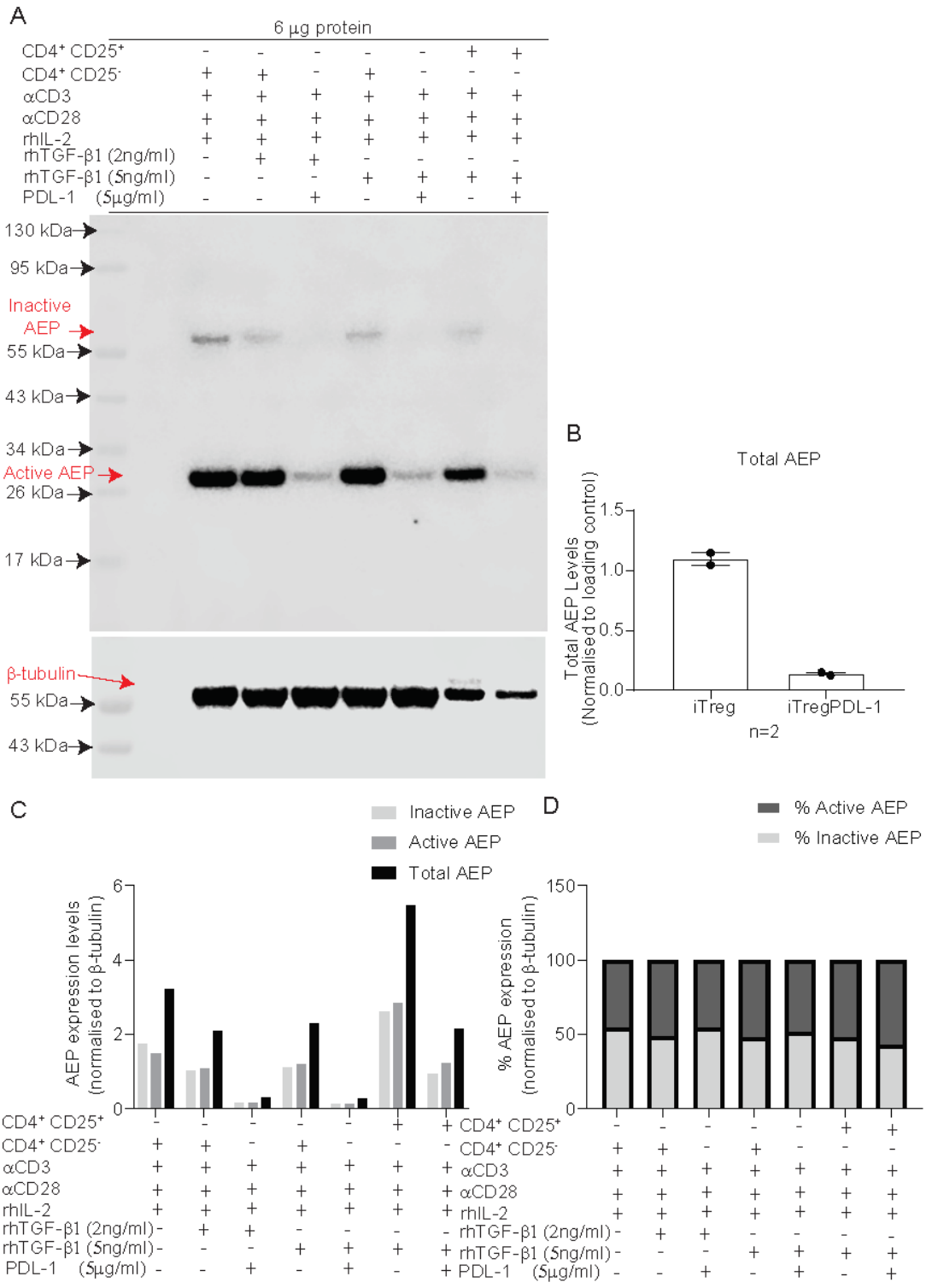
A
6 µg protein
CD4+ CD25+
CD4+ CD25-
αCD3
αCD28
rhIL-2
rhTGF-β1 (2ng/ml)
rhTGF-β1 (5ng/ml)
PDL-1 (5µg/ml)
130 kDa
95 kDa
Inactive AEP
55 kDa
43 kDa
34 kDa
Active AEP
26 kDa
17 kDa
β-tubulin
55 kDa
43 kDa
B
Total AEP
Total AEP Levels (Normalised to loading control)
1.5
1.0
0.5
0.0
iTreg
iTregPDL-1
n=2
C
Inactive AEP
Active AEP
Total AEP
AEP expression levels (normalised to β-tubulin)
6
4
2
0
D
% Active AEP
% Inactive AEP
% AEP expression (normalised to β-tubulin)
150
100
50
0

Figure 3.9 AEP expression in expanded murine iTreg cells – mouse 3. $CD4^+CD25^-$ and $CD4^+CD25^+$ T cells from WT splenocytes were isolated using the Miltenyi kit. Cells were cultured *in vitro* at 1 million cells/ml for 72 hrs in complete DMEM media in αCD3-coated plates (5 μg/ml) in the presence of αIL-4 (10 μg/ml) and αIFN-γ (10 μg/ml) with the addition of αCD28 (2 μg/ml), rhIL-2 (80 ng/ml) and rhTGF-β1 (2 or 5 ng/ml) and PDL-1 (5 μg/ml, coated wells) where appropriate. Cells from each condition were harvested using RIPA lysis buffer in preparation for protein analysis via western blotting. Lysates were reduced and boiled and run under reducing conditions on a precast, 4-12% Bis-Tris gradient gel. **A.** Western blot image showing AEP expression in each of the culture conditions. Stripped and re-probed western blot membrane was imaged for β-tubulin. **B.** Bar graph showing total AEP expression in iTreg cells cultured in the presence or absence of PDL-1. **C.** Bar graph showing the expression levels of active, inactive and total AEP in each of the conditions. Bands were normalised to β-tubulin. **D.** Bar graph showing the percentage ratio of active and inactive AEP expressed in each of the culture conditions. AEP bands were quantified using ImageJ. The active and inactive AEP bands were normalised to β-tubulin and the normalised values were divided by the total AEP and then multiplied by 100. N=1

3.3.5 *AEP deficiency alters Treg cell numbers and frequency in an in vivo model of B16 melanoma*

If AEP is a regulator of Foxp3 in Treg cells, then the Treg cells from *Lgmn*$^{-/-}$ mice may possess greater suppression capacity and stability than WT T cells. It is therefore hypothesised that *Lgmn*$^{-/-}$ mice will exhibit higher frequencies of TIL Treg cells compared to WT controls with potential implications in tumour sizes and tumour progression/metastasis. To test the function of AEP in activated Treg cells and determine whether the PD-1 and AEP pathways are interlinked, an *in vivo* mouse model of B16F10 melanoma was used.

In this disease model, WT and *Lgmn*$^{-/-}$ mice were subcutaneously injected with 0.3 million mouse B16F10 melanoma cells and tumours were left to grow for 11 days. Mouse cohorts also received intraperitoneal injections of either an isotype or PDL-1-blocking antibody on days 5, 7 and 9 post tumour injection by Dr. Shoba Amarnath. Tumours were harvested on day 11 and digested into single cell suspensions. The frequencies of tumour infiltrating $CD4^+Foxp3^+$ Treg cells (gated on $CD4^+$ T cells) were then determined (figure 3.10A).

Results from this experiment demonstrated that *Lgmn*$^{-/-}$ mice exhibited significantly increased frequencies of CD4^{+}Foxp3^{+} Treg cells within tumours (9.3% with αPDL-1 treatment, 9.8% with isotype) compared to WT mice (p=0.046) (3.5% with αPDL-1 treatment, 7.4% with isotype) irrespective of PDL-1 blockade treatment (figure 3.10B-C). In addition, there was no difference in the tumour growth rate or size between the two cohorts (data not shown). WT mice on the other hand showed a significant decrease in Treg cell frequencies after blocking PDL-1 (p=0.027) (figure 3.10B-C). In addition, there were less metastatic lesions observed in mice treated with anti-PDL-1 (counted visible black lesions during mouse dissection, data not shown). This suggests that PDL-1 signalling downregulates AEP function in these cells thus restricting the degradation of Foxp3 and promoting Treg cell stability. Collectively, these results demonstrate that Treg cells are modulated by AEP in a PD-1-dependent manner *in vivo*.

A

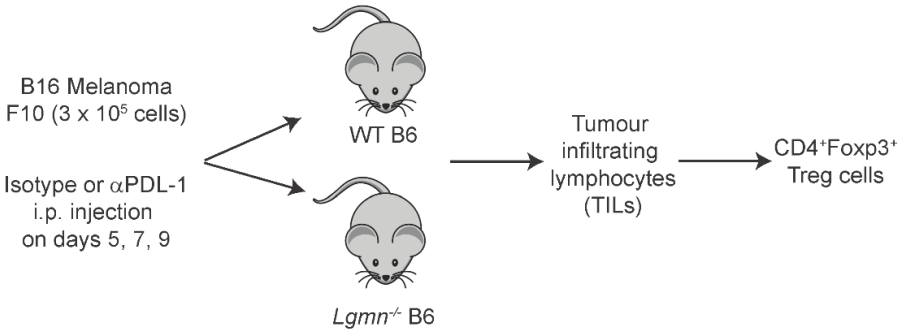
B16 Melanoma
F10 (3 x 10^5 cells)
Isotype or αPDL-1
i.p. injection
on days 5, 7, 9
WT B6
Lgmn-/- B6
Tumour
infiltrating
lymphocytes
(TILs)
CD4+Foxp3+
Treg cells

B

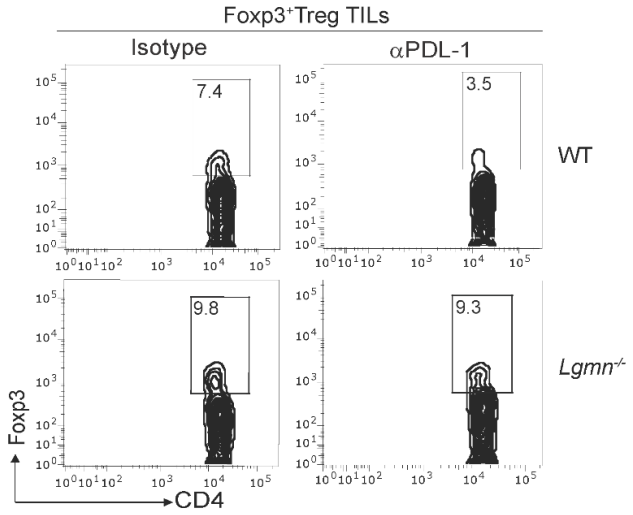
Foxp3+Treg TILs
Isotype
αPDL-1
7.4
3.5
9.8
9.3
WT
Lgmn-/-
Foxp3
CD4

C

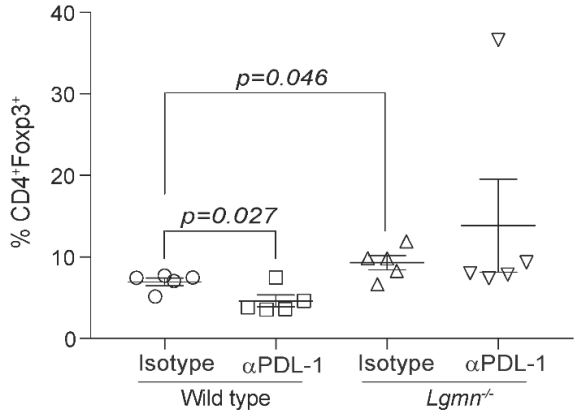
% CD4+Foxp3+
40
30
20
10
0
p=0.046
p=0.027
Isotype
αPDL-1
Isotype
αPDL-1
Wild type
Lgmn-/-

Figure 3.10 B16 melanoma mouse model. WT and *Lgmn*$^{-/-}$ mice were subcutaneously injected with 0.3 million mouse B16F10 melanoma cells and tumours left to grow for 11 days. Mouse cohorts received intraperitoneal injections of either isotype or PDL-1-blocking antibody (250 μg in 200 μl) on days 5, 7 and 9. Tumours were harvested on day 11 and digested into single cell suspensions. The frequencies of Treg cells within the tumours were then determined (gated on CD4$^+$ T cells). **A.** Schematic diagram of the experimental methodology. **B.** Representative flow plots illustrating the frequency of CD4$^+$Foxp3$^+$ T cells within tumours in mice that received either isotype or αPDL-1 treatment. **C.** Summary graph showing the frequency of CD4$^+$Foxp3$^+$ T cells among TILs (within tumours) in mice that received either isotype or αPDL-1 treatment. The Shapiro-Wilk normality test was used to confirm normal distribution of data and the One Way Anova test was used for variance analysis. P values ≤0.05 were defined as statistically significant. N=5. Processing of melanoma cells and mouse i.p. injections were performed with Dr. Shoba Amarnath.

3.4 Conclusion

This chapter focused on the role of AEP specifically in mouse Treg cells and aimed to study the signals that regulate its expression in these cells. Results from this chapter are discussed here briefly while a more detailed discussion is presented in chapter 6.

Phenotypic characterisation of *Lgmn*$^{-/-}$ mice has demonstrated that AEP modulates Treg cells in the periphery as reflected in the increased frequencies of CD4$^+$Foxp3$^+$ T cells within the spleen (16.3%). In addition, Foxp3 turnover assays demonstrated a proteolytic mechanism of Foxp3 regulation by AEP as *Lgmn*$^{-/-}$ iTreg cells maintained higher Foxp3 protein levels compared to WT iTreg cells. Cell cultures of WT mouse T cells demonstrated that TGF-β1 was the cytokine inducing the highest levels of AEP expression while PDL-1 stimulation had the opposite effect. Although Foxp3 expression correlated with increased total AEP levels, Foxp3 expression did not correlate with either active or inactive AEP expression. However, it should be mentioned that Foxp3 expression was here assessed by studying the frequency of Foxp3$^+$ T cells and not Foxp3 protein levels in each culture condition. Determining whether Foxp3 protein levels correlate with either active or inactive AEP would give an indication on whether induction of AEP expression serves as a homeostatic negative feedback loop regulating Treg cell function.

Finally, the role of AEP in regulating Treg cells was also confirmed *in vivo* in a mouse model of B16 melanoma where it was shown that AEP deficiency led to increased Treg cell frequencies within tumours (9.8%) that was refractory to PDL-1 blockade (9.3%). The fact that tumour growth rates in *Lgmn*$^{-/-}$ mice with melanoma were similar to those in WT mice, indicates that enhanced Treg cell stability due to lack of AEP expression does not confer a selective advantage to tumours in terms of growth rate but it does make them resistant to PDL-1 blockade. Also, the overall difference in the frequency of TIL Treg cells in *Lgmn*$^{-/-}$ versus WT mice was much smaller (9.8% and 7.4% respectively) compared to that observed in the spleens of untreated, normal WT and *Lgmn*$^{-/-}$ mice (12% and 16% respectively). This could explain the lack of tumour hyperprogression in the knock-out mice. However, in order to fully elucidate the function of AEP within tumours, detailed characterisation of the tumour microenvironment would have to be performed which is beyond the scope of this study.

Finally, it would be interesting to study the function of the cleaved Foxp3 protein in mouse Treg cells in order to further assess the biological significance of AEP expression in mouse Treg cells. It has been shown that AEP cleavage does not destabilise the nuclear localisation domain of Foxp3 therefore Foxp3 may still elicit its function in the nucleus (Stathopoulou *et al.*, 2018). However, its function there may be altered. To address this question, future studies would have to include genome wide CHIP-seq analysis to identify full length and cleaved Foxp3 mediated transcriptional regulation of the T cell genome.

In conclusion, this chapter demonstrated that:

- *Lgmn*$^{-/-}$ mice exhibit an increased frequency of peripheral Treg cells compared to WT mice
- AEP expression negatively regulates Foxp3 protein abundance in mouse iTreg cells
- TGF-β1 induces the highest levels of AEP expression *in vitro*
- PDL-1 stimulation downregulates AEP expression in mouse iTreg cells and that

- AEP deficiency results in increased Treg cell frequency within tumours of mice with melanoma irrespective of PDL-1 blockade.

Chapter 4. AEP Expression in Human T Cells

4.1 Introduction

The role of AEP in human T cell subsets remains unclear. *In vivo* and *in vitro* studies have shown that AEP regulates Foxp3 in mouse Treg cells and that AEP is specifically upregulated in mouse Treg and Th17 cells (Hou *et al.*, 2015; Stathopoulou *et al.*, 2018). Whether a similar mechanism exists in human Treg cells is unknown. There is evidence in the published literature that AEP is expressed and plays a role in human Th1 and Th17 cell function (Aschenbrenner *et al.*, 2018; Freeley *et al.*, 2018). Specifically, CD46 activation (the receptor for complement component C3b) has been shown to induce AEP expression in human $CD4^+$ T cells *in vitro* leading to the activation of cathepsin L (Freeley *et al.*, 2018). Cathepsin L further processes C3 into C3b thus activating CD46 in a positive feedback loop leading to IFN-γ production and the promotion of Th1 cell differentiation (Freeley *et al.*, 2018). Inhibition of AEP in $CD4^+$ T cells downregulated Th1 cell responses while it had no effect on Th2 cell responses *in vitro* (Freeley *et al.*, 2018). Notably, AEP inhibition in combination with CD3 and CD46 stimulation in $CD4^+$ T cells had a restrictive effect on Th17 cell responses (Freeley *et al.*, 2018). Consistent with the hypothesis of AEP regulating Th17 cell responses, transcriptome analysis of immunoregulatory IL-10^+ Th17 cells showed the upregulation of cMAF and AEP mRNA while this phenomenon was not observed in proinflammatory IL-10^- Th17 cells (Aschenbrenner *et al.*, 2018). This indicates that AEP may be regulating the Th17/Treg axis (Aschenbrenner *et al.*, 2018). Interestingly, transcriptome analysis of transduced human conventional T cells overexpressing GARP (receptor for the latent form of TGF-β) showed the induction of a Treg cell phenotype and function which correlated with the upregulation of FOXP3 and AEP (Probst-Kepper *et al.*, 2009). This lends support to the hypothesis that TGF-β plays a role in AEP expression in human T cells and that AEP expression is associated with FOXP3 and the Treg cell lineage. In addition, transduction of FOXP3 in conventional T cells led to the upregulation of AEP while transduction with AEP led to an increase of FOXP3 mRNA but not FOXP3 protein levels (Probst-Kepper *et al.*, 2009). This indicates that AEP regulates FOXP3 post-transcriptionally (Probst-Kepper *et al.*, 2009).

Therefore, it is here hypothesised that AEP is expressed in human Treg cells and that signalling mechanisms associated with establishing the Treg cell lineage regulate AEP expression.

4.2 Aims

This chapter focuses on characterising AEP expression in human Treg cells in more detail to identify signals that may regulate its expression *in vitro*. The hypothesis is that AEP is associated with the Treg cell lineage as AEP expression may regulate FOXP3 in human Treg cells. To characterise human Treg cell subsets for AEP expression, AEP expression was studied in:

- freshly isolated naïve and Treg cells and
- expanded Treg cells.

4.3 Results

4.3.1 *Phenotypic characterisation*

Treg cells from healthy human PBMCs were characterised by flow cytometry to determine their phenotype and frequency. This knowledge was subsequently used to estimate the amount of blood or number of PBMCs that was required for the extraction of adequate numbers of naïve and Treg cells to be used for western blots and cell culture. This experiment was also performed to determine the expression of particular co-receptors correlated with the Treg cell lineage which would also give an indication on whether any co-receptor signalling pathways may be interlinked with the AEP signalling pathway in human Treg cells.

Characterisation of human PBMCs showed that a significantly higher frequency of PD-1^+ T cells was found among the $FOXP3^+$ (4.21%) rather than in $FOXP3^-$ T cells (0.8%) (figure 4.1). This is in accordance with the published literature where PD-1 stimulation has been shown to promote Treg cell generation in mice as well as studies that have shown PD-1 regulating FOXP3 through AEP in mouse Treg cells (Francisco *et al.*, 2009; Stathopoulou *et al.*, 2018).

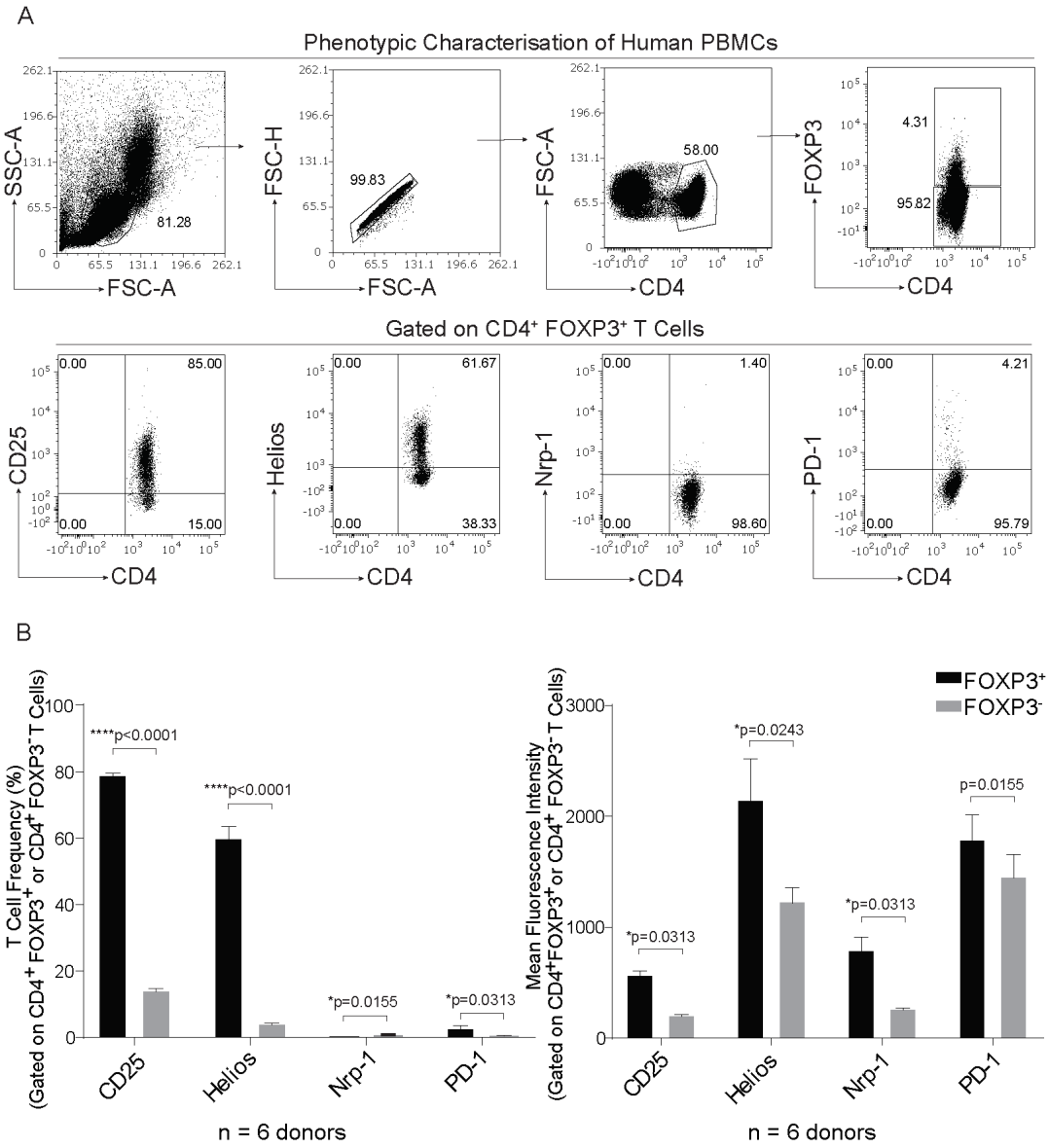

Figure 4.1 Phenotypic characterisation of human Treg cells. Human peripheral blood mononuclear cells (PBMCs) were characterised for CD4, CD25, FOXP3, Helios, Nrp-1 and PD-1 expression. **A.** Flow plots illustrating the gating strategy used for identifying Treg cells and expression of Helios, PD-1, Nrp-1 and CD25 within the $CD4^+$ $FOXP3^+$ T cell (Treg) population. **B.** Summary graphs of the T cell frequencies of positive cells (left) and mean fluorescence intensity values (right) for each marker within the $CD4^+FOXP3^+$ and $CD4^+FOXP3^-$ T cell populations. The Shapiro-Wilk normality test was used to confirm normal distribution of data. For normal distributions, a paired Student's t test was used. For non-normal distributions, the nonparametric Wilcoxon test was used. P values ≤0.05 were defined as statistically significant (n = 6 donors).

4.3.2 *Optimisation of AEP detection*

A titration experiment was then performed to optimise the concentration of the primary and secondary antibodies that were planned to be used for

detecting AEP expression on western blot membranes. It was decided that the concentration of 0.1 μg/ml for the primary polyclonal antibody and a 1:1000 dilution for the secondary Ab was to be used for future experiments (figure 4.2).

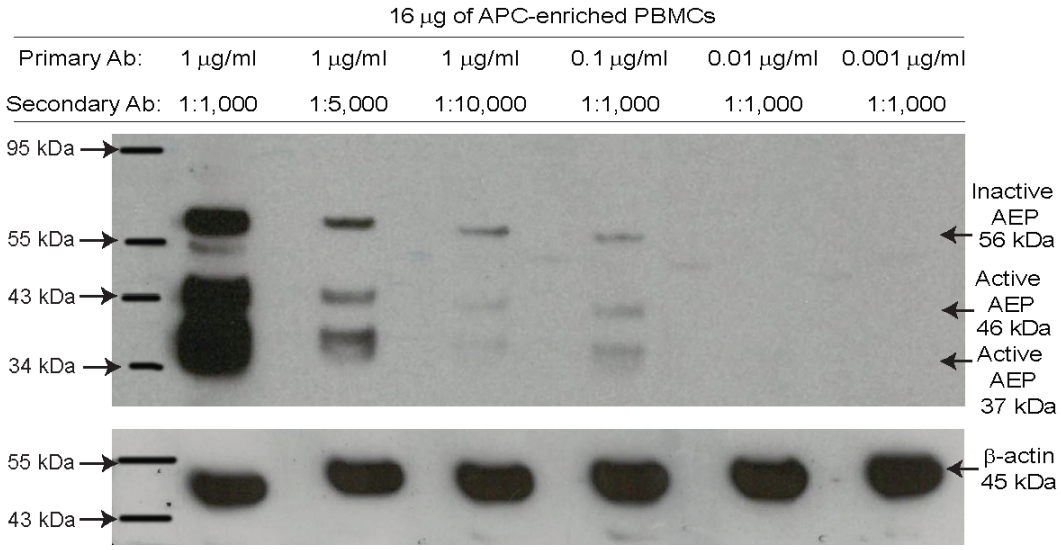

Figure 4.2 Optimisation of AEP detection via western blotting. A series of primary and secondary antibody concentrations were tested for AEP detection on western blots. The lysate were reduced and boiled and run under reducing conditions on a precast, 4-12% Bis-Tris gradient gel. Western blot image showing AEP expression in a lysate of APC-enriched PBMCs (leftover PBMCs following the isolation of $CD4^+$ T cells using the Miltenyi kit).

4.3.3 *AEP is expressed in freshly isolated $CD4^+CD25^-$ and $CD4^+CD25^+$ T cells*

AEP mRNA expression has been previously demonstrated in human T cell subsets (Beyer *et al.*, 2011; Schmidleithner *et al.*, 2019) (figure 4.3). Specifically, $CD4^+CD25^+$ T cells that were expanded *in vitro* showed significantly higher expression levels of AEP mRNA compared to freshly isolated naïve T cells and Treg cells ($p<0.0001$) (figure 4.3). However, little is known about AEP expression in human T cell subsets at protein level. In order to determine AEP expression in human naïve and Treg cells, PBMCs were isolated from the blood of healthy donors and the cell populations of interest were then sorted using the Miltenyi Treg isolation kit. This kit uses magnetic beads for the negative selection of naïve $CD4^+CD25^-$ T cells from a pre-enriched $CD4^+$ T cell population. Pre-enrichment occurs after depletion of platelets, erythrocytes, monocytes, granulocytes, epithelial cells, fibroblasts, haematopoietic progenitors, γ/δ T cells and activated lymphocytes and NK cells from the sample. The unwanted populations are stained with biotin-conjugated Abs for cell-specific markers and magnetic microbeads conjugated to anti-biotin Abs. Stained cells are captured and retained in the magnetic column allowing only the population of interest to pass through and get eluted. The eluted $CD4^+$ T cells are then labelled with microbeads conjugated to anti-CD25 antibodies and run through a separate column. The naïve $CD4^+CD25^-$ T cell population is eluted while the retained $CD4^+CD25^+$ population is manually flashed through the column to collect the Treg cell population.

Sorting of naïve T cells using the Miltenyi kit yielded purities of 92-95% (figure 4.4). As sorting of $CD4^+CD25^+$ T cells yielded a small number of cells (<200,000 cells), a purity test by means of flow cytometry was not possible. Membranes were probed for FOXP3 expression instead. The appearance of a double FOXP3 band indicates the presence of the two FOXP3 isoforms found in humans which is also consistent with the FOXP3 Ab data sheet. A large amount of debris was noted in the naïve T cell compartment in the first two donors which could potentially confound the results by giving false positives (figure 4.4A-B). The presence of platelets in the sorted populations was confirmed by microscopy. However, whether platelets express AEP

remains unknown. After optimisation of the lymphoprep protocol by adding extra washing steps to remove platelets, the amount of debris present in the third donor's PBMC sample was reduced. This was reflected in the fewer number of bands on the western blot (figure 4.4C**,** figure 4.5C). A minor contamination of the sorted naïve T cell population with $CD4^{+}CD25^{+}$ T cells was confirmed by the appearance of FOXP3 bands in the third donor (figure 4.5C). For this reason, only the results from the $CD4^{+}CD25^{+}$ T cells from the third donor were included in collective data analysis. In summary, western blot analysis of lysates from three separate donors suggests that both active and inactive AEP is expressed in freshly sorted naïve and Treg cells (figure 4.5).

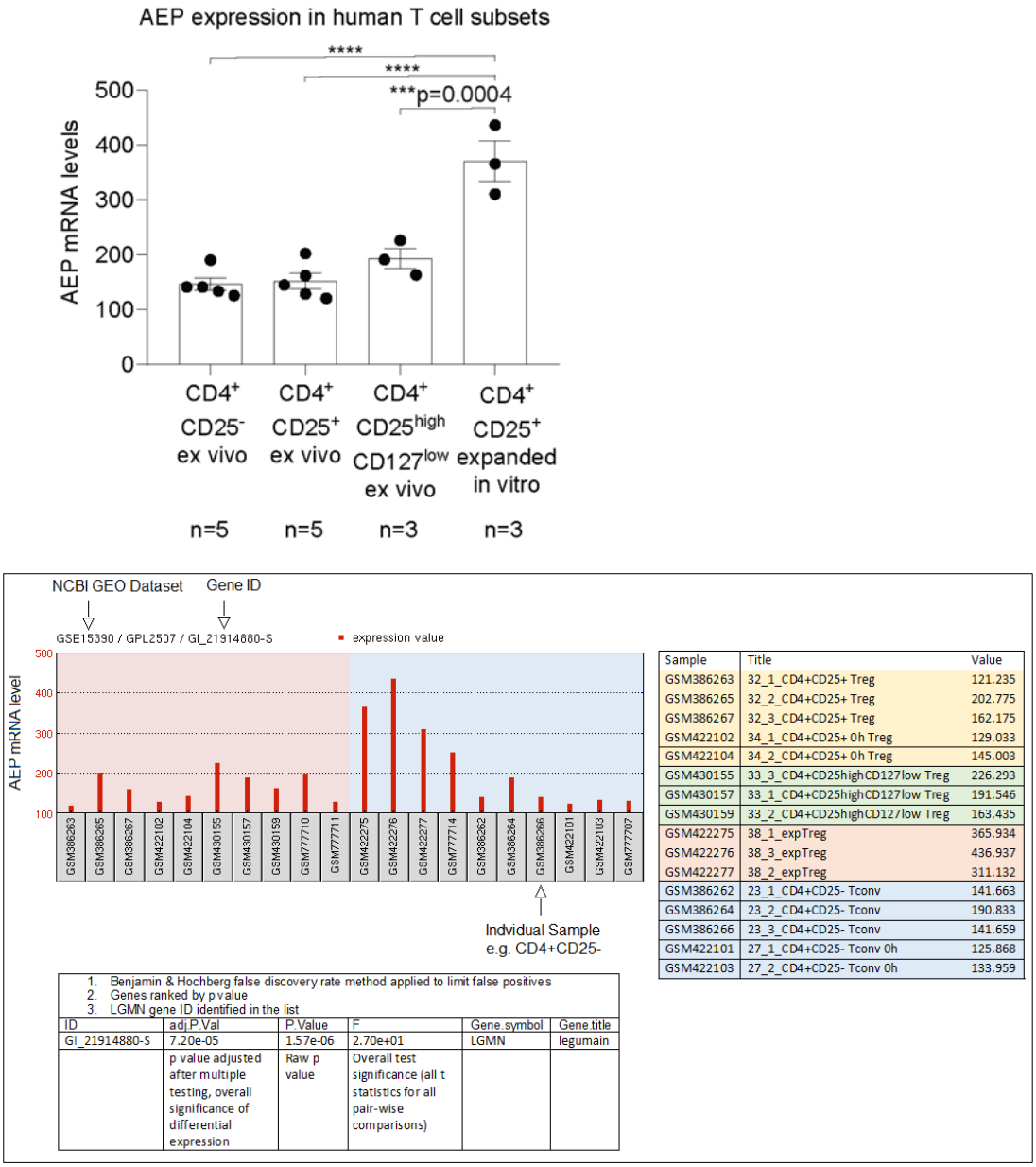

Figure 4.3 AEP mRNA expression in human T cell subsets (public data mining). Bar graph showing AEP mRNA levels in freshly isolated $CD4^+CD25^-$ (n=5), $CD4^+CD25^+$ (n=5) and $CD4^+CD25^+CD127^-$ (n=3) T cells as well as $CD4^+CD25^+$ T cells expanded *in vitro* (n=3). The Shapiro-Wilk normality test was used to confirm normal distribution of data. The One Way Anova test was used for variance analysis. P values ≤0.05 were defined as statistically significant. Dataset accession number: GSE15390. The layout of the data output is shown in the outlined panel below the main bar graph alongside descriptive annotations.

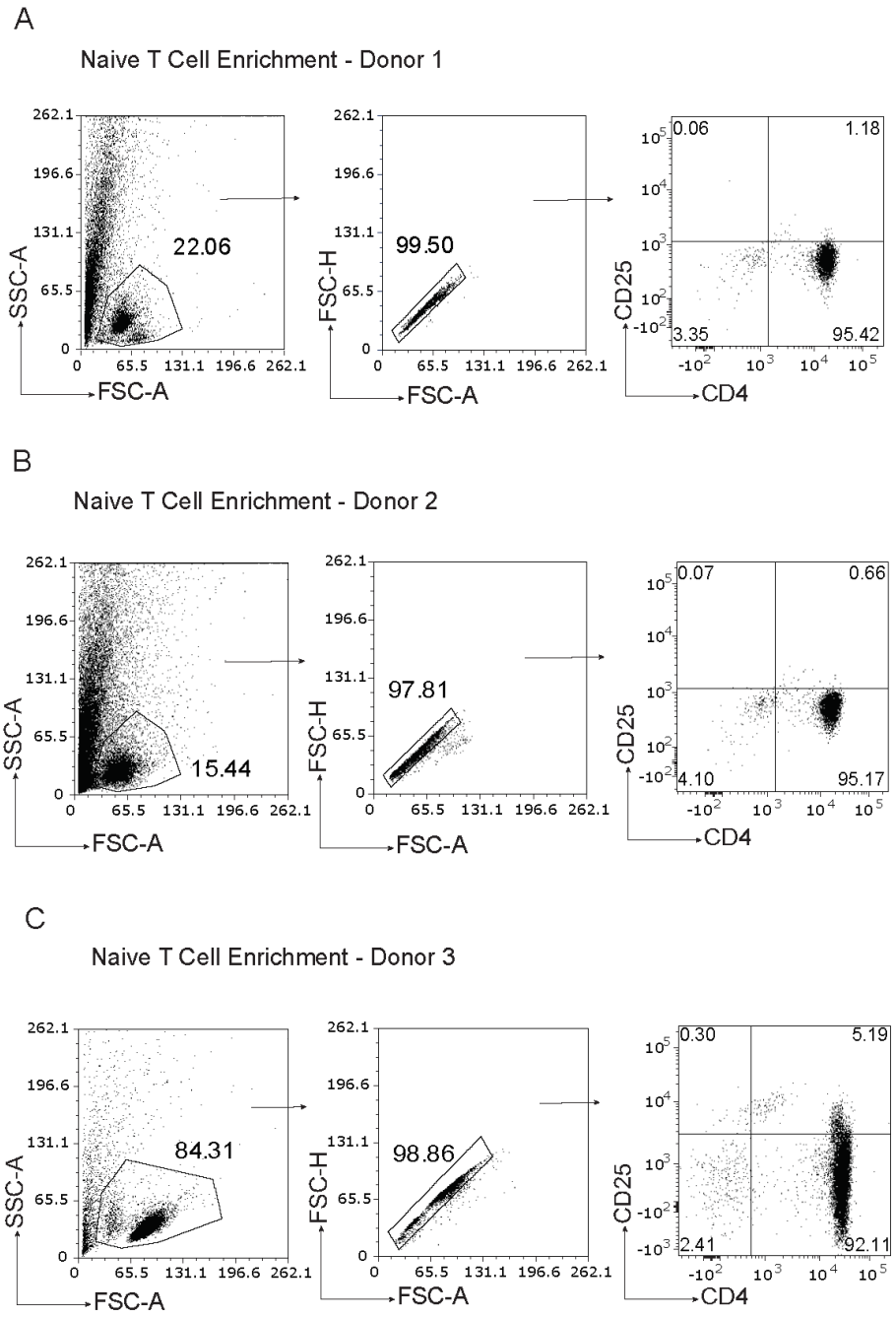

Figure 4.4 Purity test of Miltenyi-sorted naïve T cells. PBMCs were isolated from blood and $CD4^+CD25^-$ and $CD4^+CD25^+$ T cells were isolated using the Miltenyi kit. APC-enriched PBMCs (leftover PBMCs following the isolation of $CD4^+$ T cells using the Miltenyi kit) were used as positive controls for AEP expression. Following isolation, cells were characterised for CD4 and CD25 expression and then lysed using a lysis buffer that contained phenylmethanesulfonyl fluoride (PMSF lysis buffer) in preparation for protein analysis via western blotting. **A,B.** Flow plots showing enrichment/purity of the isolated naïve T cell population in donors 1 and 2 respectively. **C.** Flow plots showing enrichment/purity of the isolated naïve T cell population in donor 3. Cells were characterised for CD4 and CD25 expression only. n=3 donors.

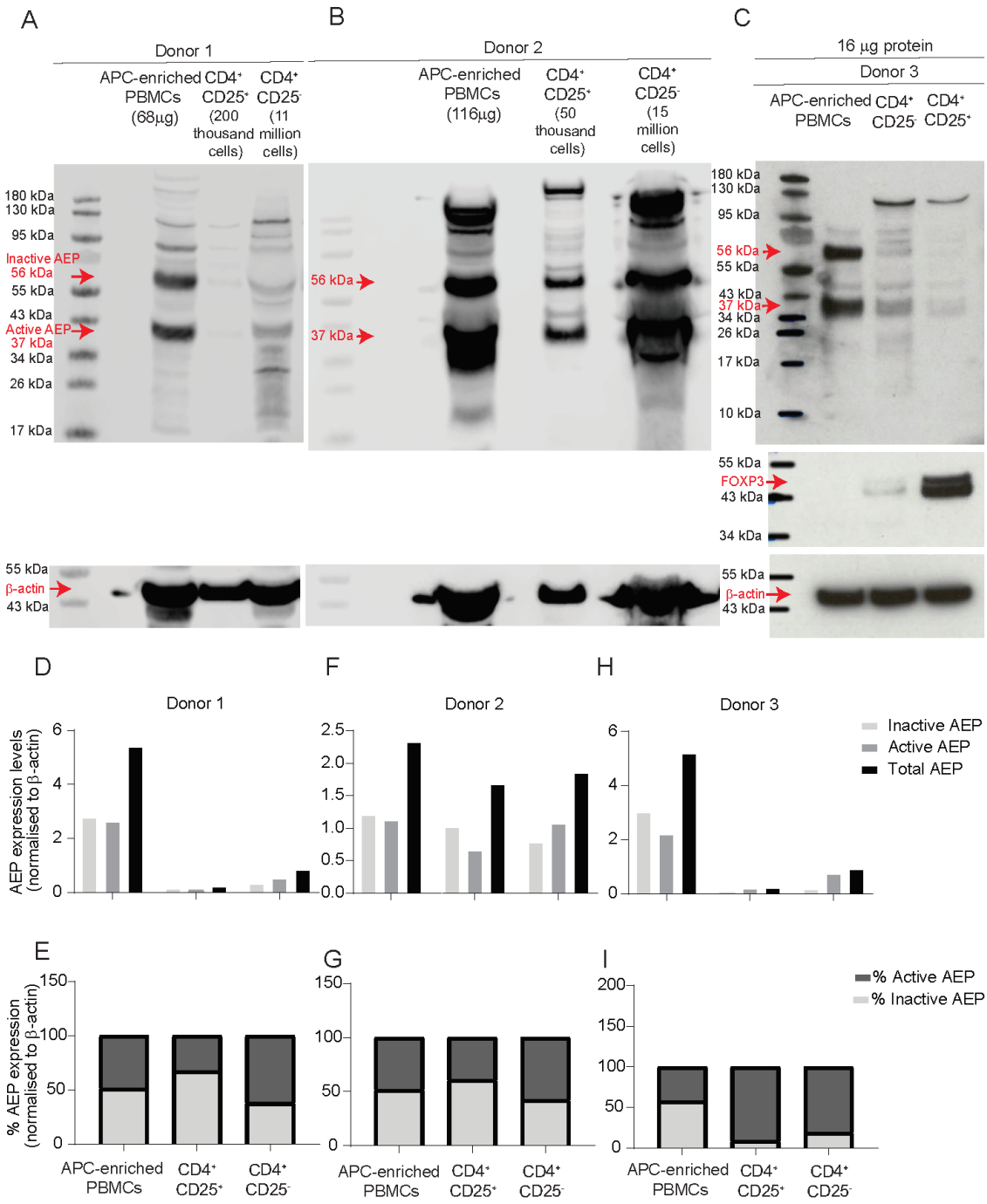
A
Donor 1
APC-enriched PBMCs (68µg)
CD4+ CD25+ (200 thousand cells)
CD4+ CD25- (11 million cells)
180 kDa
130 kDa
95 kDa
Inactive AEP
56 kDa
55 kDa
43 kDa
Active AEP
37 kDa
34 kDa
26 kDa
17 kDa
55 kDa
β-actin
43 kDa
B
Donor 2
APC-enriched PBMCs (116µg)
CD4+ CD25+ (50 thousand cells)
CD4+ CD25- (15 million cells)
56 kDa
37 kDa
55 kDa
β-actin
43 kDa
C
16 µg protein
Donor 3
APC-enriched PBMCs
CD4+ CD25-
CD4+ CD25+
180 kDa
130 kDa
95 kDa
56 kDa
55 kDa
43 kDa
37 kDa
34 kDa
26 kDa
17 kDa
10 kDa
55 kDa
FOXP3
43 kDa
34 kDa
55 kDa
β-actin
43 kDa
D
Donor 1
AEP expression levels (normalised to β-actin)
F
Donor 2
H
Donor 3
Inactive AEP
Active AEP
Total AEP
E
% AEP expression (normalised to β-actin)
APC-enriched PBMCs
CD4+ CD25+
CD4+ CD25-
G
I
% Active AEP
% Inactive AEP

Figure 4.5 AEP expression in Miltenyi-sorted naïve and $CD4^+CD25^+$ T cells. PBMCs were isolated from blood and $CD4^+CD25^-$ and $CD4^+CD25^+$ T cells were isolated using the Miltenyi kit. APC-enriched PBMCs (leftover PBMCs following the isolation of $CD4^+$ T cells using the Miltenyi kit) were used as positive controls for AEP expression. Following isolation, cells were characterised for CD4, CD25 and FOXP3 expression and then lysed using PMSF lysis buffer in preparation for protein analysis via western blotting. Lysates were reduced and boiled and run under reducing conditions on a precast, 4-12% Bis-Tris gradient gel. **A-C.** Western blot images showing AEP, FOXP3 and β-actin expression in each of the sorted populations in each donor. The 56 and 37 kDa AEP bands were quantified using ImageJ and normalised to the respective β-actin loading control bands. **D,F,H.** Bar graphs showing the expression levels of active, inactive and total AEP in each cell population in each donor. **E,G,I.** Bar graphs showing the percentage ratio of active and inactive AEP expressed in each cell population in each donor. n=3 donors.

4.3.4 *AEP is expressed in iTreg and expanded Treg cells*

Following these observations, induction of AEP expression was studied in expanded naïve and Treg cells from three separate donors. Cells were stimulated with combinations of cytokines in addition to TCR stimulation *in vitro* in order to identify the signalling pathways associated with the induction of AEP expression. $CD4^+CD25^-$ (naïve) and $CD4^+CD25^+$ (Treg) human T cells were sorted from human PBMCs using the Miltenyi kit (as described in sections 2.17 and 4.3.3) and cultured for 5 days in αCD3-coated plates (5 μg/ml) in the presence of αIL-4 (10 μg/ml) and αIFN-γ (10 μg/ml) with the addition of αCD28 (2 μg/ml), rhIL-2 (100 ng/ml) and rhTGF-β1 (5 ng/ml) where appropriate. Cells were expanded for an additional 7 days in the presence of rhIL-2 which was added every 2 days and then harvested on day 12 using a RIPA-based lysis buffer.

In donor 1, culturing naïve T cells under iTreg conditions induced the highest levels of total, active and inactive AEP out of all conditions (figure 4.6). In addition, $CD4^+CD25^+$ T cells cultured under iTreg conditions were the only ones that expressed more active AEP than inactive AEP (figure 4.6). The highest levels of active AEP were noted in cells cultured under iTreg conditions suggesting that TGF-β1 induced the highest level of AEP expression although TCR activation and IL-2 stimulation also induced its expression which is in accordance with the published literature (Freeley *et al.*, 2018).

In donor 2, a similar pattern of T cell expansion was observed however, since no FOXP3 expression was detected in cells that were cultured under iTreg conditions, these data were excluded from the analysis (figure 4.7).

In donor 3, the cell expansion pattern was consistent with the previous two donors, however, no FOXP3 expression was noted in the iTreg population (figure 4.8). The reason for this could be multifactorial associated with technical alterations or the donor cells could have been suboptimal. For instance, cell expansion in this donor was suboptimal compared to donor 1 (expansion graph in figure 4.6E). Cultured $CD4^{+}CD25^{+}$ T cells showed the highest levels of AEP expression including active and inactive AEP (figure 4.8). They were also the only ones that expressed more active AEP than inactive AEP which is consistent with donor1 (figure 4.6 and 4.8). This provides further support to the hypothesis that TGF-$\beta 1$ induces the highest level of total AEP expression in human T cells.

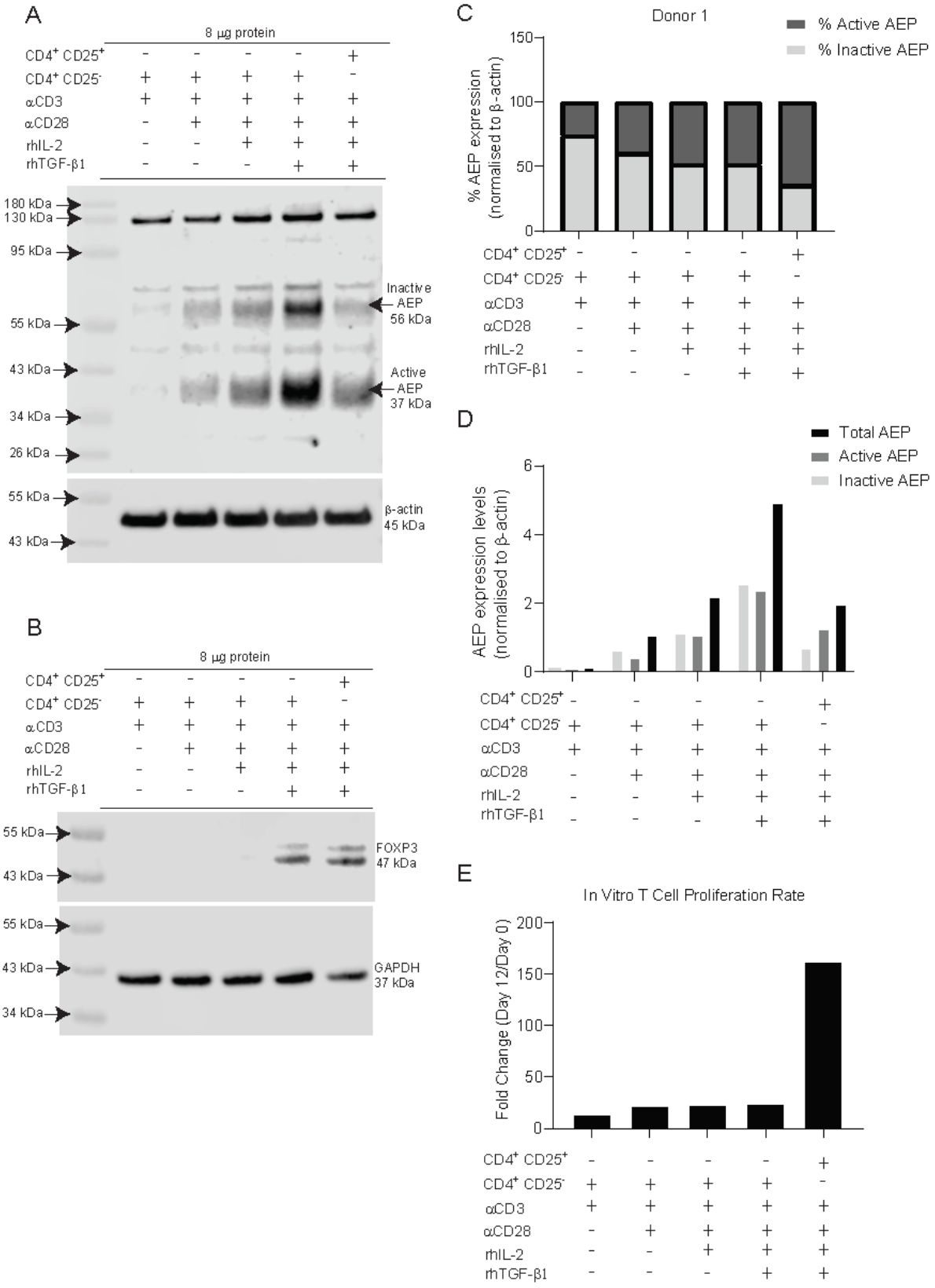
A
8 µg protein
CD4+ CD25+
CD4+ CD25-
αCD3
αCD28
rhIL-2
rhTGF-β1
180 kDa
130 kDa
95 kDa
55 kDa
43 kDa
34 kDa
26 kDa
Inactive AEP 56 kDa
Active AEP 37 kDa
55 kDa
43 kDa
β-actin 45 kDa
B
8 µg protein
55 kDa
43 kDa
FOXP3 47 kDa
55 kDa
43 kDa
34 kDa
GAPDH 37 kDa
C
Donor 1
% Active AEP
% Inactive AEP
% AEP expression (normalised to β-actin)
150
100
50
0
D
Total AEP
Active AEP
Inactive AEP
AEP expression levels (normalised to β-actin)
6
4
2
0
E
In Vitro T Cell Proliferation Rate
Fold Change (Day 12/Day 0)
200
150
100
50
0

Figure 4.6 AEP expression in expanded human iTreg cells *in vitro* - Donor 1. $CD4^+CD25^-$ and $CD4^+CD25^+$ T cells were isolated from human PBMCs using the Miltenyi Treg isolation kit. Cells were cultured *in vitro* at 1 million cells/ml for 5 days in αCD3-coated plates (5 μg/ml) in the presence of αIL-4 (10 μg/ml) and αIFN-γ (10 μg/ml) with the addition of αCD28 (2 μg/ml), rhIL-2 (100 ng/ml) and rhTGF-β1 (5 ng/ml) where appropriate. Cells were expanded for an additional 7 days in the presence of rhIL-2 which was added every 2 days and then harvested on day 12 using RIPA lysis buffer in preparation for protein analysis via western blotting. Lysates were reduced and boiled and run under reducing conditions on a precast, 4-12% Bis-Tris gradient gel. **A.** Western blot image showing AEP expression in each of the culture conditions. **B.** Stripped and re-probed western blot membrane was imaged for FOXP3 expression in each of the culture conditions. **C.** Bar graph showing the percentage ratio of active and inactive AEP expressed in each of the culture conditions. The 56 and 37 kDa AEP bands were quantified using ImageJ. The active and inactive AEP bands were normalised to β-actin and the normalised values were divided by the total AEP and then multiplied by 100. **D.** Bar graph showing the expression levels of active, inactive and total AEP in each of the conditions. Bands were normalised to β-actin. **E.** Bar graph showing the rate of T cell expansion at the end of the culture. The expansion rate is presented as a fold change in number of cells at the end of culture (day 12) divided by the initial number of plated cells (day 0). n =1 donor.

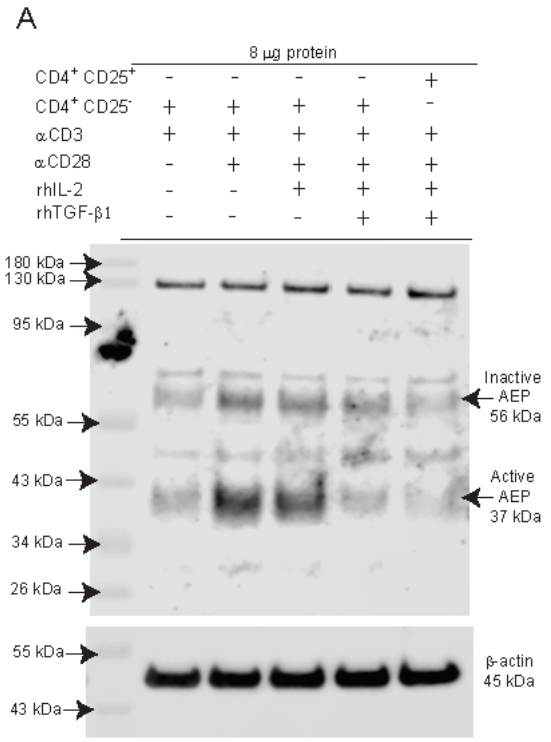
A
8 µg protein
CD4+ CD25+
CD4+ CD25-
αCD3
αCD28
rhIL-2
rhTGF-β1
180 kDa
130 kDa
95 kDa
55 kDa
43 kDa
34 kDa
26 kDa
Inactive AEP 56 kDa
Active AEP 37 kDa
55 kDa
43 kDa
β-actin 45 kDa

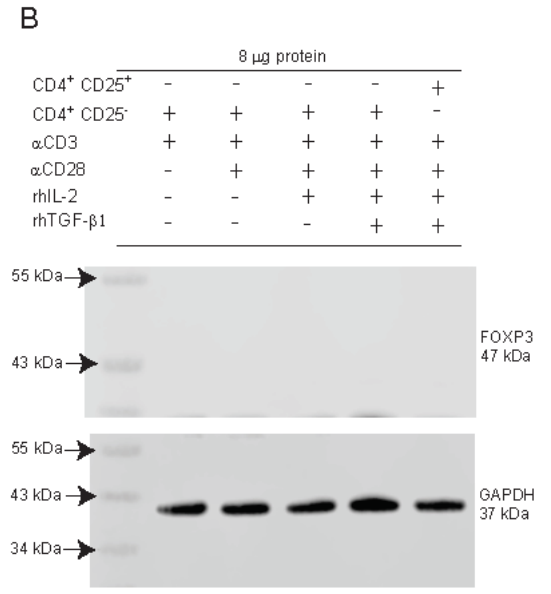
B
8 µg protein
CD4+ CD25+
CD4+ CD25-
αCD3
αCD28
rhIL-2
rhTGF-β1
55 kDa
43 kDa
FOXP3 47 kDa
55 kDa
43 kDa
34 kDa
GAPDH 37 kDa

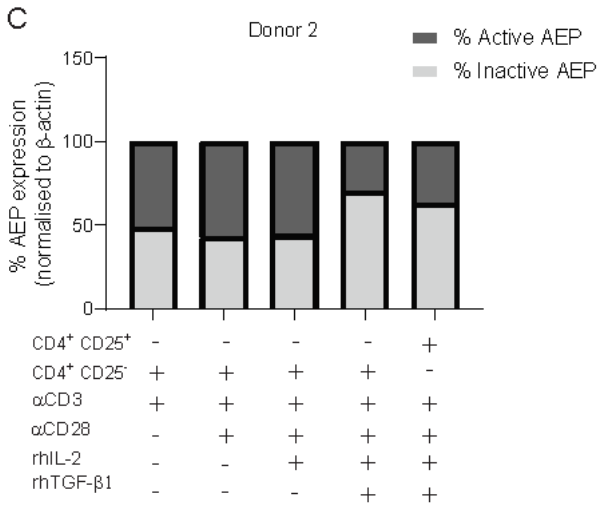
C
Donor 2
% Active AEP
% Inactive AEP
% AEP expression (normalised to β-actin)
150
100
50
0
CD4+ CD25+
CD4+ CD25-
αCD3
αCD28
rhIL-2
rhTGF-β1

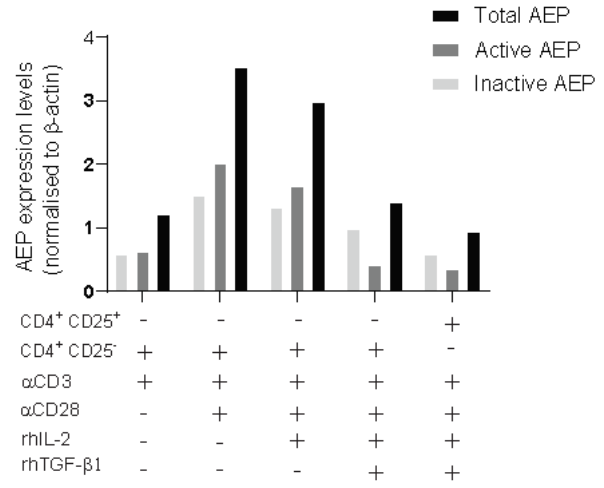
D
Total AEP
Active AEP
Inactive AEP
AEP expression levels (normalised to β-actin)
4
3
2
1
0
CD4+ CD25+
CD4+ CD25-
αCD3
αCD28
rhIL-2
rhTGF-β1

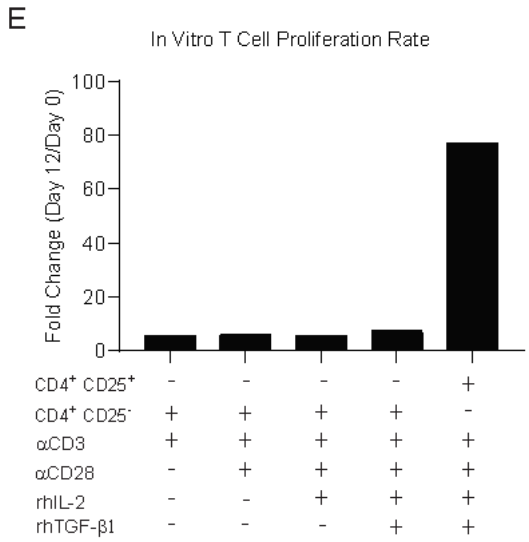
E
In Vitro T Cell Proliferation Rate
Fold Change (Day 12/Day 0)
100
80
60
40
20
0
CD4+ CD25+
CD4+ CD25-
αCD3
αCD28
rhIL-2
rhTGF-β1

Figure 4.7 AEP expression in expanded human iTreg cells *in vitro* - Donor 2. $CD4^+CD25^-$ and $CD4^+CD25^+$ T cells were isolated from human PBMCs using the Miltenyi Treg isolation kit. Cells were cultured *in vitro* at 1 million cells/ml for 5 days in αCD3-coated plates (5 μg/ml) in the presence of αIL-4 (10 μg/ml) and αIFN-γ (10 μg/ml) with the addition of αCD28 (2 μg/ml), rhIL-2 (100 ng/ml) and rhTGF-β1 (5 ng/ml) where appropriate. Cells were expanded for an additional 7 days in the presence of rhIL-2 which was added every 2 days and then harvested on day 12 using RIPA lysis buffer in preparation for protein analysis via western blotting. Lysates were reduced and boiled and run under reducing conditions on a precast, 4-12% Bis-Tris gradient gel. **A.** Western blot image showing AEP expression in each of the culture conditions. **B.** Stripped and re-probed western blot membrane was imaged for FOXP3 expression in each of the culture conditions. **C.** Bar graph showing the percentage ratio of active and inactive AEP expressed in each of the culture conditions. The 56 and 37 kDa AEP bands were quantified using ImageJ. The active and inactive AEP bands were normalised to β-actin and the normalised values were divided by the total AEP and then multiplied by 100. **D.** Bar graph showing the expression levels of active, inactive and total AEP in each of the conditions. Bands were normalised to β-actin. **E.** Bar graph showing the rate of T cell expansion at the end of the culture. The expansion rate is presented as a fold change in number of cells at the end of culture (day 12) divided by the initial number of plated cells (day 0). n =1 donor.

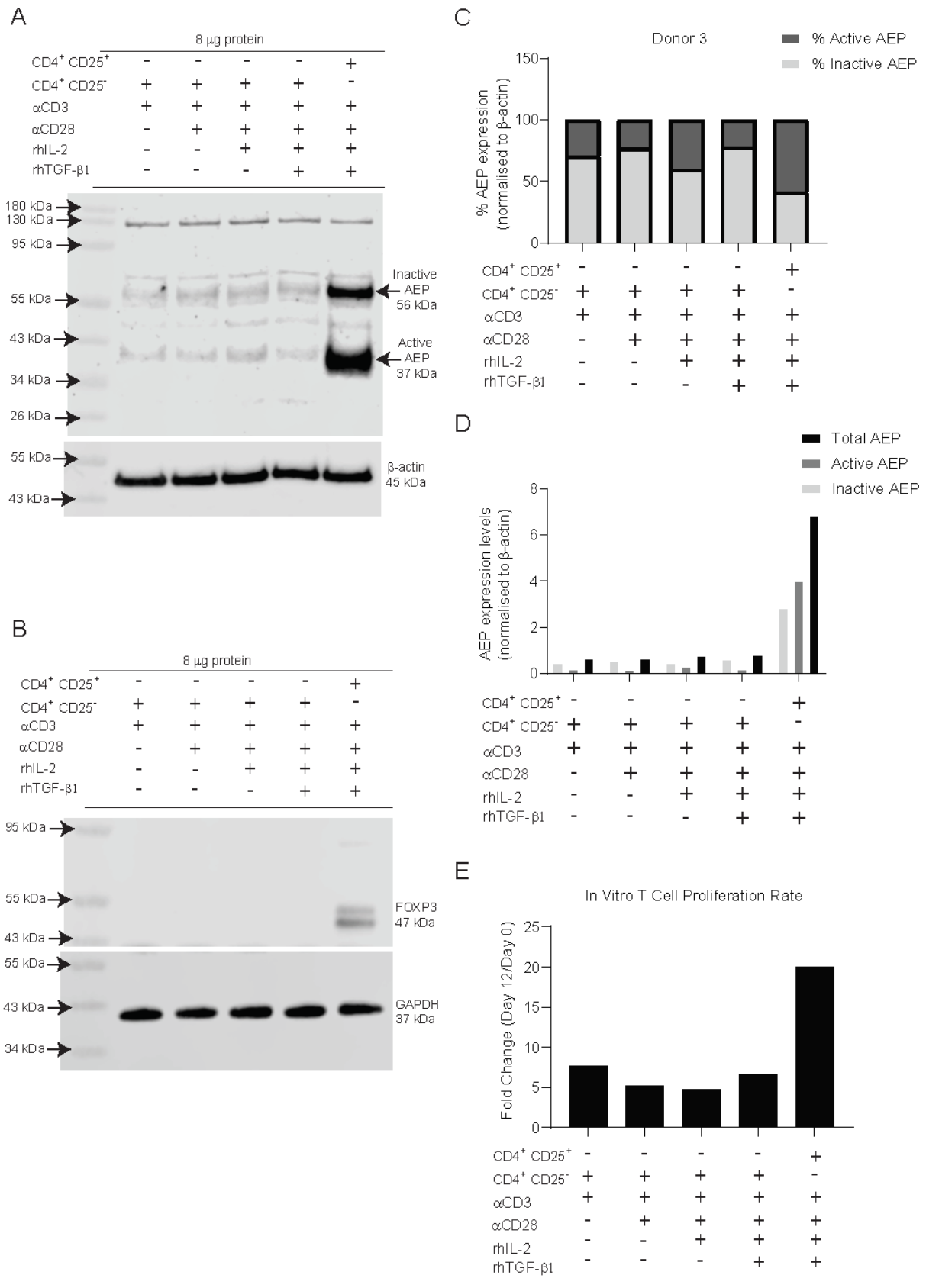
A
8 µg protein
CD4+ CD25+
CD4+ CD25-
αCD3
αCD28
rhIL-2
rhTGF-β1
180 kDa
130 kDa
95 kDa
55 kDa
43 kDa
34 kDa
26 kDa
Inactive AEP 56 kDa
Active AEP 37 kDa
55 kDa
43 kDa
β-actin 45 kDa
B
8 µg protein
95 kDa
55 kDa
43 kDa
FOXP3 47 kDa
GAPDH 37 kDa
34 kDa
C
Donor 3
% Active AEP
% Inactive AEP
% AEP expression (normalised to β-actin)
D
Total AEP
Active AEP
Inactive AEP
AEP expression levels (normalised to β-actin)
E
In Vitro T Cell Proliferation Rate
Fold Change (Day 12/Day 0)

Figure 4.8 AEP expression in expanded human iTreg cells *in vitro* - Donor 3. $CD4^+CD25^-$ and $CD4^+CD25^+$ T cells were isolated from human PBMCs using the Miltenyi Treg isolation kit. Cells were cultured *in vitro* at 1 million cells/ml for 5 days in αCD3-coated plates (5 μg/ml) in the presence of αIL-4 (10 μg/ml) and αIFN-γ (10 μg/ml) with the addition of αCD28 (2 μg/ml), rhIL-2 (100 ng/ml) and rhTGF-β1 (5 ng/ml) where appropriate. Cells were expanded for an additional 7 days in the presence of rhIL-2 which was added every 2 days and then harvested on day 12 using RIPA lysis buffer in preparation for protein analysis via western blotting. Lysates were reduced and boiled and run under reducing conditions on a precast, 4-12% Bis-Tris gradient gel. **A.** Western blot image showing AEP expression in each of the culture conditions. **B.** Stripped and re-probed western blot membrane was imaged for FOXP3 expression in each of the culture conditions. **C.** Bar graph showing the percentage ratio of active and inactive AEP expressed in each of the culture conditions. The 56 and 37 kDa AEP bands were quantified using ImageJ. The active and inactive AEP bands were normalised to β-actin and the normalised values were divided by the total AEP and then multiplied by 100. **D.** Bar graph showing the expression levels of active, inactive and total AEP in each of the conditions. Bands were normalised to β-actin. **E.** Bar graph showing the rate of T cell expansion at the end of the culture. The expansion rate is presented as a fold change in number of cells at the end of culture (day 12) divided by the initial number of plated cells (day 0). n =1 donor.

4.3.5 *AEP is expressed in freshly isolated $CD4^+CD25^-CD127^+CD45RA^+$ and $CD4^+CD25^{high}CD127^{low}$ T cells*

In order to validate the data obtained from the populations sorted using the Miltenyi kit, a more stringent sorting technique was used. Here, naïve and Treg cells were sorted from 74 – 88 million PBMCs using a FACS sorting machine based on expression of multiple markers namely CD4, CD25, CD127 and CD45RA. Monocytes, B cells and NK cells were effectively gated out. For these experiments, $CD4^+CD25^-CD127^+CD45RA^+$ were characterised as naïve while $CD4^+CD25^{high}CD127^{low}$ T cells were characterised as Treg cells. Sorting of naïve T cells using this methodology yielded purities of 96% or higher with frequencies of cell populations being similar across all three donors (figure 4.9). As sorting of Treg cells yielded a small number of cells, a purity test by means of flow cytometry was not possible (~300,000 cells). Membranes were probed for FOXP3 expression instead (figure 4.10). In accordance with previous experiments shown in figure 4.5, active and inactive AEP was detected in both naïve and Treg cells in all three donors (figure 4.10). In addition, naïve T cells consistently

expressed mostly inactive AEP with some active AEP detected but its expression levels were significantly less than in positive controls (figure 4.10). A strong 32kDa band was uniquely detected in the Treg population which indicates the presence of active AEP (figure 4.10). This potentially indicates a Treg-specific AEP peptide that has undergone further processing by other lysosomal proteases as autocatalytic processing has been reported to yield band sizes of up to 37/36 kDa in size (Li *et al.*, 2003). This idea is reinforced by the fact that sorted Treg cells expressed less active AEP that was 37 kDa in size than both naïve T cells and the positive controls indicating a Treg-specific processing mechanism of AEP (figure 4.10). Furthermore, this 32kDa band seems to disappear upon culturing these cells under iTreg conditions *in vitro* as shown in figures 4.12, 4.17, 4.19, 4.21 and 4.25. Sorted Treg cells expressed the highest amounts of inactive AEP out of all the sorted populations (figure 4.10). The fact that FOXP3 expression was only detected in Treg cells, eliminates the possibility that activated naïve T cells or Treg cells contaminated the sorted naïve T cell population (figure 4.10). Also, the absence of a strong 37kDa band in the naïve and Treg populations indicates that there is no contamination with any $CD4^-$ lymphocytes that in this case were used as positive controls (figure 4.10). These data have been observed in all three donors (figure 4.10). In conclusion, AEP expression was confirmed in both naïve and human Treg cells with different active to inactive AEP ratios observed in each population.

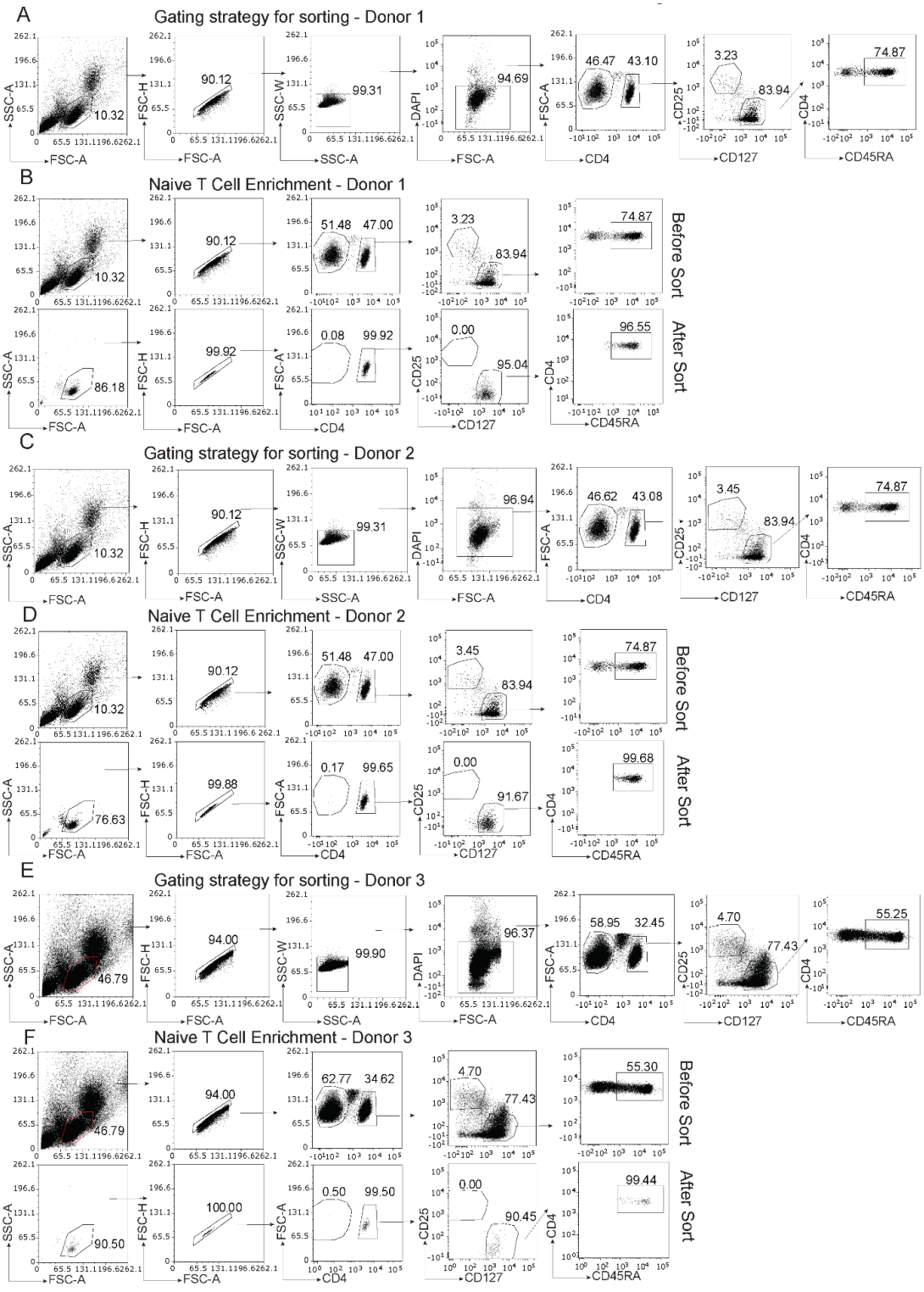
A
Gating strategy for sorting - Donor 1
10.32
90.12
99.31
94.69
46.47
43.10
3.23
83.94
74.87
B
Naive T Cell Enrichment - Donor 1
10.32
90.12
51.48
47.00
3.23
83.94
74.87
Before Sort
86.18
99.92
0.08
99.92
0.00
95.04
96.55
After Sort
C
Gating strategy for sorting - Donor 2
10.32
90.12
99.31
96.94
46.62
43.08
3.45
83.94
74.87
D
Naive T Cell Enrichment - Donor 2
10.32
90.12
51.48
47.00
3.45
83.94
74.87
Before Sort
76.63
99.88
0.17
99.65
0.00
91.67
99.68
After Sort
E
Gating strategy for sorting - Donor 3
46.79
94.00
99.90
96.37
58.95
32.45
4.70
77.43
55.25
F
Naive T Cell Enrichment - Donor 3
46.79
94.00
62.77
34.62
4.70
77.43
55.30
Before Sort
90.50
100.00
0.50
99.50
0.00
90.45
99.44
After Sort
SSC-A
FSC-A
FSC-H
SSC-W
SSC-A
DAPI
FSC-A
CD4
CD25
CD127
CD4
CD45RA

Figure 4.9 Purity test of sorted naïve T cells. PBMCs were isolated from blood and $CD4^+CD25^-CD127^+CD45RA^+$ (naïve) and $CD4^+CD25^{high}CD127^{low}$ T cells were isolated using cell sorting. $CD4^-$ lymphocytes were also sorted to be used as positive controls for AEP expression. PBMCs were counted and stained with CD4-FITC, CD25-APC, CD127-PE.CY7, CD45RA-PE and DAPI in Miltenyi buffer prior to sorting. Following sorting, cells were lysed using PMSF lysis buffer in preparation for protein analysis via western blotting. **A,C,E.** Flow plots illustrating the gating strategy used for sorting $CD4^-$ lymphocytes, $CD4^+CD25^-CD127^+CD45RA^+$ and $CD4^+CD25^{high}CD127^{low}$ T cells from donors 1, 2 and 3 respectively. **B,D,F.** Flow plots showing enrichment/purity of the naïve T cell population before and after cell sorting in donors 1, 2 and 3 respectively. n=3 donors.

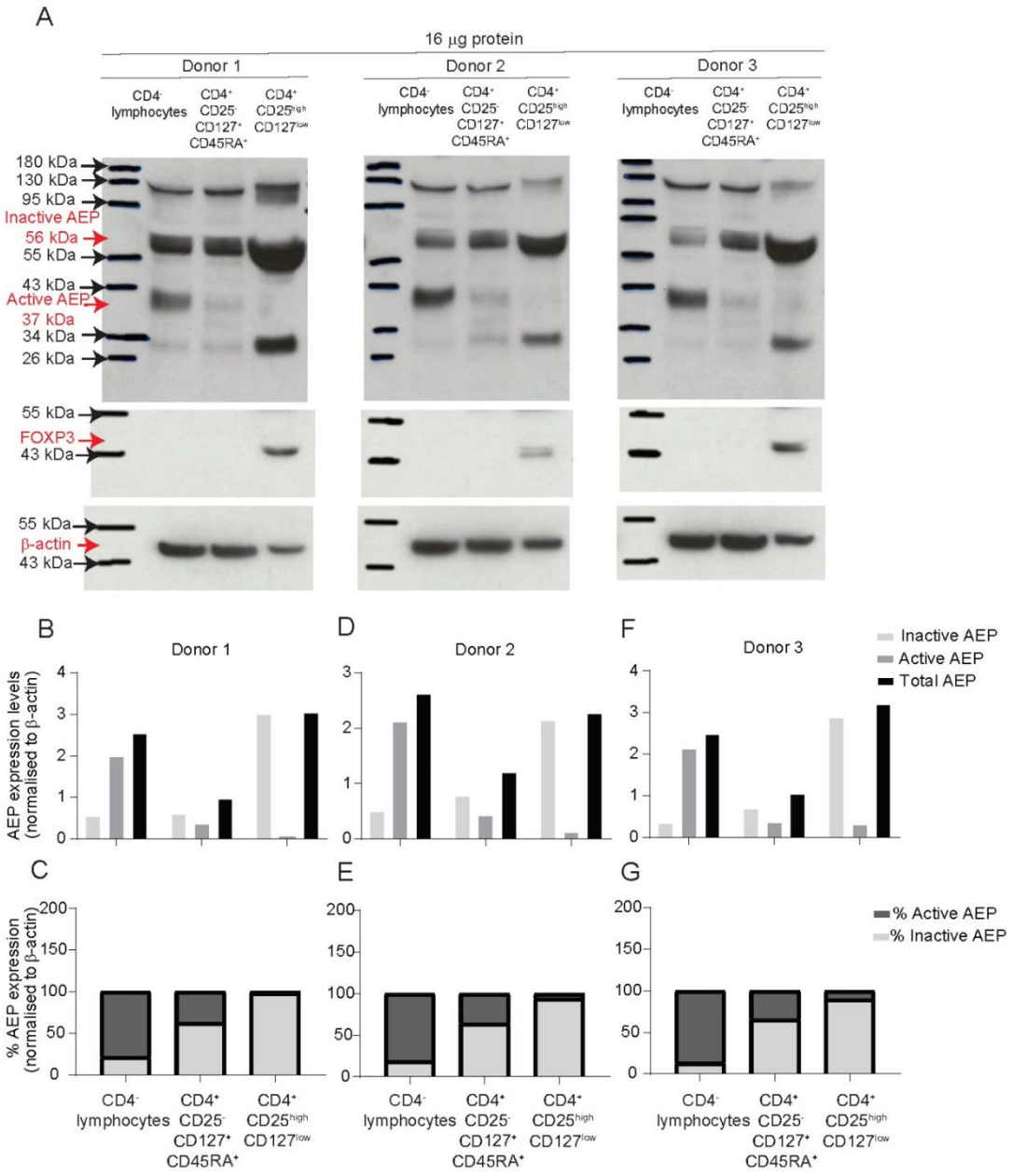
A
16 µg protein
Donor 1
Donor 2
Donor 3
CD4- lymphocytes
CD4+ CD25- CD127+ CD45RA+
CD4+ CD25high CD127low
180 kDa
130 kDa
95 kDa
Inactive AEP
56 kDa
55 kDa
43 kDa
Active AEP
37 kDa
34 kDa
26 kDa
55 kDa
FOXP3
43 kDa
55 kDa
β-actin
43 kDa
B
D
F
Donor 1
Donor 2
Donor 3
Inactive AEP
Active AEP
Total AEP
AEP expression levels (normalised to β-actin)
C
E
G
% AEP expression (normalised to β-actin)
% Active AEP
% Inactive AEP

Figure 4.10 AEP expression in sorted naïve and $CD4^+CD25^{high}CD127^{low}$ T cells. PBMCs were isolated from blood and $CD4^+CD25^-CD127^+CD45RA^+$ (naïve) and $CD4^+CD25^{high}CD127^{low}$ T cells were isolated using cell sorting. $CD4^-$ lymphocytes were also sorted to be used as positive controls for AEP expression. Following sorting, cells were lysed using PMSF lysis buffer in preparation for protein analysis via western blotting. Lysates were reduced and boiled and run under reducing conditions on a precast, 4-12% Bis-Tris gradient gel. **A.** Western blot image showing AEP, FOXP3 and β-actin expression in each of the sorted populations. The 56 and 37 kDa AEP bands were quantified using ImageJ and normalised to the respective β-actin loading control bands. **B,D,F.** Bar graphs showing the expression levels of active, inactive and total AEP in each cell population in each donor. **C,E,G.** Bar graphs showing the percentage ratio of active and inactive AEP expressed in each cell population in each donor. The active and inactive AEP bands were normalised to β-actin and the normalised values were divided by the total AEP and then multiplied by 100. n=3 donors.

4.3.6 *AEP is expressed in iTreg and expanded Treg cells*

In order to validate data obtained from the expanded populations that were sorted using the Miltenyi kit, populations from 7 different donors (donors 4-10) were sorted using the methodology described above and stimulated with combinations of cytokines and stimulatory molecules *in vitro* in order to identify the signalling pathways associated with the induction of AEP expression. Cells were cultured for 5 days in αCD3-coated plates (5 μg/ml) in the presence of αIL-4 (10 μg/ml) and αIFN-γ (10 μg/ml) with the addition of αCD28 (2 μg/ml), rhIL-2 (100 ng/ml) and rhTGF-β1 (5 ng/ml) where appropriate. Cells were expanded for an additional 7 days in the presence of rhIL-2 which was added every 2 days and then harvested on day 12 using either a RIPA-based or PMSF-based lysis buffer. FOXP3 expression was confirmed on Day 12 by flow cytometry and western blotting.

In donor 4, naïve and Treg cells were isolated from human PBMCs based on CD4 and CD25 expression using FACS sorting which allowed the selection for high CD25 expression for the isolation of Treg cells. At the end of the culture, only 20% of iTreg cells were FOXP3 positive while no FOXP3 expression was detected on WB membranes (figure 4.11**,** figure 4.12). For this reason, this condition was excluded from the analysis. Sorted Treg cells that were cultured under iTreg conditions expanded the least out of all the conditions (1.45-fold change) (figure 4.12D). Although there was not enough

Treg cells on day 12 for flow cytometry (20,000 cells), FOXP3 expression was detected by western blotting (figure 4.12A). In an effort to increase band intensity, a higher amount of protein was used but that failed to increase band intensity (figure 4.12B). When lysates were acetone precipitated, band intensity was increased (figure 4.12C). Only the non-acetone precipitated lysates were used for the analysis (figure 4.12A). As seen in figures 4.6 and 4.8, the highest level of total AEP expression seemed to be induced by TGF-β1 (figure 4.12). As confirmation of the role of TGF-β1 in activation of AEP, the role of IL-2 stimulation was next assessed to see whether AEP expression levels would go up. Therefore, at the end of the culture, cells from each condition (apart from Treg cells) were stimulated with IL-2 for 15, 30 and 60 minutes (figure 4.13). This experiment showed that IL-2 did not play a role in inducing AEP as AEP expression levels did not increase following stimulation with IL-2 (figure 4.13).

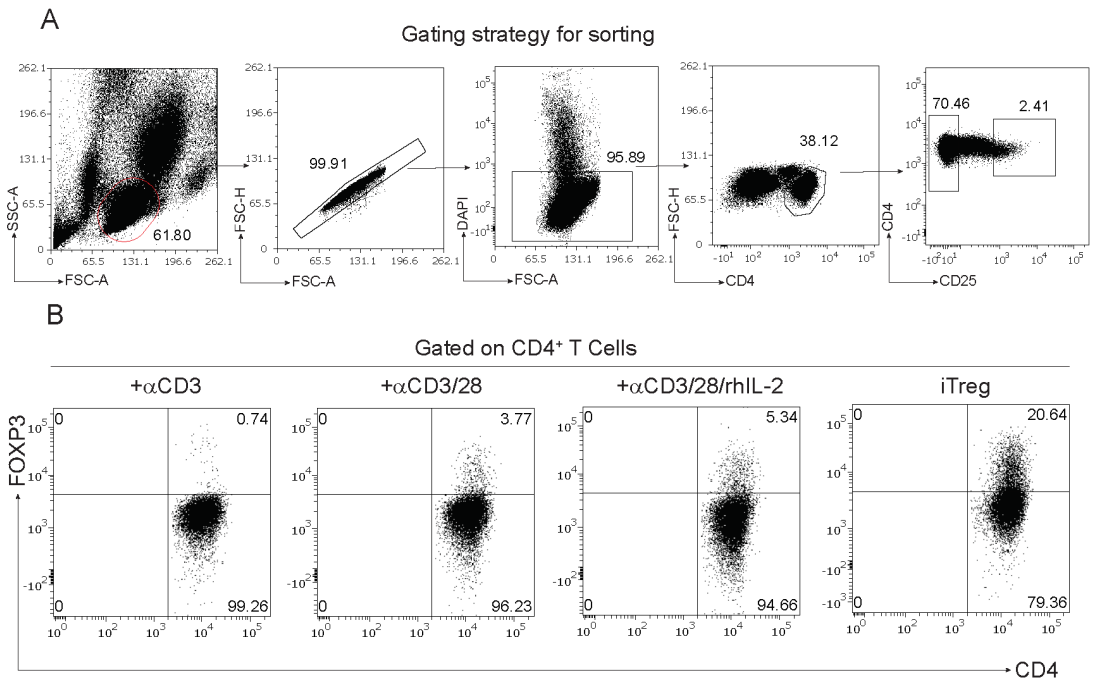
A
Gating strategy for sorting
SSC-A
FSC-A
61.80
FSC-H
99.91
DAPI
95.89
38.12
CD4
70.46
2.41
CD25
B
Gated on CD4⁺ T Cells
+αCD3
+αCD3/28
+αCD3/28/rhIL-2
iTreg
FOXP3
0.74
99.26
3.77
96.23
5.34
94.66
20.64
79.36
CD4
C
Donor 4
% CD4⁺ FOXP3⁺ T Cells (Gated on CD4⁺ T cells)
CD4⁺ CD25⁻
αCD3
αCD28
rhIL-2
rhTGF-β1

Figure 4.11 FOXP3 expression in expanded iTreg cells - Donor 4. $CD4^+CD25^-$ and $CD4^+CD25^{high}$ T cells were isolated from human PBMCs using a cell sorter. PBMCs were counted and stained with CD4-FITC, CD25-APC and DAPI in Miltenyi buffer prior to sorting. Following sorting, cells were cultured *in vitro* at 0.5 million cells/ml for 5 days in αCD3-coated plates (5 μg/ml) in the presence of αIL-4 (10 μg/ml) and αIFN-γ (10 μg/ml) with the addition of αCD28 (2 μg/ml), rhIL-2 (100 ng/ml) and rhTGF-β1 (5 ng/ml) where appropriate. Cells were expanded for an additional 7 days in the presence of rhIL-2 which was added every 2 days. On day 12, cells from each condition were characterised for CD4 and FOXP3 expression. The rest were harvested using RIPA lysis buffer in preparation for protein analysis via western blotting. **A.** Flow plots illustrating the gating strategy used for sorting $CD4^+CD25^-$ and $CD4^+CD25^{high}$ T cells. **B.** Flow plots showing the frequency of $CD4^+FOXP3^+$ present within the $CD4^+$ T cell population in each culture condition on day 12. **C.** Bar graph showing the percentage frequency of $CD4^+FOXP3^+$ T cells in each culture condition (gated on $CD4^+$ T cells). n =1 donor.

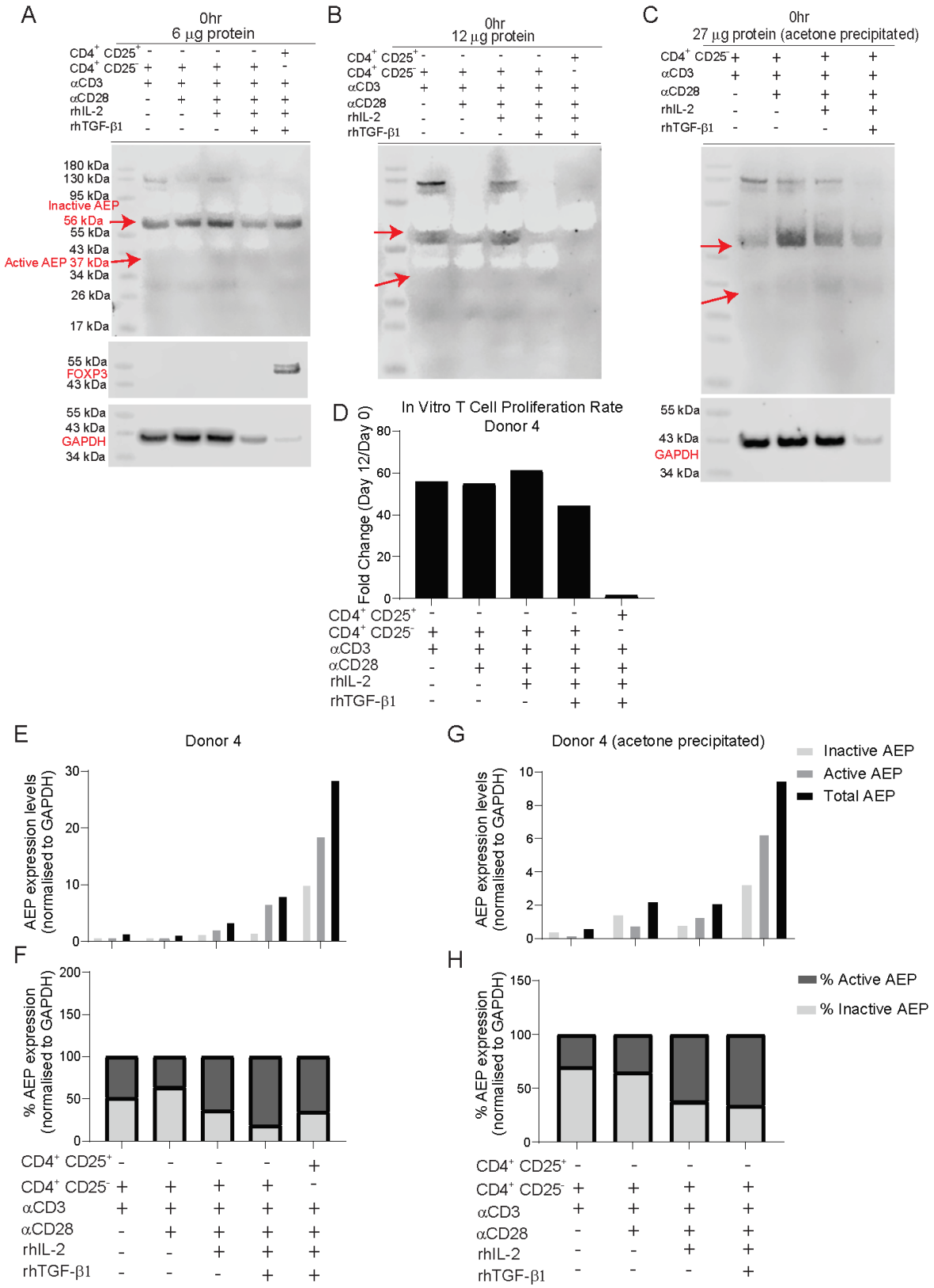
A
0hr
6 µg protein
CD4+ CD25+
CD4+ CD25-
αCD3
αCD28
rhIL-2
rhTGF-β1
180 kDa
130 kDa
95 kDa
Inactive AEP
56 kDa
55 kDa
43 kDa
Active AEP 37 kDa
34 kDa
26 kDa
17 kDa
55 kDa
FOXP3
43 kDa
55 kDa
43 kDa
GAPDH
34 kDa
B
0hr
12 µg protein
C
0hr
27 µg protein (acetone precipitated)
55 kDa
43 kDa
GAPDH
34 kDa
D
In Vitro T Cell Proliferation Rate
Donor 4
Fold Change (Day 12/Day 0)
E
Donor 4
AEP expression levels (normalised to GAPDH)
F
% AEP expression (normalised to GAPDH)
G
Donor 4 (acetone precipitated)
Inactive AEP
Active AEP
Total AEP
H
% Active AEP
% Inactive AEP

Figure 4.12 AEP expression in expanded human iTreg cells *in vitro* - Donor 4. $CD4^+CD25^-$ and $CD4^+CD25^{high}$ T cells were isolated from human PBMCs using a cell sorter. Following sorting, cells were cultured *in vitro* at 0.5 million cells/ml for 5 days in αCD3-coated plates (5 μg/ml) in the presence of αIL-4 (10 μg/ml) and αIFN-γ (10 μg/ml) with the addition of αCD28 (2 μg/ml), rhIL-2 (100 ng/ml) and rhTGF-β1 (5 ng/ml) where appropriate. Cells were expanded for an additional 7 days in the presence of rhIL-2 which was added every 2 days. On day 12, cells were harvested using RIPA lysis buffer in preparation for protein analysis via western blotting. Lysates were reduced and boiled and run under reducing conditions on a precast, 4-12% Bis-Tris gradient gel. **A.** Western blot image showing AEP, FOXP3 and GAPDH expression in each of the culture conditions. The 56 and 37 kDa AEP bands were quantified using ImageJ and normalised to the respective GAPDH loading control bands. **B.** Non-acetone-precipitated lysates of higher protein concentration were run on a separate western blot gel and the membrane was probed for AEP expression. **C.** Acetone-precipitated lysates were run on a separate western blot gel and the membrane was probed for AEP expression. **D.** Bar graph showing the rate of T cell expansion at the end of the culture. The expansion rate is presented as a fold change in number of cells at the end of culture (day 12) divided by the initial number of plated cells (day 0). **E.** Bar graph showing the expression levels of active, inactive and total AEP in each of the conditions. **F.** Bar graph showing the percentage ratio of active and inactive AEP expressed in each of the culture conditions. The active and inactive AEP bands were normalised to GAPDH and the normalised values were divided by the total AEP and then multiplied by 100. **G.** Bar graph showing the expression levels of active, inactive and total AEP in each of the conditions in the acetone-precipitated lysates. **H.** Bar graph showing the percentage ratio of active and inactive AEP expressed in each of the culture conditions in the acetone-precipitated lysates. The active and inactive AEP bands were normalised to GAPDH and the normalised values were divided by the total AEP and then multiplied by 100. n = 1 donor.

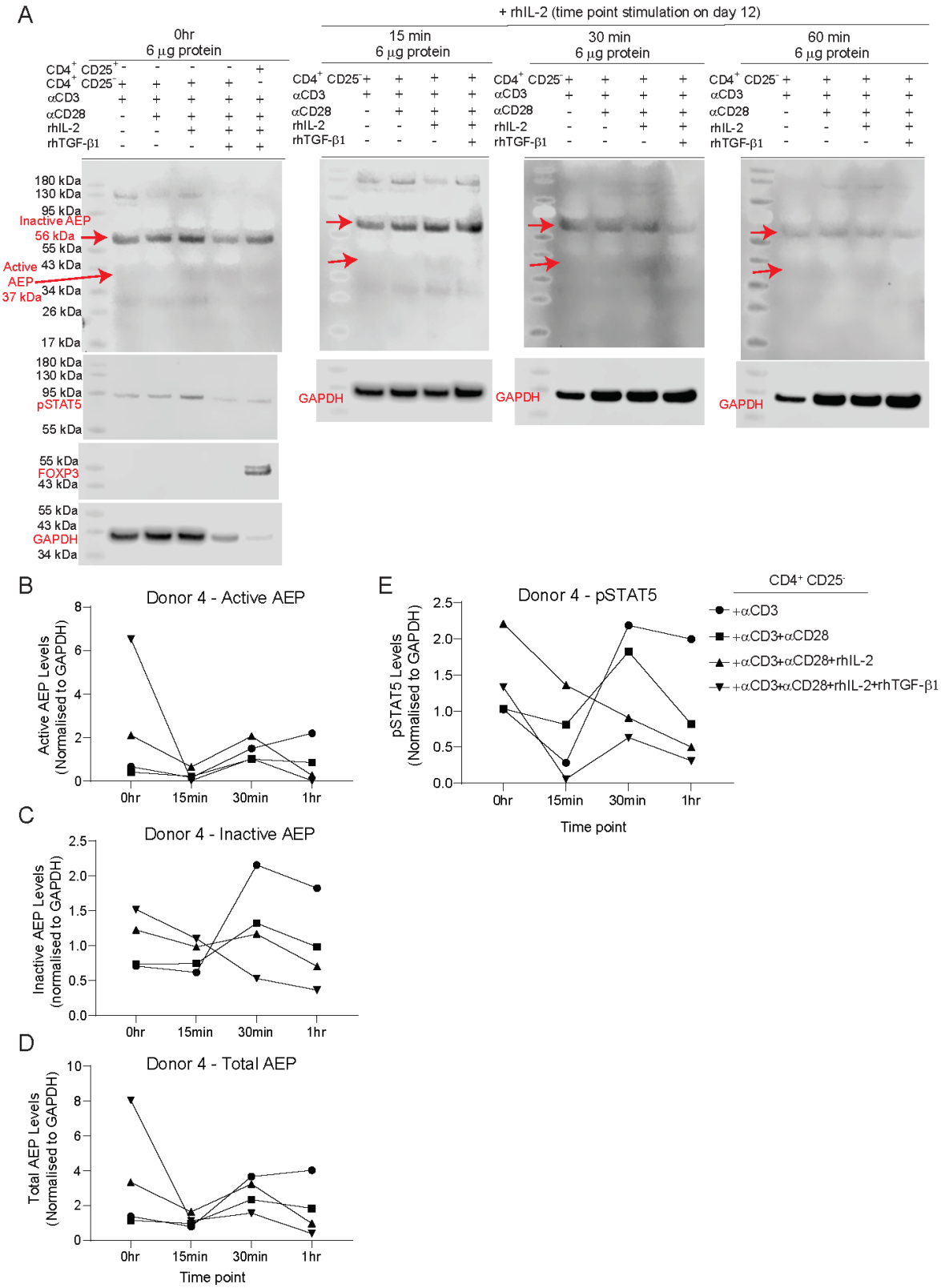
A
+ rhIL-2 (time point stimulation on day 12)
0hr
6 μg protein
15 min
6 μg protein
30 min
6 μg protein
60 min
6 μg protein
CD4+ CD25+
CD4+ CD25-
αCD3
αCD28
rhIL-2
rhTGF-β1
180 kDa
130 kDa
95 kDa
Inactive AEP
56 kDa
55 kDa
Active AEP
43 kDa
34 kDa
37 kDa
26 kDa
17 kDa
pSTAT5
FOXP3
43 kDa
GAPDH
34 kDa
B
Donor 4 - Active AEP
Active AEP Levels (Normalised to GAPDH)
0hr
15min
30min
1hr
C
Donor 4 - Inactive AEP
Inactive AEP Levels (normalised to GAPDH)
D
Donor 4 - Total AEP
Total AEP Levels (Normalised to GAPDH)
Time point
E
Donor 4 - pSTAT5
pSTAT5 Levels (Normalised to GAPDH)
CD4+ CD25-
+αCD3
+αCD3+αCD28
+αCD3+αCD28+rhIL-2
+αCD3+αCD28+rhIL-2+rhTGF-β1

Figure 4.13 AEP expression in expanded human iTreg cells *in vitro* in response to IL-2 stimulation - Donor 4. $CD4^+CD25^-$ and $CD4^+CD25^{high}$ T cells were isolated from human PBMCs using a cell sorter. Following sorting, cells were cultured *in vitro* at 0.5 million cells/ml for 5 days in αCD3-coated plates (5 μg/ml) in the presence of αIL-4 (10 μg/ml) and αIFN-γ (10 μg/ml) with the addition of αCD28 (2 μg/ml), rhIL-2 (100 ng/ml) and rhTGF-β1 (5 ng/ml) where appropriate. Cells were expanded for an additional 7 days in the presence of rhIL-2 which was added every 2 days. On day 12, cells from each condition were harvested using RIPA lysis buffer in preparation for protein analysis via western blotting while. Prior to lysis, 1 million cells were also taken from each condition on day 12 and cultured at 1 million cells/ml, stimulated with rhIL-2 (100 ng/ml) for 15min, 30min, 1hr, 3hr, 6hr and 24hr and then harvested for protein analysis. Lysates were reduced and boiled and run under reducing conditions on a precast, 4-12% Bis-Tris gradient gel. **A.** Western blot image showing AEP, phosphoSTAT5, FOXP3 and GAPDH expression in each of the culture conditions in each time point following rhIL-2 stimulation. The 56 and 37 kDa AEP bands were quantified using ImageJ and normalised to the respective GAPDH loading control bands. **B.** Histogram showing the changes in active AEP expression levels in each of the culture conditions over time following stimulation with rhIL-2. **C.** Histogram showing the changes in inactive AEP expression levels in each of the culture conditions over time following stimulation with rhIL-2. **D.** Histogram showing the changes in total AEP expression levels in each of the culture conditions over time following stimulation with rhIL-2. **E.** Histogram showing the changes in pSTAT5 expression levels in each of the culture conditions over time following stimulation with rhIL-2. n = 1 donor.

To validate these results, additional markers were added to the sorting panel which would restrict selection of cells and increase sample purity (figure 4.14). In this experiment (donor 5), cultured Treg cells expanded the least but the cells could not be revived by day 12 (0.4-fold change) (figure 4.15). As 12 μg of protein lysate yielded very faint bands, lysates were acetone-precipitated and used for the analysis instead (figure 4.15). As stimulation with IL-2 seemed to increase expression of AEP in this scenario, iTreg cells were stimulated with IL-2 for 15 and 60 minutes to test whether AEP expression would go up (figure 4.15). In accordance with donor 4, IL-2 stimulation failed to increase AEP expression *in vitro* (figure 4.15).

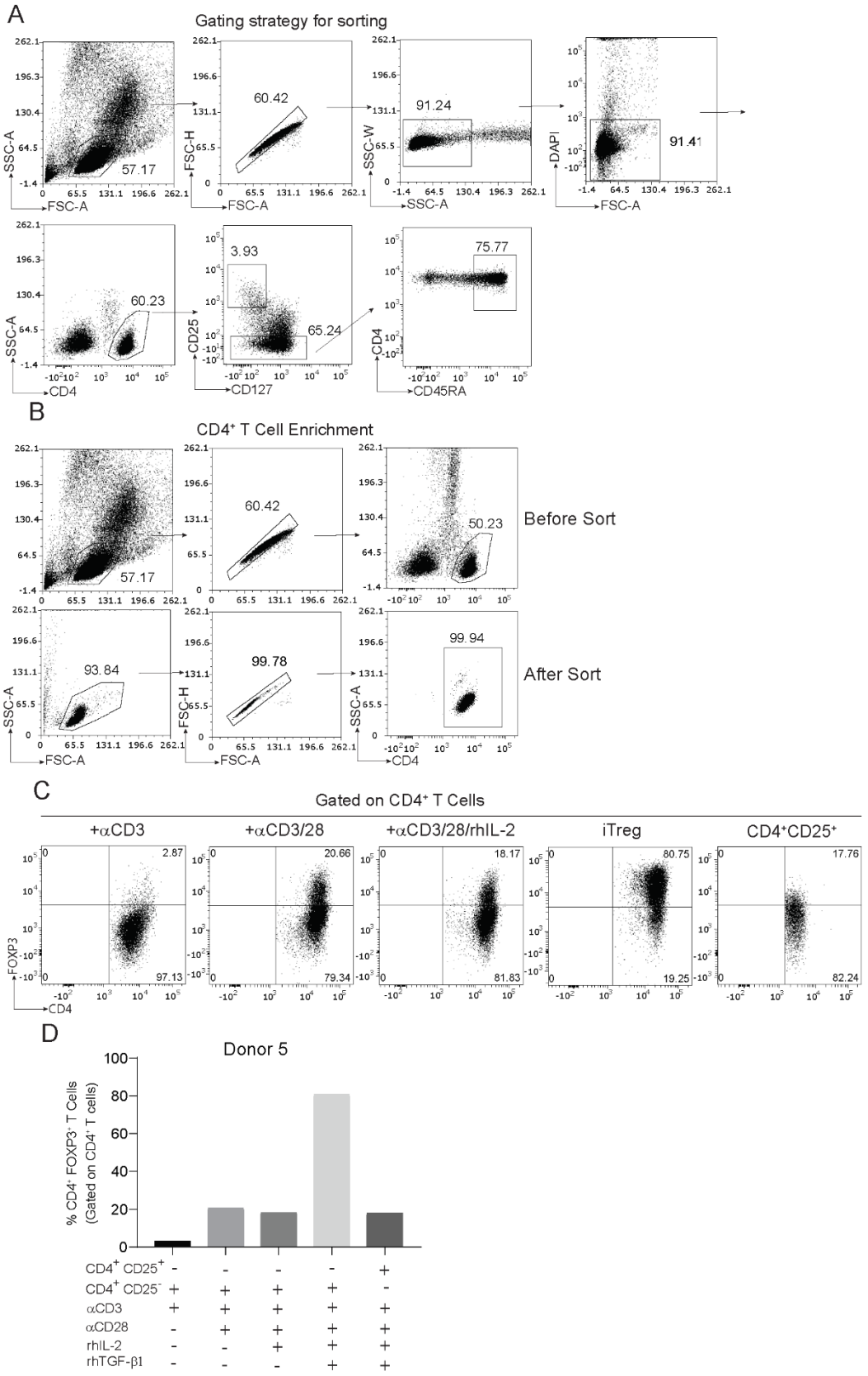
A
Gating strategy for sorting
SSC-A
FSC-A
57.17
FSC-H
60.42
SSC-W
91.24
DAPI
91.41
CD4
60.23
CD25
CD127
3.93
65.24
CD45RA
75.77
B
CD4+ T Cell Enrichment
50.23
Before Sort
93.84
99.78
99.94
After Sort
C
Gated on CD4+ T Cells
+αCD3
+αCD3/28
+αCD3/28/rhIL-2
iTreg
CD4+CD25+
FOXP3
2.87
97.13
20.66
79.34
18.17
81.83
80.75
19.25
17.76
82.24
D
Donor 5
% CD4+ FOXP3+ T Cells
(Gated on CD4+ T cells)
CD4+ CD25+
CD4+ CD25-
αCD3
αCD28
rhIL-2
rhTGF-β1

Figure 4.14 FOXP3 expression in expanded iTreg cells - Donor 5. $CD4^+CD25^-CD127^+CD45RA^+$ and $CD4^+CD25^{high}CD127^{low}$ T cells were isolated from human PBMCs using a cell sorter. PBMCs were counted and stained with CD4-FITC, CD25-APC, CD127-PE.CY7, CD45RA-PE and DAPI in Miltenyi buffer prior to sorting. Following sorting, cells were cultured *in vitro* at 1 million cells/ml for 5 days in αCD3-coated plates (5 μg/ml) in the presence of αIL-4 (10 μg/ml) and αIFN-γ (10 μg/ml) with the addition of αCD28 (2 μg/ml), rhIL-2 (100 ng/ml) and rhTGF-β1 (5 ng/ml) where appropriate. Cells were expanded for an additional 7 days in the presence of rhIL-2 which was added every 2 days. On day 12, cells from each condition were characterised for CD4 and FOXP3 expression. The rest were harvested using RIPA lysis buffer in preparation for protein analysis via western blotting. **A.** Flow plots illustrating the gating strategy used for sorting $CD4^+CD25^-CD127^+CD45RA^+$ and $CD4^+CD25^{high}CD127^{low}$ T cells. **B.** Flow plots showing enrichment of the $CD4^+$ T cell population within the naïve T cell compartment before and after cell sorting. **C.** Flow plots showing the frequency of $CD4^+FOXP3^+$ present within the $CD4^+$ T cell population in each culture condition on day 12. **D.** Bar graph showing the percentage frequency of $CD4^+FOXP3^+$ T cells present within the $CD4^+$ T cell population in each culture condition on day 12. n = 1 donor.

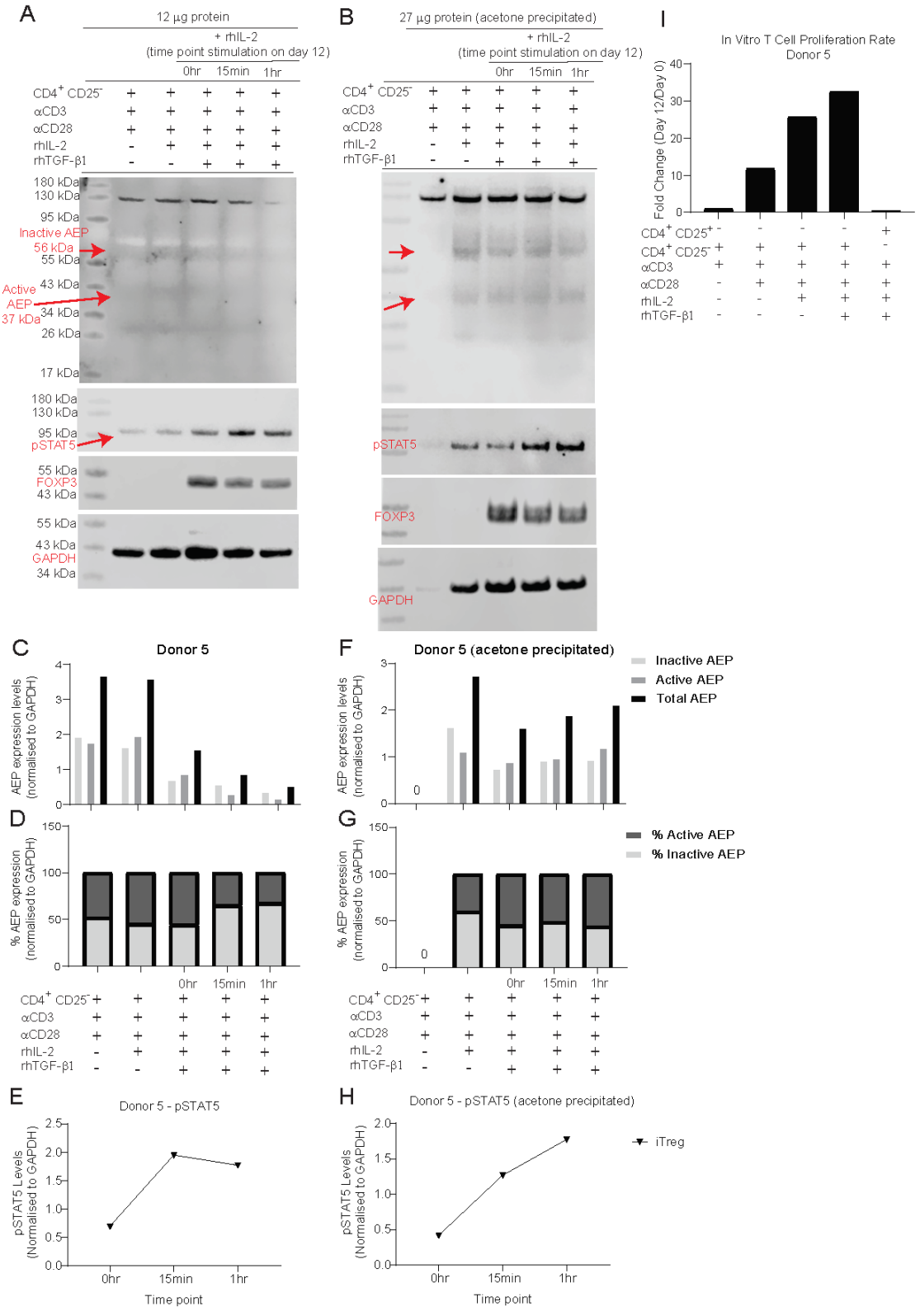
A
12 µg protein
+ rhIL-2
(time point stimulation on day 12)
0hr 15min 1hr
CD4+ CD25-
αCD3
αCD28
rhIL-2
rhTGF-β1
180 kDa
130 kDa
95 kDa
Inactive AEP
56 kDa
55 kDa
Active AEP
43 kDa
37 kDa
34 kDa
26 kDa
17 kDa
pSTAT5
FOXP3
GAPDH
B
27 µg protein (acetone precipitated)
C
Donor 5
AEP expression levels (normalised to GAPDH)
D
% AEP expression (normalised to GAPDH)
E
Donor 5 - pSTAT5
pSTAT5 Levels (Normalised to GAPDH)
Time point
F
Donor 5 (acetone precipitated)
Inactive AEP
Active AEP
Total AEP
G
% Active AEP
% Inactive AEP
H
Donor 5 - pSTAT5 (acetone precipitated)
iTreg
I
In Vitro T Cell Proliferation Rate
Donor 5
Fold Change (Day 12/Day 0)
CD4+ CD25+
CD4+ CD25-

Figure 4.15 AEP expression in expanded human iTreg cells *in vitro* - Donor 5. $CD4^+CD25^-CD127^+CD45RA^+$ and $CD4^+CD25^{high}CD127^{low}$ T cells were isolated from human PBMCs using a cell sorter. Following sorting, cells were cultured *in vitro* at 1 million cells/ml for 5 days in αCD3-coated plates (5 μg/ml) in the presence of αIL-4 (10 μg/ml) and αIFN-γ (10 μg/ml) with the addition of αCD28 (2 μg/ml), rhIL-2 (100 ng/ml) and rhTGF-β1 (5 ng/ml) where appropriate. Cells were expanded for an additional 7 days in the presence of rhIL-2 which was added every 2 days. On day 12, cells were harvested using RIPA lysis buffer in preparation for protein analysis via western blotting. Prior to lysis, 1 million iTreg cells were taken on day 12 and cultured at 1 million cells/ml, stimulated with rhIL-2 (100 ng/ml) for 15min and 1hr and then harvested for protein analysis. Lysates were reduced and boiled and run under reducing conditions on a precast, 4-12% Bis-Tris gradient gel. **A.** Western blot image showing AEP, phosphoSTAT5, FOXP3 and GAPDH expression in each of the culture conditions. The 56 and 37 kDa AEP bands were quantified using ImageJ and normalised to the respective GAPDH loading control bands. **B.** Acetone-precipitated lysates were run on a separate western blot gel and the membrane was probed for AEP, phosphoSTAT5, FOXP3 and GAPDH expression. **C.** Bar graph showing the expression levels of active, inactive and total AEP in each of the conditions. **D.** Bar graph showing the percentage ratio of active and inactive AEP expressed in each of the culture conditions. **E.** Histogram showing the changes in pSTAT5 expression levels in each of the culture conditions over time following stimulation with rhIL-2. **F.** Bar graph showing the expression levels of active, inactive and total AEP in each of the conditions in the acetone-precipitated lysates. **G.** Bar graph showing the percentage ratio of active and inactive AEP expressed in each of the culture conditions in the acetone-precipitated lysates. **H.** Histogram showing the changes in pSTAT5 expression levels in each of the culture conditions over time following stimulation with rhIL-2 in the acetone-precipitated lysates. **I.** Bar graph showing the rate of T cell expansion of cells cultured under different culture conditions at the end of the culture. The expansion rate is presented as a fold change in number of cells at the end of culture (day 12) divided by the initial number of plated cells (day 0). n = 1 donor.

The culture was repeated in donor 6 to include Treg condition which failed in the previous donor. Within this experiment, all the conditions successfully expanded *in vitro* with cultured Treg cells expanding less than iTreg cells (19.21 and 31 – 40-fold change respectively) (figure 4.16-17). All conditions except for cultured Treg cells, expressed more inactive than active AEP (figure 4.17) something that was also observed in donors 1 and 3. Cultured iTreg and Treg cells had the highest expression of AEP out of all conditions (figure 4.17). This is in support of the hypothesis that the highest level of total AEP expression is induced by TGF-β1. No significant difference was

observed in AEP expression levels in iTreg cells that were stimulated with either 5 or 10 ng/ml of TGF-β1 (figure 4.17).

Repetition of this experiment in donor 7 confirmed these results in cultured Treg cells as the iTreg condition failed to show any AEP expression despite FOXP3 being expressed (figure 4.18-19). Stimulation of iTreg and Treg cells with IL-2 for 15 minutes, 1 and 3 hours failed to increase AEP expression consistent with previous experiments (figure 4.13, 4.15, 4.19).

In donor 8, 40% of iTreg cells were FOXP3 positive therefore this condition was excluded from the analysis (figure 4.20). All conditions except for the cultured Treg cells expressed more inactive than active AEP consistent with donors 1 and 3 (figure 4.21). In this case the highest level of total AEP expression seems to be induced by both IL-2 and TGF-β1 (figure 4.21).

In donor 9, all conditions except for the IL-2 and cultured Treg cells expressed more inactive than active AEP (figure 4.22-23). Again, the highest level of total AEP expression seemed to be induced by TGF-β1 (figure 4.23).

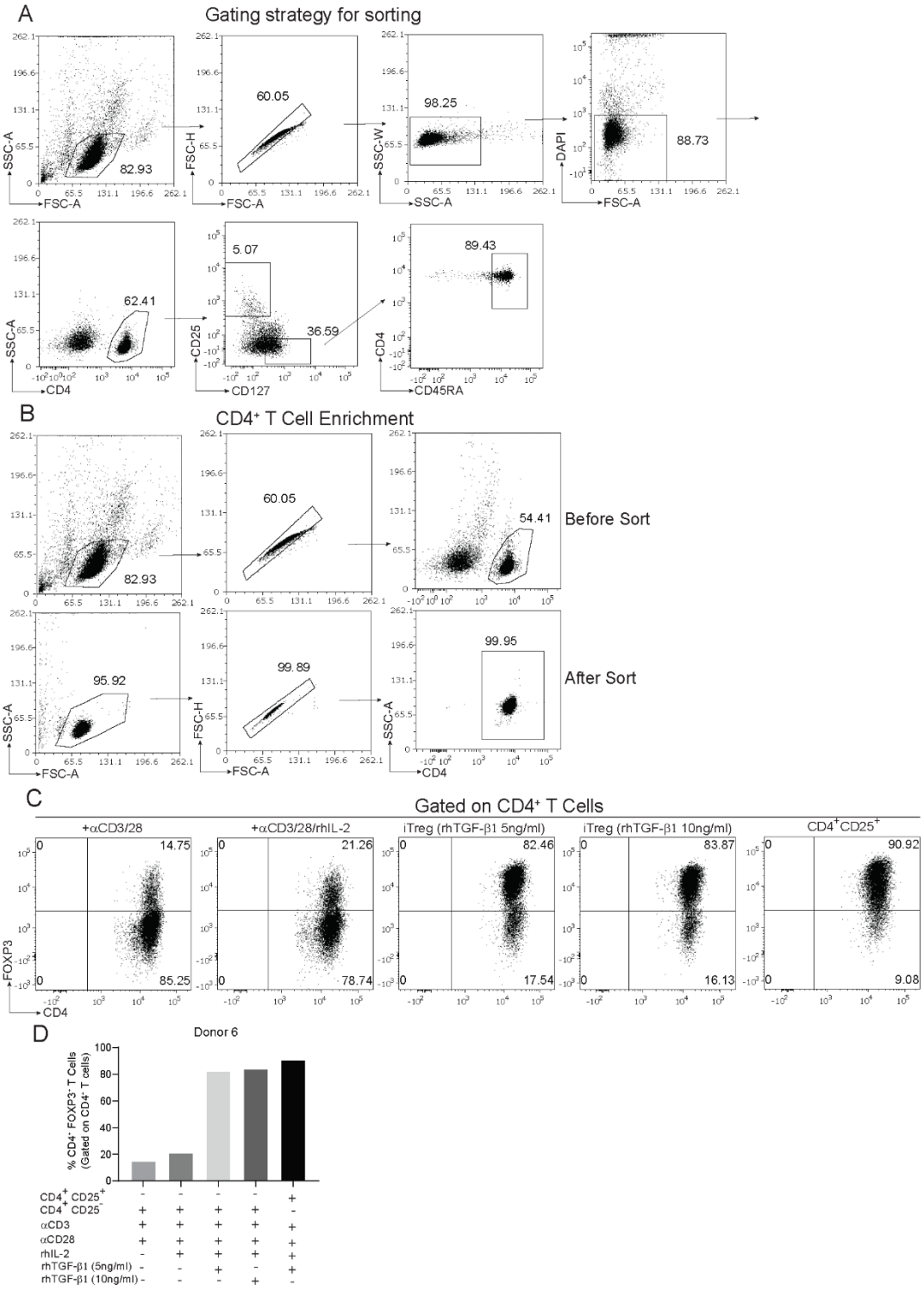
A
Gating strategy for sorting
SSC-A
FSC-A
82.93
FSC-H
60.05
SSC-W
98.25
DAPI
88.73
62.41
CD4
5.07
CD25
CD127
36.59
89.43
CD45RA
B
CD4⁺ T Cell Enrichment
54.41
Before Sort
95.92
99.89
99.95
After Sort
C
Gated on CD4⁺ T Cells
+αCD3/28
+αCD3/28/rhIL-2
iTreg (rhTGF-β1 5ng/ml)
iTreg (rhTGF-β1 10ng/ml)
CD4+CD25+
FOXP3
14.75
85.25
21.26
78.74
82.46
17.54
83.87
16.13
90.92
9.08
D
Donor 6
% CD4+ FOXP3+ T Cells (Gated on CD4+ T cells)
CD4+ CD25+
CD4+ CD25-
αCD3
αCD28
rhIL-2
rhTGF-β1 (5ng/ml)
rhTGF-β1 (10ng/ml)

Figure 4.16 FOXP3 expression in expanded iTreg cells - Donor 6. $CD4^+CD25^-CD127^+CD45RA^+$ and $CD4^+CD25^{high}CD127^{low}$ T cells were isolated from human PBMCs using a cell sorter. PBMCs were counted and stained with CD4-FITC, CD25-APC, CD127-PE.CY7, CD45RA-PE and DAPI in Miltenyi buffer prior to sorting. Following sorting, cells were cultured *in vitro* at 1 million cells/ml for 5 days in αCD3-coated plates (5 μg/ml) in the presence of αIL-4 (10 μg/ml) and αIFN-γ (10 μg/ml) with the addition of αCD28 (2 μg/ml), rhIL-2 (100 ng/ml) and rhTGF-β1 where appropriate. rhTGF-β1 was added to the iTreg condition at either 5 ng/ml or 10 ng/ml while sorted $CD4^+CD25^{high}CD127^{low}$ T cells were stimulated with 5 ng/ml rhTGF-β1. Cells were expanded for an additional 7 days in the presence of rhIL-2 which was added every 2 days. On day 12, cells from each condition were characterised for CD4 and FOXP3 expression. The rest were harvested using PMSF lysis buffer in preparation for protein analysis via western blotting. **A.** Flow plots illustrating the gating strategy used for sorting $CD4^+CD25^-CD127^+CD45RA^+$ and $CD4^+CD25^{high}CD127^{low}$ T cells. **B.** Flow plots showing enrichment of the $CD4^+$ T cell population within the naïve T cell compartment before and after cell sorting. **C.** Flow plots showing the frequency of $CD4^+FOXP3^+$ present within the $CD4^+$ T cell population in each culture condition on day 12. **D.** Bar graph showing the percentage frequency of $CD4^+FOXP3^+$ T cells present within the $CD4^+$ T cell population in each culture condition on day 12. n = 1 donor.

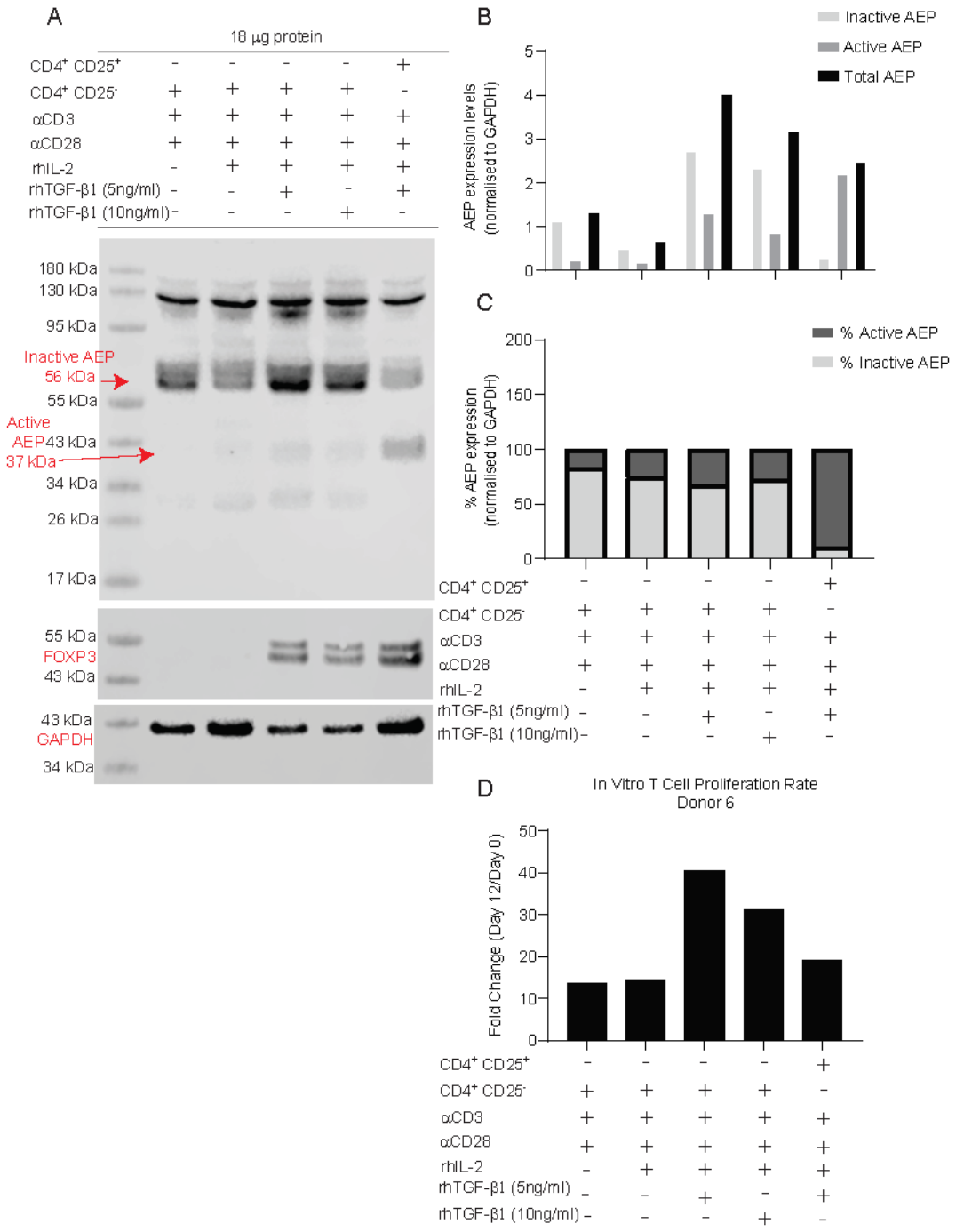
A
18 µg protein
CD4+ CD25+
CD4+ CD25-
αCD3
αCD28
rhIL-2
rhTGF-β1 (5ng/ml)
rhTGF-β1 (10ng/ml)
180 kDa
130 kDa
95 kDa
Inactive AEP
56 kDa
55 kDa
Active AEP
43 kDa
37 kDa
34 kDa
26 kDa
17 kDa
55 kDa
FOXP3
43 kDa
43 kDa
GAPDH
34 kDa
B
Inactive AEP
Active AEP
Total AEP
AEP expression levels (normalised to GAPDH)
C
% Active AEP
% Inactive AEP
% AEP expression (normalised to GAPDH)
D
In Vitro T Cell Proliferation Rate
Donor 6
Fold Change (Day 12/Day 0)

Figure 4.17 AEP expression in expanded human iTreg cells *in vitro* - Donor 6. $CD4^+CD25^-CD127^+CD45RA^+$ and $CD4^+CD25^{high}CD127^{low}$ T cells were isolated from human PBMCs using a cell sorter. Following sorting, cells were cultured *in vitro* at 1 million cells/ml for 5 days in αCD3-coated plates (5 μg/ml) in the presence of αIL-4 (10 μg/ml) and αIFN-γ (10 μg/ml) with the addition of αCD28 (2 μg/ml), rhIL-2 (100 ng/ml) and rhTGF-β1 where appropriate. rhTGF-β1 was added to the iTreg condition at either 5 ng/ml or 10 ng/ml while sorted $CD4^+CD25^{high}CD127^{low}$ T cells were stimulated with 5 ng/ml rhTGF-β1. Cells were expanded for an additional 7 days in the presence of rhIL-2 which was added every 2 days. On day 12, cells were harvested using PMSF lysis buffer in preparation for protein analysis via western blotting. Lysates were reduced and boiled and run under reducing conditions on a precast, 4-12% Bis-Tris gradient gel. **A.** Western blot image showing AEP, FOXP3 and GAPDH expression in each of the culture conditions. The 56 and 37 kDa AEP bands were quantified using ImageJ and normalised to the respective GAPDH loading control bands. **B.** Bar graph showing the expression levels of active, inactive and total AEP in each of the conditions. **C.** Bar graph showing the percentage ratio of active and inactive AEP expressed in each of the culture conditions. **D.** Bar graph showing the rate of T cell expansion of cells cultured under different culture conditions at the end of the culture. The expansion rate is presented as a fold change in number of cells at the end of culture (day 12) divided by the initial number of plated cells (day 0). n =1 donor.

A

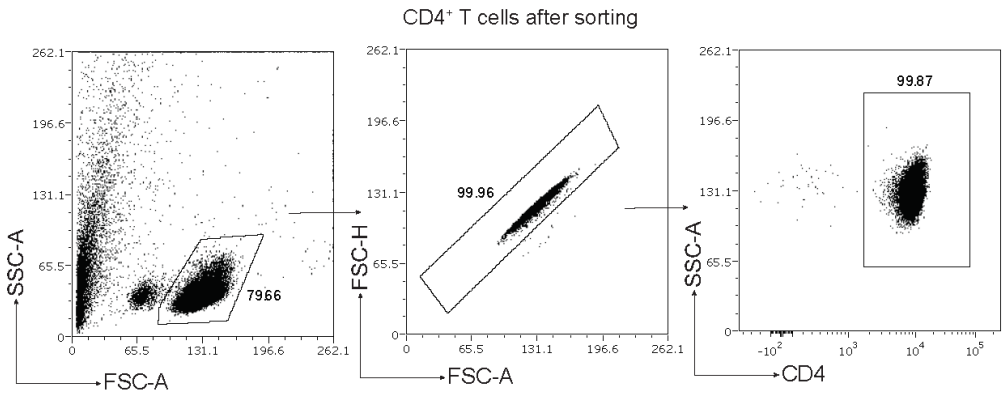
CD4⁺ T cells after sorting
SSC-A
FSC-A
79.66
FSC-H
99.96
CD4
99.87

B

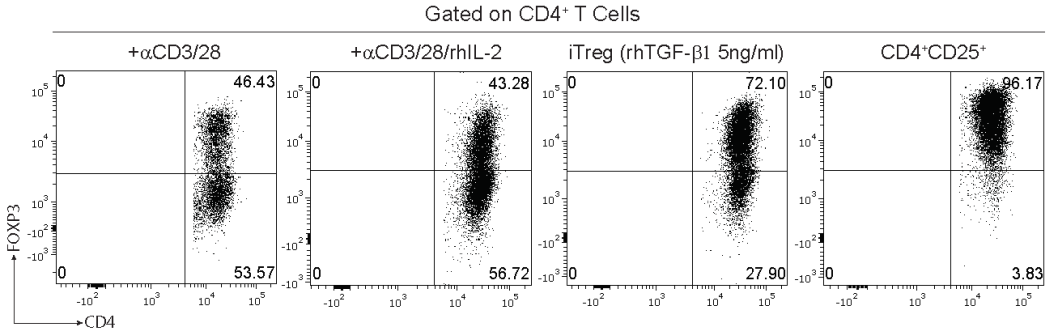
Gated on CD4⁺ T Cells
+αCD3/28
+αCD3/28/rhIL-2
iTreg (rhTGF-β1 5ng/ml)
CD4⁺CD25⁺
FOXP3
CD4
46.43
53.57
43.28
56.72
72.10
27.90
96.17
3.83

C

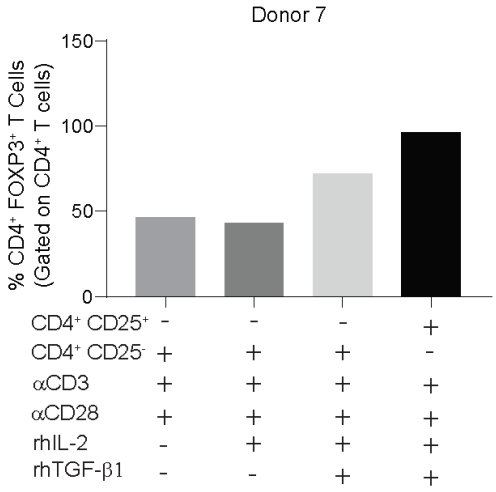
Donor 7
% CD4⁺ FOXP3⁺ T Cells (Gated on CD4⁺ T cells)
150
100
50
0
CD4⁺ CD25⁺ - - - +
CD4⁺ CD25⁻ + + + -
αCD3 + + + +
αCD28 + + + +
rhIL-2 - + + +
rhTGF-β1 - - + +

Figure 4.18 FOXP3 expression in expanded iTreg cells - Donor 7. $CD4^+CD25^-CD127^+CD45RA^+$ and $CD4^+CD25^{high}CD127^{low}$ T cells were isolated from human PBMCs using a cell sorter. PBMCs were counted and stained with CD4-FITC, CD25-APC, CD127-PE.CY7, CD45RA-PE and DAPI in Miltenyi buffer prior to sorting. Following sorting, cells were cultured *in vitro* at 1 million cells/ml for 5 days in αCD3-coated plates (5 μg/ml) in the presence of αIL-4 (10 μg/ml) and αIFN-γ (10 μg/ml) with the addition of αCD28 (2 μg/ml), rhIL-2 (100 ng/ml) and rhTGF-β1 (5 ng/ml) where appropriate. Cells were expanded for an additional 7 days in the presence of rhIL-2 which was added every 2 days. On day 12, cells from each condition were characterised for CD4 and FOXP3 expression. The rest were harvested using PMSF lysis buffer in preparation for protein analysis via western blotting. **A.** Flow plots showing enrichment of the $CD4^+$ T cell population within the naïve T cell compartment after cell sorting. **B.** Flow plots showing the frequency of $CD4^+FOXP3^+$ present within the $CD4^+$ T cell population in each culture condition on day 12. **C.** Bar graph showing the percentage frequency of $CD4^+FOXP3^+$ T cells present within the $CD4^+$ T cell population in each culture condition on day 12. n =1 donor.

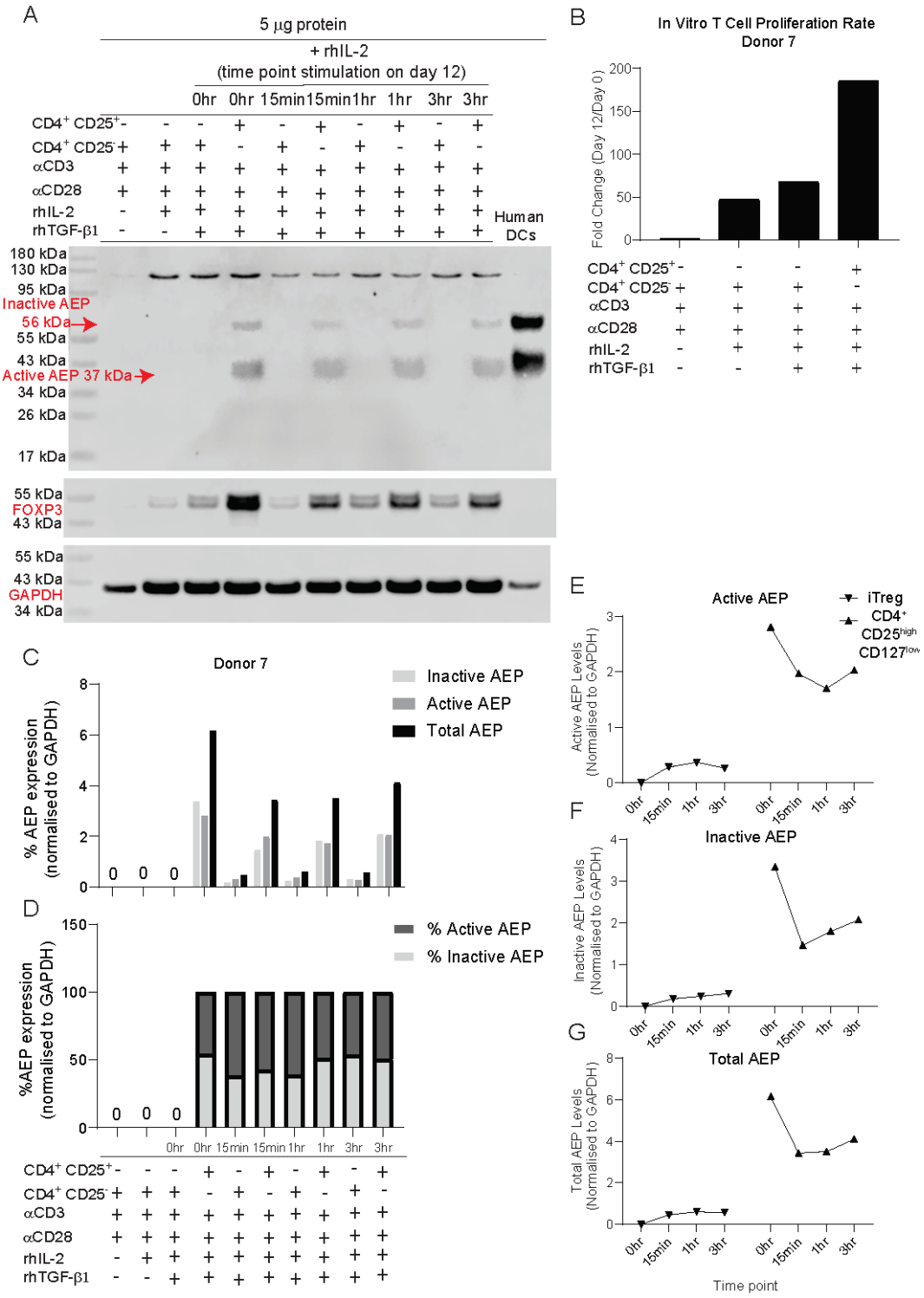
A
5 μg protein
+ rhIL-2
(time point stimulation on day 12)
0hr 0hr 15min 15min 1hr 1hr 3hr 3hr
CD4+ CD25+
CD4+ CD25-
αCD3
αCD28
rhIL-2
rhTGF-β1
Human DCs
180 kDa
130 kDa
95 kDa
Inactive AEP
56 kDa
55 kDa
43 kDa
Active AEP 37 kDa
34 kDa
26 kDa
17 kDa
55 kDa
FOXP3
43 kDa
55 kDa
43 kDa
GAPDH
34 kDa
B
In Vitro T Cell Proliferation Rate
Donor 7
Fold Change (Day 12/Day 0)
200
150
100
50
0
CD4+ CD25+
CD4+ CD25-
αCD3
αCD28
rhIL-2
rhTGF-β1
C
Donor 7
% AEP expression (normalised to GAPDH)
Inactive AEP
Active AEP
Total AEP
D
%AEP expression (normalised to GAPDH)
% Active AEP
% Inactive AEP
0hr 0hr 15min 15min 1hr 1hr 3hr 3hr
CD4+ CD25+
CD4+ CD25-
αCD3
αCD28
rhIL-2
rhTGF-β1
E
Active AEP
iTreg
CD4+ CD25high CD127low
Active AEP Levels (Normalised to GAPDH)
F
Inactive AEP
Inactive AEP Levels (Normalised to GAPDH)
G
Total AEP
Total AEP Levels (Normalised to GAPDH)
0hr 15min 1hr 3hr 0hr 15min 1hr 3hr
Time point

Figure 4.19 AEP expression in expanded human iTreg cells *in vitro* in response to IL-2 stimulation - Donor 7. $CD4^+CD25^-CD127^+CD45RA^+$ and $CD4^+CD25^{high}CD127^{low}$ T cells were isolated from human PBMCs using a cell sorter. Following sorting, cells were cultured *in vitro* at 1 million cells/ml for 5 days in αCD3-coated plates (5 μg/ml) in the presence of αIL-4 (10 μg/ml) and αIFN-γ (10 μg/ml) with the addition of αCD28 (2 μg/ml), rhIL-2 (100 ng/ml) and rhTGF-β1 (5 ng/ml) where appropriate. Cells were expanded for an additional 7 days in the presence of rhIL-2 which was added every 2 days. On day 12, cells from each condition were harvested using PMSF lysis buffer in preparation for protein analysis via western blotting. Prior to lysis, 1 million cells were also taken from the iTreg and cultured $CD4^+CD25^{high}CD127^{low}$ conditions on day 12 and cultured at 1 million cells/ml, stimulated with rhIL-2 (100 ng/ml) for 15min, 1hr and 3hr and then harvested for protein analysis. Lysates were reduced and boiled and run under reducing conditions on a precast, 4-12% Bis-Tris gradient gel. **A.** Western blot image showing AEP, FOXP3 and GAPDH expression in each of the culture conditions including in each time point following IL-2 stimulation. The 56 and 37 kDa AEP bands were quantified using ImageJ and normalised to the respective GAPDH loading control bands. **B.** Bar graph showing the rate of T cell expansion of cells cultured under different culture conditions at the end of the culture. The expansion rate is presented as a fold change in number of cells at the end of culture (day 12) divided by the initial number of plated cells (day 0). **C.** Bar graph showing the expression levels of active, inactive and total AEP in each of the conditions. **D.** Bar graph showing the percentage ratio of active and inactive AEP expressed in each of the culture conditions. **E.** Histogram showing the changes in active AEP expression levels in the iTreg and $CD4^+CD25^{high}CD127^{low}$ culture conditions over time following stimulation with IL-2. **F.** Histogram showing the changes in inactive AEP expression levels in the iTreg and $CD4^+CD25^{high}CD127^{low}$ culture conditions over time following stimulation with IL-2. **G.** Histogram showing the changes in total AEP expression levels in the iTreg and $CD4^+CD25^{high}CD127^{low}$ culture conditions over time following stimulation with IL-2. n =1 donor.

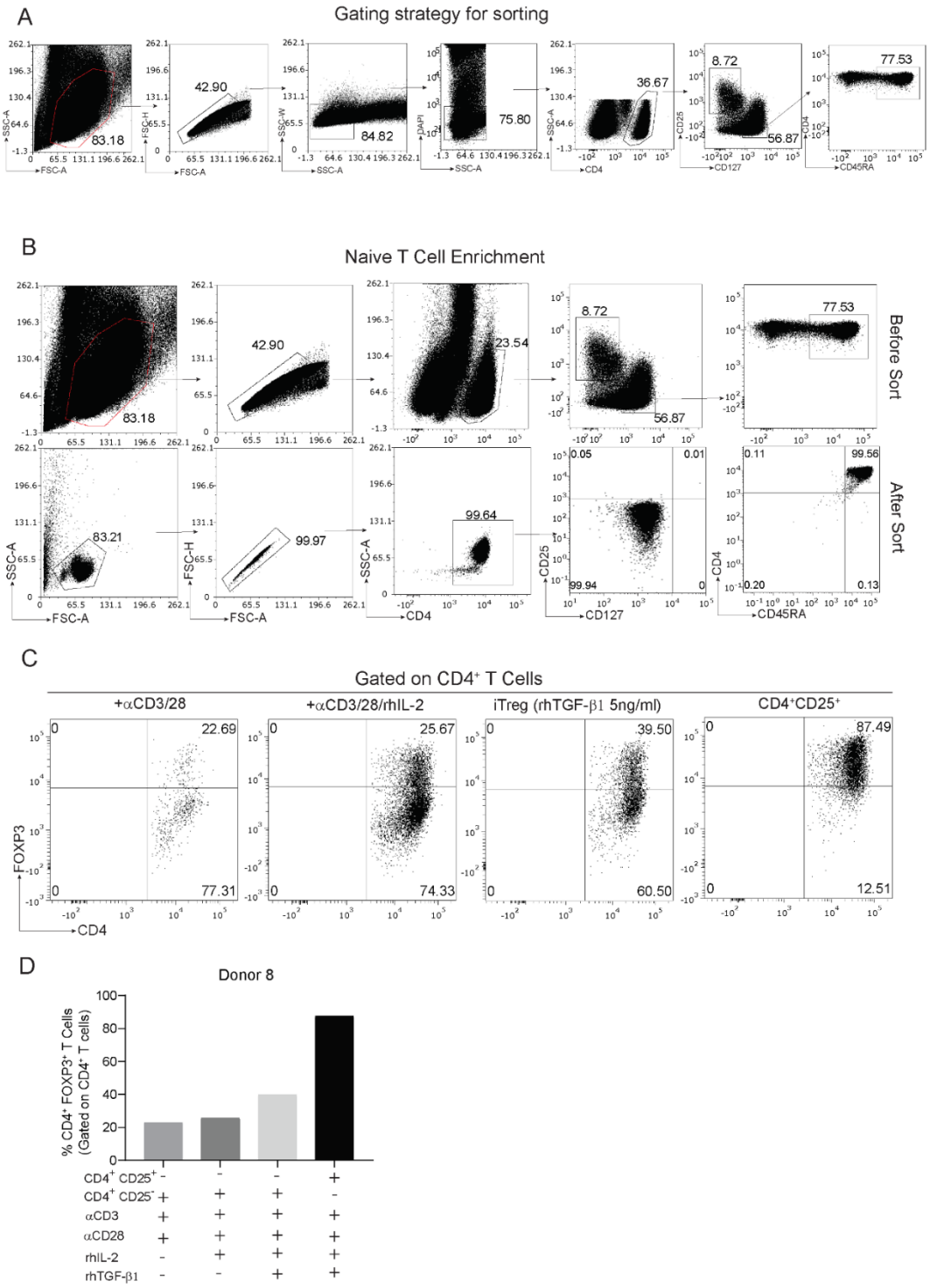
A
Gating strategy for sorting
SSC-A
FSC-A
83.18
FSC-H
42.90
SSC-W
84.82
DAPI
75.80
36.67
CD4
CD25
CD127
8.72
56.87
CD45RA
77.53
B
Naive T Cell Enrichment
Before Sort
After Sort
23.54
99.64
99.97
83.21
0.05
0.01
99.94
0.11
99.56
0.20
0.13
C
Gated on CD4⁺ T Cells
+αCD3/28
+αCD3/28/rhIL-2
iTreg (rhTGF-β1 5ng/ml)
CD4⁺CD25⁺
FOXP3
22.69
77.31
25.67
74.33
39.50
60.50
87.49
12.51
D
Donor 8
% CD4⁺ FOXP3⁺ T Cells (Gated on CD4⁺ T cells)
CD4⁺ CD25⁺
CD4⁺ CD25⁻
αCD3
αCD28
rhIL-2
rhTGF-β1

Figure 4.20 FOXP3 expression in expanded iTreg cells - Donor 8. $CD4^+CD25^-CD127^+CD45RA^+$ and $CD4^+CD25^{high}CD127^{low}$ T cells were isolated from human PBMCs using a cell sorter. PBMCs were counted and stained with CD4-FITC, CD25-APC, CD127-PE.CY7, CD45RA-PE and DAPI in Miltenyi buffer prior to sorting. Following sorting, cells were cultured *in vitro* at 1 million cells/ml for 5 days in αCD3-coated plates (5 μg/ml) in the presence of αIL-4 (10 μg/ml) and αIFN-γ (10 μg/ml) with the addition of αCD28 (2 μg/ml), rhIL-2 (100 ng/ml) and rhTGF-β1 (5 ng/ml) where appropriate. Cells were expanded for an additional 7 days in the presence of rhIL-2 which was added every 2 days. On day 12, cells from each condition were characterised for CD4 and FOXP3 expression. The rest were harvested using PMSF lysis buffer in preparation for protein analysis via western blotting. **A.** Flow plots illustrating the gating strategy used for sorting $CD4^+CD25^-CD127^+CD45RA^+$ and $CD4^+CD25^{high}CD127^{low}$ T cells. **B.** Flow plots showing enrichment of the naïve T cell population before and after cell sorting. **C.** Flow plots showing the frequency of $CD4^+FOXP3^+$ present within the $CD4^+$ T cell population in each culture condition on day 12. **D.** Bar graph showing the percentage frequency of $CD4^+FOXP3^+$ T cells present within the $CD4^+$ T cell population in each culture condition on day 12. n =1 donor.

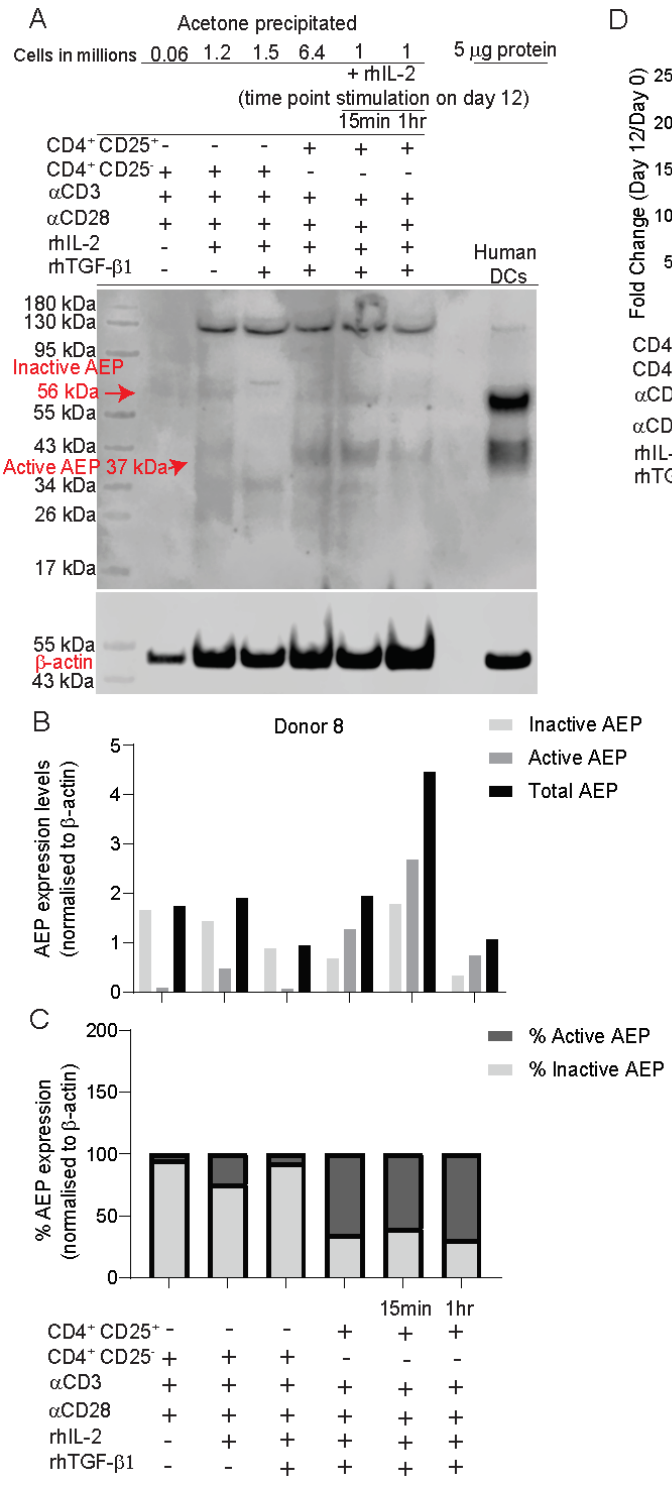
A
Acetone precipitated
Cells in millions 0.06 1.2 1.5 6.4 1 1
5 µg protein
+ rhIL-2
(time point stimulation on day 12)
15min 1hr
CD4+ CD25+ - - - + + +
CD4+ CD25- + + + - - -
αCD3 + + + + + +
αCD28 + + + + + +
rhIL-2 - + + + + +
rhTGF-β1 - - + + + +
Human DCs
180 kDa
130 kDa
95 kDa
Inactive AEP
56 kDa
55 kDa
43 kDa
Active AEP 37 kDa
34 kDa
26 kDa
17 kDa
55 kDa
β-actin
43 kDa
B
Donor 8
Inactive AEP
Active AEP
Total AEP
AEP expression levels (normalised to β-actin)
C
% Active AEP
% Inactive AEP
% AEP expression (normalised to β-actin)
15min 1hr
CD4+ CD25+ - - - + + +
CD4+ CD25- + + + - - -
αCD3 + + + + + +
αCD28 + + + + + +
rhIL-2 - + + + + +
rhTGF-β1 - - + + + +
D
In Vitro T Cell Proliferation Rate
Donor 8
Fold Change (Day 12/Day 0)
CD4+ CD25+ - - - +
CD4+ CD25- + + + -
αCD3 + + + +
αCD28 + + + +
rhIL-2 - + + +
rhTGF-β1 - - + +

Figure 4.21 AEP expression in expanded human iTreg cells *in vitro* in response to IL-2 stimulation - Donor 8. $CD4^+CD25^-CD127^+CD45RA^+$ and $CD4^+CD25^{high}CD127^{low}$ T cells were isolated from human PBMCs using a cell sorter. Following sorting, cells were cultured *in vitro* at 1 million cells/ml for 5 days in αCD3-coated plates (5 μg/ml) in the presence of αIL-4 (10 μg/ml) and αIFN-γ (10 μg/ml) with the addition of αCD28 (2 μg/ml), rhIL-2 (100 ng/ml) and rhTGF-β1 (5 ng/ml) where appropriate. Cells were expanded for an additional 7 days in the presence of rhIL-2 which was added every 2 days. On day 12, cells from each condition were harvested using PMSF lysis buffer in preparation for protein analysis via western blotting. Prior to lysis, 1 million cells were also taken from the cultured $CD4^+CD25^{high}CD127^{low}$ conditions on day 12 and cultured at 1 million cells/ml, stimulated with rhIL-2 (100 ng/ml) for 15min and 1hr and then harvested for protein analysis. All lysates were acetone precipitated. Lysates were reduced and boiled and run under reducing conditions on a precast, 4-12% Bis-Tris gradient gel. **A.** Western blot image showing AEP and β-actin expression in each of the culture conditions including in each time point following IL-2 stimulation. The 56 and 37 kDa AEP bands were quantified using ImageJ and normalised to the respective β-actin loading control bands. **B.** Bar graph showing the expression levels of active, inactive and total AEP in each of the conditions. **C.** Bar graph showing the percentage ratio of active and inactive AEP expressed in each of the culture conditions. **D.** Bar graph showing the rate of T cell expansion of cells cultured under different culture conditions at the end of the culture. The expansion rate is presented as a fold change in number of cells at the end of culture (day 12) divided by the initial number of plated cells (day 0). n=1 donor.

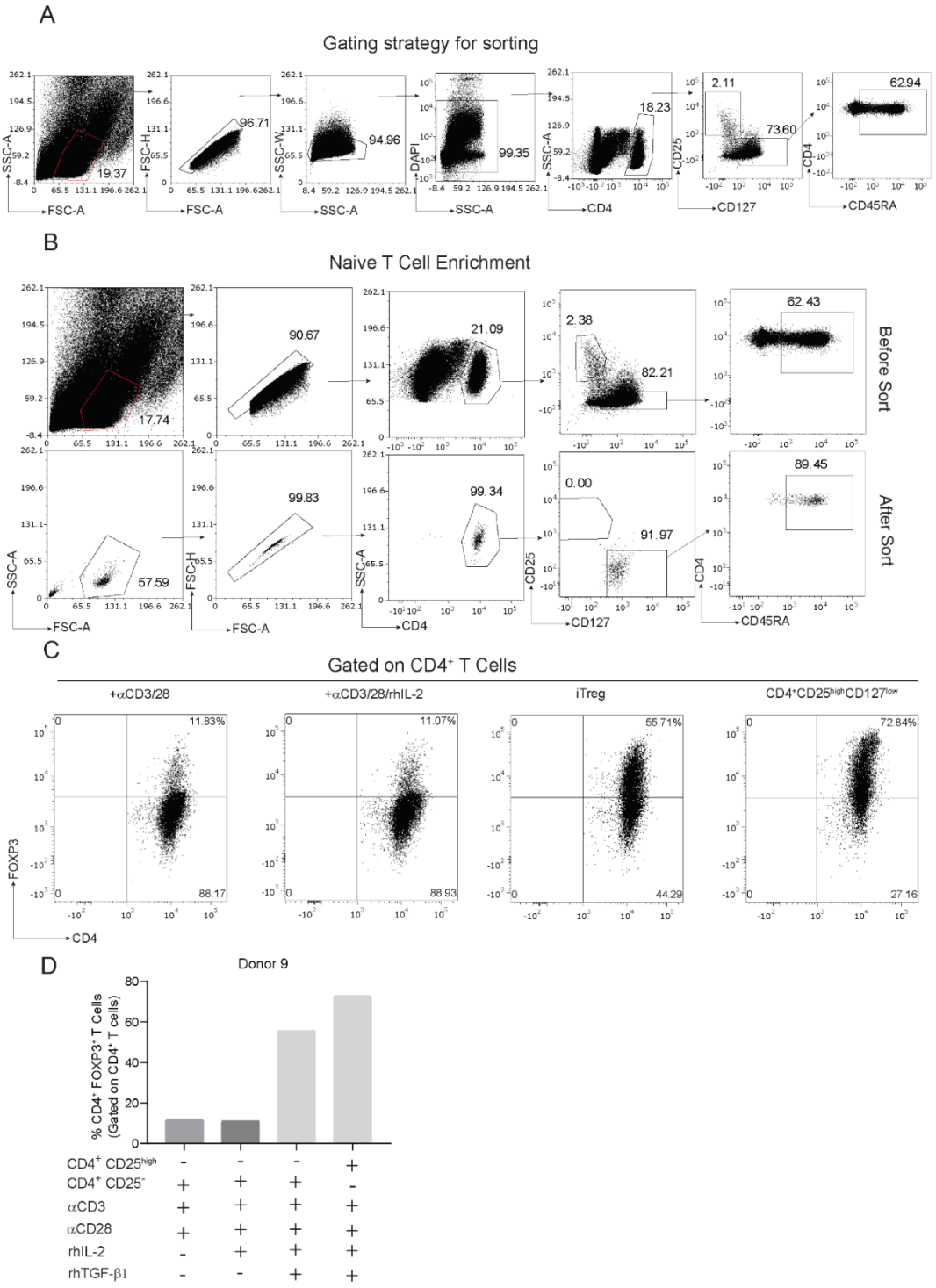
A
Gating strategy for sorting
SSC-A
FSC-A
19.37
FSC-H
96.71
SSC-W
94.96
DAPI
99.35
SSC-A
CD4
18.23
CD25
CD127
2.11
73.60
CD4
CD45RA
62.94
B
Naive T Cell Enrichment
17.74
90.67
21.09
2.38
82.21
62.43
Before Sort
57.59
99.83
99.34
0.00
91.97
89.45
After Sort
C
Gated on CD4+ T Cells
+αCD3/28
+αCD3/28/rhIL-2
iTreg
CD4+CD25highCD127low
11.83%
88.17
11.07%
88.93
55.71%
44.29
72.84%
27.16
FOXP3
CD4
D
Donor 9
% CD4+ FOXP3+ T Cells (Gated on CD4+ T cells)
CD4+ CD25high
CD4+ CD25-
αCD3
αCD28
rhIL-2
rhTGF-β1

Figure 4.22 FOXP3 expression in expanded iTreg cells - Donor 9. PBMCs were isolated from blood and $CD4^+CD25^-CD127^+CD45RA^+$ and $CD4^+CD25^{high}CD127^{low}$ T cells were isolated using cell sorting. PBMCs were counted and stained with CD4-FITC, CD25-APC, CD127-PE.CY7, CD45RA-PE and DAPI in Miltenyi buffer prior to sorting. Following sorting, cells were cultured *in vitro* at 1 million cells/ml for 5 days in αCD3-coated plates (5 μg/ml) in the presence of αIL-4 (10 μg/ml) and αIFN-γ (10 μg/ml) with the addition of αCD28 (2 μg/ml), rhIL-2 (100 ng/ml) and rhTGF-β1 (5 ng/ml) where appropriate. Cells were expanded for an additional 7 days in the presence of rhIL-2 which was added every 2 days. On day 12, cells from each condition were characterised for CD4 and FOXP3 expression. The rest were harvested using PMSF lysis buffer in preparation for protein analysis via western blotting. **A.** Flow plots illustrating the gating strategy used for sorting $CD4^+CD25^-CD127^+CD45RA^+$ and $CD4^+CD25^{high}CD127^{low}$ T cells. **B.** Flow plots showing enrichment of the naïve T cell population before and after cell sorting. **C.** Flow plots showing the frequency of $CD4^+FOXP3^+$ present within the $CD4^+$ T cell population in each culture condition on day 12. **D.** Bar graph showing the percentage frequency of $CD4^+FOXP3^+$ T cells present within the $CD4^+$ T cell population in each culture condition on day 12. n=1 donor.

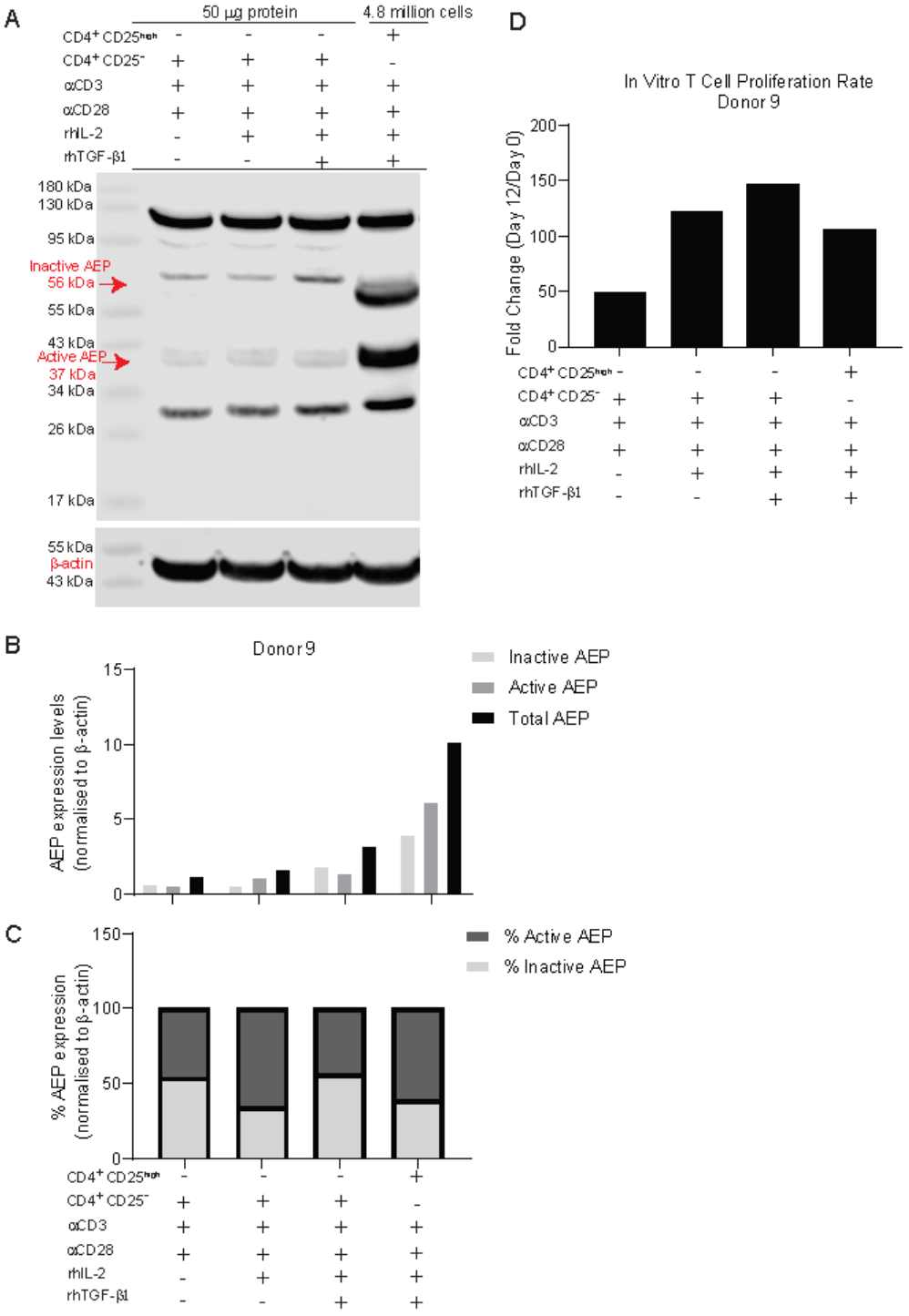
A
50 µg protein
4.8 million cells
CD4+ CD25high
CD4+ CD25-
αCD3
αCD28
rhIL-2
rhTGF-β1
180 kDa
130 kDa
95 kDa
Inactive AEP
56 kDa
55 kDa
43 kDa
Active AEP
37 kDa
34 kDa
26 kDa
17 kDa
55 kDa
β-actin
43 kDa
D
In Vitro T Cell Proliferation Rate
Donor 9
Fold Change (Day 12/Day 0)
200
150
100
50
0
B
Donor 9
Inactive AEP
Active AEP
Total AEP
AEP expression levels
(normalised to β-actin)
15
10
5
0
C
% Active AEP
% Inactive AEP
% AEP expression
(normalised to β-actin)
150
100
50
0

Figure 4.23 AEP expression in expanded human iTreg cells *in vitro* in response to IL-2 stimulation - Donor 9. PBMCs were isolated from blood and $CD4^+CD25^-CD127^+CD45RA^+$ and $CD4^+CD25^{high}CD127^{low}$ T cells were isolated using cell sorting. Following sorting, cells were cultured *in vitro* at 1 million cells/ml for 5 days in αCD3-coated plates (5 μg/ml) in the presence of αIL-4 (10 μg/ml) and αIFN-γ (10 μg/ml) with the addition of αCD28 (2 μg/ml), rhIL-2 (100 ng/ml) and rhTGF-β1 (5 ng/ml) where appropriate. Cells were expanded for an additional 7 days in the presence of rhIL-2 which was added every 2 days. On day 12, cells from each condition were harvested using PMSF lysis buffer in preparation for protein analysis via western blotting. Lysates were reduced and boiled and run under reducing conditions on a precast, 4-12% Bis-Tris gradient gel. **A.** Western blot image showing AEP and β-actin expression in each of the culture conditions. The 56 and 37 kDa AEP bands were quantified using ImageJ and normalised to the respective β-actin loading control bands. **B.** Bar graph showing the expression levels of active, inactive and total AEP in each of the conditions. **C.** Bar graph showing the percentage ratio of active and inactive AEP expressed in each of the culture conditions. **D.** Bar graph showing the rate of T cell expansion of cells cultured under different culture conditions at the end of the culture. The expansion rate is presented as a fold change in number of cells at the end of culture (day 12) divided by the initial number of plated cells (day 0). n=1 donor.

In order to further assess the role of TGF-β1 in inducing AEP expression, cells were cultured in serum-free media (donor 10). The iTreg condition did not express sufficient levels of FOXP3 therefore it was excluded from the analysis (figure 4.24). All the rest of the conditions with the exception of cultured Treg cells expressed more inactive than active AEP (figure 4.25). A marked decrease of AEP was noted in the IL-2 condition (figure 4.25). However, it has been reported in the literature that TCR stimulation in addition to CD28 co-stimulation can induce apoptosis leading to the release of TGF-β1 which could account for the slightly increased levels of AEP when compared to the IL-2 condition (Krammer *et al.*, 2007). This effect was exacerbated in the absence of serum as the percent of apoptosis is lower in complete media cultures. Therefore, the IL-2 condition, which provides survival signals in T cell cultures, constitutes a better control in serum-free media. Taking this into consideration, the highest level of total AEP expression seemed to be induced by TGF-β1 (figure 4.25).

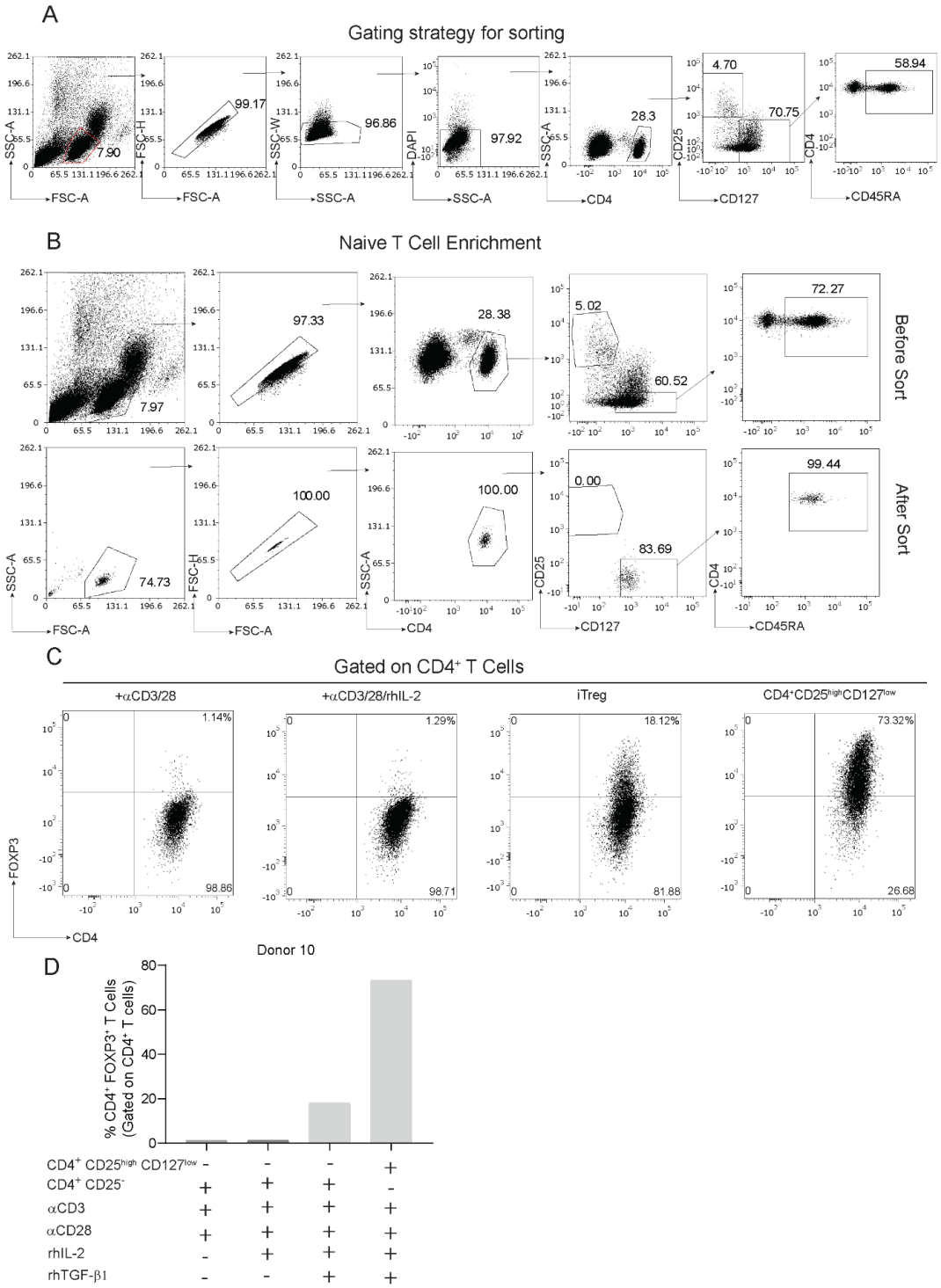
A
Gating strategy for sorting
SSC-A
FSC-A
7.90
FSC-H
99.17
SSC-W
96.86
DAPI
97.92
28.3
CD4
CD25
CD127
4.70
70.75
CD45RA
58.94
B
Naive T Cell Enrichment
7.97
97.33
28.38
5.02
60.52
72.27
Before Sort
74.73
100.00
100.00
0.00
83.69
99.44
After Sort
C
Gated on CD4+ T Cells
+αCD3/28
+αCD3/28/rhIL-2
iTreg
CD4+CD25highCD127low
FOXP3
1.14%
98.86
1.29%
98.71
18.12%
81.88
73.32%
26.68
D
Donor 10
% CD4+ FOXP3+ T Cells (Gated on CD4+ T cells)
CD4+ CD25high CD127low
CD4+ CD25-
αCD3
αCD28
rhIL-2
rhTGF-β1

Figure 4.24 FOXP3 expression in expanded iTreg cells - Donor 10. PBMCs were isolated from blood and $CD4^+CD25^-CD127^+CD45RA^+$ and $CD4^+CD25^{high}CD127^{low}$ T cells were isolated using cell sorting. PBMCs were counted and stained with CD4-FITC, CD25-APC, CD127-PE.CY7, CD45RA-PE and DAPI in Miltenyi buffer prior to sorting. Following sorting, cells were cultured *in vitro* at 1 million cells/ml in serum free X-vivo media for 5 days in αCD3-coated plates (5 μg/ml) in the presence of αIL-4 (10 μg/ml) and αIFN-γ (10 μg/ml) with the addition of αCD28 (2 μg/ml), rhIL-2 (100 ng/ml) and rhTGF-β1 (5 ng/ml) where appropriate. Cells were expanded for an additional 7 days in the presence of rhIL-2 which was added every 2 days. On day 12, cells from each condition were characterised for CD4 and FOXP3 expression. The rest were harvested using PMSF lysis buffer in preparation for protein analysis via western blotting. **A.** Flow plots illustrating the gating strategy used for sorting $CD4^+CD25^-CD127^+CD45RA^+$ and $CD4^+CD25^{high}CD127^{low}$ T cells. **B.** Flow plots showing enrichment of the naïve T cell population before and after cell sorting. **C.** Flow plots showing the frequency of $CD4^+FOXP3^+$ present within the $CD4^+$ T cell population in each culture condition on day 12. **D.** Bar graph showing the percentage frequency of $CD4^+FOXP3^+$ T cells present within the $CD4^+$ T cell population in each culture condition on day 12. n=1 donor.

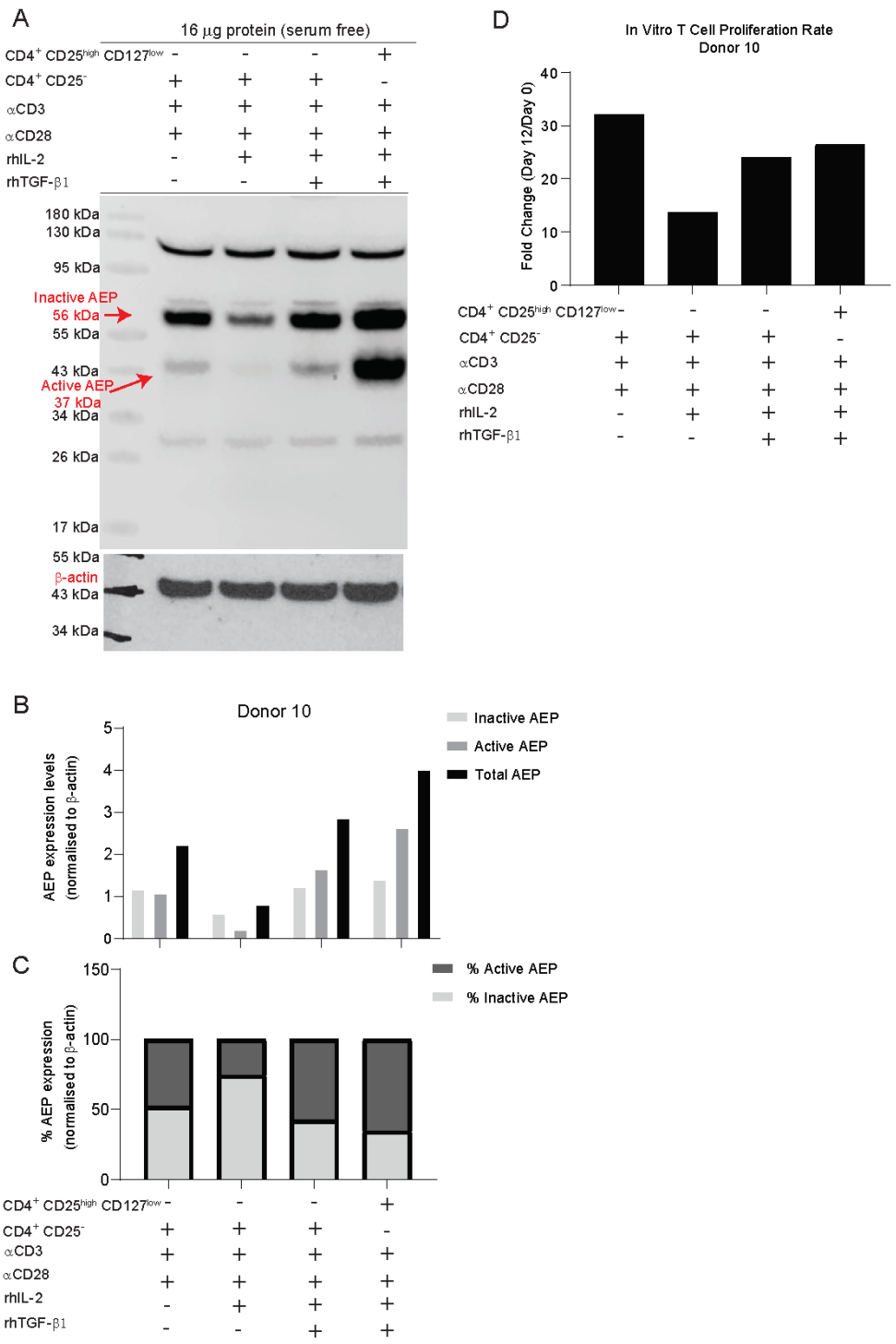
A
16 µg protein (serum free)
CD4+ CD25high CD127low
CD4+ CD25-
αCD3
αCD28
rhIL-2
rhTGF-β1
180 kDa
130 kDa
95 kDa
Inactive AEP
56 kDa
55 kDa
43 kDa
Active AEP
37 kDa
34 kDa
26 kDa
17 kDa
55 kDa
β-actin
43 kDa
34 kDa
D
In Vitro T Cell Proliferation Rate
Donor 10
Fold Change (Day 12/Day 0)
40
30
20
10
0
B
Donor 10
Inactive AEP
Active AEP
Total AEP
AEP expression levels
(normalised to β-actin)
5
4
3
2
1
0
C
% Active AEP
% Inactive AEP
% AEP expression
(normalised to β-actin)
150
100
50
0

Figure 4.25 AEP expression in expanded human iTreg cells *in vitro* - Donor 10. PBMCs were isolated from blood and $CD4^+CD25^-CD127^+CD45RA^+$ and $CD4^+CD25^{high}CD127^{low}$ T cells were isolated using cell sorting. Following sorting, cells were cultured *in vitro* at 1 million cells/ml in serum free X-vivo media for 5 days in αCD3-coated plates (5 μg/ml) in the presence of αIL-4 (10 μg/ml) and αIFN-γ (10 μg/ml) with the addition of αCD28 (2 μg/ml), rhIL-2 (100 ng/ml) and rhTGF-β1 (5 ng/ml) where appropriate. Cells were expanded for an additional 7 days in the presence of rhIL-2 which was added every 2 days. On day 12, cells from each condition were harvested using PMSF lysis buffer in preparation for protein analysis via western blotting. Lysates were reduced and boiled and run under reducing conditions on a precast, 4-12% Bis-Tris gradient gel. **A.** Western blot image showing AEP and β-actin expression in each of the culture conditions. The 56 and 37 kDa AEP bands were quantified using ImageJ and normalised to the respective β-actin loading control bands. **B.** Bar graph showing the expression levels of active, inactive and total AEP in each of the conditions. **C.** Bar graph showing the percentage ratio of active and inactive AEP expressed in each of the culture conditions. **D.** Bar graph showing the rate of T cell expansion of cells cultured under different culture conditions at the end of the culture. The expansion rate is presented as a fold change in number of cells at the end of culture (day 12) divided by the initial number of plated cells (day 0). n=1 donor.

Collective analysis of data demonstrated that freshly isolated naïve and Treg cells expressed more inactive AEP than active AEP (figure 4.26). However, freshly isolated Treg cells expressed more inactive AEP and less active AEP than naïve T cells (figure 4.26). Consistent with the hypothesis, the fact that freshly isolated Treg cells expressed more inactive AEP than naïve T cells reinforces the idea that AEP plays a role in the Treg cell signature (figure 4.26).

When data from expanded T cells were analysed, AEP was shown to be expressed in expanded Treg and iTreg cells. Culture of freshly isolated Treg cells under iTreg conditions increased expression of active AEP levels (figure 4.26). In addition to this, these cells expressed more active than inactive AEP which is the opposite of what was observed in the freshly isolated Treg cell population (figure 4.26). TGF-β1 seemed to induce the highest level of AEP expression *in vitro* as iTreg cells tended to express more total AEP than naïve T cells stimulated *in vitro* with αCD3, αCD28 or rhIL-2 (figure 4.26). Higher AEP levels were observed in cultured Treg cells than in iTreg cells *in vitro* (figure 4.26). In addition, culture of freshly isolated Treg cells under iTreg conditions led to a significant increase in active AEP

levels (p=0.0294) (figure 4.26). In addition, cultured Treg cells along with freshly isolated Treg cells tended to express the highest level of total AEP

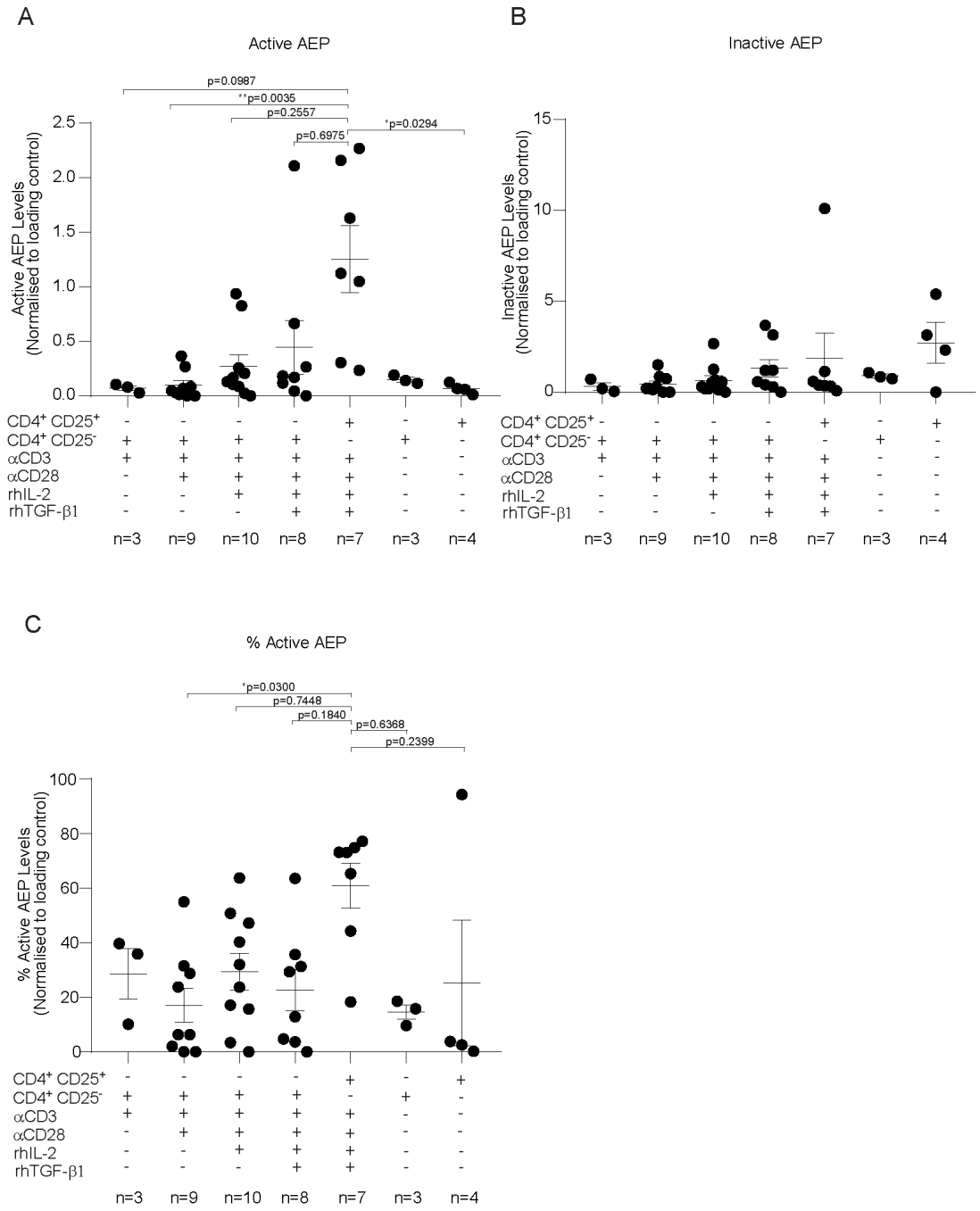

(figure 4.26).

Figure 4.26 Summary of AEP expression in human Treg cells. Collective analysis of AEP expression in human donors. Only cultures with sufficient (>50%) FOXP3 expression within the Treg cell compartment were included in the analysis and where cytometry data were not available, cultures where FOXP3 expression was detected using western blotting were analysed. The 56 (inactive) and 37 (active) kDa AEP bands were quantified using ImageJ and normalised to the respective loading control bands. **A.** Summary graph showing the expression levels of active AEP in each of the culture conditions. **B.** Summary graph showing the expression levels of inactive AEP in each of the conditions. **C.** Summary graph showing the percentage ratio of active AEP expressed in each of the culture conditions normalised to total AEP levels (100%). The Shapiro-Wilk normality test was used to confirm normal distribution of data and the nonparametric Kruskal-Wallis test was used for variance analysis. P values ≤0.05 were defined as statistically significant. A total of 14 donors were tested (n=14).

4.4 Conclusion

The role of proteases in T cell differentiation has not been widely studied in either mice or human T cells. However, studies have shown that proteases have different biological functions and the induction of their expression is therefore hypothesised to play a role in determining T helper subset function (Zhang *et al.*, 2017; Aschenbrenner *et al.*, 2018). Differential expression of proteases and protease inhibitors can play a role in determining T cell signatures and function. Studies have demonstrated that TGF-β1 and STAT3 signalling regulate AEP expression in mice (Zhang *et al.*, 2017; Martinez-Fabregas *et al.*, 2018). Downregulation of AEP in mouse T cells correlates with a decrease in Th17 induction and an increase in Treg cell induction which is in accordance with the data presented in chapter 3 (Hou *et al.*, 2015). In humans, downregulation of AEP correlates with a decrease in Th1 and Th17 responses and its expression is involved in regulating the Treg/Th17 axis (Aschenbrenner *et al.*, 2018; Freeley *et al.*, 2018).

In order to study AEP expression in human T cell subsets, a Treg isolation kit was used to sort human naïve and Treg cells and AEP expression was then detected using western blotting. Although AEP expression was studied in multiple human T cell subsets including Th1 and Th2 cells, lack of proper controls, stimulation experiments and cytokine expression profiling made it unclear as to whether the cultured T cells were indeed Th1 or Th2 etc. (appendix B). However, it was shown that AEP is expressed in freshly sorted

naïve and Treg cells. Following this observation, AEP expression was tested in iTreg cells. For this purpose, naïve T cells were expanded and stimulated *in vitro* with different combinations of cytokines in addition to TCR stimulation. It was shown that AEP is expressed in human iTreg cells and that TGF-β1 consistently induced the highest level of AEP expression *in vitro*. This indicates that a negative feedback loop may be in place in Treg cells that regulates AEP and FOXP3 expression. However, this methodology was not used to establish a correlation between active AEP levels and FOXP3 protein levels in cultured Treg cells. In order to do this, FOXP3 levels would have to be determined in Treg cells cultured under Treg stabilising conditions such as in the presence of an AEP inhibitor and/or PDL-1 stimulation. Also, a FOXP3 turnover assay using CHX and an AEP inhibitor could give an indication on whether increased active AEP levels correlate with reduced FOXP3 levels.

IL-2 was also shown to increase AEP expression but this was observed in only one of the donors (donor5). Taking into consideration that IL-2 and TGF-β1 are both involved in T cell differentiation into the Treg cell lineage and that AEP can regulate the Treg master transcription factor Foxp3 in mice, the question of whether IL-2 – in addition to TGF-β1 - increases AEP expression in human Treg cells was addressed (Chen *et al.*, 2003). As confirmation of the role of TGF-β1, human Treg cells were stimulated with IL-2 to test whether AEP expression levels would increase. Time point stimulation with IL-2 consistently failed to increase AEP expression in human Treg cells (donor4, donor5, donor7). It could be argued that the presence of TGF-β1-containing cell debris (donor7) in the initial sorted population that went into culture could have skewed the results. Therefore, to further investigate the role of TGF-β1 in the induction of AEP expression, cells were cultured in serum free media. This was done to remove any platelets (which are normally present in the supplementing serum) from the culture thus reducing the overall levels of TGF-β1 present in the medium. A marked decrease of AEP expression was noted in the IL-2 condition of the serum-free culture while a marked increase was observed in the αCD3/28 condition. This could be explained by the fact that TCR stimulation in combination with αCD28 in the absence of serum causes greater apoptosis

compared to cultures in complete media (Krammer *et al.*, 2007). Therefore, the IL-2 condition which provides survival signals in T cell cultures constitutes a better control in serum free media.

Despite all this, it is worth mentioning some of the limitations and pitfalls of this part of the project. This chapter started with an effort to identify AEP expression in T cell subsets but it was hard to establish a pattern. However, when data was analysed retrospectively, a pattern was emerging that identified TGF-β1 as an inducer of AEP expression which was also confirmed in the serum free culture. Therefore, stimulation experiments were performed in naïve and Treg cells *in vitro* in multiple donors. Since AEP is a novel protein and its expression has not been established in T cell subsets and T helper cell subsets in humans, every assay used in this methodology for the detection of AEP expression had to be validated and optimised. Due to the complexity of human donors (between donor variability), the experiments were repeated multiple times and each donor was presented separately. Furthermore, it is worth noting that this study relied solely on fresh PBMCs isolated from donated blood taken on the day of the experiment. This limited the number of cells used for sorting and as a result, led to a poor yield of Treg cells which typically comprise only 1% of the $CD4^+$ T cells found in the peripheral blood. Therefore, it was not possible to do a purity check of this population prior to cell culture or a functional assay at the end of the cultures. An attempt was made to detect AEP expression in human Treg cells using flow cytometry (appendix A). However, this methodology was not pursued further due to lack of proper controls and the limited availability of the primary Ab for AEP. Also, results from the acetone-precipitated lysates should be interpreted with caution as this methodology may have resulted in suboptimal protein solubilisation due to leftover acetone while a disruption of epitopes is also possible. Furthermore, there was some inconsistency regarding the number and sizes of AEP bands across the donors. This could be due to the reducing sample processing and reducing gel running conditions which could have altered protein epitopes and therefore Ab binding. However, it should be noted that the gel running conditions used for all these experiments were the same as those indicated in the data sheet that came with the purchased

polyclonal primary Ab. For all these reasons, the data presented in this chapter should only be considered as an indication of AEP expression in these cells and not interpreted as full proof data.

In conclusion, this chapter demonstrated that:

- human naïve T cells express both active and inactive AEP
- human Treg cells consistently express more inactive AEP that active AEP
- culturing of human Treg cells under iTreg conditions increases the levels of active AEP
- TGF-β1 stimulation induces the highest levels of AEP expression
- IL-2 stimulation does not play a role in AEP expression.

Chapter 5. Stimuli That Regulate AEP in Human T Cells

5.1 Introduction

In the previous chapter, it was demonstrated that TGF-β1 consistently induced the highest level of AEP expression *in vitro* as culturing human T cells under iTreg conditions led to an increase in active as well as total AEP protein levels. This is consistent with the mouse studies presented in chapter 3 and with a study by Zhang et al. where it was shown that IL-6 stimulation in combination with inhibition of TGFBR-I in SMAD4 KO $CD4^+$ mouse T cells leads to the downregulation of AEP mRNA levels (Zhang *et al.*, 2017). However, in addition to TGF-β1 and PD-1, other stimuli have been associated with upregulating or downregulating AEP expression levels in mice (Zhang *et al.*, 2017; Martinez-Fabregas *et al.*, 2018; Stathopoulou *et al.*, 2018). *Lgmn*$^{-/-}$ mouse embryonic fibroblasts (MEF) and proximal tubular cells (PTCs) have been shown to express increased levels of active STAT3 while STAT3 inhibition in these cells leads to the downregulation of AEP (Martinez-Fabregas *et al.*, 2018). Inhibition of AEP in these cells leads to a dose-dependent increase in pSTAT3 levels accompanied with an increase in expression levels of other lysosomal hydrolases such as cathepsin D (Martinez-Fabregas *et al.*, 2018). Additionally, 3T3 fibroblasts expressing constitutively active STAT3 show increased levels of AEP and cathepsin D activity (Martinez-Fabregas *et al.*, 2018). In humans, AEP inhibition in PTCs results in increased STAT3 and cathepsin D activation (Martinez-Fabregas *et al.*, 2018). This study demonstrates that STAT3 signalling is also implicated in the regulation of AEP in both mice and humans (Martinez-Fabregas *et al.*, 2018). However, whether this mechanism exists in other types of human cells is unknown. Therefore, it is here hypothesised that STAT3 regulates AEP function in human lymphocytes also.

Since the role of PD-1 signalling in AEP regulation in human lymphocytes has not been assessed previously and to further validate the significance of TGF-β1, PD-1 and STAT3 signalling in regulating AEP function in human lymphocytes, a functional assay was used that specifically measured AEP activity levels.

5.2 Aims

The aim of this chapter is to determine stimuli that regulate AEP activity in human T cells. For this purpose, human T lymphocytes from isolated PBMCs were expanded *in vitro* and relevant signalling pathways were targeted pharmacologically. Changes in AEP activity were then studied using an AEP enzyme activity assay which relies on AEP-specific cleavage of a fluorescently-labelled substrate as outlined in sections 2.2.4 and 2.27.

5.3 Results

5.3.1 *AEP enzyme activity development and optimisation*

To determine AEP enzyme activity levels, an activity assay was developed and optimised based on published methodology (Johansen *et al.*, 1999; Li *et al.*, 2003; Haugen *et al.*, 2013; Stathopoulou *et al.*, 2018). AMC standards of different concentrations were tested using a fluorimeter (POLARstar Omega, BMG LABTECH, UK) and the settings of the plate reader were adjusted accordingly to optimise the standard curve.

In the first experiment, AMC standards of lower concentrations came up lower than blank controls so no standard curve could be produced (figure 5.1A). This was due to not specifying the detection range limits of the machine at the beginning of the experiment.

After adjusting the settings in the machine, the experiment was repeated two more times. More standards of lower concentrations were included in experiments 2 and 3 to accurately calculate enzyme activity levels in samples of low AEP content which are expected to emit low fluorescence intensity (F.I.) signals. Assay buffer pH was lowered from pH 5.5 to 5 while for AMC standards of higher concentrations (≥ 400 μM), the detection filter was getting saturated leading to inaccurate measurements of higher intensity signals (figure 5.1B-C). However, all samples that were subsequently screened for AEP activity during this project emitted signals that fell within the range of 6 μM and 0 μM.

Following standard curve optimisation, 10 μg of DC lysate that expresses high levels of AEP was tested. This experiment was also performed to determine the length of incubation in activation buffer needed to activate the total amount of enzyme present in the lysate as well as determine whether

a concentration of 100μM of substrate was enough for AEP activity detection. Readings were taken at regular intervals to determine the optimum length of incubation with the substrate before activity levels could be detected (figure 5.2C). Based on the results of this experiment, the optimum time length of incubation with activation buffer was determined to be 2 hours at 1:1 dilution of lysate (pH 5.8) and activation buffer (pH 4). The optimum duration of incubation with the substrate (in assay buffer of pH 5) was 90 minutes (Manoury *et al.*, 2002) with a final substrate concentration of 100 μM. Fluorescence intensity values that were detected fell within the range of the 12 – 0 μM standards so in future assays 13 standards were used. Also, 10 μg of DC lysate were used as positive controls in all future experiments. In subsequent experiments, readings were taken at 90 minutes after substrate addition and AEP activity levels were normalised to the amount of protein present in the lysate. An equal amount of protein lysate was used in experiments.

Studies have shown that AEP is resistant to selective protease inhibitors such as E-64 (cysteine protease inhibitor), PMSF (cysteine protease inhibitor) and pepstatin A as well as leupeptin (cysteine, serine and threonine protease inhibitor) (Johansen *et al.*, 1999; Li *et al.*, 2003; Teng *et al.*, 2009). To check substrate specificity, DC lysates were activated in the presence of the protease inhibitor pepstatin A (5 μM) and activity levels were measured (figure 5.3). Pepstatin A is an inhibitor of aspartate and aspartyl proteases but not cysteine, thiol or serine proteases (Marciniszyn *et al.*, 1976). In accordance with the literature, no inhibition of AEP activity was observed in the presence of pepstsatin A (figure 5.3C). However, it should be noted that additional controls would have to be included in the assay to increase confidence in the substrate specificity. For instance, an AEP-specific inhibitor could be added to the reaction as well as a more general inhibitor such as cystatin E which is known to inhibit AEP function (Dall and Brandstetter, 2013; Dall and Brandstetter, 2016).

A

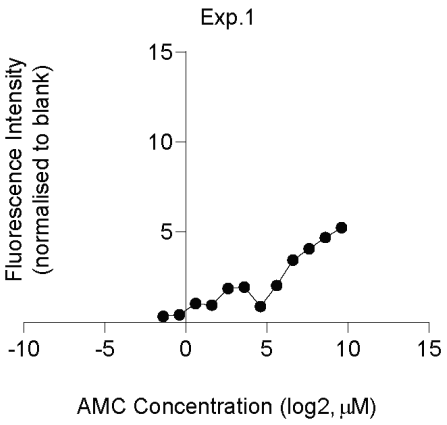
Exp.1
Fluorescence Intensity
(normalised to blank)
15
10
5
-10
-5
0
5
10
15
AMC Concentration (log2, μM)

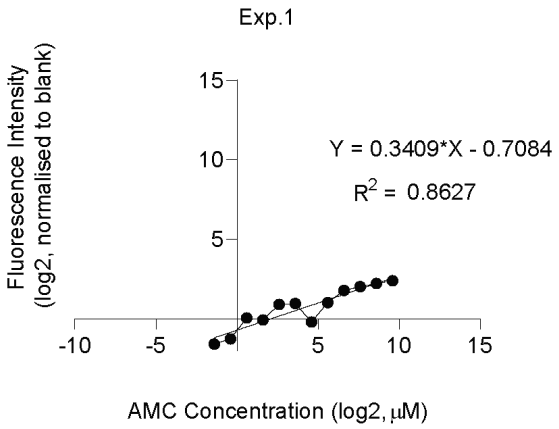
Exp.1
Fluorescence Intensity
(log2, normalised to blank)
Y = 0.3409*X - 0.7084
R2 = 0.8627
15
10
5
-10
-5
5
10
15
AMC Concentration (log2, μM)

B

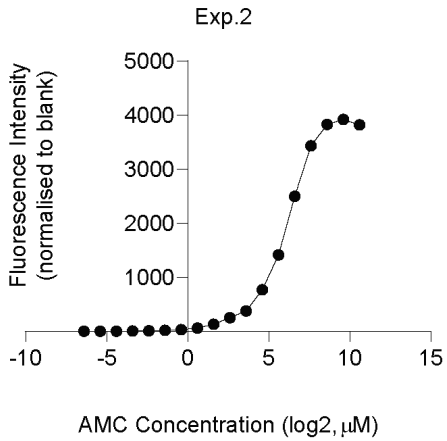
Exp.2
Fluorescence Intensity
(normalised to blank)
5000
4000
3000
2000
1000
-10
-5
0
5
10
15
AMC Concentration (log2, μM)

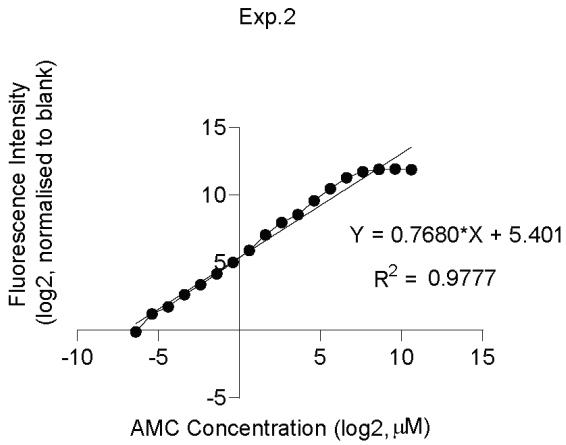
Exp.2
Fluorescence Intensity
(log2, normalised to blank)
Y = 0.7680*X + 5.401
R2 = 0.9777
15
10
5
-5
-10
-5
5
10
15
AMC Concentration (log2, μM)

C

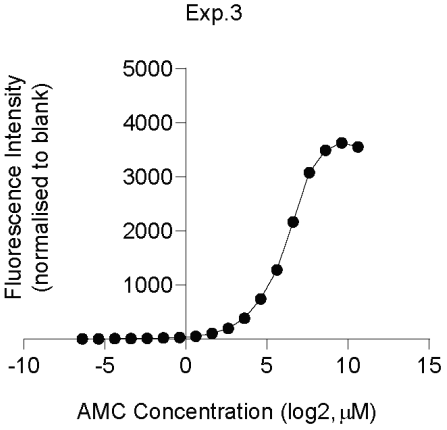
Exp.3
Fluorescence Intensity
(normalised to blank)
5000
4000
3000
2000
1000
-10
-5
0
5
10
15
AMC Concentration (log2, μM)

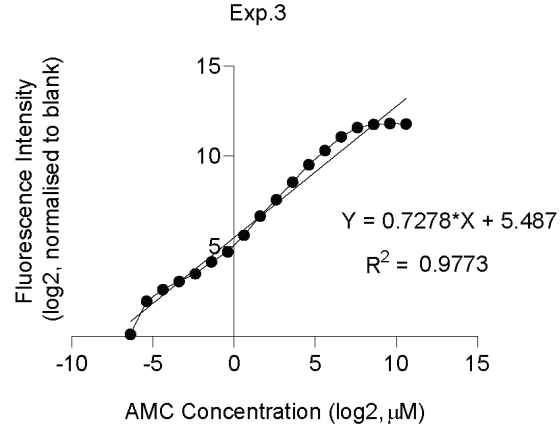
Exp.3
Fluorescence Intensity
(log2, normalised to blank)
Y = 0.7278*X + 5.487
R2 = 0.9773
15
10
5
-10
-5
0
5
10
15
AMC Concentration (log2, μM)

Figure 5.1 AEP enzyme activity assay – standard curve optimisation. Different concentrations of AMC were tested. AMC standards were prepared in 100 μl assay buffer and fluorescence was detected using a POLARstar Omega (BMG LABTECH, UK) fluorimeter. **A.** 13 standards of AMC ranging from 800 μM to 0 μM were prepared in assay buffer with pH 5.5. No minimum or maximum values were specified in the plate reader's settings. **B.** 19 standards of AMC ranging from 1600 μM to 0 μM were prepared in assay buffer with pH 5. The detection range limits of the plate reader were specified at the beginning of the experiment. The standard with the highest concentration of 1600 μM was set to 90% of the total signal detected by the plate reader. **C.** The experiment was repeated using the same settings as in the second experiment. In all experiments, blank controls containing only assay buffer were included in the plate to determine background noise levels. Readouts for every single standard were averaged and normalised to blank. The linearity of the regression model was tested by plotting the log2 values of the normalised fluorescent intensity (FI) values against the log2 values of the standard concentrations (μM). n=3 donors.

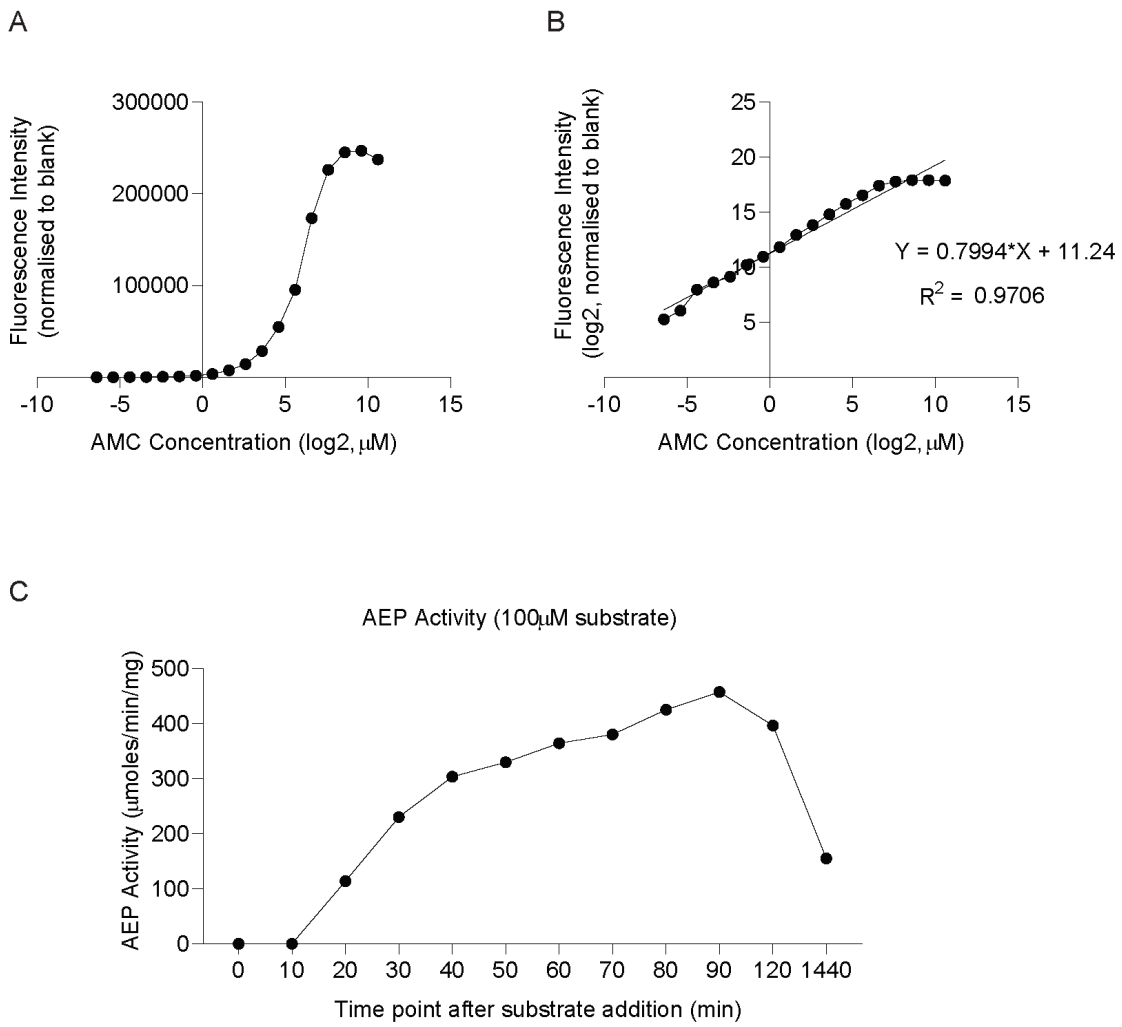

Figure 5.2 AEP enzyme activity assay – standard curve optimisation. A. 19 standards of AMC ranging from 1600 μM to 0 μM were prepared in assay buffer with pH 5. The detection range limits of the plate reader were specified at the beginning of the experiment. The standard with the highest concentration of 1600 μM was set to 75% of the total signal detected by the plate reader. Blank controls containing only assay buffer were included in the plate to determine background noise levels. Readouts for every single standard were averaged and normalised to blank. **B.** The linearity of the regression model was tested by plotting the log2 values of the normalised fluorescent intensity (FI) values against the log2 values of the standard concentrations (μM). **C.** Human tolerogenic dendritic cells were lysed using n-octyl lysis buffer and 10 μg of protein lysate were diluted with activation buffer at 1:1 ratio and incubated for 2hrs at 37°C to activate AEP. The reaction mixture was topped up to 100 μl with assay buffer and AEP-specific substrate. A final concentration of 100 μM of substrate was used. A blank control containing only substrate of 100 μM in assay buffer was included. Readouts were taken at regular intervals. Activity levels were normalised to the relevant controls. N=1

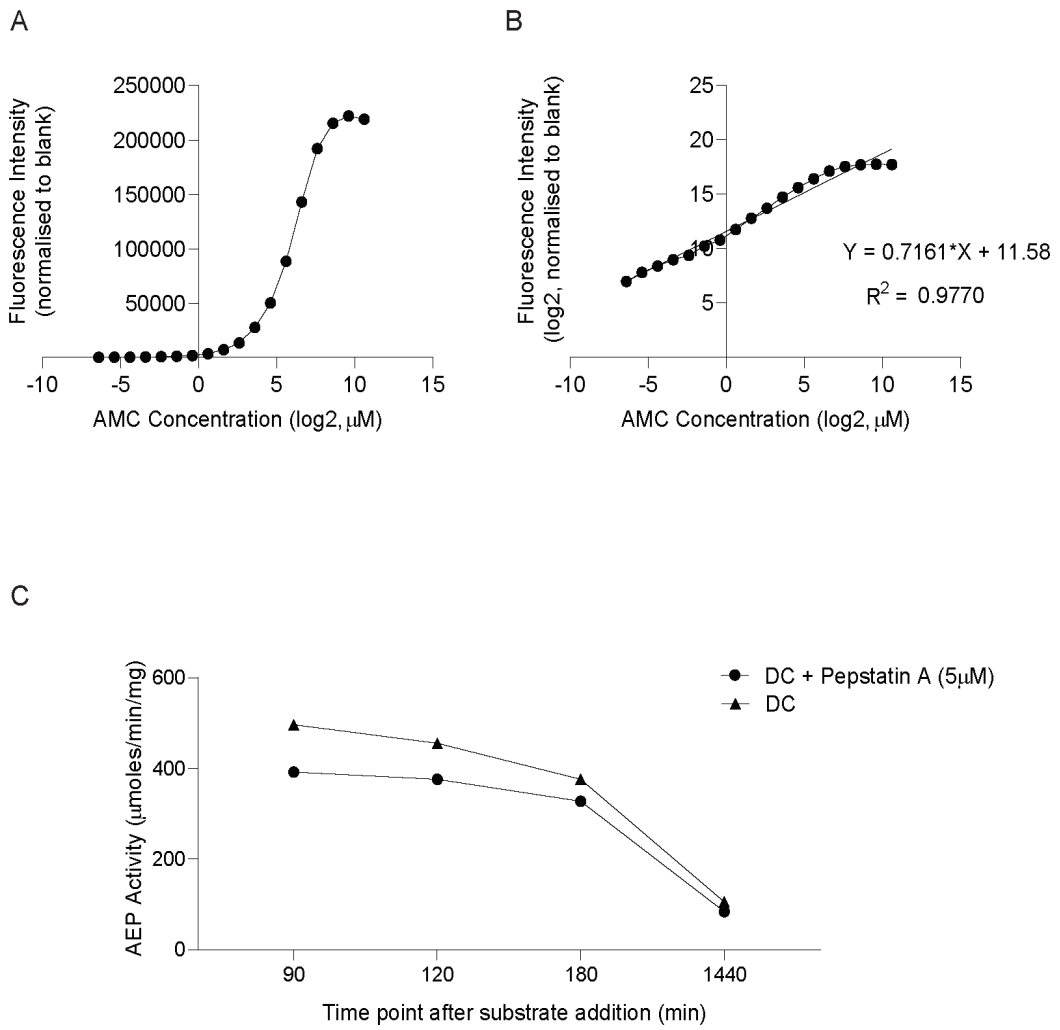

Figure 5.3 AEP enzyme activity assay – substrate specificity. A. 19 standards of AMC ranging from 1600 μM to 0 μM were prepared in assay buffer with pH 5. The detection range limits of the plate reader were specified at the beginning of the experiment. The standard with the highest concentration of 1600 μM was set to 75% of the total signal detected by the plate reader. Blank controls containing only assay buffer were included in the plate to determine background noise levels. Readouts for every single standard were averaged and normalised to blank. **B.** The linearity of the regression model was tested by plotting the log2 values of the normalised fluorescent intensity (FI) values against the log2 values of the standard concentrations (μM). **C.** Human mature dendritic cells were lysed using n-octyl lysis buffer and 10 μg of protein lysate were diluted with activation buffer at 1:1 ratio and incubated for 2hrs at 37°C to activate AEP with the addition of 5 μM pepstatin A final concentration. The reaction mixture was topped up to 100 μl with assay buffer and AEP-specific substrate to a final concentration of 100 μM. A blank control containing 100 μM substrate in assay buffer was included. Readouts were taken at regular intervals and activity levels were normalised to the blank control. N=1

5.3.2 *TGF-β1 inhibition blocks AEP activity in human lymphocytes*

In order to determine whether TGF-β1 played a role in AEP activity, publically available datasets of mouse T cells with a SMAD4-specific deletion were mined and analysed. Naïve $CD4^+$ T cells from *Cd4cre;Smad4$^{fl/fl}$* mice that were activated in the presence of IL-6 and a TGFβR inhibitor for 3 hours showed a significant decrease in AEP mRNA levels compared to WT controls (p=0.0073) (figure 5.4) (Zhang *et al.*, 2017). This indicates that TGF-β1 is important for upregulating AEP mRNA expression. However, this effect was not observed after 12 hours of stimulation suggesting that IL-6 is able to eventually compensate for the loss of TGF-β1 signalling. Collectively, these results indicate that TGF-β1 signalling is involved in initial AEP expression which is stabilised by IL-6.

To validate the results from the western blotting experiments presented in chapter 4 and to further examine the significance of TGF-β1 signalling in inducing AEP expression, an AEP enzyme activity assay was performed using lysates of human lymphocytes. Specifically, human PBMCs were expanded *in vitro* in the presence of the mitogen PHA that promotes the proliferation of lymphocytes and a specific inhibitor for TGFBR-I. After five days of culture, cells were lysed and AEP activity measured.

In order to optimise lymphocyte expansion with PHA, total PBMCs from three separate donors were cultured in the presence of PHA for five days and the frequency of T cells assessed on day 0 and day 5 (figure 5.5). Whilst lymphocytes did not expand more than 1-fold in 5 days, monocytes and APCs were eliminated after 5 days of culture (figure 5.5). Also, there was a significant increase in the frequency of T cells ($CD3^+$, >80% of single cells, p=0.0226) and $CD4^+$ T cells (35 - 45% of single cells, p=0.0459) after 5 days of culture with PHA (figure 5.6).

The experiment was repeated with the addition of TGFBR-I inhibitor at different concentrations and this showed a pattern whereby TGFBR-I inhibition decreased AEP activity levels supporting the hypothesis (figure 5.7).

A

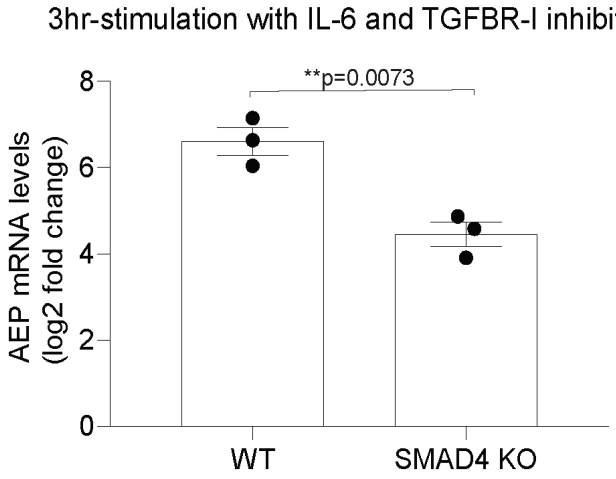

B

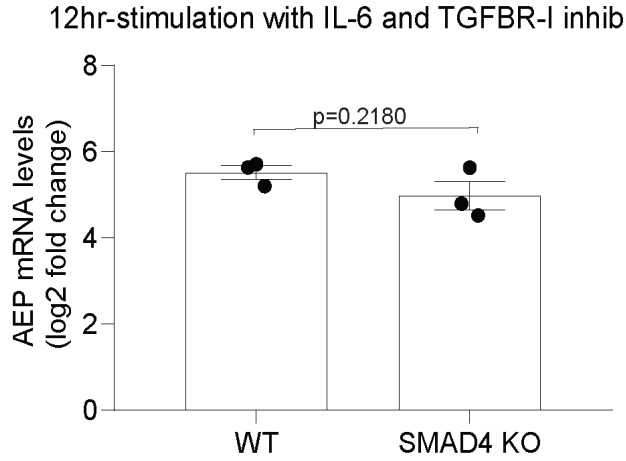

KO 12hr IL6SB 1	4.520914956
KO 12hr IL6SB 2	4.794614729
KO 12hr IL6SB 3	5.627314442
KO 3hr IL6SB 2	3.908340255
KO 3hr IL6SB 3	4.871671981
KO 3hr IL6SB 1	4.581117373
WT 12hr IL6SB 2	5.636315169
WT 12hr IL6SB 3	5.712718429
WT 12hr IL6SB 1	5.206616338
WT 3hr IL6SB 2	6.045835526
WT 3hr IL6SB 3	6.634018928
WT 3hr IL6SB 1	7.149207048

Figure 5.4 Inhibition of TGFBR-I downregulates AEP mRNA levels in murine, naïve, SMAD4 KO T cells (public data mining). Sorted $CD4^{+}CD25^{-}CD44^{low}CD62L^{high}$ T cells were isolated from the spleen of *Smad4*$^{fl/fl}$ C57BL/6 mice and cultured in complete RPMI medium in the presence of αIL-4 (20 μg/ml), αIFN-γ (20 μg/ml), IL-6 (40 ng/ml) and TGFBR-I inhibitor (10 μM). **A.** Bar graph showing AEP mRNA levels as log2 fold change after 3 hours of stimulation with IL-6 and the TGFBR-I inhibitor. Log2 fold change values were normalised to IL-6-treated cells. **B.** Bar graph showing AEP levels as log2 fold change after 12 hours of stimulation with IL-6 and the TGFBR-I inhibitor. Sample values were normalised to the IL-6-only condition. The Shapiro-Wilk normality test was used to confirm normal distribution of data. An unpaired, 2-tailed Student's t test was used for variance analysis. P values ≤0.05 were defined as statistically significant. N=3. Dataset accession number: GSE101527.

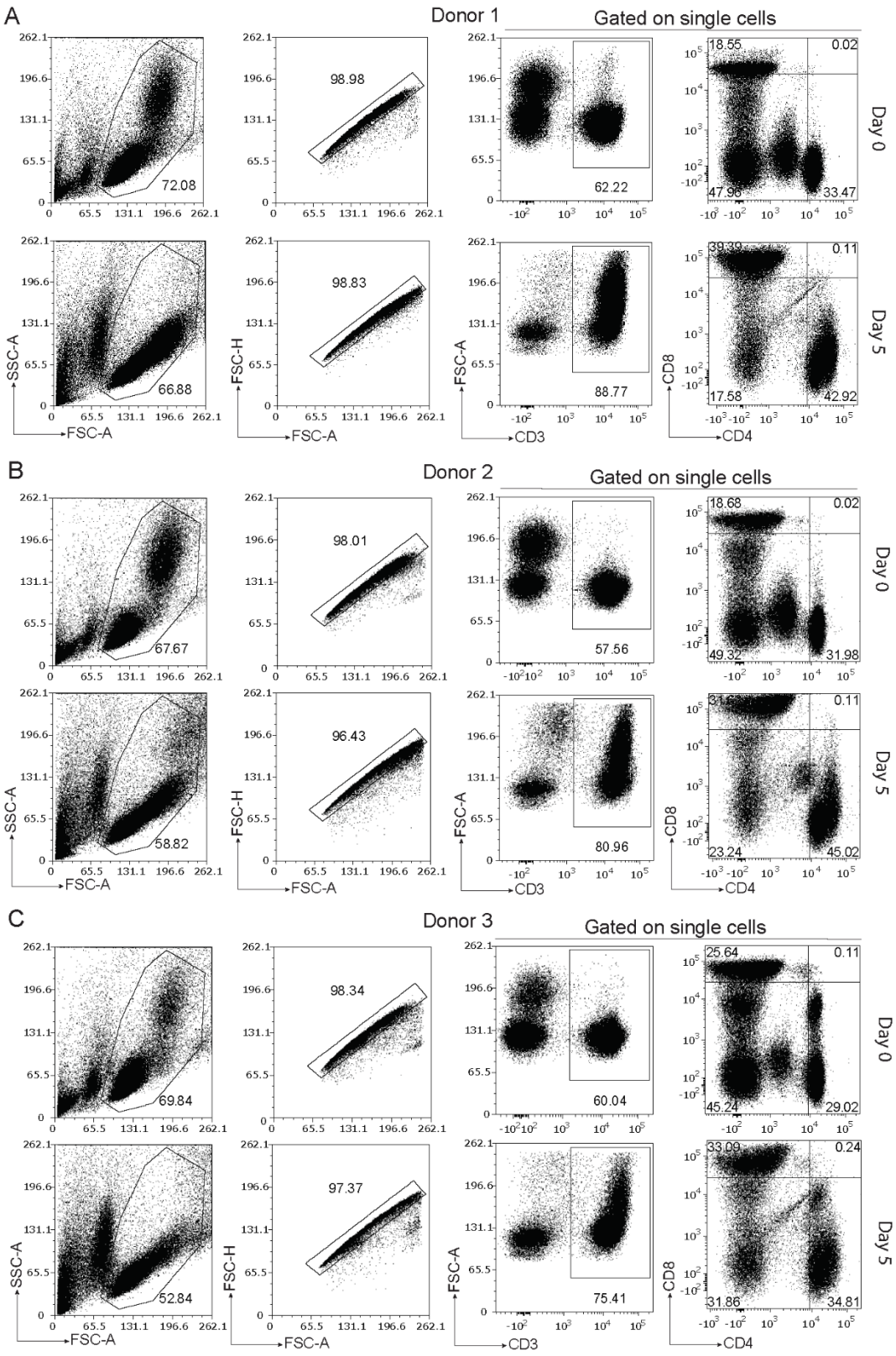
A
Donor 1
Gated on single cells
Day 0
Day 5
72.08
98.98
62.22
18.55
0.02
47.96
33.47
66.88
98.83
88.77
39.30
0.11
17.58
42.92
B
Donor 2
Gated on single cells
67.67
98.01
57.56
18.68
0.02
49.32
31.98
58.82
96.43
80.96
0.11
23.24
45.02
C
Donor 3
Gated on single cells
69.84
98.34
60.04
25.64
0.11
45.24
29.02
52.84
97.37
75.41
33.09
0.24
31.86
34.81
SSC-A
FSC-A
FSC-H
CD3
CD8
CD4

Figure 5.5 Optimisation of lymphocyte expansion with Phytohemagglutinin–M (PHA). PBMCs from healthy human donors were cultured in 48-well plates at 1 million cells per ml in complete RPMI media. The cells were stimulated with 2 μg/ml of PHA and expanded for 5 days at 37^{o}C. One million cells were taken on day 0 and day 5 and stained with CD3 – APC, CD4 – Percpcy5.5, CD8 – PE and Fc block. **A-C.** Flow plots illustrating the gating strategy used for the characterisation of lymphocytes on day 0 and day 5 in three different donors. N=3

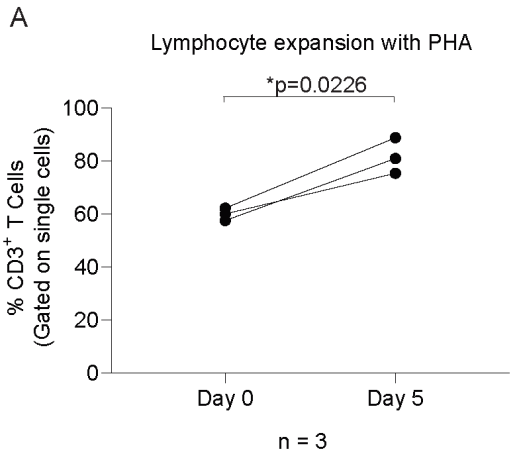
A
Lymphocyte expansion with PHA
*p=0.0226
% CD3+ T Cells
(Gated on single cells)
100
80
60
40
20
0
Day 0
Day 5
n = 3

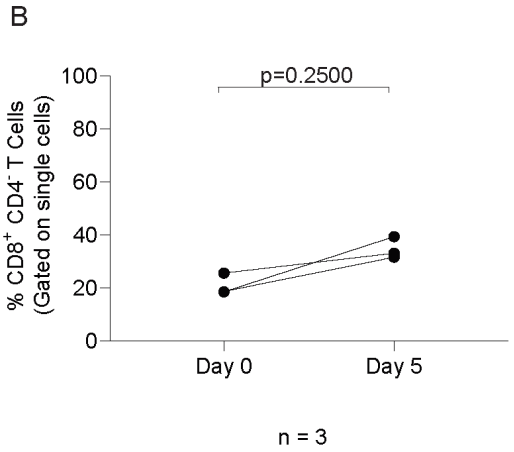
B
p=0.2500
% CD8+ CD4- T Cells
(Gated on single cells)
100
80
60
40
20
0
Day 0
Day 5
n = 3

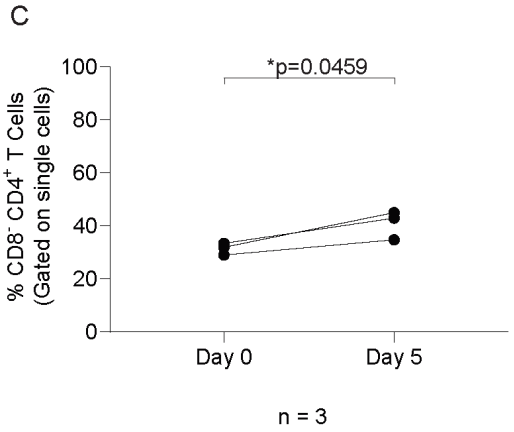
C
*p=0.0459
% CD8- CD4+ T Cells
(Gated on single cells)
100
80
60
40
20
0
Day 0
Day 5
n = 3

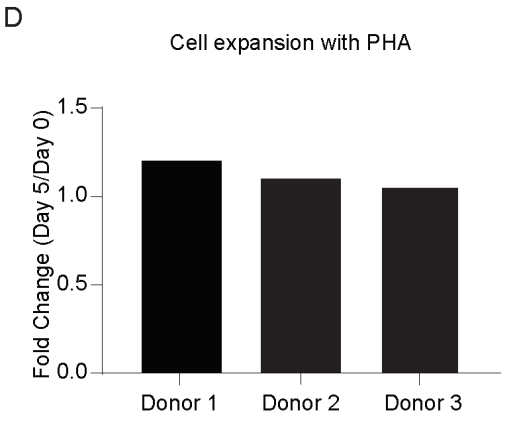
D
Cell expansion with PHA
Fold Change (Day 5/Day 0)
1.5
1.0
0.5
0.0
Donor 1
Donor 2
Donor 3

Figure 5.6 Expansion of human T lymphocytes with PHA. PBMCs from healthy human donors were cultured in 48-well plates at 1 million cells per ml in complete RPMI media. The cells were stimulated with 2 μg/ml of PHA and expanded for 5 days at 37ºC. One million cells were taken on day 0 and day 5 and stained with CD3 – APC, CD4 – Percpcy5.5, CD8 – PE and Fc block. **A-C.** Histograms showing the frequency of $CD3^+$, $CD8^+$ and $CD4^+$ T cell populations on day 0 and day 5 in 3 donors. **D.** Bar graph showing the rate of cell expansion in each donor. The expansion rate is presented as a fold change in number of cells at the end of culture (day 5) divided by the initial number of plated cells (day 0). The Shapiro-Wilk normality test was used to confirm normal distribution of data. The One Way Anova test was used for normally distributed data. Alternatively, the nonparametric Kruskal-Wallis test was used for variance analysis. P values ≤0.05 were defined as statistically significant. N=3

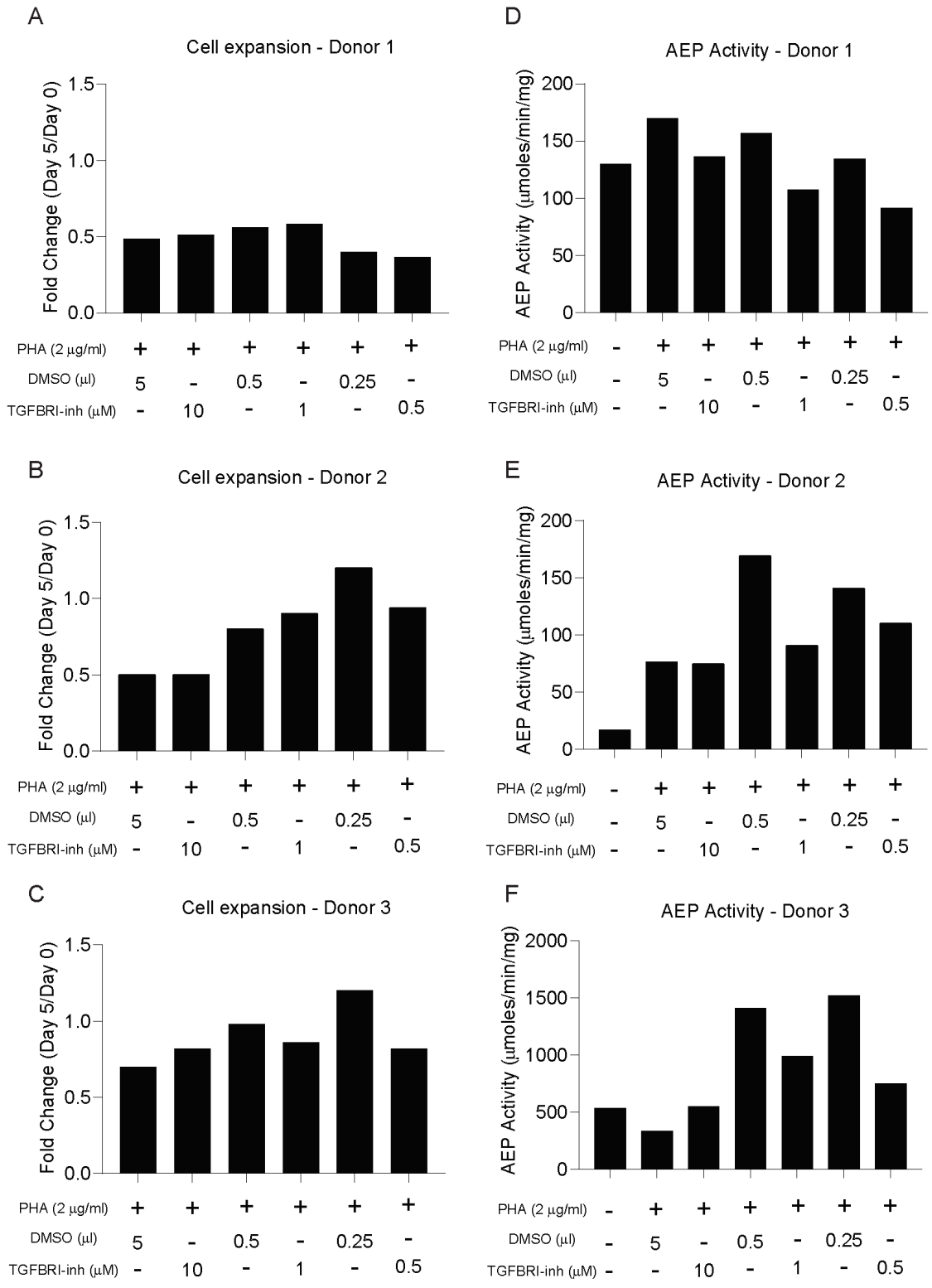
A
Cell expansion - Donor 1
Fold Change (Day 5/Day 0)
1.5
1.0
0.5
0.0
PHA (2 µg/ml) + + + + + +
DMSO (µl) 5 - 0.5 - 0.25 -
TGFBRI-inh (µM) - 10 - 1 - 0.5
D
AEP Activity - Donor 1
AEP Activity (µmoles/min/mg)
200
150
100
50
0
PHA (2 µg/ml) - + + + + + +
DMSO (µl) - 5 - 0.5 - 0.25 -
TGFBRI-inh (µM) - - 10 - 1 - 0.5
B
Cell expansion - Donor 2
Fold Change (Day 5/Day 0)
1.5
1.0
0.5
0.0
PHA (2 µg/ml) + + + + + +
DMSO (µl) 5 - 0.5 - 0.25 -
TGFBRI-inh (µM) - 10 - 1 - 0.5
E
AEP Activity - Donor 2
AEP Activity (µmoles/min/mg)
200
150
100
50
0
PHA (2 µg/ml) - + + + + + +
DMSO (µl) - 5 - 0.5 - 0.25 -
TGFBRI-inh (µM) - - 10 - 1 - 0.5
C
Cell expansion - Donor 3
Fold Change (Day 5/Day 0)
1.5
1.0
0.5
0.0
PHA (2 µg/ml) + + + + + +
DMSO (µl) 5 - 0.5 - 0.25 -
TGFBRI-inh (µM) - 10 - 1 - 0.5
F
AEP Activity - Donor 3
AEP Activity (µmoles/min/mg)
2000
1500
1000
500
0
PHA (2 µg/ml) - + + + + + +
DMSO (µl) - 5 - 0.5 - 0.25 -
TGFBRI-inh (µM) - - 10 - 1 - 0.5

Figure 5.7 Inhibition of TGFBR-I downregulates AEP activity. PBMCs from healthy human donors were cultured in 48-well plates at 1 million cells per ml in complete RPMI media. The cells were stimulated with 2 μg/ml of PHA and expanded for 5 days at 37ºC in the presence of either DMSO or TGFBR-I inhibitor at 10, 1 or 0.5 μM final concentration. An equal volume of the TGFBR-I inhibitor and DMSO was added to the relevant conditions. Cells from day 0 and day 5 were harvested using n-octyl lysis buffer in preparation for the enzyme activity assay. **A-C.** Bar graphs showing the rate of cell expansion in each culture condition in each donor. The expansion rate is presented as a fold change in number of cells at the end of culture (day 5) divided by the initial number of plated cells (day 0). **D-F.** Bar graphs showing AEP activity levels on day 0 and day 5 in each culture condition in each donor. Readouts were taken at 90 min after the addition of substrate and activity levels were normalised to the blank control. N=3

5.3.3 *STAT3-associated cytokines increase AEP activity in human lymphocytes*

Publicly mined datasets have shown that IL-2 does not play a role in inducing AEP mRNA expression in human T cells as Treg cells treated with IL-2 for 24 hours did not show any changes in AEP mRNA levels (figure 5.8) (Yu *et al.*, 2015).

In mice, IL-6 can induce AEP while inhibition of STAT3 signalling leads to downregulation of AEP expression (Zhang *et al.*, 2017; Martinez-Fabregas *et al.*, 2018). In support of this, knocking out STAT3 in Foxp3^{+} T cells promoted the Treg cell signature (Laurence *et al.*, 2012). STAT3 knock-out nTreg cells showed increased expression of Foxp3 and decreased expression of IL-17A when they were stimulated with IL-6 and IL-27 *in vitro* (Laurence *et al.*, 2012). *In vivo*, mice that received bone marrow transplants with naïve T cells that were conditional knock outs for STAT3 (*Foxp3-GFP;CD4-Cre;Stat3$^{fl/fl}$*) showed enhanced survival rates than those that received WT naïve T cells (*Foxp3-GFP;Stat3$^{fl/fl}$*) (Laurence *et al.*, 2012). This demonstrated that STAT3 expression destabilised iTreg cells in mice with GvHD leading to decreased survival rates (Laurence *et al.*, 2012). In humans, AEP expression has been shown to be increased in immunoregulatory IL-10^{+} Th17 cells rather than pro-inflammatory IL-10^{-} Th17 cells (Aschenbrenner *et al.*, 2018). Collectively, these studies support the hypothesis that STAT3 and AEP expression play a role in regulating the Treg/Th17 axis.

Therefore, the next step was to explore whether STAT3 induced AEP expression in human lymphocytes using a methodology similar to that described in 5.3.2. Treatment of cells with the STAT3 inhibitor demonstrated a significant decrease ($p=0.0021$) in AEP activity levels *in vitro* which is in accordance with the published literature (figure 5.9-10).

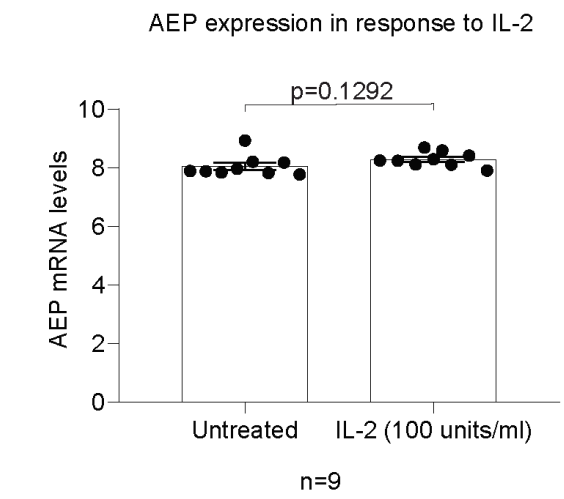

GSE49817 / GPL6244 / 7980958

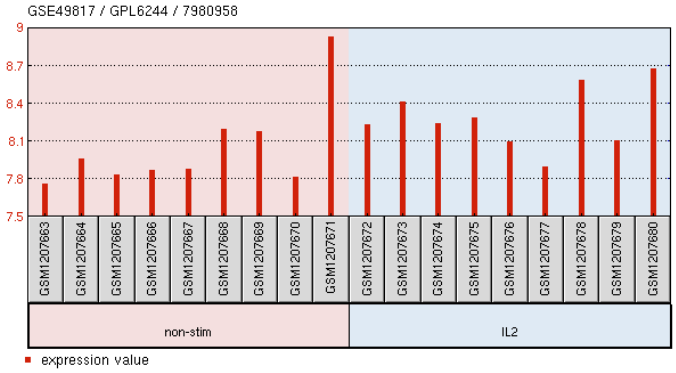

Sample	Title	Value
GSM1207663	Media-1	7.76943
GSM1207664	Media-2	7.96378
GSM1207665	Media-3	7.83445
GSM1207666	Media-4	7.87712
GSM1207667	Media-5	7.88576
GSM1207668	Media-6	8.20123
GSM1207669	Media-7	8.1793
GSM1207670	Media-8	7.82365
GSM1207671	Media-9	8.93266
GSM1207672	IL-2-1	8.23358
GSM1207673	IL-2-2	8.41491
GSM1207674	IL-2-3	8.24622
GSM1207675	IL-2-4	8.29111
GSM1207676	IL-2-5	8.10232
GSM1207677	IL-2-6	7.90384
GSM1207678	IL-2-7	8.58459
GSM1207679	IL-2-8	8.11167
GSM1207680	IL-2-9	8.68348

ID	adj.P.Val	P.Value	t	B	logFc	Gene.symbol	Gene.title
7980958	4.66E-01	1.04E-01	1.7027211	5.10246	0.2338156	LGMN	legumain
	p value adjusted after multiple testing, overall significance of differential expression	Raw p value	Overall test significance (when two groups are compared)	B-statistic or log-odds that the gene is differentially expressed (when two groups are compared)	Log2 Fold Change		

Figure 5.8 Regulation of AEP mRNA expression in human Treg cells (public data mining). Bar graph showing AEP mRNA levels in human $CD4^{+}CD25^{high}CD127^{-}$ Treg cells in response to 24hr stimulation with IL-2. $CD4^{+}$ T cells isolated from PBMCs were cultured in complete RPMI in the presence of IL-2 (100 units/ml) and Treg cells sorted and RNA purified. The Shapiro-Wilk normality test was used to confirm normal distribution of data. An unpaired, 2-tailed Student's t test was used for variance analysis. P values ≤0.05 were defined as statistically significant. N=9. Dataset accession number: GSE49817. The layout of the data output is shown in the outlined panel below the main bar graph.

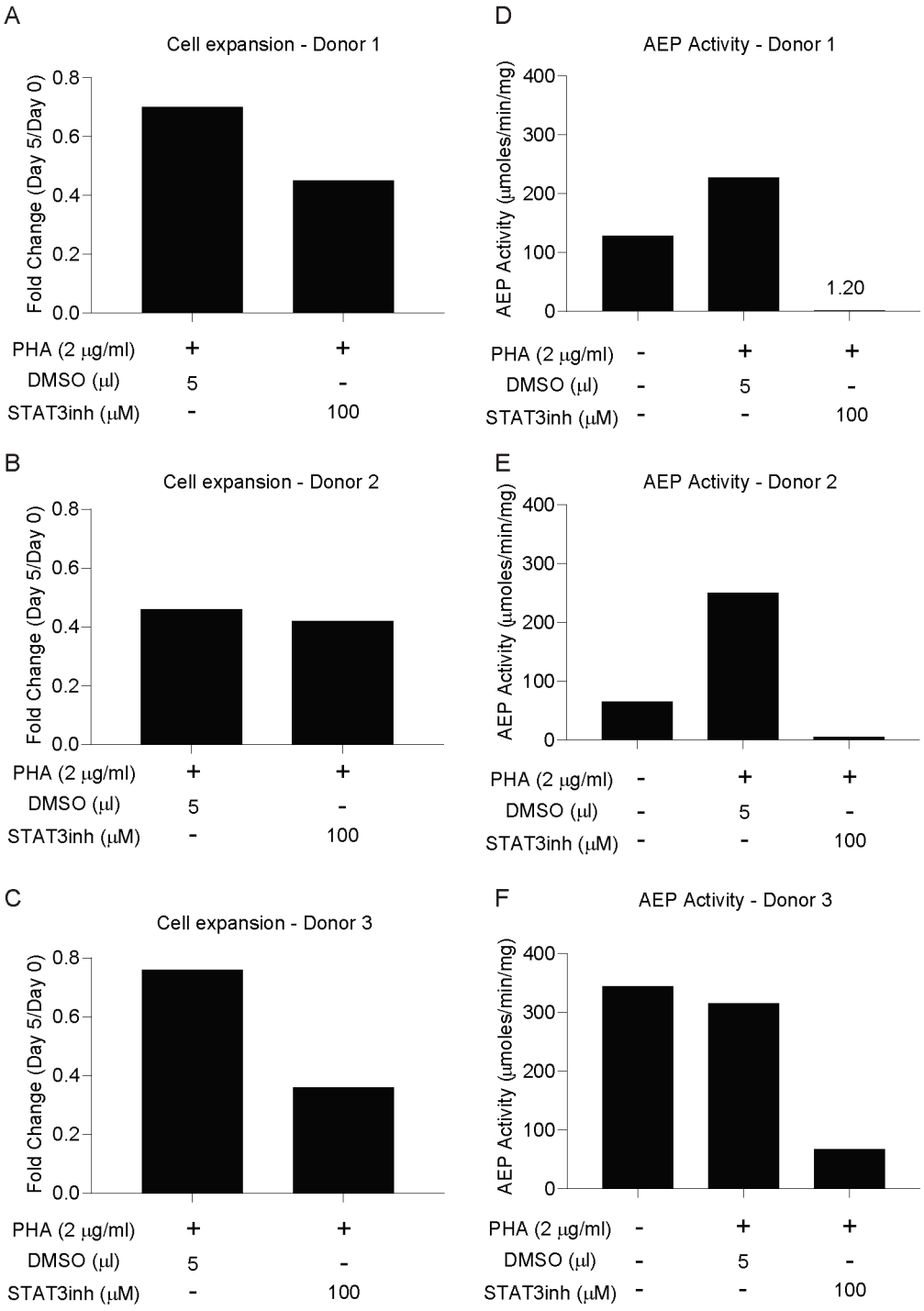
A
Cell expansion - Donor 1
Fold Change (Day 5/Day 0)
0.0
0.2
0.4
0.6
0.8
PHA (2 μg/ml) + +
DMSO (μl) 5 -
STAT3inh (μM) - 100
D
AEP Activity - Donor 1
AEP Activity (μmoles/min/mg)
0
100
200
300
400
1.20
PHA (2 μg/ml) - + +
DMSO (μl) - 5 -
STAT3inh (μM) - - 100
B
Cell expansion - Donor 2
Fold Change (Day 5/Day 0)
0.0
0.2
0.4
0.6
0.8
PHA (2 μg/ml) + +
DMSO (μl) 5 -
STAT3inh (μM) - 100
E
AEP Activity - Donor 2
AEP Activity (μmoles/min/mg)
0
100
200
300
400
PHA (2 μg/ml) - + +
DMSO (μl) - 5 -
STAT3inh (μM) - - 100
C
Cell expansion - Donor 3
Fold Change (Day 5/Day 0)
0.0
0.2
0.4
0.6
0.8
PHA (2 μg/ml) + +
DMSO (μl) 5 -
STAT3inh (μM) - 100
F
AEP Activity - Donor 3
AEP Activity (μmoles/min/mg)
0
100
200
300
400
PHA (2 μg/ml) - + +
DMSO (μl) - 5 -
STAT3inh (μM) - - 100

Figure 5.9 Inhibition of STAT3 downregulates AEP activity. PBMCs from healthy human donors were cultured in 48-well plates at 1 million cells per ml in complete RPMI media. The cells were stimulated with 2 μg/ml of PHA and expanded for 5 days at 37°C in the presence of either DMSO or STAT3 inhibitor at 100 μM final concentration. An equal volume of the STAT3 inhibitor and DMSO was added to the relevant conditions. Cells from day 0 and day 5 were harvested using n-octyl lysis buffer in preparation for the enzyme activity assay. **A-C.** Bar graphs showing the rate of cell expansion in each culture condition in each donor. The expansion rate is presented as a fold change in number of cells at the end of culture (day 5) divided by the initial number of plated cells (day 0). **D-F.** Bar graphs showing AEP activity levels on day 0 and day 5 in each culture condition in each donor. Readouts were taken at 90 min after the addition of substrate and activity levels were normalised to the blank control. N=3

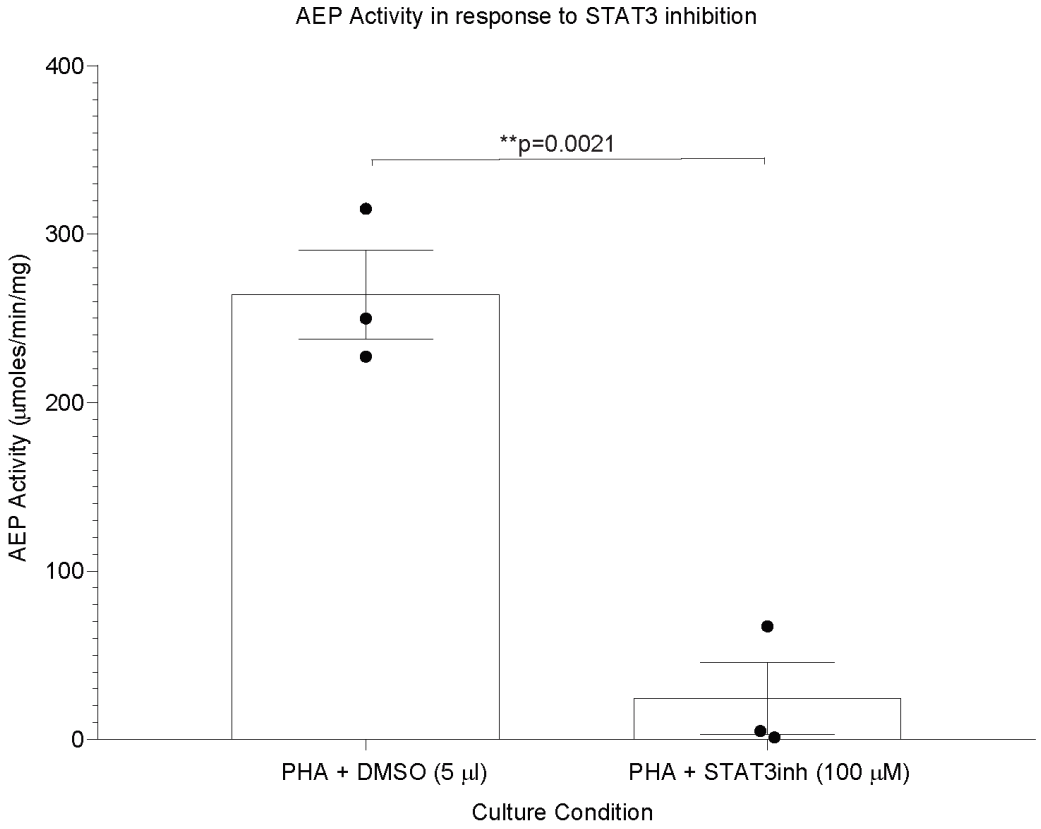

Figure 5.10 Inhibition of STAT3 downregulates AEP activity. Summarising bar graph showing AEP activity levels on day 0 and day 5 in each culture condition in each donor. The Shapiro-Wilk normality test was used to confirm normal distribution of data. An unpaired, 2-tailed Student's t test was used for variance analysis. P values ≤0.05 were defined as statistically significant. N=3

5.3.4 *PD-1 signalling downregulates AEP activity in human lymphocytes*

Following the observation that TGF-β1 and STAT3 positively regulate AEP expression, the next step was to investigate signals that downregulate AEP. PD-1 has been shown to downregulate AEP expression in mouse iTreg cells (Stathopoulou *et al.*, 2018). Therefore, the question of whether PD-1 downregulated AEP expression in human lymphocytes was explored. Human lymphocytes that were expanded with PHA were treated with a PD-1 blocking antibody and AEP activity levels measured (figure 5.11). Results from this experiment showed that there is a significant increase (p=0.0467) of AEP activity levels in response to PD-1 blockade which is in accordance with the mouse studies (figure 5.12).

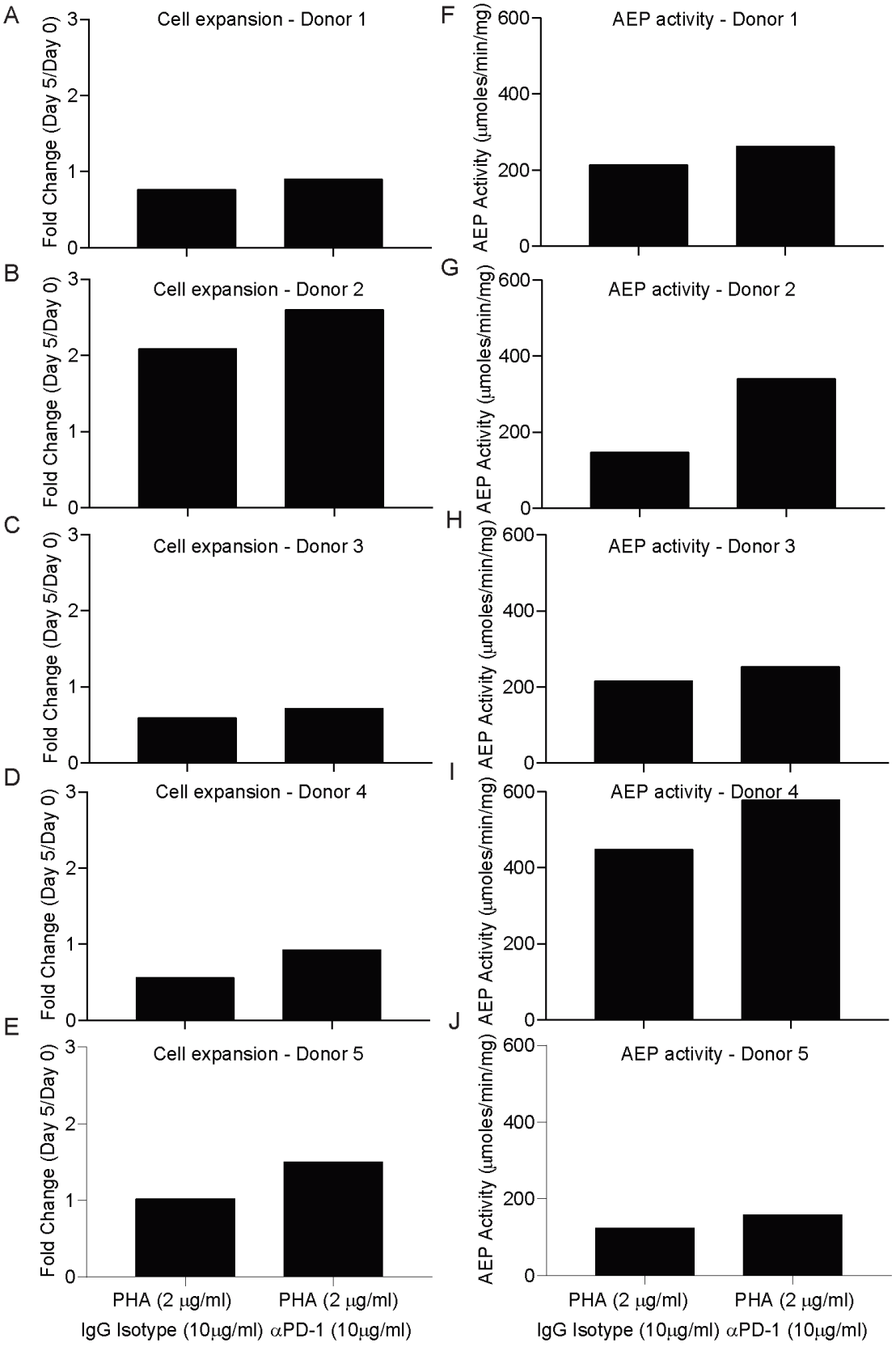
A
Cell expansion - Donor 1
Fold Change (Day 5/Day 0)
B
Cell expansion - Donor 2
C
Cell expansion - Donor 3
D
Cell expansion - Donor 4
E
Cell expansion - Donor 5
F
AEP activity - Donor 1
AEP Activity (µmoles/min/mg)
G
AEP activity - Donor 2
H
AEP activity - Donor 3
I
AEP activity - Donor 4
J
AEP activity - Donor 5
PHA (2 µg/ml)
IgG Isotype (10µg/ml)
PHA (2 µg/ml)
αPD-1 (10µg/ml)

Figure 5.11 Blocking PD-1 increases AEP activity. PBMCs from healthy human donors were cultured in 48-well plates at 1 million cells per ml in complete RPMI media. The cells were stimulated with 2 μg/ml of PHA and expanded for 5 days at 37°C in the presence of either αPD-1 or IgG isotype at 10 μg/ml final concentration (soluble). Cells from day 0 and day 5 were harvested using n-octyl lysis buffer in preparation for the enzyme activity assay. **A-E.** Bar graphs showing the rate of cell expansion in each culture condition in each donor. The expansion rate is presented as a fold change in number of cells at the end of culture (day 5) divided by the initial number of plated cells (day 0). **F-J.** Bar graphs showing AEP activity levels on day 0 and day 5 in each culture condition in each donor. Readouts were taken at 90 min after the addition of substrate and activity levels were normalised to the blank control. N=5

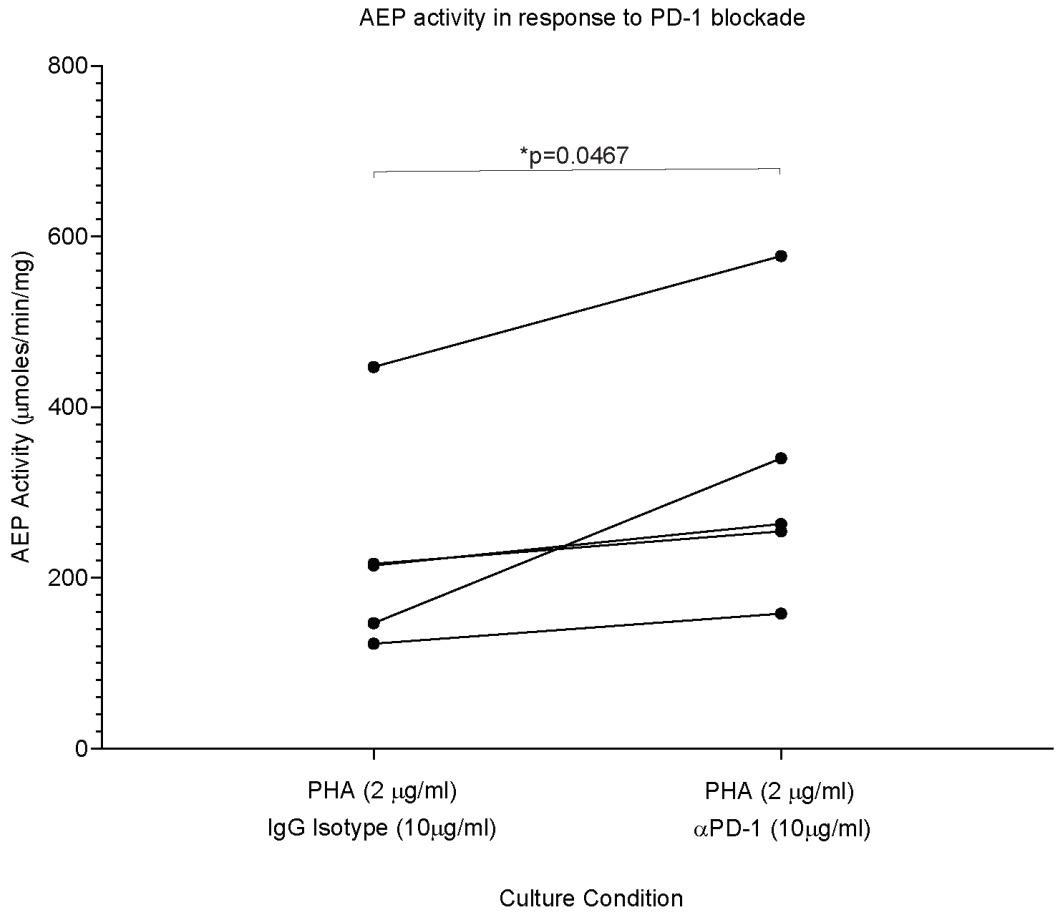

Figure 5.12 Blocking PD-1 increases AEP activity. Summarising bar graph showing AEP activity levels on day 0 and day 5 in each culture condition in each donor. The Shapiro-Wilk normality test was used to confirm normal distribution of data. An unpaired, 2-tailed Student's t test was used for variance analysis where the αPD-1 and isotype conditions were compared. P values ≤0.05 were defined as statistically significant. N=5

5.4 Conclusion

Studies have suggested that AEP expression is involved in regulating Treg/Th17 balance in mice (Zhang *et al.*, 2017; Martinez-Fabregas *et al.*, 2018). In order to investigate which signals induce AEP activity in human lymphocytes, cells were expanded with PHA to specifically select for T cells over monocytes. These experiments showed that TGF-β1 consistently increased AEP activity levels while blocking STAT3 led to a marked decrease of AEP activity. As confirmation of the mouse studies, PD-1 blockade led to an increase in AEP activity levels in human lymphocytes (Stathopoulou *et al.*, 2018). However, it remains unclear which signals are dominant. It is possible that PD-1 signalling may override TGF-β1/STAT3 signalling to maintain Treg cell stability. In order to study this, T cells would

have to be cultured in the presence of combinations of inhibitors and blocking antibodies.

This study focused on TGF-β1, STAT3 and PD-1 as the key players in regulating AEP activity levels based on data obtained in chapters 3 and 4 as well as the current published literature. In addition, as this study is primarily focused on human T cells, it would be worth repeating the experiments in more donors. However, even with limited n numbers, a pattern was observed and significance level was achieved in certain cases.

Future directions include testing AEP activity specifically in human T helper cell subsets in response to cytokine stimulations in the presence or absence of an AEP-specific inhibitor as well as investigating downstream signalling of involved pathways including assessing pSTAT3 levels via western blotting and flow cytometry. It would also be worth using more inhibitors to validate these findings such as SMAD2/3/4 inhibitors as well as other molecules signalling through the same pathways including activin which is a member of the TGF-β superfamily.

In conclusion, this chapter demonstrated that:

- TGF-β1 and STAT3 signalling increased AEP activity while
- PD-1 signalling decreased AEP activity in human lymphocytes.

Chapter 6. Discussion

AEP function was initially discovered in APCs where it is involved in antigen processing for MHC class II presentation. Since then, AEP protein expression has been demonstrated in mouse and human T cells where it is implicated in T cell differentiation and function particularly that of the Th1, Th17 and Treg cell lineages (Probst-Kepper *et al.*, 2009; Aschenbrenner *et al.*, 2018; Freeley *et al.*, 2018; Stathopoulou *et al.*, 2018). However, very little is known about the mechanisms that regulate AEP expression in mouse and human Treg cells specifically.

Previous work performed by Dr Shoba Amarnath has demonstrated that PDL-1-treated Tbet$^+$iTreg cells were more potent at alleviating GvHD and colitis in mice than Tbet$^+$iTreg cells (figure 1 in appendix D). Subsequent microarray analysis performed by Dr Shoba Amarnath showed the downregulation of AEP transcripts in the PDL-1-treated population (figure 2 in appendix D). In addition, published data have demonstrated that PDL-1 signalling enhances Treg cell differentiation and function through the reinforcement of Foxp3 expression (Francisco *et al.*, 2009). Also, degradation assays performed *in vitro* have shown that AEP is able to degrade Foxp3 but not Tbet indicating that Foxp3 is a specific target of AEP (Stathopoulou *et al.*, 2018). The colocalisation of active AEP and Foxp3 in the nucleus of activated human CD4$^+$ T has also been demonstrated while PDL-1 treatment of these cells seems to restrict active AEP levels in the nucleus (Freeley *et al.*, 2018; Stathopoulou *et al.*, 2018). Although T cell activation seems to be driving AEP localisation to the nucleus, the mechanism by which AEP relocates and how it can function in this compartment where the pH is neutral remains unknown (Freeley *et al.*, 2018). It may be possible that complexes of AEP with other proteins may stabilise its function in these conditions and further experiments such as co-IP experiments and mass spectrometry analysis would need to be performed to assess this. An NLS sequence has been identified within the enzyme's AP domain close to the C terminus which remains intact in the active 47 kDa peptide but gets disrupted by further processing (Dall and Brandstetter, 2016). Disruption of this sequence has been shown to have a positive effect on Foxp3 expression indicating the functional significance of

nuclear AEP (Stathopoulou *et al.*, 2018). Collectively, these studies proposed a model whereby Foxp3 and subsequently Treg cell function and stability may be regulated by AEP in a PD-1 dependent manner.

To test the hypothesis and investigate the role of AEP in mouse Treg cells, Treg cells from AEP deficient mice were phenotyped and the importance of AEP in Treg cell function was assessed *in vivo* in a mouse model of melanoma. Although it should be taken into consideration that the process of generation of this KO mouse strain may also have affected the mouse phenotype through disruption of genes surrounding the AEP gene, these experiments showed that *Lgmn*$^{-/-}$ mice were able to maintain higher frequencies of Treg cells in the periphery compared to WT mice. *In vitro*, *Lgmn*$^{-/-}$ iTreg cells maintained higher protein levels of Foxp3 in a protein turnover assay while *in vivo*, *Lgmn*$^{-/-}$ mice with melanoma exhibited higher frequencies of Treg cells within tumours compared to WT cohorts.

In vitro stimulation experiments indicated that TGF-β1 was the key cytokine inducing the highest levels of AEP expression in mouse T cells cultured under iTreg cell conditions. Although TCR and/or IL-2 stimulation were able to induce expression of AEP in freshly isolated naïve and nTreg cells, AEP levels were the highest in cultures stimulated with TGF-β1. In support of this, studies have shown that inhibition of the TGFB receptor leads to a reduction of AEP mRNA levels in murine SMAD4 deficient CD4^{+} T cells compared to WT controls (Zhang *et al.*, 2017). In addition to TGF-β1, PDL-1 stimulation was also able to regulate AEP protein expression in mouse iTreg cells. Specifically, PDL-1 downregulated AEP expression in iTreg cells *in vitro* which is consistent with the mouse melanoma experiment where it was shown that the increased frequency of tumour resident Treg cells in *Lgmn*$^{-/-}$ mice was refractory to PDL-1 blockade.

In summary, the work presented here has demonstrated that AEP regulates mouse Treg cell stability and function through its ability to selectively target Foxp3 for proteolytic degradation.

Having established that AEP can regulate mouse Treg cells and determined TGF-β1 and PDL-1 as key regulators of AEP expression, the importance of AEP expression in human Treg cells was then investigated.

In contrast to mice, freshly isolated naïve and Treg cells expressed AEP *ex vivo*. However, similarly to mice, TGF-β1 was able to induce the highest levels of AEP expression *in vitro*. TCR and IL-2 stimulation was able to induce AEP expression at lower levels compared to TGF-β1. However, time point stimulation experiments with IL-2 failed to show an increase in AEP expression in human Treg cells. In support of that, studies have shown the upregulation of AEP mRNA levels in human Treg and naïve T cells activated *ex vivo* in the presence of αCD3, αCD28 and IL-2 (Probst-Kepper *et al.*, 2009). In addition, upregulation of AEP mRNA was associated with the Treg cell lineage signature as it was observed in FOXP3-overexpressing Th cells that acquired a regulatory phenotype and function (Probst-Kepper *et al.*, 2009). However, overexpression of AEP in Th cells failed to upregulate Treg-associated protein expression (including FOXP3) indicating that AEP acts as a post-transcriptional regulator of FOXP3 which is in agreement with the results from the mouse studies (Probst-Kepper *et al.*, 2009).

In addition to TGF-β1 and PD-1, other stimuli have been associated with upregulating or downregulating AEP expression levels. STAT3 and STAT3-inducing cytokines in particular have been shown to play a role in regulating AEP expression and function in mice (Zhang *et al.*, 2017; Martinez-Fabregas *et al.*, 2018; Stathopoulou *et al.*, 2018). However, little is known about the regulation of AEP expression and function in human lymphocytes. To assess the significance of TGF-β1, PD-1 and STAT3 signalling in regulating AEP function in human lymphocytes, a functional assay was used that specifically measured AEP activity levels. These studies showed that blocking TGF-β and STAT3 signalling leads to a decrease in AEP activity levels while blocking PD-1 has the opposite effect which is in accordance with the *in vitro* studies.

In summary, this study explored the significance of AEP expression in mouse Treg cells and elucidated some of the mechanisms regulating AEP expression in both mice and human lymphocytes. Specifically, it demonstrated that AEP expression contributes to mouse Treg cell lineage instability through the degradation of the Treg master transcription factor Foxp3 and that PDL-1 signalling can reverse this effect by downregulating

AEP expression. In addition, this study showed that similar mechanisms of AEP regulation exist in both mouse and human T cells as TGF-β1 was shown to be inducing the highest levels of AEP expression *in vitro*. Also, PDL-1 signalling downregulated AEP expression in mouse Treg cells while in human lymphocytes, blockade of PD-1 led to an increase in AEP activity levels. Finally, studies have shown that STAT3 can positively regulate AEP expression in mice which is in accordance with data presented here whereby blockade of STAT3 in human lymphocytes leads to a significant decrease in AEP activity levels ($p=0.0021$) (Zhang *et al.*, 2017; Martinez-Fabregas *et al.*, 2018; Stathopoulou *et al.*, 2018).

6.1 Limitations and future directions

However, it is worth mentioning some of the major limitations of this study.

For instance, to better assess the rate of Foxp3 degradation in *Lgmn*$^{-/-}$ Treg cells, more stimulation time-points would have to be included as longer incubation with CHX may have revealed a greater difference in the levels of Foxp3 protein between WT and *Lgmn*$^{-/-}$ iTreg cells. However, previous experiments performed by Dr Amarnath have demonstrated the loss of Foxp3 expression in *Lgmn*$^{-/-}$ iTreg cells that were transduced to overexpress AEP after 7 days of culture while *Lgmn*$^{-/-}$ iTreg cells were shown to be more efficient at preventing GvHD than WT iTreg cells (Stathopoulou *et al.*, 2018). Also, a different, less abundant, internal control should be used in future degradation assays to avoid band saturation. An example of such a protein is the nuclear housekeeping protein lamin. Alternatively, loading less protein on the gel may resolve this issue.

Finally, although the cell sorting technique used for the isolation of mouse naïve T cells (and their differentiation into iTreg cells) is known to yield samples of high purity (>80%) and mouse T cell cultures were performed over short periods of time, it would be worth phenotyping cultured iTreg cells for Foxp3 expression to safely exclude the possibility of culture contamination which could have skewed the results.

Treg cell isolation using the Miltenyi kit relies on the isolation of cells expressing general surface activation markers that are not restricted to the Treg cell lineage thus increasing the risk of sample contamination. The

purity of the isolated mouse Treg cells and the cultured iTreg cells was assessed in subsequent experiments by assessing Foxp3 expression by IC flow cytometry, however, additional validation experiments such as a Treg cell suppression assay was attempted (appendix C). In the end, this methodology was deemed impractical due to the low availability of mouse spleens, the low Treg and iTreg cell numbers as well as the technical difficulties that resulted in suboptimal assays (appendix C).

Issues associated with faint bands of β-tubulin were restricted to the sorted Treg cells that were cultured under iTreg cell conditions. Initially, it was proposed that excessive membrane stripping may have removed some of the protein but that failed to explain why the other bands remained unaffected. Therefore, it is hypothesised that this is a cell-specific and/or condition-specific effect. In support of this, cell confluency during cell culture has been shown to impact the expression levels of certain housekeeping genes including β-tubulin and GAPDH (Samantha Greer *et al.*, 2010). TGF-β which is included in the iTreg cell condition has also been shown to affect β-tubulin expression though this did not affect internal control levels in iTreg cells (Lomri and Marie, 1990). Also, it is worth mentioning that human DCs were shown to express low levels of GAPDH but high levels of β-actin, even though an equal amount of protein was loaded on the gel in both cases. Collectively, these data support the hypothesis that this is a cell-specific effect. However, more validation experiments need to be done to assess variation in housekeeping gene expression in each experimental context. A future direction could involve the use of total protein staining as a more accurate method of protein normalisation.

Similar limitations were noted in the human studies where AEP expression was studied in human T cell subsets. Specifically, poor yield of sorted Treg cells from the PBMCs of healthy donors made it impossible to do a purity test or perform a suppression assay at the end of cell culture. However, FOXP3 expression was assessed by both IC flow cytometry and western blotting. In terms of AEP expression, although it was assessed by western blotting and positive controls such as DC lysates were included in certain gels, the inclusion of negative controls for AEP could have been included to

further validate results. Such a negative control could include blocking the primary Ab with an Ab-specific peptide inhibitor such as the immunogen used to raise the Ab (in this case mouse myeloma cell line NS0-derived recombinant human Legumain, Ile18-Tyr433, R&D systems, MN, USA). Attempts were made to study AEP expression using flow cytometry, but this methodology was not pursued due to lack of a proper Ab for AEP designed to be used for flow cytometry, limited availability of the primary WB Ab for AEP and the lack of proper controls (appendix A).

In addition, multiple AEP bands of inconsistent band sizes were detected across multiple donors. Although donor variability cannot be excluded, the running conditions such as the use of gradient gels may have interfered with protein migration while the reducing conditions used for sample processing and sample running may have altered protein epitopes and therefore affected Ab binding. This could explain why in some cultures AEP bands appeared very faint even though an adequate amount of total protein was loaded in the gel. However, it should be noted that the reducing running conditions were consistent with those used in the product data sheet and the experimental methodology was kept consistent across all donors. In the cases where AEP bands appeared very faint, acetone precipitation was performed to further condense samples so that the entire lysate could be run. However, risks associated with this process include leftover acetone which could have interfered with protein solubilisation and epitope disruption.

In order to further study the signalling mechanisms involved in the induction of AEP expression, AEP protein levels were assessed in multiple human T cell subsets including Th1 and Th2 cells (appendix B). However, lack of purity tests, proper controls during flow cytometry and lack of extensive cytokine expression profiling using techniques such as ELISA made it unclear as to whether the cultured T cells differentiated into the intended cell lineages.

Finally, AEP enzyme activity was measured in expanded human lymphocytes and although AEP substrate specificity was tested in the presence of pepstatin A, additional controls should have been included such

as AEP-specific inhibitors or other protease inhibitors known to inhibit AEP protease activity such as cystatin E (Dall and Brandstetter, 2013; Dall and Brandstetter, 2016).

In summary, results from the studies presented here constitute very preliminary data and there is still a lot that remains unknown regarding AEP regulation in human lymphocytes. It would be worth mentioning potential future directions that could advance knowledge in the field and provide valuable insight into AEP function in human T cells.

To further elucidate the signalling pathways that regulate AEP in human T cells, AEP expression and activity would have to be studied in individual human T helper cell subsets. In order to do this, human naïve T cells would have to be isolated and differentiated into individual T helper subsets. Following differentiation and expansion, populations could be stimulated with individual cytokines or treated with specific inhibitors and then AEP expression and activity levels measured.

In addition, since AEP has been found in the nucleus of T cells where its function is unknown, nuclear and cytoplasmic AEP levels could be determined by cell fractionation during the cell lysis process or by confocal microscopy using an AEP-specific probe which would provide insight into the nuclear activity of AEP.

Finally, to assess the importance of AEP function specifically in human T cells, FOXP3 could be mutated in human naïve T cells via lentiviral transduction to provide resistance to AEP-mediated cleavage and then the potency of the cells could be tested *in vivo* in a humanised mouse model of GvHD as well as *in vitro* in Treg cell suppression assays. Also, it would be very interesting to study whether AEP deficiency affects the levels of FOXP3 isoforms in human T cells and whether this affects their function. Finally, *in silico* analysis of the FOXP3 sequence could identify sites that are targeted by proteases for cleavage which would give an indication of protease-mediated regulation of FOXP3.

In conclusion, this study has demonstrated that proteases can have a highly specialised function and can play an important role in regulating T cell function. AEP inhibition in Treg cell expansion regimes could boost the

immunosuppressive function of these cells leading to more effective forms of cell therapy for GvHD and autoimmunity. Recently, a phase I clinical trial using Treg cell therapy for the prevention of kidney transplant rejection has demonstrated the safety of polyclonal Treg cell infusion which also correlated with 100% survival rates two years after transplantation (Mathew *et al.*, 2018). Clinical trials involving Treg cell therapy for autoimmune diseases such as type 1 diabetes have shown different rates of success and so far, required combinatorial treatment of patients with other immunosuppressive drugs (Duggleby *et al.*, 2018). Collectively, these studies demonstrate that Treg cell therapy can be applied in many disease settings and that current methodologies used for the expansion of Treg cells need to be further optimised. AEP inhibition during polyclonal Treg cell expansion could help boost Treg cell persistence and sustain long-term peripheral tolerance following engraftment. In addition to autoimmunity, AEP expression levels within Treg cell populations found in solid tumours could be used as a biomarker to predict patient response to immunotherapies such as PD-1/PDL-1. It is possible that differences in AEP expression levels between patients could partly account for the variation seen in patient response to immunotherapy therefore the role of AEP as a resistance mechanism is something worth investigating. In consistence with this hypothesis, Treg cell depletion resulting from the combinatorial treatment of melanoma patients with PD-1 and CTLA-4 blockade correlates with reduced rates of tumour hyperprogressive disease (Larkin *et al.*, 2015). Therefore, the role of additional Treg-associated inhibitory coreceptors such as CTLA-4 on AEP expression could be investigated to further elucidate the mechanisms of AEP regulation in Treg cells.

The field of protease-mediated regulation of T cell lineage stability and function has remained largely unexplored mainly due to challenges involving the purification of proteolytic enzymes, the fact that there is extensive functional overlap among them and a relative lack of protease-specific inhibitors. Nonetheless, understanding how protease expression and function is regulated in different T cell lineages promises to open new avenues of exploiting these mechanisms for the treatment of a wide array of immune system disorders.

Appendix A

AEP Expression is Associated with FOXP3 Expression.

In order to further validate AEP expression in human Treg cells, an alternative method of detecting AEP was used. Here, cells from donor 6 (figures 4.16-17) were characterised for CD4, FOXP3 and AEP (LGMN) expression at the end of the culture. Specifically, iTreg and cultured Treg cells were stained with the same antibody used for western blotting and then stained with a secondary goat IgG-PE (R&D systems, MN, USA; 2μl/100μl) that would bind to the primary anti-AEP antibody (figures 1 and 2). These experiments were performed in two distinct donors (donors 6 and 7) and showed that AEP is expressed in human Treg cells *in vitro* as the majority of $FOXP3^+$ cells were AEP^+ (figures 1 and 2). However, due to the lack of proper controls and the limited availability of the primary antibody, this methodology was not used in further experiments.

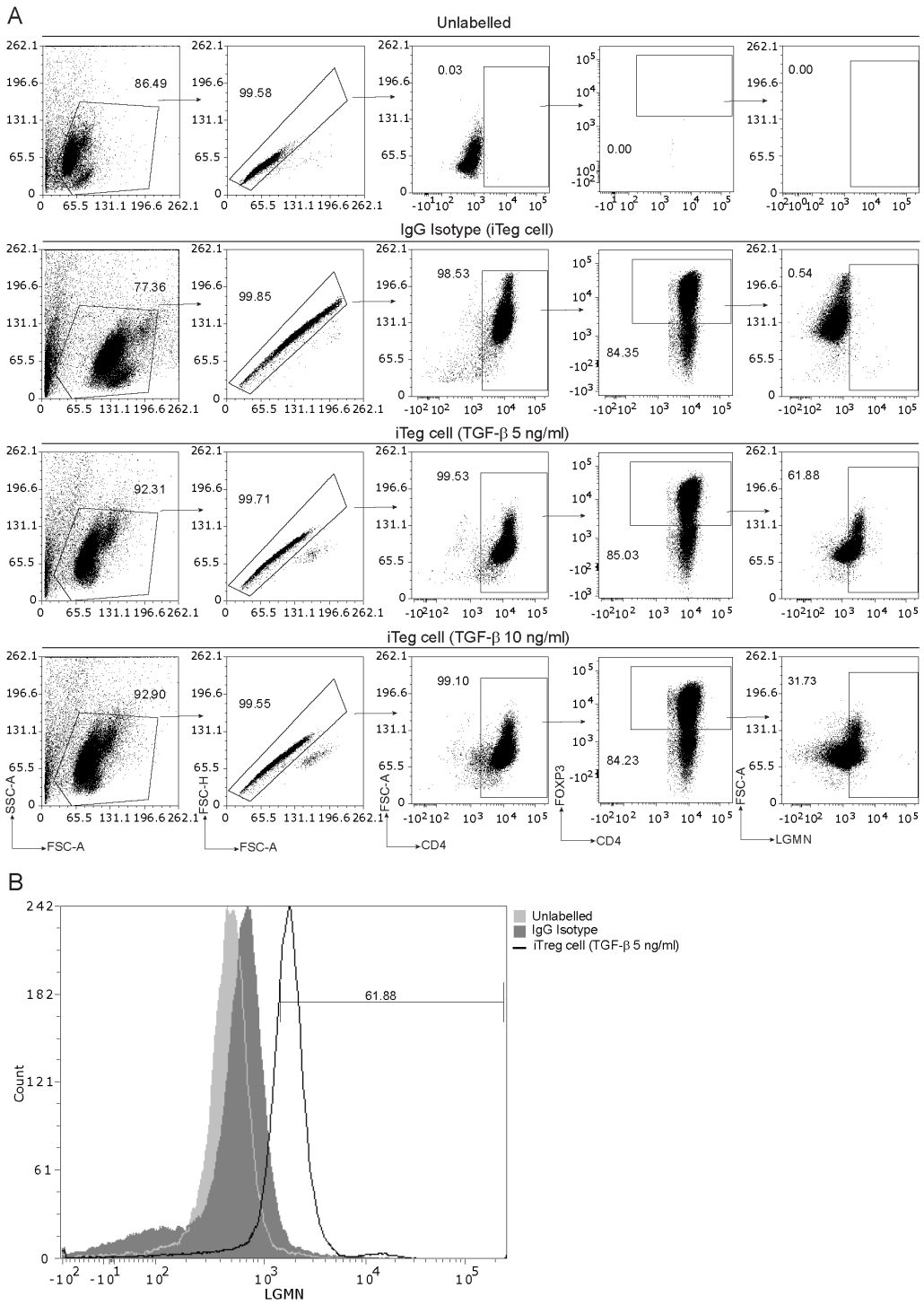
A
Unlabelled
86.49
99.58
0.03
0.00
0.00
IgG Isotype (iTeg cell)
77.36
99.85
98.53
84.35
0.54
iTeg cell (TGF-β 5 ng/ml)
92.31
99.71
99.53
85.03
61.88
iTeg cell (TGF-β 10 ng/ml)
92.90
99.55
99.10
84.23
31.73
SSC-A
FSC-A
FSC-H
FSC-A
FSC-A
CD4
FOXP3
CD4
FSC-A
LGMN
B
Unlabelled
IgG Isotype
iTreg cell (TGF-β 5 ng/ml)
61.88
Count
LGMN

Figure 1. AEP expression in iTreg cells. Cells from donor 6 (figures 4.15-16) were characterised for CD4, FOXP3 and AEP (LGMN) expression on day 12. iTreg cells were stained with the WB Ab for AEP at 0.5 μg/100 μl and then stained with goat IgG-PE. An unlabelled and an isotype-only control was included. The rest of the cells were harvested using PMSF lysis buffer in preparation for protein analysis via western blotting. **A.** Flow plots showing the frequency of $LGMN^+$ iTreg cells on day 12. **B.** Histogram showing the percentage frequency of $LGMN^+$ iTreg cells on day 12. n = 1 donor.

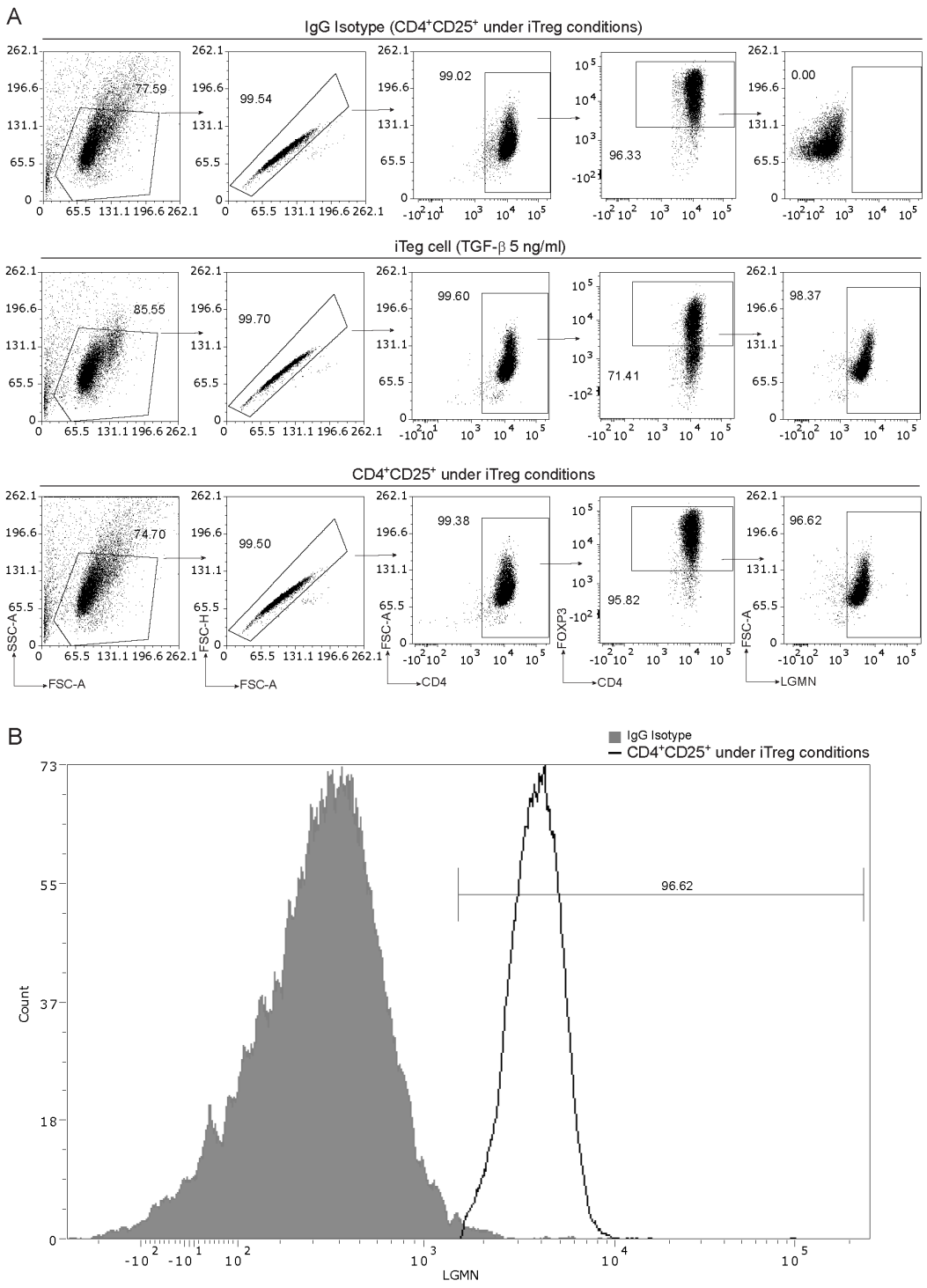
A
IgG Isotype (CD4+CD25+ under iTreg conditions)
77.59
99.54
99.02
96.33
0.00
iTeg cell (TGF-β 5 ng/ml)
85.55
99.70
99.60
71.41
98.37
CD4+CD25+ under iTreg conditions
74.70
99.50
99.38
95.82
96.62
SSC-A
FSC-A
FSC-H
FSC-A
FSC-A
CD4
FOXP3
CD4
FSC-A
LGMN
B
IgG Isotype
CD4+CD25+ under iTreg conditions
96.62
Count
LGMN

Figure 2. AEP expression in iTreg and $CD4^+CD25^{high}CD127^{low}$ cells cultured under iTreg conditions. iTreg and $CD4^+CD25^{high}CD127^{low}$ cells from donor 7 (figures 4.17-18) were characterised for CD4, FOXP3 and AEP (LGMN) expression on day 12. Cells were stained with the WB Ab for AEP at 0.5 μg/100 μl and then stained with goat IgG-PE. An isotype-only control was included. The rest of the cells were harvested using PMSF lysis buffer in preparation for protein analysis via western blotting. **A.** Flow plots showing the frequency of $LGMN^+$ iTreg and $CD4^+CD25^{high}CD127^{low}$ cells on day 12. **B.** Histogram showing the percentage frequency of $LGMN^+$ iTreg and $CD4^+CD25^{high}CD127^{low}$ cells on day 12. n = 1 donor.

Appendix B

Human T Helper Cell Subsets Express AEP *In Vitro*.

AEP expression has been observed in human Th1 and Th17 cells (Aschenbrenner *et al.*, 2018; Freeley *et al.*, 2018). In order to study the patterns of AEP expression in human T helper cell subsets which would give an indication of the cytokines that may play a role in inducing AEP expression, naïve T cells were cultured under Th1 and Th2 inducing conditions. Naïve T cells were isolated from PBMCs using the Miltenyi Treg isolation kit (as described in sections 2.17 and 4.3.3). FOXP3 expression was then confirmed via western blotting. Any culture conditions - with the exception of iTreg cells - where FOXP3 expression was observed, were excluded from the analysis. The experiment was repeated in three separate donors.

Sorted naïve T cells were differentiated into Th1, Th2, Th17 and iTreg cells with Th0 used as controls. Cells were cultured in 96-well plates previously coated with anti-CD3 (BioLegend, CA, USA; clone:OKT3;5µg/m) for 3hrs at 37ºC. The wells were washed three times with PBS and cells were plated at a concentration of $1x10^6$ c/ml. To induce differentiation, soluble anti-CD28 (BioLegend, CA, USA; clone:CD28.2;2µg/ml) was added along with anti-IL4 (BioLegend, CA, USA;clone: MP4-25D2;10µg/ml), anti-IFNγ (BioLegend, CA, USA; clone:B27;10µg/ml), rhIL-4 (Peprotech, London, UK, 20ng/ml), rhIL-1β (Peprotech, London, UK, 20ng/ml) rhIL-6 (MACS Miltenyi Biotec, Bergisch Gladbach, Germany; 20ng/ml), rhIL-12 (MACS Miltenyi Biotec, Bergisch Gladbach, Germany; 20ng/ml), rhIL-23 (MACS Miltenyi Biotec, Bergisch Gladbach, Germany; 20ng/ml), rhTGF-β1 (R&D systems, MN, USA; 5 ng/ml) and rhIL-2 (Peprotech, London, UK, 80ng/ml) as appropriate. The cells were cultured for 5 days and then expanded for an additional 7 days at 37ºC, CO_2 5%, humidity 95% with rhIL-2 added on days 5, 7, 9 and 11. On day 12 the cells were stimulated with PMA (Sigma, MO, UK; 10µg/ml) and ionomycin (Sigma, MO, UK; 1µg/ml) for two hours at 37ºC and then, they were treated with Brefeldin/Golgiplug (BioLegend, CA, USA; 5 µg/ml) and Monensin A/Golgistop (BioLegend, CA, USA; 2µM) for another

two hours at 37°C. The cells were characterised by flow cytometry and cell lysates were obtained for AEP protein analysis by western blotting.

Human cells were stained for CD4 (BioLegend, CA, USA; clone A161A1), CD25 (BioLegend, CA, USA; clone BC96), CD127 (BioLegend, CA, USA; clone A019D5), FOXP3 (BioLegend, CA, USA; clone 259D), PD-1 (BioLegend, CA, USA; clone EH12.2H7), CD45RA (BioLegend, CA, USA; clone HI100), IL-17A (BioLegend, CA, USA; clone BL168), RORγt (BD Pharmingen, CA, USA; clone: Q21-559), IL-4 (BioLegend, CA, USA; clone 8D4-8), GATA3 (eBioscience,CA, USA; clone TWAJ), IFN-γ (BioLegend, CA, USA; clone 4S.B3), Tbet (BioLegend, CA, USA; clone 4B10), DAPI (Invitrogen, CA, USA; 5 μg/ml) and anti-human Trustain Fc block (BioLegend, CA, USA). The Foxp3 Transcription Factor Staining Buffer Kit was used (Thermo Fisher Scientific, MA, UK).

In all donors, TGF-β1 seemed to induce the highest expression of AEP as iTreg cells expressed the highest amount of AEP (figure 1). They also expressed more inactive than active AEP (figure 1). In addition, FOXP3 expression seems to be associated with AEP expression (figure 1).

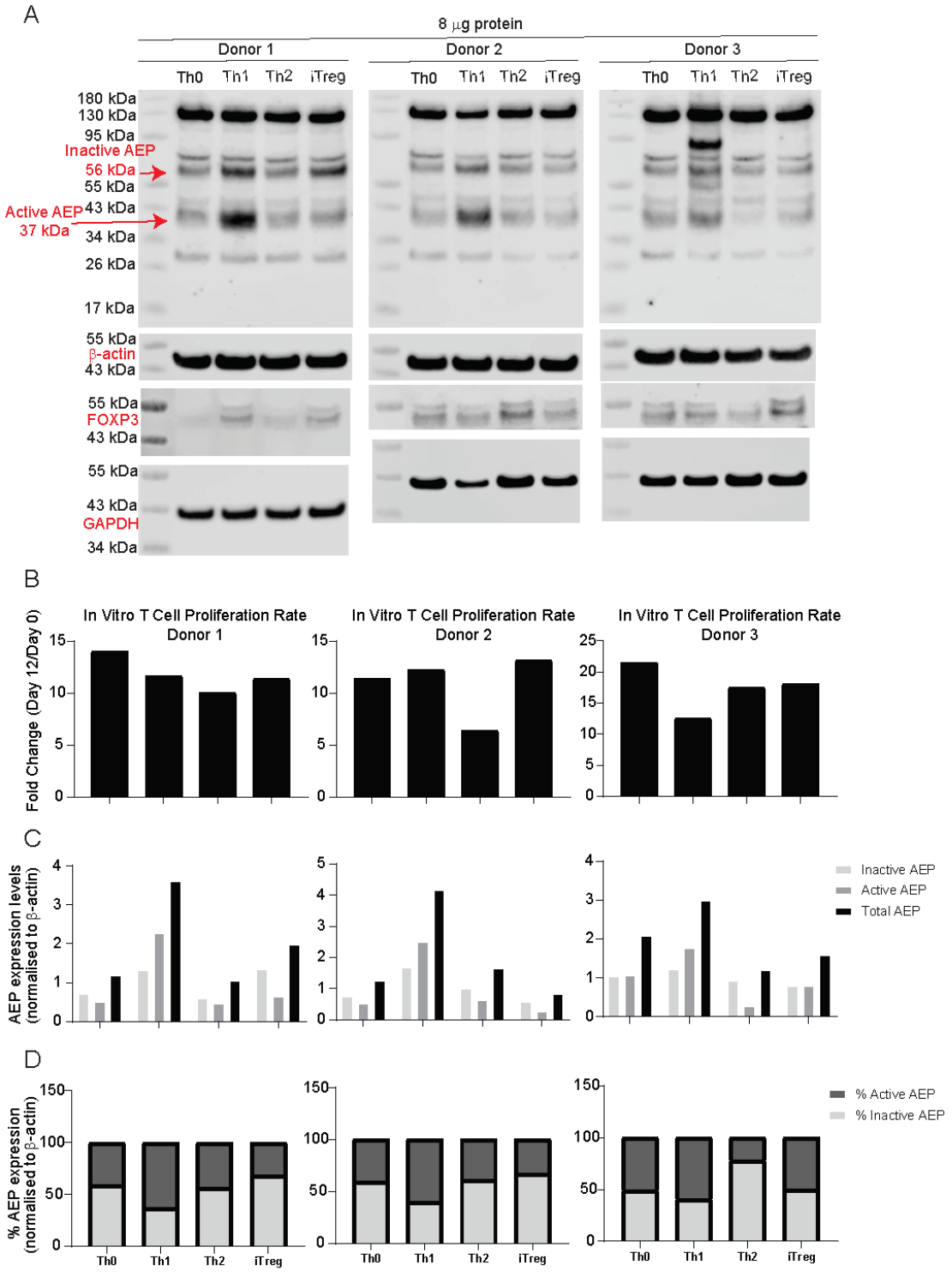
A
8 μg protein
Donor 1
Donor 2
Donor 3
Th0
Th1
Th2
iTreg
180 kDa
130 kDa
95 kDa
Inactive AEP
56 kDa
55 kDa
Active AEP
43 kDa
37 kDa
34 kDa
26 kDa
17 kDa
55 kDa
β-actin
43 kDa
55 kDa
FOXP3
43 kDa
55 kDa
43 kDa
GAPDH
34 kDa
B
In Vitro T Cell Proliferation Rate
Donor 1
In Vitro T Cell Proliferation Rate
Donor 2
In Vitro T Cell Proliferation Rate
Donor 3
Fold Change (Day 12/Day 0)
C
AEP expression levels
(normalised to β-actin)
Inactive AEP
Active AEP
Total AEP
D
% AEP expression
(normalised to β-actin)
% Active AEP
% Inactive AEP

Figure 1. AEP expression in cultured human Th cell subsets. $CD4^+CD25^-$ and $CD4^+CD25^+$ T cells were isolated from human PBMCs using the Miltenyi Treg isolation kit. Cells were cultured at 1 million cells/ml for 5 days in αCD3-coated plates (5 μg/ml) in the presence of αIL-4 (10 μg/ml) and αIFN-γ (10 μg/ml), αCD28 (2 μg/ml) with the addition of rhIL-2 (100 ng/ml), rhTGF-β1 (5 ng/ml), IL-4 (20 ng/ml) and IL-12 (20 ng/ml) where appropriate. Cells were expanded for an additional 7 days in the presence of rhIL-2 which was added every 2 days. On day 12, cells were harvested using RIPA lysis buffer in preparation for protein analysis via western blotting. Lysates were reduced and boiled and run under reducing conditions on a precast, 4-12% Bis-Tris gradient gel. **A.** Western blot images showing AEP expression in each of the culture conditions in each donor. The 56 and 37 kDa AEP bands were quantified using ImageJ and normalised to the respective β-actin loading control bands. **B.** Bar graphs showing the rate of T cell expansion of cells cultured under different culture conditions at the end of the culture. The expansion rate is presented as a fold change in number of cells at the end of culture (day 12) divided by the initial number of plated cells (day 0). **C.** Bar graphs showing the expression levels of active, inactive and total AEP in each of the conditions. Bands were normalised to β-actin. **D.** Bar graphs showing the percentage ratio of active and inactive AEP expressed in each of the culture conditions. The active and inactive AEP bands were normalised to β-actin and the normalised values were divided by the total AEP and then multiplied by 100. n=3 donors.

In order to validate the data obtained from the populations sorted using the Miltenyi kit, a more stringent sorting technique was used whereby naïve and Treg cells were sorted from PBMCs based on expression of CD4, CD25, CD127 and CD45RA as described previously (donors 9 and 10). These experiments showed that cultured Treg cells expressed the highest levels of AEP out of all the conditions even in the absence of serum (donor 10) (figure 2). In addition, AEP expression was also confirmed in Th17 and Th1 cells (figure 2). No active AEP was detected in Th2 cells (figure 2). Following culture, cells from each condition were stimulated with PMA and ionomycin and then characterised for cytokine expression (figures 3-4). Stimulation of Th1 cells led to an increase in IFN-γ levels whereas stimulation of Th17 cells showed an increase in IL-17 expression (figures 3-4).

In summary, different patterns of active and inactive AEP expression were observed in human Treg, iTreg, Th1, Th2 and Th17 cells *in vitro*. AEP expression has been confirmed in human Treg cells as well as Th1 and Th17 cells in accordance with the published literature. Treg cells expressed

the highest levels of AEP expression out of all the subsets while Th1 and Th17 cells were shown to express active AEP.

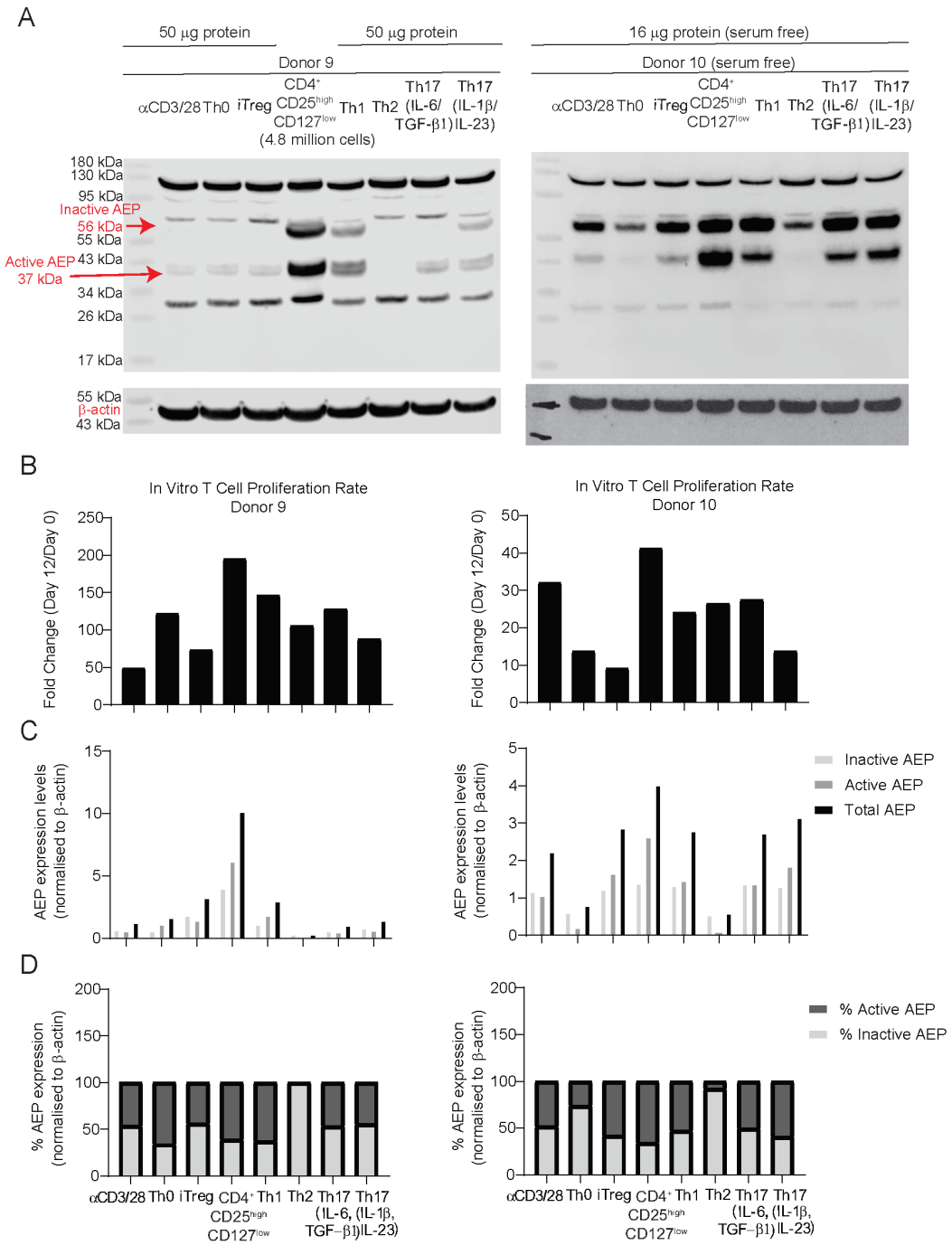

Figure 2. AEP expression in cultured human Th cell subsets. PBMCs were isolated from blood and $CD4^+CD25^-CD127^+CD45RA^+$ and $CD4^+CD25^{high}CD127^{low}$ T cells were isolated using cell sorting. Donors 9 and 10 are the same as those in figures 22 and 24 respectively. Following sorting, cells were cultured at 1 million cells/ml for 5 days in αCD3-coated plates (5 μg/ml) in the presence of αIL-4 (10 μg /ml) and αIFN-γ (10 μg /ml), αCD28 (2 μg/ml), rhIL-2 (100 ng/ml), rhTGF-β1 (5 ng/ml), IL-4 (20 ng/ml), IL-12 (20 ng/ml), IL-6 (20 ng/ml), IL-1β (20 ng/ml) and IL-23 (20 ng/ml) where appropriate. Cells were expanded for an additional 7 days in the presence of rhIL-2 which was added every 2 days. On day 12, cells from each condition were harvested using PMSF lysis buffer in preparation for protein analysis via western blotting. Lysates were reduced and boiled and run under reducing conditions on a precast, 4-12% Bis-Tris gradient gel. **A.** Western blot images showing AEP and β-actin expression in each of the culture conditions in each donor. The 56 and 37 kDa AEP bands were quantified using ImageJ and normalised to the respective β-actin loading control bands. **B.** Bar graphs showing the rate of T cell expansion of cells cultured under different culture conditions at the end of the culture. The expansion rate is presented as a fold change in number of cells at the end of culture (day 12) divided by the initial number of plated cells (day 0). **C.** Bar graphs showing the expression levels of active, inactive and total AEP in each of the conditions. **D.** Bar graphs showing the percentage ratio of active and inactive AEP expressed in each of the culture conditions. The active and inactive AEP bands were normalised to β-actin and the normalised values were divided by the total AEP and then multiplied by 100. n=2 donors.

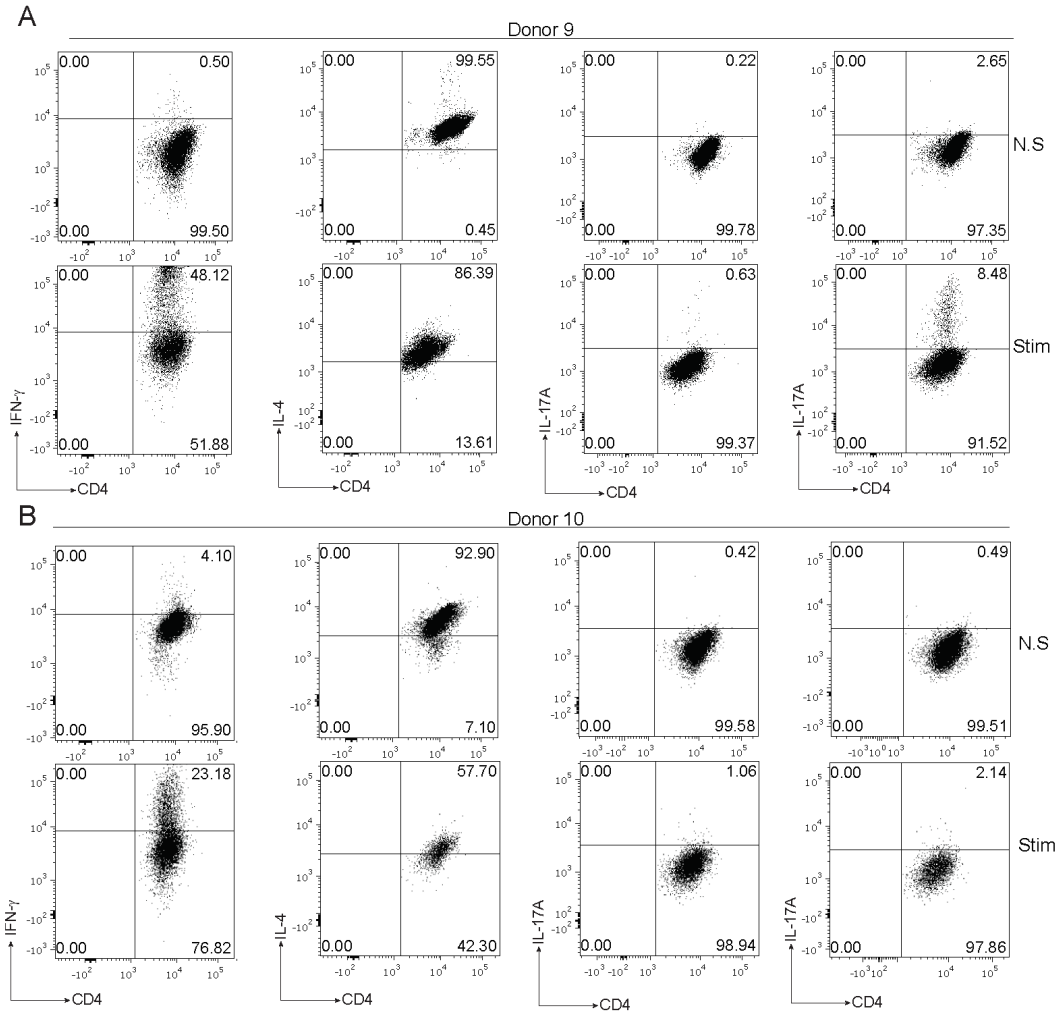

Figure 3. Cytokine profiling of cultured Th cell subsets. PBMCs were isolated from blood and $CD4^+CD25^-CD127^+CD45RA^+$ and $CD4^+CD25^{high}CD127^{low}$ T cells were isolated using cell sorting. The donors are the same as those in figures 4.21-24. Following sorting, cells were cultured at 1 million cells/ml for 5 days in αCD3-coated plates (5 μg/ml) in the presence of αIL-4 (10 μg/ml) and αIFN-γ (10 μg/ml), αCD28 (2 μg/ml), rhIL-2 (100 ng/ml), rhTGF-β1 (5 ng/ml), IL-4 (20 ng/ml), IL-12 (20 ng/ml), IL-6 (20 ng/ml), IL-1β (20 ng/ml) and IL-23 (20 ng/ml) where appropriate. Cells were expanded for an additional 7 days in the presence of rhIL-2 which was added every 2 days. On day 12, cells from each condition were stimulated with PMA (10 μg/ml) and ionomycin (1 μg/ml) for 2 hours at 37°C and then treated with brefeldin (5 μg/ml) and monensin (2 μM) for 2 more hours at 37°C. Following stimulation, cells were characterised for CD4, Tbet, GATA3, RORγt and IL-17A via flow cytometry. **A-B.** Flow plots showing the frequency of $CD4^+IFNγ^+$, $CD4^+IL\text{-}4^+$ and $CD4^+IL17A^+$ T cells in each condition in each donor on day 12. n=2 donors.

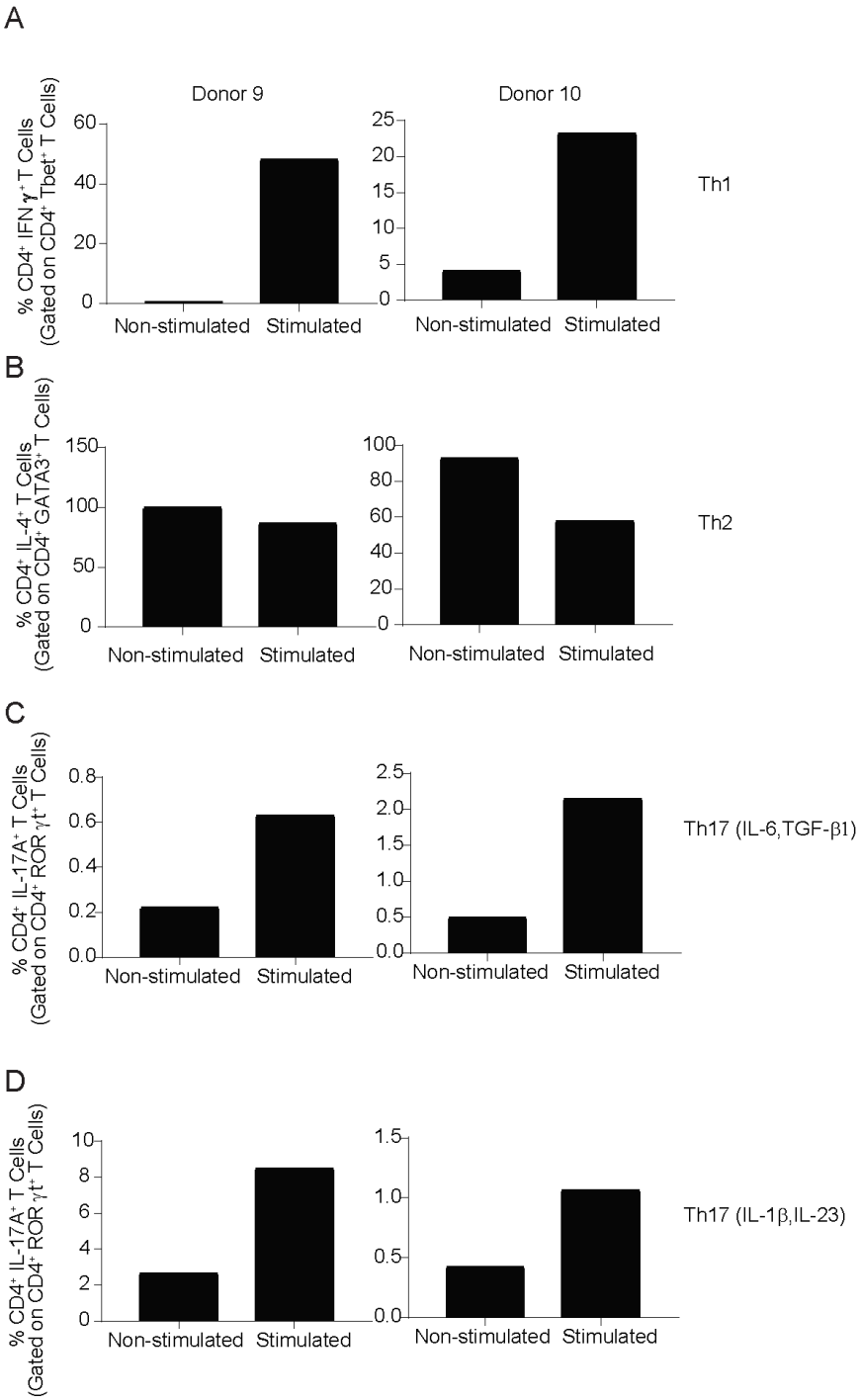

Figure 4. Cytokine profiling of cultured Th cell subsets – summary graphs. A-D. Bar graphs showing the percentage frequency of $CD4^+IFN\gamma^+$, $CD4^+IL\text{-}4^+$ and $CD4^+IL17\text{-}A^+$ T cells in each condition in each donor on day 12 before and after stimulation with PMA and ionomycin. n=2 donors.

Appendix C

Mouse T Cell Proliferation and Treg Cell Suppression Assays

Foxp3 is critical for mouse Treg cell function. In order to assess whether Treg cell isolation and Treg cell culture was performed correctly, Foxp3 expression was primarily assessed via intracellular flow cytometry. However, as a complimentary validation experiment for the efficiency of Treg cell isolation and culture, a functional Treg cell suppression assay was attempted as follow.

First, to optimise the functional assay, a simple proliferation assay was performed using WT mouse splenocytes (figure 1). The spleen of a C57BL/6 WT mouse was isolated. The spleen cells were RBC lysed, washed and resuspended at 10 x 10^6 cells/ml in warm, sterile PBS. The cells were then labelled with CellTrace Violet (Life technologies, CA, USA). Briefly, 20 µl of DMSO were added in a tube of cell trace violet and 1 µl of the cell trace mixture was added per ml of PBS. The cells were then incubated for 20 minutes at 37ºC. Complete media was then added and the cells were further incubated for 10 minutes at 37ºC to enhance the absorption of any unbound dye by the cells. Finally, cells were re-suspended at 1 x 10^6 cells/ml in complete media and then cultured in 96-well, round bottom plates in 200µl per well. Finally, the cells were stimulated with soluble αnti-CD3 (BD Pharmingen, CA, USA; clone:145-2C11; 0.5µg/ml) with or without αnti-CD28 (BD Pharmingen, CA, USA; clone:37.51;2µg/ml) for 72 hrs at 37ºC, CO_2 5%, humidity 95%, to drive cell proliferation. Cell proliferation was assessed by flow cytometry. Expansion of lymphocytes was maximum after stimulation with both αnti-CD3 and αnti-CD28 as opposed to αnti-CD3 alone as reflected by the proliferation index (Pi 2 and 3 respectively) (figure 1B,C). Formulas for the cell proliferation analysis were obtained from (Roederer, 2011).

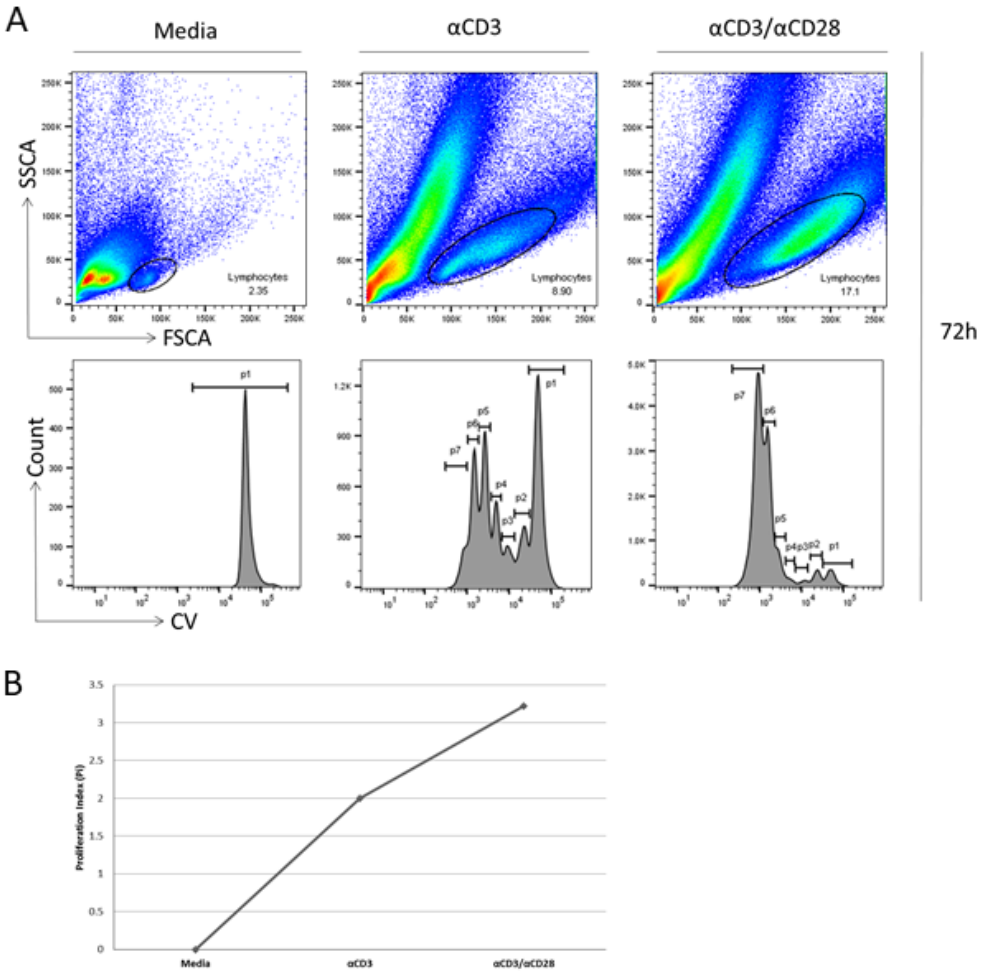

C

*P1=P0	Formula	Media	αCD3	αCD3/αCD28
total no. of cells at t0	*f = P1+P2/2+P3/4+P4/8+P5/16+P6/32+P7/64*	5044	20505	10536
total no. of divisions	*f = P2/2+(P3/4)*2+(P4/8)*3+(P5/16)*4+(P6/32)*5+(P7/64)*6*	0	9632	16448
total no. of cells that divided	*f = total no. of cells at t0 - no. of cells at P1*	0	4823	5108
Di = no. of divisions/ no. of cells at t0	*f = total no. of divisions / total no. of cells at t0*	0	0	2
Pi = no. of divisions/ no. of cells that divided	*f = total no. of divisions / total no. of cells that divided*	0	2	3

Figure 1. Optimisation of cell trace violet (CV) staining and measuring proliferation by flow cytometry. Spleen cells from a WT C57BL/6 mouse were stained with cell trace violet (CV), stimulated with anti-CD3 (0.5µg/ml) and anti-CD28 (2µg/ml) and cultured in complete media for 72 hours. Cell proliferation was measured by flow cytometry. **A.** Gating strategy for the selection of lymphocytes and histograms of cell count versus CV signal intensity which were used to assess the number of cell divisions indicated by peaks (each peak represents a cell generation/division). **B.** Cells were cultured for 72h in complete media alone or treated with αnti-CD3 or αnti-CD3 & αnti-CD28. Treatment of cells with both αnti-CD3 and αnti-CD28 increased the proliferation index (Pi) of lymphocytes. **C.** Formulas used for calculating the Pi. Formulas taken from (Roederer, 2011). N=1

Following the optimisation of the proliferation assay, a Treg cell suppression assay was next performed (figure 2). For this purpose, murine $CD4^{+}CD25^{-}$

and $CD4^+CD25^+$T cells were isolated from the spleen of a WT C57BL/6 mouse using the Miltenyi Biotech Treg isolation kit (as described in sections 2.7 and 3.3.2). Purified $CD4^+CD25^-$ cells ($5x10^4$) were first labelled with CellTrace Violet prior to culture. Briefly, 20 µl of DMSO were added in a tube of cell trace violet. $CD4^+CD25^-$ cells were re-suspended in warm sterile PBS at 10 x 10^6 cells/ml and 1 µl of the cell trace mixture was added per ml of PBS. The cells were then incubated for 20 minutes at 37°C. Complete media was then added and the cells were further incubated for 10 minutes at 37°C to enhance the absorption of any unbound dye by the cells. Finally, cells were re-suspended at 1 x 10^6 cells/ml and then cultured in 96-well round bottom plates in 200µl complete media along with 2 x 10^5 irradiated T cell-depleted spleen cells (irradiated at 3000 cGY) functioning as APCs. Soluble anti-CD3 (0.5µg/ml) was added along with $CD4^+CD25^+$ T cell populations at the indicated ratios. Cells were incubated at 37°C for 72hrs and proliferation/suppression was monitored by flow cytometry. Proliferation of responder naïve T cells was evaluated by CelllTrace Violet dilution on a FACS CANTO II machine. Though not optimal, the addition of effector

$CD4^+CD25^+$ cells resulted in a decrease in the proliferation index (figure 2B).

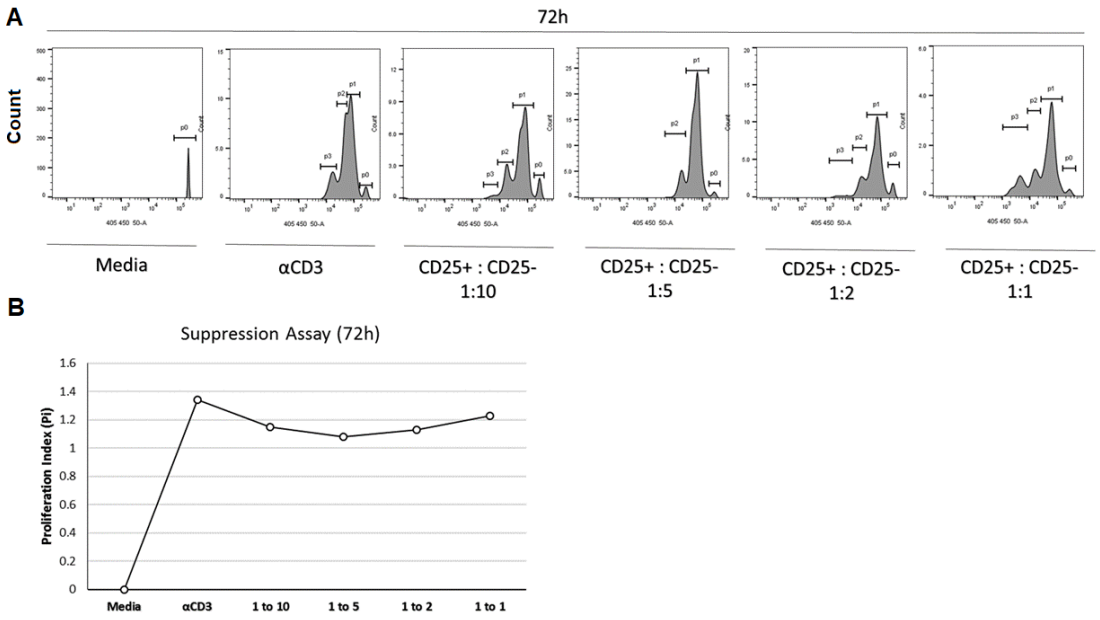

Figure 2. Cell proliferation assay in response to different culture conditions. WT naïve $CD4^+CD25^-$ T cells were stained with cell trace violet and co-cultured with WT $CD4^+CD25^+$ T cells and irradiated spleenocytes in complete media, in the presence of anti-CD3 stimulation (0.5µg/ml). Cells were cultured for 72 hrs and cell proliferation was measured by flow cytometry. **A.** Histograms of cell count versus CV signal intensity which were used to assess the number of cell divisions indicated by peaks (each peak represents a cell generation/division). 'Media' = irradiated spleenocytes plus naïve T cells. 'Anti-CD3' = irradiated spleenocytes plus naïve T cells plus anti-CD3. The rest of the conditions = irradiated spleenocytes plus naïve ($CD25^-$) T cells plus anti-CD3 plus $CD4^+CD25^+$ ($CD25^+$) T cells at indicated ratios. **B.** Summary histogram of the proliferation index of naïve T cells in each culture condition. N=1

Since the attempted suppression assay was not optimal and Treg cell numbers from the *in vitro* cultures were not enough to allow flow cytometry, western blotting and suppression assays to be performed, this methodology was not pursued. As a result, an *in vitro* comparison of the immunosuppressive capacity of *Lgmn*$^{-/-}$ versus WT Treg cells was not performed.

Appendix D

Publication Figures

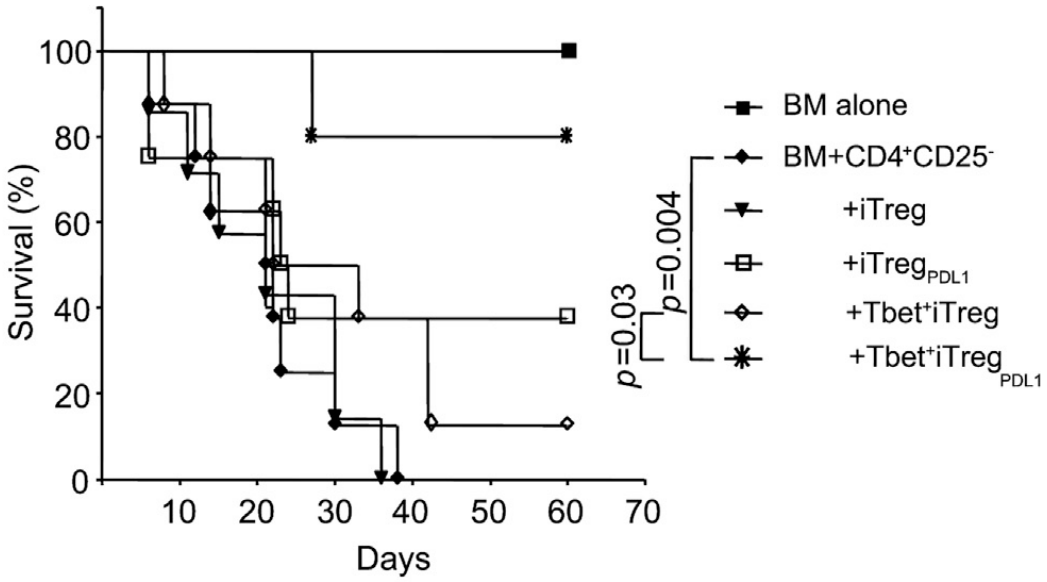

Figure 1. Survival curve of GvHD mice. Mouse cohorts and their respective survival rates. The experiment was performed and analysed by Dr Shoba Amarnath. Figure taken from (Stathopoulou et al., 2018).

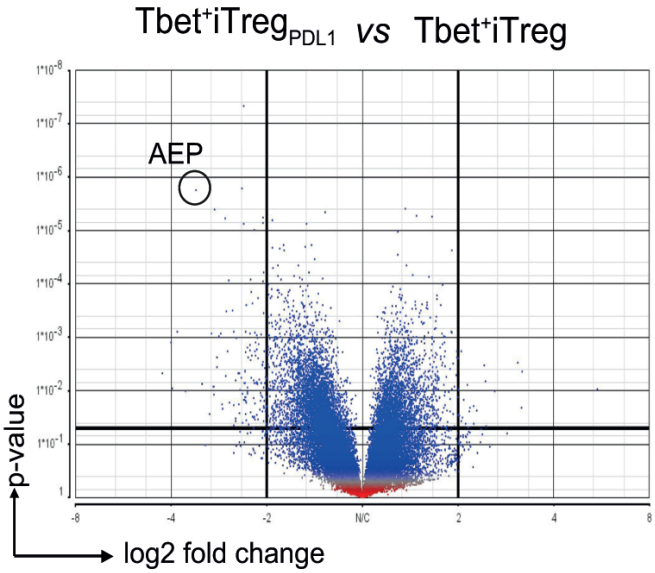

Figure 2. Microarray analysis of AEP mRNA expression in PDL-1-treated Tbet$^+$Treg versus Tbet$^+$Treg cells. AEP is downregulated in Tbet$^+$Treg cells that have been stimulated with PDL-1. The experiment was performed and analysed by Dr Shoba Amarnath. Figure taken from (Stathopoulou et al., 2018).

Appendix E

Posters, Presentations, Publications, Activities, Seminars/Training Courses & Memberships.

Posters

Poster presentation at BSI Congress on the 6th of December 2017 - Potentiating cancer immunotherapy by targeting the tumour microenvironment – 'Asparaginyl endopeptidase deficiency enhances T regulatory cell frequency within the melanoma tumour microenvironment'.

Poster presentation at BSI Congress on the 5th of December 2017 - Battling it out: Regulatory T cells versus inflammation: 'Programmed death 1 signalling maintains FoxP3 stability in Tbet+iTregs by inhibiting asparaginyl endopeptidase'.

Presentations

Oral presentation for the ICM seminar program, Newcastle University, 2017 & 2019

Oral presentation for III Theme meeting, 2017

Publications

Taylor, S., et al., PD-1 regulates KLRG1(+) group 2 innate lymphoid cells. J Exp Med, 2017. 214(6): p. 1663-1678.

Stathopoulou, C., et al., PD-1 Inhibitory Receptor Downregulates Asparaginyl Endopeptidase and Maintains Foxp3 Transcription Factor Stability in Induced Regulatory T Cells. Immunity, 2018.

Stathopoulou, C., Amarnath, S., Differential Regulation of Treg Cells Through Co-receptor Signalling (manuscript written – to be submitted for publication).

Activities

Genetics Matters - Public Engagement event, Centre for Life, Newcastle upon Tyne, 24 February 2018; poster presentation and public engagement activities.

Seminars/Training courses

SPSS Advanced

The Basics in Mass Spectrometry

Data Handling and Spreadsheet Skills

Statistical Considerations in Experimental Research

Introduction to Learning and Teaching one day workshop - demonstrator workshop (ILTHE)

Licensee training course PIL AB - Personal licence category B training course

Memberships

Member of the British Society for Immunology (BSI) since October 2017 – student membership.

References

Abbas, A.K., Benoist, C., Bluestone, J.A., Campbell, D.J., Ghosh, S., Hori, S., Jiang, S., Kuchroo, V.K., Mathis, D., Roncarolo, M.G., Rudensky, A., Sakaguchi, S., Shevach, E.M., Vignali, D.A. and Ziegler, S.F. (2013) 'Regulatory T cells: recommendations to simplify the nomenclature', *Nat Immunol*, 14(4), pp. 307-8.

Allan, S.E., Passerini, L., Bacchetta, R., Crellin, N., Dai, M., Orban, P.C., Ziegler, S.F., Roncarolo, M.G. and Levings, M.K. (2005) 'The role of 2 FOXP3 isoforms in the generation of human CD4+ Tregs', *J Clin Invest*, 115(11), pp. 3276-84.

Aluvihare, V.R., Kallikourdis, M. and Betz, A.G. (2004) 'Regulatory T cells mediate maternal tolerance to the fetus', *Nat Immunol*, 5(3), pp. 266-71.

Antoniou, A.N., Blackwood, S.L., Mazzeo, D. and Watts, C. (2000) 'Control of antigen presentation by a single protease cleavage site', *Immunity*, 12(4), pp. 391-8.

Aschenbrenner, D., Foglierini, M., Jarrossay, D., Hu, D., Weiner, H.L., Kuchroo, V.K., Lanzavecchia, A., Notarbartolo, S. and Sallusto, F. (2018) 'An immunoregulatory and tissue-residency program modulated by c-MAF in human TH17 cells', *Nat Immunol*, 19(10), pp. 1126-1136.

Aschenbrenner, K., D'Cruz, L.M., Vollmann, E.H., Hinterberger, M., Emmerich, J., Swee, L.K., Rolink, A. and Klein, L. (2007) 'Selection of Foxp3+ regulatory T cells specific for self antigen expressed and presented by Aire+ medullary thymic epithelial cells', *Nat Immunol*, 8(4), pp. 351-8.

Attisano, L. and Wrana, J.L. (1996) 'Signal transduction by members of the transforming growth factor-beta superfamily', *Cytokine Growth Factor Rev*, 7(4), pp. 327-39.

Bandukwala, H.S., Wu, Y., Feuerer, M., Chen, Y., Barboza, B., Ghosh, S., Stroud, J.C., Benoist, C., Mathis, D., Rao, A. and Chen, L. (2011) 'Structure of a domain-swapped FOXP3 dimer on DNA and its function in regulatory T cells', *Immunity*, 34(4), pp. 479-91.

Basu, S., Golovina, T., Mikheeva, T., June, C.H. and Riley, J.L. (2008) 'Cutting edge: Foxp3-mediated induction of pim 2 allows human T regulatory cells to preferentially expand in rapamycin', *J Immunol*, 180(9), pp. 5794-8.

Basurto-Islas, G., Grundke-Iqbal, I., Tung, Y.C., Liu, F. and Iqbal, K. (2013) 'Activation of asparaginyl endopeptidase leads to Tau hyperphosphorylation in Alzheimer disease', *J Biol Chem*, 288(24), pp. 17495-507.

Bennett, C.L., Christie, J., Ramsdell, F., Brunkow, M.E., Ferguson, P.J., Whitesell, L., Kelly, T.E., Saulsbury, F.T., Chance, P.F. and Ochs, H.D. (2001) 'The immune dysregulation, polyendocrinopathy, enteropathy, X-linked syndrome (IPEX) is caused by mutations of FOXP3', *Nat Genet*, 27(1), pp. 20-1.

Bensinger, S.J., Bandeira, A., Jordan, M.S., Caton, A.J. and Laufer, T.M. (2001) 'Major histocompatibility complex class II-positive cortical epithelium mediates the selection of CD4(+)25(+) immunoregulatory T cells', *J Exp Med*, 194(4), pp. 427-38.

Bettini, M.L., Pan, F., Bettini, M., Finkelstein, D., Rehg, J.E., Floess, S., Bell, B.D., Ziegler, S.F., Huehn, J., Pardoll, D.M. and Vignali, D.A. (2012) 'Loss of epigenetic modification driven by the Foxp3 transcription factor leads to regulatory T cell insufficiency', *Immunity*, 36(5), pp. 717-30.

Beyer, M., Thabet, Y., Muller, R.U., Sadlon, T., Classen, S., Lahl, K., Basu, S., Zhou, X., Bailey-Bucktrout, S.L., Krebs, W., Schonfeld, E.A., Bottcher, J., Golovina, T., Mayer, C.T., Hofmann, A., Sommer, D., Debey-Pascher, S., Endl, E., Limmer, A., Hippen, K.L., Blazar, B.R., Balderas, R., Quast, T., Waha, A., Mayer, G., Famulok, M., Knolle, P.A., Wickenhauser, C., Kolanus, W., Schermer, B., Bluestone, J.A., Barry, S.C., Sparwasser, T., Riley, J.L. and Schultze, J.L. (2011) 'Repression of the genome organizer SATB1 in regulatory T cells is required for suppressive function and inhibition of effector differentiation', *Nat Immunol*, 12(9), pp. 898-907.

Brabletz, T., Pfeuffer, I., Schorr, E., Siebelt, F., Wirth, T. and Serfling, E. (1993) 'Transforming growth factor beta and cyclosporin A inhibit the inducible activity of the interleukin-2 gene in T cells through a noncanonical octamer-binding site', *Mol Cell Biol*, 13(2), pp. 1155-62.

Brandacher, G., Margreiter, R. and Fuchs, D. (2008) 'Clinical relevance of indoleamine 2,3-dioxygenase for alloimmunity and transplantation', *Curr Opin Organ Transplant*, 13(1), pp. 10-5.

Brunkow, M.E., Jeffery, E.W., Hjerrild, K.A., Paeper, B., Clark, L.B., Yasayko, S.A., Wilkinson, J.E., Galas, D., Ziegler, S.F. and Ramsdell, F.

(2001) 'Disruption of a new forkhead/winged-helix protein, scurfin, results in the fatal lymphoproliferative disorder of the scurfy mouse', *Nat Genet*, 27(1), pp. 68-73.

Burchill, M.A., Yang, J., Vang, K.B., Moon, J.J., Chu, H.H., Lio, C.W., Vegoe, A.L., Hsieh, C.S., Jenkins, M.K. and Farrar, M.A. (2008) 'Linked T cell receptor and cytokine signaling govern the development of the regulatory T cell repertoire', *Immunity*, 28(1), pp. 112-21.

Burchill, M.A., Yang, J., Vogtenhuber, C., Blazar, B.R. and Farrar, M.A. (2007) 'IL-2 receptor beta-dependent STAT5 activation is required for the development of Foxp3+ regulatory T cells', *J Immunol*, 178(1), pp. 280-90.

Burster, T., Beck, A., Tolosa, E., Marin-Esteban, V., Rotzschke, O., Falk, K., Lautwein, A., Reich, M., Brandenburg, J., Schwarz, G., Wiendl, H., Melms, A., Lehmann, R., Stevanovic, S., Kalbacher, H. and Driessen, C. (2004) 'Cathepsin G, and not the asparagine-specific endoprotease, controls the processing of myelin basic protein in lysosomes from human B lymphocytes', *J Immunol*, 172(9), pp. 5495-503.

Chaudhry, A., Rudra, D., Treuting, P., Samstein, R.M., Liang, Y., Kas, A. and Rudensky, A.Y. (2009) 'CD4+ regulatory T cells control TH17 responses in a Stat3-dependent manner', *Science*, 326(5955), pp. 986-91.

Chen, L., Wu, J., Pier, E., Zhao, Y. and Shen, Z. (2013) 'mTORC2-PKBalpha/Akt1 Serine 473 phosphorylation axis is essential for regulation of FOXP3 Stability by chemokine CCL3 in psoriasis', *J Invest Dermatol*, 133(2), pp. 418-28.

Chen, W., Frank, M.E., Jin, W. and Wahl, S.M. (2001) 'TGF-beta released by apoptotic T cells contributes to an immunosuppressive milieu', *Immunity*, 14(6), pp. 715-25.

Chen, W., Jin, W., Hardegen, N., Lei, K.J., Li, L., Marinos, N., McGrady, G. and Wahl, S.M. (2003) 'Conversion of peripheral CD4+CD25- naive T cells to CD4+CD25+ regulatory T cells by TGF-beta induction of transcription factor Foxp3', *J Exp Med*, 198(12), pp. 1875-86.

Chen, W., Jin, W. and Wahl, S.M. (1998) 'Engagement of cytotoxic T lymphocyte-associated antigen 4 (CTLA-4) induces transforming growth factor beta (TGF-beta) production by murine CD4(+) T cells', *J Exp Med*, 188(10), pp. 1849-57.

Chen, Y., Chen, C., Zhang, Z., Liu, C.C., Johnson, M.E., Espinoza, C.A., Edsall, L.E., Ren, B., Zhou, X.J., Grant, S.F., Wells, A.D. and Chen, L. (2015) 'DNA binding by FOXP3 domain-swapped dimer suggests mechanisms of long-range chromosomal interactions', *Nucleic Acids Res*, 43(2), pp. 1268-82.

Cipolletta, D., Feuerer, M., Li, A., Kamei, N., Lee, J., Shoelson, S.E., Benoist, C. and Mathis, D. (2012) 'PPAR-gamma is a major driver of the accumulation and phenotype of adipose tissue Treg cells', *Nature*, 486(7404), pp. 549-53.

Coffer, P.J. and Burgering, B.M. (2004) 'Forkhead-box transcription factors and their role in the immune system', *Nat Rev Immunol*, 4(11), pp. 889-99.

Collado, J.A., Guitart, C., Ciudad, M.T., Alvarez, I. and Jaraquemada, D. (2013) 'The Repertoires of Peptides Presented by MHC-II in the Thymus and in Peripheral Tissue: A Clue for Autoimmunity?', *Front Immunol*, 4, p. 442.

Crespo, J., Sun, H., Welling, T.H., Tian, Z. and Zou, W. (2013) 'T cell anergy, exhaustion, senescence, and stemness in the tumor microenvironment', *Curr Opin Immunol*, 25(2), pp. 214-21.

Creusot, F., Acs, G. and Christman, J.K. (1982) 'Inhibition of DNA methyltransferase and induction of Friend erythroleukemia cell differentiation by 5-azacytidine and 5-aza-2'-deoxycytidine', *J Biol Chem*, 257(4), pp. 2041-8.

Dall, E. and Brandstetter, H. (2013) 'Mechanistic and structural studies on legumain explain its zymogenicity, distinct activation pathways, and regulation', *Proc Natl Acad Sci U S A*, 110(27), pp. 10940-5.

Dall, E. and Brandstetter, H. (2016) 'Structure and function of legumain in health and disease', *Biochimie*, 122, pp. 126-50.

Deng, G., Song, X., Fujimoto, S., Piccirillo, C.A., Nagai, Y. and Greene, M.I. (2019) 'Foxp3 Post-translational Modifications and Treg Suppressive Activity', *Front Immunol*, 10, p. 2486.

Deng, G., Xiao, Y., Zhou, Z., Nagai, Y., Zhang, H., Li, B. and Greene, M.I. (2012) 'Molecular and biological role of the FOXP3 N-terminal domain in immune regulation by T regulatory/suppressor cells', *Exp Mol Pathol*, 93(3), pp. 334-8.

Derynck, R. and Zhang, Y.E. (2003) 'Smad-dependent and Smad-independent pathways in TGF-beta family signalling', *Nature*, 425(6958), pp. 577-84.

Duggleby, R., Danby, R.D., Madrigal, J.A. and Saudemont, A. (2018) 'Clinical Grade Regulatory CD4(+) T Cells (Tregs): Moving Toward Cellular-Based Immunomodulatory Therapies', *Front Immunol*, 9, p. 252.

Fadok, V.A., Bratton, D.L., Rose, D.M., Pearson, A., Ezekewitz, R.A. and Henson, P.M. (2000) 'A receptor for phosphatidylserine-specific clearance of apoptotic cells', *Nature*, 405(6782), pp. 85-90.

Feng, Y., Arvey, A., Chinen, T., van der Veeken, J., Gasteiger, G. and Rudensky, A.Y. (2014) 'Control of the inheritance of regulatory T cell identity by a cis element in the Foxp3 locus', *Cell*, 158(4), pp. 749-63.

Feuerer, M., Herrero, L., Cipolletta, D., Naaz, A., Wong, J., Nayer, A., Lee, J., Goldfine, A.B., Benoist, C., Shoelson, S. and Mathis, D. (2009) 'Lean, but not obese, fat is enriched for a unique population of regulatory T cells that affect metabolic parameters', *Nat Med*, 15(8), pp. 930-9.

Fiebiger, E., Meraner, P., Weber, E., Fang, I.F., Stingl, G., Ploegh, H. and Maurer, D. (2001) 'Cytokines regulate proteolysis in major histocompatibility complex class II-dependent antigen presentation by dendritic cells', *J Exp Med*, 193(8), pp. 881-92.

Fife, B.T., Pauken, K.E., Eagar, T.N., Obu, T., Wu, J., Tang, Q., Azuma, M., Krummel, M.F. and Bluestone, J.A. (2009) 'Interactions between PD-1 and PD-L1 promote tolerance by blocking the TCR-induced stop signal', *Nat Immunol*, 10(11), pp. 1185-92.

Floess, S., Freyer, J., Siewert, C., Baron, U., Olek, S., Polansky, J., Schlawe, K., Chang, H.D., Bopp, T., Schmitt, E., Klein-Hessling, S., Serfling, E., Hamann, A. and Huehn, J. (2007) 'Epigenetic control of the foxp3 locus in regulatory T cells', *PLoS Biol*, 5(2), p. e38.

Fontenot, J.D., Dooley, J.L., Farr, A.G. and Rudensky, A.Y. (2005) 'Developmental regulation of Foxp3 expression during ontogeny', *J Exp Med*, 202(7), pp. 901-6.

Francisco, L.M., Salinas, V.H., Brown, K.E., Vanguri, V.K., Freeman, G.J., Kuchroo, V.K. and Sharpe, A.H. (2009) 'PD-L1 regulates the development,

maintenance, and function of induced regulatory T cells', *J Exp Med*, 206(13), pp. 3015-29.

Freeley, S., Cardone, J., Gunther, S.C., West, E.E., Reinheckel, T., Watts, C., Kemper, C. and Kolev, M.V. (2018) 'Asparaginyl Endopeptidase (Legumain) Supports Human Th1 Induction via Cathepsin L-Mediated Intracellular C3 Activation', *Front Immunol*, 9, p. 2449.

Freeman, M. (2000) 'Feedback control of intercellular signalling in development', *Nature*, 408(6810), pp. 313-9.

Gavin, M.A., Rasmussen, J.P., Fontenot, J.D., Vasta, V., Manganiello, V.C., Beavo, J.A. and Rudensky, A.Y. (2007) 'Foxp3-dependent programme of regulatory T-cell differentiation', *Nature*, 445(7129), pp. 771-5.

Genestier, L., Kasibhatla, S., Brunner, T. and Green, D.R. (1999) 'Transforming growth factor beta1 inhibits Fas ligand expression and subsequent activation-induced cell death in T cells via downregulation of c-Myc', *J Exp Med*, 189(2), pp. 231-9.

Germain, R.N. (1994) 'MHC-dependent antigen processing and peptide presentation: providing ligands for T lymphocyte activation', *Cell*, 76(2), pp. 287-99.

Germain, R.N. (2002) 'T-cell development and the CD4-CD8 lineage decision', *Nat Rev Immunol*, 2(5), pp. 309-22.

Gershon, R.K. and Kondo, K. (1970) 'Cell interactions in the induction of tolerance: the role of thymic lymphocytes', *Immunology*, 18(5), pp. 723-37.

Gershon, R.K. and Kondo, K. (1971) 'Infectious immunological tolerance', *Immunology*, 21(6), pp. 903-14.

Gorelik, L., Fields, P.E. and Flavell, R.A. (2000) 'Cutting Edge: TGF- Inhibits Th Type 2 Development Through Inhibition of GATA-3 Expression', *The Journal of Immunology*, 165(9), pp. 4773-4777.

Gorelik, L. and Flavell, R.A. (2002) 'Transforming growth factor-beta in T-cell biology', *Nat Rev Immunol*, 2(1), pp. 46-53.

Grewal, I.S. and Flavell, R.A. (1998) 'CD40 and CD154 in cell-mediated immunity', *Annu Rev Immunol*, 16, pp. 111-35.

Guerau-de-Arellano, M., Martinic, M., Benoist, C. and Mathis, D. (2009) 'Neonatal tolerance revisited: a perinatal window for Aire control of autoimmunity', *J Exp Med*, 206(6), pp. 1245-52.

Halim, L., Romano, M., McGregor, R., Correa, I., Pavlidis, P., Grageda, N., Hoong, S.J., Yuksel, M., Jassem, W., Hannen, R.F., Ong, M., McKinney, O., Hayee, B., Karagiannis, S.N., Powell, N., Lechler, R.I., Nova-Lamperti, E. and Lombardi, G. (2017) 'An Atlas of Human Regulatory T Helper-like Cells Reveals Features of Th2-like Tregs that Support a Tumorigenic Environment', *Cell Rep*, 20(3), pp. 757-770.

Hancock, W.W. and Ozkaynak, E. (2009) 'Three distinct domains contribute to nuclear transport of murine Foxp3', *PLoS One*, 4(11), p. e7890.

Hannenhalli, S. and Kaestner, K.H. (2009) 'The evolution of Fox genes and their role in development and disease', *Nat Rev Genet*, 10(4), pp. 233-40.

Haugen, M.H., Johansen, H.T., Pettersen, S.J., Solberg, R., Brix, K., Flatmark, K. and Maelandsmo, G.M. (2013) 'Nuclear legumain activity in colorectal cancer', *PLoS One*, 8(1), p. e52980.

Haxhinasto, S., Mathis, D. and Benoist, C. (2008) 'The AKT-mTOR axis regulates de novo differentiation of CD4+Foxp3+ cells', *J Exp Med*, 205(3), pp. 565-74.

Hill, J.A., Feuerer, M., Tash, K., Haxhinasto, S., Perez, J., Melamed, R., Mathis, D. and Benoist, C. (2007) 'Foxp3 transcription-factor-dependent and -independent regulation of the regulatory T cell transcriptional signature', *Immunity*, 27(5), pp. 786-800.

Hori, S., Nomura, T. and Sakaguchi, S. (2003) 'Control of regulatory T cell development by the transcription factor Foxp3', *Science*, 299(5609), pp. 1057-61.

Hori, S. and Sakaguchi, S. (2004) 'Foxp3: a critical regulator of the development and function of regulatory T cells', *Microbes Infect*, 6(8), pp. 745-51.

Hou, L., Cooley, J., Swanson, R., Ong, P.C., Pike, R.N., Bogyo, M., Olson, S.T. and Remold-O'Donnell, E. (2015) 'The protease cathepsin L regulates Th17 cell differentiation', *J Autoimmun*, 65, pp. 56-63.

Hsieh, C.S., Lee, H.M. and Lio, C.W. (2012) 'Selection of regulatory T cells in the thymus', *Nat Rev Immunol*, 12(3), pp. 157-67.

Ishii, S. (1993) '[Asparaginylendopeptidase: an enzyme probably responsible to post-translational proteolysis and transpeptidation of proconcanavalin A]', *Seikagaku*, 65(3), pp. 185-9.

Johansen, H.T., Knight, C.G. and Barrett, A.J. (1999) 'Colorimetric and fluorimetric microplate assays for legumain and a staining reaction for detection of the enzyme after electrophoresis', *Anal Biochem*, 273(2), pp. 278-83.

Kaestner, K.H., Knochel, W. and Martinez, D.E. (2000) 'Unified nomenclature for the winged helix/forkhead transcription factors', *Genes Dev*, 14(2), pp. 142-6.

Kanamori, M., Nakatsukasa, H., Okada, M., Lu, Q. and Yoshimura, A. (2016) 'Induced Regulatory T Cells: Their Development, Stability, and Applications', *Trends Immunol*, 37(11), pp. 803-811.

Kaplan, M.H., Sun, Y.L., Hoey, T. and Grusby, M.J. (1996) 'Impaired IL-12 responses and enhanced development of Th2 cells in Stat4-deficient mice', *Nature*, 382(6587), pp. 174-7.

Keir, M.E., Butte, M.J., Freeman, G.J. and Sharpe, A.H. (2008) 'PD-1 and its ligands in tolerance and immunity', *Annu Rev Immunol*, 26, pp. 677-704.

Kim, H.P. and Leonard, W.J. (2007) 'CREB/ATF-dependent T cell receptor-induced FoxP3 gene expression: a role for DNA methylation', *J Exp Med*, 204(7), pp. 1543-51.

Koch, M.A., Tucker-Heard, G., Perdue, N.R., Killebrew, J.R., Urdahl, K.B. and Campbell, D.J. (2009) 'The transcription factor T-bet controls regulatory T cell homeostasis and function during type 1 inflammation', *Nat Immunol*, 10(6), pp. 595-602.

Kojima, A. and Prehn, R.T. (1981) 'Genetic susceptibility to post-thymectomy autoimmune diseases in mice', *Immunogenetics*, 14(1-2), pp. 15-27.

Konkel, J.E., Jin, W., Abbatiello, B., Grainger, J.R. and Chen, W. (2014) 'Thymocyte apoptosis drives the intrathymic generation of regulatory T cells', *Proc Natl Acad Sci U S A*, 111(4), pp. E465-73.

Krammer, P.H., Arnold, R. and Lavrik, I.N. (2007) 'Life and death in peripheral T cells', *Nat Rev Immunol*, 7(7), pp. 532-42.

Larkin, J., Chiarion-Sileni, V., Gonzalez, R., Grob, J.J., Cowey, C.L., Lao, C.D., Schadendorf, D., Dummer, R., Smylie, M., Rutkowski, P., Ferrucci, P.F., Hill, A., Wagstaff, J., Carlino, M.S., Haanen, J.B., Maio, M., Marquez-Rodas, I., McArthur, G.A., Ascierto, P.A., Long, G.V., Callahan, M.K.,

Postow, M.A., Grossmann, K., Sznol, M., Dreno, B., Bastholt, L., Yang, A., Rollin, L.M., Horak, C., Hodi, F.S. and Wolchok, J.D. (2015) 'Combined Nivolumab and Ipilimumab or Monotherapy in Untreated Melanoma', *N Engl J Med*, 373(1), pp. 23-34.

Laurence, A., Amarnath, S., Mariotti, J., Kim, Y.C., Foley, J., Eckhaus, M., O'Shea, J.J. and Fowler, D.H. (2012) 'STAT3 transcription factor promotes instability of nTreg cells and limits generation of iTreg cells during acute murine graft-versus-host disease', *Immunity*, 37(2), pp. 209-22.

Lee, H.M. and Hsieh, C.S. (2009) 'Rare development of Foxp3+ thymocytes in the CD4+CD8+ subset', *J Immunol*, 183(4), pp. 2261-6.

Lee, J.H., Kang, S.G. and Kim, C.H. (2007) 'FoxP3+ T cells undergo conventional first switch to lymphoid tissue homing receptors in thymus but accelerated second switch to nonlymphoid tissue homing receptors in secondary lymphoid tissues', *J Immunol*, 178(1), pp. 301-11.

Lee, S.M., Gao, B. and Fang, D. (2008) 'FoxP3 maintains Treg unresponsiveness by selectively inhibiting the promoter DNA-binding activity of AP-1', *Blood*, 111(7), pp. 3599-606.

Lenschow, D.J., Zeng, Y., Thistlethwaite, J.R., Montag, A., Brady, W., Gibson, M.G., Linsley, P.S. and Bluestone, J.A. (1992) 'Long-term survival of xenogeneic pancreatic islet grafts induced by CTLA4lg', *Science*, 257(5071), pp. 789-92.

Letterio, J.J. and Roberts, A.B. (1998) 'Regulation of immune responses by TGF-beta', *Annu Rev Immunol*, 16, pp. 137-61.

Li, B., Samanta, A., Song, X., Iacono, K.T., Brennan, P., Chatila, T.A., Roncador, G., Banham, A.H., Riley, J.L., Wang, Q., Shen, Y., Saouaf, S.J. and Greene, M.I. (2007) 'FOXP3 is a homo-oligomer and a component of a supramolecular regulatory complex disabled in the human XLAAD/IPEX autoimmune disease', *Int Immunol*, 19(7), pp. 825-35.

Li, D.N., Matthews, S.P., Antoniou, A.N., Mazzeo, D. and Watts, C. (2003) 'Multistep autoactivation of asparaginyl endopeptidase in vitro and in vivo', *J Biol Chem*, 278(40), pp. 38980-90.

Linsley, P.S., Greene, J.L., Brady, W., Bajorath, J., Ledbetter, J.A. and Peach, R. (1994) 'Human B7-1 (CD80) and B7-2 (CD86) bind with similar

avidities but distinct kinetics to CD28 and CTLA-4 receptors', *Immunity*, 1(9), pp. 793-801.

Liu, Y., Zhang, P., Li, J., Kulkarni, A.B., Perruche, S. and Chen, W. (2008a) 'A critical function for TGF-beta signaling in the development of natural CD4+CD25+Foxp3+ regulatory T cells', *Nat Immunol*, 9(6), pp. 632-40.

Liu, Z., Jang, S.W., Liu, X., Cheng, D., Peng, J., Yepes, M., Li, X.J., Matthews, S., Watts, C., Asano, M., Hara-Nishimura, I., Luo, H.R. and Ye, K. (2008b) 'Neuroprotective actions of PIKE-L by inhibition of SET proteolytic degradation by asparagine endopeptidase', *Mol Cell*, 29(6), pp. 665-78.

Loak, K., Li, D.N., Manoury, B., Billson, J., Morton, F., Hewitt, E. and Watts, C. (2003) 'Novel cell-permeable acyloxymethylketone inhibitors of asparaginyl endopeptidase', *Biol Chem*, 384(8), pp. 1239-46.

Lomri, A. and Marie, P.J. (1990) 'Effects of transforming growth factor type beta on expression of cytoskeletal proteins in endosteal mouse osteoblastic cells', *Bone*, 11(6), pp. 445-51.

Long, M., Park, S.G., Strickland, I., Hayden, M.S. and Ghosh, S. (2009) 'Nuclear factor-kappaB modulates regulatory T cell development by directly regulating expression of Foxp3 transcription factor', *Immunity*, 31(6), pp. 921-31.

Lopes, J.E., Torgerson, T.R., Schubert, L.A., Anover, S.D., Ocheltree, E.L., Ochs, H.D. and Ziegler, S.F. (2006) 'Analysis of FOXP3 reveals multiple domains required for its function as a transcriptional repressor', *J Immunol*, 177(5), pp. 3133-42.

Luo, Y., Zhou, H., Krueger, J., Kaplan, C., Lee, S.H., Dolman, C., Markowitz, D., Wu, W., Liu, C., Reisfeld, R.A. and Xiang, R. (2006) 'Targeting tumor-associated macrophages as a novel strategy against breast cancer', *J Clin Invest*, 116(8), pp. 2132-2141.

Maehr, R., Hang, H.C., Mintern, J.D., Kim, Y.M., Cuvillier, A., Nishimura, M., Yamada, K., Shirahama-Noda, K., Hara-Nishimura, I. and Ploegh, H.L. (2005) 'Asparagine endopeptidase is not essential for class II MHC antigen presentation but is required for processing of cathepsin L in mice', *J Immunol*, 174(11), pp. 7066-74.

Magg, T., Mannert, J., Ellwart, J.W., Schmid, I. and Albert, M.H. (2012) 'Subcellular localization of FOXP3 in human regulatory and nonregulatory T cells', *Eur J Immunol*, 42(6), pp. 1627-38.

Mailer, R.K., Joly, A.L., Liu, S., Elias, S., Tegner, J. and Andersson, J. (2015) 'IL-1beta promotes Th17 differentiation by inducing alternative splicing of FOXP3', *Sci Rep*, 5, p. 14674.

Mailer, R.K.W. (2018) 'Alternative Splicing of FOXP3-Virtue and Vice', *Front Immunol*, 9, p. 530.

Malek, T.R. (2008) 'The biology of interleukin-2', *Annu Rev Immunol*, 26, pp. 453-79.

Maloy, K.J. and Powrie, F. (2001) 'Regulatory T cells in the control of immune pathology', *Nat Immunol*, 2(9), pp. 816-22.

Manoury, B., Hewitt, E.W., Morrice, N., Dando, P.M., Barrett, A.J. and Watts, C. (1998) 'An asparaginyl endopeptidase processes a microbial antigen for class II MHC presentation', *Nature*, 396(6712), pp. 695-9.

Manoury, B., Mazzeo, D., Fugger, L., Viner, N., Ponsford, M., Streeter, H., Mazza, G., Wraith, D.C. and Watts, C. (2002) 'Destructive processing by asparagine endopeptidase limits presentation of a dominant T cell epitope in MBP', *Nat Immunol*, 3(2), pp. 169-74.

Marciniszyn, J., Jr., Hartsuck, J.A. and Tang, J. (1976) 'Mode of inhibition of acid proteases by pepstatin', *J Biol Chem*, 251(22), pp. 7088-94.

Marie, J.C., Letterio, J.J., Gavin, M. and Rudensky, A.Y. (2005) 'TGF-beta1 maintains suppressor function and Foxp3 expression in CD4+CD25+ regulatory T cells', *J Exp Med*, 201(7), pp. 1061-7.

Martinez-Fabregas, J., Prescott, A., van Kasteren, S., Pedrioli, D.L., McLean, I., Moles, A., Reinheckel, T., Poli, V. and Watts, C. (2018) 'Lysosomal protease deficiency or substrate overload induces an oxidative-stress mediated STAT3-dependent pathway of lysosomal homeostasis', *Nat Commun*, 9(1), p. 5343.

Martinez, G.J., Zhang, Z., Reynolds, J.M., Tanaka, S., Chung, Y., Liu, T., Robertson, E., Lin, X., Feng, X.H. and Dong, C. (2010) 'Smad2 positively regulates the generation of Th17 cells', *J Biol Chem*, 285(38), pp. 29039-43.

Martinon, F., Burns, K. and Tschopp, J. (2002) 'The inflammasome: a molecular platform triggering activation of inflammatory caspases and processing of proIL-beta', *Mol Cell*, 10(2), pp. 417-26.

Mathew, J.M., J, H.V., LeFever, A., Konieczna, I., Stratton, C., He, J., Huang, X., Gallon, L., Skaro, A., Ansari, M.J. and Leventhal, J.R. (2018) 'A Phase I Clinical Trial with Ex Vivo Expanded Recipient Regulatory T cells in Living Donor Kidney Transplants', *Sci Rep*, 8(1), p. 7428.

Matthews, S.P., Werber, I., Deussing, J., Peters, C., Reinheckel, T. and Watts, C. (2010) 'Distinct protease requirements for antigen presentation in vitro and in vivo', *J Immunol*, 184(5), pp. 2423-31.

Matzinger, P. (1994) 'Tolerance, danger, and the extended family', *Annu Rev Immunol*, 12, pp. 991-1045.

Matzinger, P. (2002) 'The danger model: a renewed sense of self', *Science*, 296(5566), pp. 301-5.

Mellor, A.L., Keskin, D.B., Johnson, T., Chandler, P. and Munn, D.H. (2002) 'Cells expressing indoleamine 2,3-dioxygenase inhibit T cell responses', *J Immunol*, 168(8), pp. 3771-6.

Miller, J.F. (1961) 'Immunological function of the thymus', *Lancet*, 2(7205), pp. 748-9.

Mosmann, T.R. and Coffman, R.L. (1989) 'Th1-Cell and Th2-Cell - Different Patterns of Lymphokine Secretion Lead to Different Functional-Properties', *Annual Review of Immunology*, 7, pp. 145-173.

Mullen, A.C., Orlando, D.A., Newman, J.J., Loven, J., Kumar, R.M., Bilodeau, S., Reddy, J., Guenther, M.G., DeKoter, R.P. and Young, R.A. (2011) 'Master transcription factors determine cell-type-specific responses to TGF-beta signaling', *Cell*, 147(3), pp. 565-76.

Munn, D.H., Shafizadeh, E., Attwood, J.T., Bondarev, I., Pashine, A. and Mellor, A.L. (1999) 'Inhibition of T cell proliferation by macrophage tryptophan catabolism', *J Exp Med*, 189(9), pp. 1363-72.

Nie, J., Li, Y.Y., Zheng, S.G., Tsun, A. and Li, B. (2015) 'FOXP3(+) Treg Cells and Gender Bias in Autoimmune Diseases', *Front Immunol*, 6, p. 493.

Nishizuka, Y. and Sakakura, T. (1969) 'Thymus and reproduction: sex-linked dysgenesia of the gonad after neonatal thymectomy in mice', *Science*, 166(3906), pp. 753-5.

O'Shea, J.J. and Paul, W.E. (2010) 'Mechanisms underlying lineage commitment and plasticity of helper CD4+ T cells', *Science*, 327(5969), pp. 1098-102.

Otsubo, K., Kanegane, H., Kamachi, Y., Kobayashi, I., Tsuge, I., Imaizumi, M., Sasahara, Y., Hayakawa, A., Nozu, K., Iijima, K., Ito, S., Horikawa, R., Nagai, Y., Takatsu, K., Mori, H., Ochs, H.D. and Miyawaki, T. (2011) 'Identification of FOXP3-negative regulatory T-like (CD4(+)CD25(+)CD127(low)) cells in patients with immune dysregulation, polyendocrinopathy, enteropathy, X-linked syndrome', *Clin Immunol*, 141(1), pp. 111-20.

Ouyang, W., Beckett, O., Ma, Q., Paik, J.H., DePinho, R.A. and Li, M.O. (2010) 'Foxo proteins cooperatively control the differentiation of Foxp3+ regulatory T cells', *Nat Immunol*, 11(7), pp. 618-27.

Pacholczyk, R., Ignatowicz, H., Kraj, P. and Ignatowicz, L. (2006) 'Origin and T cell receptor diversity of Foxp3+CD4+CD25+ T cells', *Immunity*, 25(2), pp. 249-59.

Pardoll, D.M. (2012) 'The blockade of immune checkpoints in cancer immunotherapy', *Nat Rev Cancer*, 12(4), pp. 252-64.

Parry, R.V., Chemnitz, J.M., Frauwirth, K.A., Lanfranco, A.R., Braunstein, I., Kobayashi, S.V., Linsley, P.S., Thompson, C.B. and Riley, J.L. (2005) 'CTLA-4 and PD-1 receptors inhibit T-cell activation by distinct mechanisms', *Mol Cell Biol*, 25(21), pp. 9543-53.

Paul, W.E. and Seder, R.A. (1994) 'Lymphocyte responses and cytokines', *Cell*, 76(2), pp. 241-51.

Pierre, P. and Mellman, I. (1998) 'Developmental regulation of invariant chain proteolysis controls MHC class II trafficking in mouse dendritic cells', *Cell*, 93(7), pp. 1135-45.

Polansky, J.K., Kretschmer, K., Freyer, J., Floess, S., Garbe, A., Baron, U., Olek, S., Hamann, A., von Boehmer, H. and Huehn, J. (2008) 'DNA methylation controls Foxp3 gene expression', *Eur J Immunol*, 38(6), pp. 1654-63.

Probst-Kepper, M., Geffers, R., Kroger, A., Viegas, N., Erck, C., Hecht, H.J., Lunsdorf, H., Roubin, R., Moharregh-Khiabani, D., Wagner, K., Ocklenburg, F., Jeron, A., Garritsen, H., Arstila, T.P., Kekalainen, E., Balling, R., Hauser,

H., Buer, J. and Weiss, S. (2009) 'GARP: a key receptor controlling FOXP3 in human regulatory T cells', *J Cell Mol Med*, 13(9B), pp. 3343-57.
Proetzel, G., Pawlowski, S.A., Wiles, M.V., Yin, M., Boivin, G.P., Howles, P.N., Ding, J., Ferguson, M.W. and Doetschman, T. (1995) 'Transforming growth factor-beta 3 is required for secondary palate fusion', *Nat Genet*, 11(4), pp. 409-14.
Ramsdell, F. (2003) 'Foxp3 and natural regulatory T cells: key to a cell lineage?', *Immunity*, 19(2), pp. 165-8.
Ramsdell, F. and Ziegler, S.F. (2014) 'FOXP3 and scurfy: how it all began', *Nat Rev Immunol*, 14(5), pp. 343-9.
Rao, S., Gerondakis, S., Woltring, D. and Shannon, M.F. (2003) 'c-Rel is required for chromatin remodeling across the IL-2 gene promoter', *J Immunol*, 170(7), pp. 3724-31.
Riley, J.L. (2009) 'PD-1 signaling in primary T cells', *Immunol Rev*, 229(1), pp. 114-25.
Roederer, M. (2011) 'Interpretation of cellular proliferation data: avoid the panglossian', *Cytometry A*, 79(2), pp. 95-101.
Rosenblum, M.D., Gratz, I.K., Paw, J.S., Lee, K., Marshak-Rothstein, A. and Abbas, A.K. (2011) 'Response to self antigen imprints regulatory memory in tissues', *Nature*, 480(7378), pp. 538-42.
Saeidi, A., Zandi, K., Cheok, Y.Y., Saeidi, H., Wong, W.F., Lee, C.Y.Q., Cheong, H.C., Yong, Y.K., Larsson, M. and Shankar, E.M. (2018) 'T-Cell Exhaustion in Chronic Infections: Reversing the State of Exhaustion and Reinvigorating Optimal Protective Immune Responses', *Front Immunol*, 9, p. 2569.
Sakaguchi, S. (2004) 'Naturally arising CD4+ regulatory t cells for immunologic self-tolerance and negative control of immune responses', *Annu Rev Immunol*, 22, pp. 531-62.
Sakaguchi, S., Fukuma, K., Kuribayashi, K. and Masuda, T. (1985) 'Organ-specific autoimmune diseases induced in mice by elimination of T cell subset. I. Evidence for the active participation of T cells in natural self-tolerance; deficit of a T cell subset as a possible cause of autoimmune disease', *J Exp Med*, 161(1), pp. 72-87.

Sakaguchi, S., Sakaguchi, N., Asano, M., Itoh, M. and Toda, M. (1995) 'Immunologic self-tolerance maintained by activated T cells expressing IL-2 receptor alpha-chains (CD25). Breakdown of a single mechanism of self-tolerance causes various autoimmune diseases', *J Immunol*, 155(3), pp. 1151-64.

Sakaguchi, S., Takahashi, T. and Nishizuka, Y. (1982) 'Study on cellular events in post-thymectomy autoimmune oophoritis in mice. II. Requirement of Lyt-1 cells in normal female mice for the prevention of oophoritis', *J Exp Med*, 156(6), pp. 1577-86.

Samantha Greer, Rice Honeywell, Mulu Geletu, Rozanne Arulanandam and Raptis, L. (2010) 'Housekeeping genes; expression levels may change with density of cultured cells', *Journal of Immunological Methods*, 355(1–2), pp. 76-79.

Sanford, L.P., Ormsby, I., Gittenberger-de Groot, A.C., Sariola, H., Friedman, R., Boivin, G.P., Cardell, E.L. and Doetschman, T. (1997) 'TGFbeta2 knockout mice have multiple developmental defects that are non-overlapping with other TGFbeta knockout phenotypes', *Development*, 124(13), pp. 2659-70.

Sansom, D.M. (2015) 'IMMUNOLOGY. Moving CTLA-4 from the trash to recycling', *Science*, 349(6246), pp. 377-8.

Sather, B.D., Treuting, P., Perdue, N., Miazgowicz, M., Fontenot, J.D., Rudensky, A.Y. and Campbell, D.J. (2007) 'Altering the distribution of Foxp3(+) regulatory T cells results in tissue-specific inflammatory disease', *J Exp Med*, 204(6), pp. 1335-47.

Sauer, S., Bruno, L., Hertweck, A., Finlay, D., Leleu, M., Spivakov, M., Knight, Z.A., Cobb, B.S., Cantrell, D., O'Connor, E., Shokat, K.M., Fisher, A.G. and Merkenschlager, M. (2008) 'T cell receptor signaling controls Foxp3 expression via PI3K, Akt, and mTOR', *Proc Natl Acad Sci U S A*, 105(22), pp. 7797-802.

Schmidleithner, L., Thabet, Y., Schonfeld, E., Kohne, M., Sommer, D., Abdullah, Z., Sadlon, T., Osei-Sarpong, C., Subbaramaiah, K., Copperi, F., Haendler, K., Varga, T., Schanz, O., Bourry, S., Bassler, K., Krebs, W., Peters, A.E., Baumgart, A.K., Schneeweiss, M., Klee, K., Schmidt, S.V., Nussing, S., Sander, J., Ohkura, N., Waha, A., Sparwasser, T., Wunderlich,

F.T., Forster, I., Ulas, T., Weighardt, H., Sakaguchi, S., Pfeifer, A., Bluher, M., Dannenberg, A.J., Ferreiros, N., Muglia, L.J., Wickenhauser, C., Barry, S.C., Schultze, J.L. and Beyer, M. (2019) 'Enzymatic Activity of HPGD in Treg Cells Suppresses Tconv Cells to Maintain Adipose Tissue Homeostasis and Prevent Metabolic Dysfunction', *Immunity*, 50(5), pp. 1232-1248 e14.

Sepulveda, F.E., Maschalidi, S., Colisson, R., Heslop, L., Ghirelli, C., Sakka, E., Lennon-Dumenil, A.M., Amigorena, S., Cabanie, L. and Manoury, B. (2009) 'Critical role for asparagine endopeptidase in endocytic Toll-like receptor signaling in dendritic cells', *Immunity*, 31(5), pp. 737-48.

Sette, A., Adorini, L., Colon, S.M., Buus, S. and Grey, H.M. (1989) 'Capacity of intact proteins to bind to MHC class II molecules', *J Immunol*, 143(4), pp. 1265-7.

Shah, D.K. and Zuniga-Pflucker, J.C. (2014) 'An overview of the intrathymic intricacies of T cell development', *J Immunol*, 192(9), pp. 4017-23.

Shevach, E.M. and Thornton, A.M. (2014) 'tTregs, pTregs, and iTregs: similarities and differences', *Immunol Rev*, 259(1), pp. 88-102.

Shirahama-Noda, K., Yamamoto, A., Sugihara, K., Hashimoto, N., Asano, M., Nishimura, M. and Hara-Nishimura, I. (2003) 'Biosynthetic processing of cathepsins and lysosomal degradation are abolished in asparaginyl endopeptidase-deficient mice', *J Biol Chem*, 278(35), pp. 33194-9.

Shull, M.M., Ormsby, I., Kier, A.B., Pawlowski, S., Diebold, R.J., Yin, M., Allen, R., Sidman, C., Proetzel, G., Calvin, D. and et al. (1992) 'Targeted disruption of the mouse transforming growth factor-beta 1 gene results in multifocal inflammatory disease', *Nature*, 359(6397), pp. 693-9.

Singh, K., Hjort, M., Thorvaldson, L. and Sandler, S. (2015) 'Concomitant analysis of Helios and Neuropilin-1 as a marker to detect thymic derived regulatory T cells in naive mice', *Sci Rep*, 5, p. 7767.

Starr, T.K., Jameson, S.C. and Hogquist, K.A. (2003) 'Positive and negative selection of T cells', *Annu Rev Immunol*, 21, pp. 139-76.

Stathopoulou, C., Gangaplara, A., Mallett, G., Flomerfelt, F.A., Liniany, L.P., Knight, D., Samsel, L.A., Berlinguer-Palmini, R., Yim, J.J., Felizardo, T.C., Eckhaus, M.A., Edgington-Mitchell, L., Martinez-Fabregas, J., Zhu, J., Fowler, D.H., van Kasteren, S.I., Laurence, A., Bogyo, M., Watts, C.,

Shevach, E.M. and Amarnath, S. (2018) 'PD-1 Inhibitory Receptor Downregulates Asparaginyl Endopeptidase and Maintains Foxp3 Transcription Factor Stability in Induced Regulatory T Cells', *Immunity*.

Swain, S.L. (1983) 'T cell subsets and the recognition of MHC class', *Immunol Rev*, 74, pp. 129-42.

Tai, X., Cowan, M., Feigenbaum, L. and Singer, A. (2005) 'CD28 costimulation of developing thymocytes induces Foxp3 expression and regulatory T cell differentiation independently of interleukin 2', *Nat Immunol*, 6(2), pp. 152-62.

Takahashi, T., Tagami, T., Yamazaki, S., Uede, T., Shimizu, J., Sakaguchi, N., Mak, T.W. and Sakaguchi, S. (2000) 'Immunologic self-tolerance maintained by CD25(+)CD4(+) regulatory T cells constitutively expressing cytotoxic T lymphocyte-associated antigen 4', *J Exp Med*, 192(2), pp. 303-10.

Takenaka, M.C. and Quintana, F.J. (2017) 'Tolerogenic dendritic cells', *Semin Immunopathol*, 39(2), pp. 113-120.

Tanaka, T., Inazawa, J. and Nakamura, Y. (1996) 'Molecular cloning of a human cDNA encoding putative cysteine protease (PRSC1) and its chromosome assignment to 14q32.1', *Cytogenet Cell Genet*, 74(1-2), pp. 120-3.

Teng, L., Wada, H. and Zhang, S. (2009) 'Identification and functional characterization of legumain in amphioxus Branchiostoma belcheri', *Biosci Rep*, 30(3), pp. 177-86.

Tivol, E.A., Borriello, F., Schweitzer, A.N., Lynch, W.P., Bluestone, J.A. and Sharpe, A.H. (1995) 'Loss of CTLA-4 leads to massive lymphoproliferation and fatal multiorgan tissue destruction, revealing a critical negative regulatory role of CTLA-4', *Immunity*, 3(5), pp. 541-7.

Tone, Y., Furuuchi, K., Kojima, Y., Tykocinski, M.L., Greene, M.I. and Tone, M. (2008) 'Smad3 and NFAT cooperate to induce Foxp3 expression through its enhancer', *Nat Immunol*, 9(2), pp. 194-202.

Tontonoz, P. and Spiegelman, B.M. (2008) 'Fat and beyond: the diverse biology of PPARgamma', *Annu Rev Biochem*, 77, pp. 289-312.

Tran, D.Q., Ramsey, H. and Shevach, E.M. (2007) 'Induction of FOXP3 expression in naive human CD4+FOXP3 T cells by T-cell receptor

stimulation is transforming growth factor-beta dependent but does not confer a regulatory phenotype', *Blood*, 110(8), pp. 2983-90.

Veldhoen, M., Hocking, R.J., Atkins, C.J., Locksley, R.M. and Stockinger, B. (2006) 'TGFbeta in the context of an inflammatory cytokine milieu supports de novo differentiation of IL-17-producing T cells', *Immunity*, 24(2), pp. 179-89.

Walker, M.R., Kasprowicz, D.J., Gersuk, V.H., Benard, A., Van Landeghen, M., Buckner, J.H. and Ziegler, S.F. (2003) 'Induction of FoxP3 and acquisition of T regulatory activity by stimulated human CD4+CD25- T cells', *J Clin Invest*, 112(9), pp. 1437-43.

Walunas, T.L., Lenschow, D.J., Bakker, C.Y., Linsley, P.S., Freeman, G.J., Green, J.M., Thompson, C.B. and Bluestone, J.A. (1994) 'CTLA-4 can function as a negative regulator of T cell activation', *Immunity*, 1(5), pp. 405-13.

Weigel, D., Jurgens, G., Kuttner, F., Seifert, E. and Jackle, H. (1989) 'The homeotic gene fork head encodes a nuclear protein and is expressed in the terminal regions of the Drosophila embryo', *Cell*, 57(4), pp. 645-58.

Wing, K., Onishi, Y., Prieto-Martin, P., Yamaguchi, T., Miyara, M., Fehervari, Z., Nomura, T. and Sakaguchi, S. (2008) 'CTLA-4 control over Foxp3+ regulatory T cell function', *Science*, 322(5899), pp. 271-5.

Wu, Y., Borde, M., Heissmeyer, V., Feuerer, M., Lapan, A.D., Stroud, J.C., Bates, D.L., Guo, L., Han, A., Ziegler, S.F., Mathis, D., Benoist, C., Chen, L. and Rao, A. (2006) 'FOXP3 controls regulatory T cell function through cooperation with NFAT', *Cell*, 126(2), pp. 375-87.

Xiao, S., Jin, H., Korn, T., Liu, S.M., Oukka, M., Lim, B. and Kuchroo, V.K. (2008) 'Retinoic acid increases Foxp3+ regulatory T cells and inhibits development of Th17 cells by enhancing TGF-beta-driven Smad3 signaling and inhibiting IL-6 and IL-23 receptor expression', *J Immunol*, 181(4), pp. 2277-84.

Xu, L., Kitani, A., Stuelten, C., McGrady, G., Fuss, I. and Strober, W. (2010) 'Positive and negative transcriptional regulation of the Foxp3 gene is mediated by access and binding of the Smad3 protein to enhancer I', *Immunity*, 33(3), pp. 313-25.

Yang, S., Fujikado, N., Kolodin, D., Benoist, C. and Mathis, D. (2015) 'Immune tolerance. Regulatory T cells generated early in life play a distinct role in maintaining self-tolerance', *Science*, 348(6234), pp. 589-94.

Yu, A., Snowhite, I., Vendrame, F., Rosenzwajg, M., Klatzmann, D., Pugliese, A. and Malek, T.R. (2015) 'Selective IL-2 responsiveness of regulatory T cells through multiple intrinsic mechanisms supports the use of low-dose IL-2 therapy in type 1 diabetes', *Diabetes*, 64(6), pp. 2172-83.

Yuan, S., Yu, X., Topf, M., Ludtke, S.J., Wang, X. and Akey, C.W. (2010) 'Structure of an apoptosome-procaspase-9 CARD complex', *Structure*, 18(5), pp. 571-83.

Yuan, X., Cheng, G. and Malek, T.R. (2014) 'The importance of regulatory T-cell heterogeneity in maintaining self-tolerance', *Immunol Rev*, 259(1), pp. 103-14.

Zhang, S., Takaku, M., Zou, L., Gu, A.D., Chou, W.C., Zhang, G., Wu, B., Kong, Q., Thomas, S.Y., Serody, J.S., Chen, X., Xu, X., Wade, P.A., Cook, D.N., Ting, J.P.Y. and Wan, Y.Y. (2017) 'Reversing SKI-SMAD4-mediated suppression is essential for TH17 cell differentiation', *Nature*, 551(7678), pp. 105-109.

Zhang, Z., Song, M., Liu, X., Kang, S.S., Kwon, I.S., Duong, D.M., Seyfried, N.T., Hu, W.T., Liu, Z., Wang, J.Z., Cheng, L., Sun, Y.E., Yu, S.P., Levey, A.I. and Ye, K. (2014) 'Cleavage of tau by asparagine endopeptidase mediates the neurofibrillary pathology in Alzheimer's disease', *Nat Med*, 20(11), pp. 1254-62.

Zheng, Y., Josefowicz, S., Chaudhry, A., Peng, X.P., Forbush, K. and Rudensky, A.Y. (2010) 'Role of conserved non-coding DNA elements in the Foxp3 gene in regulatory T-cell fate', *Nature*, 463(7282), pp. 808-12.

Ziegler, S.F. (2006) 'FOXP3: of mice and men', *Annu Rev Immunol*, 24, pp. 209-26.

Article

Immunity

PD-1 Inhibitory Receptor Downregulates Asparaginyl Endopeptidase and Maintains Foxp3 Transcription Factor Stability in Induced Regulatory T Cells

Graphical Abstract

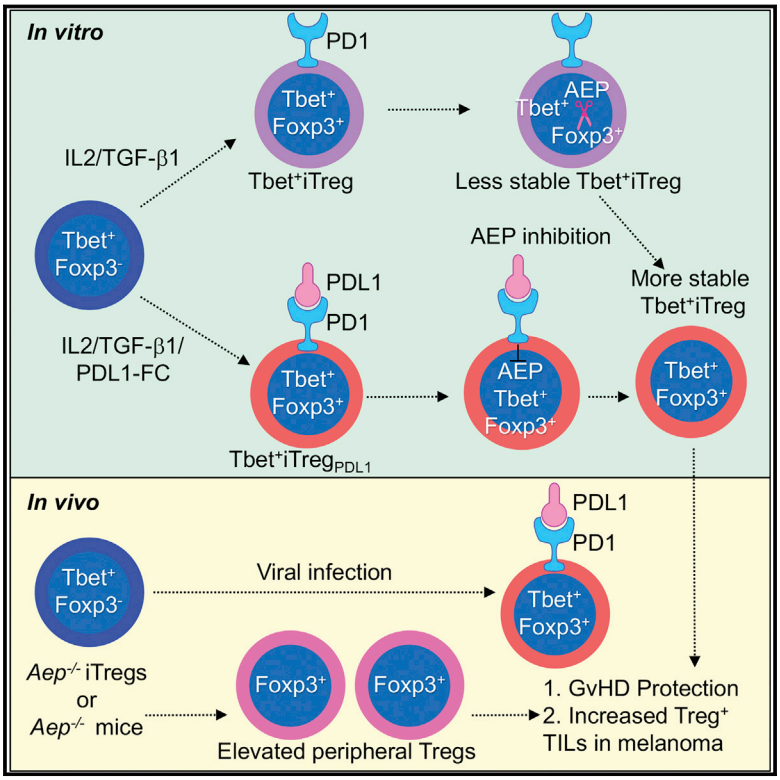

Highlights

- Asparaginyl endopeptidase (AEP) is expressed in induced regulatory T cells
- AEP cleaves Foxp3 and *Aep*$^{-/-}$ mice have elevated numbers of peripheral Treg cells
- AEP deficiency increases Treg cell frequency and numbers in GvHD and melanoma
- PD-1 signaling maintains Foxp3 protein expression by inhibiting AEP

Authors

Chaido Stathopoulou, Arunakumar Gangaplara, Grace Mallett, ..., Colin Watts, Ethan M. Shevach, Shoba Amarnath

Correspondence

shoba.amarnath@newcastle.ac.uk

In Brief

Th1 cells are known for their enhanced stability, so mechanisms that mediate their flexibility are poorly studied. Here, Stathopoulou et al. demonstrate that plasticity of Th1 cells to Tbet^{+}iTreg cells is mediated by PD-1 signaling via asparaginyl endopeptidase (AEP). AEP inhibition enhanced iTreg cells in GvHD and tumor models.

Stathopoulou et al., 2018, Immunity *49*, 247–263
August 21, 2018
https://doi.org/10.1016/j.immuni.2018.05.006

CellPress

Immunity
Article

PD-1 Inhibitory Receptor Downregulates Asparaginyl Endopeptidase and Maintains Foxp3 Transcription Factor Stability in Induced Regulatory T Cells

Chaido Stathopoulou,[1,13] Arunakumar Gangaplara,[2,13] Grace Mallett,[1,13] Francis A. Flomerfelt,[3] Lukasz P. Liniany,[1] David Knight,[4] Leigh A. Samsel,[5] Rolando Berlinguer-Palmini,[1] Joshua J. Yim,[6] Tania C. Felizardo,[3] Michael A. Eckhaus,[7] Laura Edgington-Mitchell,[6,8] Jonathan Martinez-Fabregas,[9] Jinfang Zhu,[2] Daniel H. Fowler,[3] Sander I. van Kasteren,[10] Arian Laurence,[1,11,12] Matthew Bogyo,[6] Colin Watts,[9] Ethan M. Shevach,[2] and Shoba Amarnath[1,14,*]
[1]Bio-Imaging Unit, Newcastle University, Newcastle upon Tyne NE2 4HH, UK
[2]Laboratory of Immunology, National Institute of Allergy and Infectious Diseases, NIH, Bethesda, MD 20892, USA
[3]Experimental Transplantation Immunology Branch, National Cancer Institute, NIH, Bethesda, MD 20892, USA
[4]Biological Mass Spectrometry Core, University of Manchester, Manchester M13 9PL, UK
[5]Flow Cytometry Core, National Heart, Lung and Blood Institute, NIH, Bethesda, MD 20892, USA
[6]School of Medicine, Stanford University, Stanford, CA 94305, USA
[7]Division of Veterinary Resources, Office of Research Services, NIH, Bethesda, MD 20892, USA
[8]Drug Discovery Biology, Monash University, Melbourne, VIC 3800, Australia
[9]College of Life Sciences, University of Dundee, Dundee DD1 4HN, UK
[10]Leiden Institute of Chemistry and Institute of Chemical Immunology, Leiden University, 2311 EZ Leiden, the Netherlands
[11]Translational Gastroenterology Unit, Experimental Medicine Division, John Radcliffe Hospital, University of Oxford, Headington, Oxford OX3 9DU, UK
[12]Department of Haematology, Northern Centre for Cancer Care, Newcastle upon Tyne NE2 4HH, UK
[13]These authors contributed equally
[14]Lead Contact
*Correspondence: shoba.amarnath@newcastle.ac.uk
https://doi.org/10.1016/j.immuni.2018.05.006

SUMMARY

CD4$^+$ T cell differentiation into multiple T helper (Th) cell lineages is critical for optimal adaptive immune responses. This report identifies an intrinsic mechanism by which programmed death-1 receptor (PD-1) signaling imparted regulatory phenotype to Foxp3$^+$ Th1 cells (denoted as Tbet$^+$iTreg$_{PDL1}$ cells) and inducible regulatory T (iTreg) cells. Tbet$^+$ iTreg$_{PDL1}$ cells prevented inflammation in murine models of experimental colitis and experimental graft versus host disease (GvHD). Programmed death ligand-1 (PDL-1) binding to PD-1 imparted regulatory function to Tbet$^+$iTreg$_{PDL1}$ cells and iTreg cells by specifically downregulating endo-lysosomal protease asparaginyl endopeptidase (AEP). AEP regulated Foxp3 stability and blocking AEP imparted regulatory function in Tbet$^+$iTreg cells. Also, *Aep*$^{-/-}$ iTreg cells significantly inhibited GvHD and maintained Foxp3 expression. PD-1-mediated Foxp3 maintenance in Tbet$^+$ Th1 cells occurred both in tumor infiltrating lymphocytes (TILs) and during chronic viral infection. Collectively, this report has identified an intrinsic function for PD-1 in maintaining Foxp3 through proteolytic pathway.

INTRODUCTION

Functional plasticity of cells belonging to the innate and adaptive immune system is necessary for the generation of robust immune responses while minimizing detrimental effects toward the host. CD4$^+$ T cell plasticity has been extensively studied in recent years (O'Shea and Paul, 2010). A plasticity index has been proposed for the various T helper cell lineage subsets, with each subset possessing different lineage flexibility (Murphy and Stockinger, 2010). Of the numerous CD4$^+$ T cell subsets, peripherally generated T regulatory (Treg) cells and T helper (Th) 17 cells are regarded as plastic (Bailey-Bucktrout et al., 2013; Boniface et al., 2010; Gagliani et al., 2015; McGeachy et al., 2007; Mukasa et al., 2010; Yang et al., 2008) whereas functional stability has been attributed toward thymic derived Treg (tTreg) cells (Miyao et al., 2012), Th1, and Th2 cell lineages. Both Th2 cells (Adeeku et al., 2008; Hegazy et al., 2010; Peine et al., 2013; Taylor et al., 2006) and tTreg cells (Feng et al., 2014; Laurence et al., 2012; Zhou et al., 2009) have been demonstrated to be plastic in disease conditions. In light of these studies, Th1 cells remain the lineage with the least evidence of functional flexibility. Furthermore, the molecular mechanisms that influence lineage stability in Th1 cells are poorly defined (Brown et al., 2015).

In contrast to work on cytokine signaling (O'Shea and Paul, 2010), the role of co-receptors in mediating functional plasticity has received minimal attention. One such co-inhibitory molecule that has been implicated in Th cell plasticity is programmed

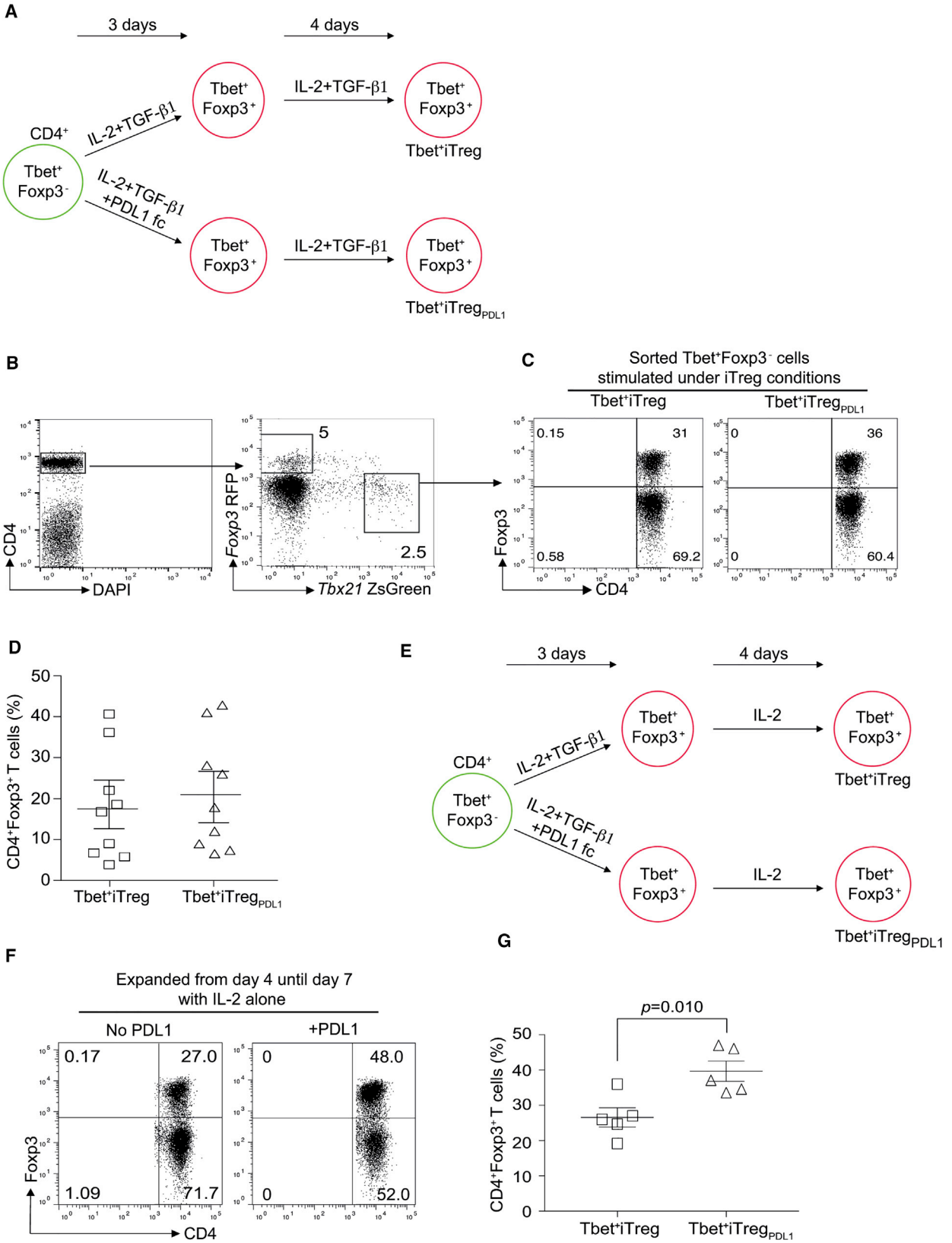

(legend on next page)

death ligand-1 (PDL-1 or B7-H1). In our previous work, we have found that PDL-1 can induce Foxp3 in human Th1 cells (Amarnath et al., 2011), consistent with work in murine naive T cells (Francisco et al., 2009). In the tumor microenvironment, PDL-1 expression coincides with increased intra-tumor Foxp3$^+$ T cells (Duraiswamy et al., 2013; Jacobs et al., 2009), suggesting that PDL-1 may play a role in maintaining Foxp3 expression in CD4$^+$ Th cell subsets. PDL-1 binds to its receptor PD-1 on T cells which signals through the inhibitory phosphatase SHP1 (Chemnitz et al., 2004). SHP1 or SHP2 recruitment results in STAT de-phosphorylation (Amarnath et al., 2011; Taylor et al., 2017), potentially destabilizing the transcriptional signature of Th1 cell lineage.

In the current study, we have elucidated an intrinsic mechanism by which PD-1 signaling maintains Foxp3 in Tbet$^+$iTreg and iTreg cells. The data presented here demonstrate that PD-1 can inhibit a functional nuclear pool of active asparaginyl endopeptidase (AEP), an endo-lysosomal protease previously implicated in antigen processing in dendritic cells (Dall and Brandstetter, 2016; Manoury et al., 1998, 2002). We show that AEP is responsible for destabilizing Foxp3 in both iTreg and Tbet$^+$iTreg cells. We found that PD-1 activation significantly enhanced Foxp3 expression in primed anti-viral and anti-tumor Tbet$^+$Th1 cells, which was reversed in the presence of a blocking antibody to PDL-1. Of note, PDL-1 blockade did not reverse Tbet$^+$Th1 cell conversion and iTreg cell induction in the absence of AEP. Therefore, this study demonstrates that downregulation of AEP is necessary for PD-1-generated Foxp3 stability.

RESULTS

PD-1 Signaling, in the Absence of TGF-β1, Reinforces Foxp3 Expression in CD4$^+$Tbet$^+$Foxp3$^-$ T Cells

To investigate whether PD-1 maintains Foxp3 in Th1 cells, previously described *Tbx21*ZsGreen reporter mice were crossed with *Foxp3*RFP mice. Flow sorted CD4$^+$Tbet$^+$Foxp3$^-$ T cells (Figures 1A, 1B, S1A, and S1B) were differentiated under iTreg cell conditions (Tbet$^+$iTreg cells) or iTreg cell conditions with PDL-1 (Tbet$^+$iTreg$_{PDL1}$ cells) (Figures 1A–1D). When subsets were maintained with interleukin-2 (IL-2) and transforming growth factor-β (TGF-β1), Foxp3 expression under both culture conditions was similar (Figure 1D). In culture conditions where TGF-β1 was omitted from day 4 until day 7 (Figure 1E), a significant loss in Foxp3 was noted within the Tbet$^+$iTreg cells compared with Tbet$^+$iTreg$_{PDL1}$ cells (Figures 1F and 1G). We next purified Foxp3$^+$ cells from both groups (denoted hereafter as Tbet$^+$iTreg cells and Tbet$^+$ iTreg$_{PDL1}$ cells) and examined their function *in vitro*. Both populations suppressed effector T cell proliferation *in vitro* to a similar extent (Figures S1C–S1E). Tbet$^+$iTreg$_{PDL1}$ cells secreted less IL-10 and IFN-γ, when compared to Tbet$^+$ Foxp3$^-$ cells (Figure S1F). These results indicate that PDL-1 signaling maintains Foxp3 expression in Tbet$^+$iTreg cells in the absence of TGF-β1.

PDL-1 Induces Stable Regulatory Phenotype in Tbet$^+$iTreg$_{PDL1}$ Cells during Experimental Autoimmune Colitis and Graft versus Host Disease (GvHD)

The *in vivo* regulatory potential of Tbet$^+$iTreg cells and Tbet$^+$ iTreg$_{PDL1}$ cells was next evaluated. *Rag2*$^{-/-}$ mice were reconstituted with CD4$^+$CD45RB^{hi}CD25$^-$ naive T effector cells alone (CD45.1$^+$) or in conjunction with various indicated flow-sorted iTreg cell populations (CD45.2$^+$). Cohorts that received either T effector cells alone or together with Tbet$^+$iTreg cells succumbed to colitis. By contrast, animals that received effector T cells and Tbet$^+$iTreg$_{PDL1}$ cells were protected from clinical weight loss (Figure S2A). We next evaluated T effector cell function in the spleen and lamina propria lymphocytes (LPLs). Adoptive transfer of Tbet$^+$iTreg$_{PDL1}$ cells significantly diminished interferon-γ (IFN-γ) production in the T effector cells in the spleen (Figures 2A and 2B) and in the LPL (Figure S2B). These results suggested that despite both groups of Th1 cells expressing Foxp3, only Tbet$^+$iTreg$_{PDL1}$ cells had a robust regulatory phenotype *in vivo* that was comparable to iTreg cells generated from naive CD4$^+$ cells. We next investigated whether the ability of Tbet$^+$iTreg$_{PDL1}$ cells to prevent colitis was attributed to Foxp3 stability in these cells. Foxp3 expression was measured within the CD45.2$^+$ cells isolated from the spleen (Figures 2C and 2D) and lamina propria (Figure S2C) at day 60 after adoptive transfer. Frequency of Foxp3-expressing Tbet$^+$iTreg$_{PDL1}$ cells was increased when compared to cohorts that received Tbet$^+$iTreg cells. Finally, we evaluated the inherent capacity of these cells to revert back to IFN-γ producers. We found that the capacity of Tbet$^+$iTreg$_{PDL1}$ cells to secrete IFN-γ was significantly diminished when compared to Tbet$^+$iTreg cells (Figure 2E).

The potency of Tbet$^+$iTreg$_{PDL1}$ cells was then tested in an allogeneic murine GvHD model. We found that BALB/c host mice that received B6 cells stimulated under iTreg cells plus PDL-1 conditions had higher survival rates, diminished weight loss, and histological manifestations compared with mice that received cells stimulated under iTreg cell conditions alone, reaching significance in cohorts with Tbet$^+$iTreg$_{PDL1}$ cells (Figures 2F, S2D, and S2E). We next measured Foxp3 expression within the CD45.2$^+$ iTreg, iTreg$_{PDL1}$, Tbet$^+$iTreg, and Tbet$^+$ iTreg$_{PDL1}$ cells at day 14 after transplant and found that significant Foxp3 expression was maintained within Tbet$^+$iTreg$_{PDL1}$ cells (Figure 2G). We next evaluated the amount of alloreactive IFN-γ expression in the cohorts that received Tbet$^+$iTreg and Tbet$^+$iTreg$_{PDL1}$ cells. A significant reduction in the

Figure 1. Purified CD4$^+$Tbet^{hi}Foxp3$^-$ Cells Can Upregulate Foxp3 under iTreg Cell Conditions

(A) Schematic representation of cell culture conditions under which sorted CD4$^+$Tbet^{hi}Foxp3$^-$ cells were expanded.

(B and C) Flow cytometry profile of *Tbx21*ZsGreen *Foxp3*RFP-expressing CD4$^+$ T helper cells (B), Foxp3 expression of CD4$^+$Tbet^{hi}Foxp3$^-$ cells in the presence of IL-2 and TGF-β1 (Tbet$^+$iTreg cells) (C), or IL-2, TGF-β1, and PDL-1 Fc chimera (Tbet$^+$iTreg$_{PDL1}$ cells) (C) after differentiation and expansion.

(D) Summary of %CD4$^+$Foxp3$^+$ cells expression in Tbet$^+$iTreg cells and Tbet$^+$iTreg$_{PDL1}$ cells.

(E) Schematic representation of alternate cell culture conditions under which sorted CD4$^+$Tbet^{hi}Foxp3$^-$ cells were expanded.

(F and G) Foxp3 expression of CD4$^+$Tbet^{hi}Foxp3$^-$ cells in the presence of IL-2 (F), and summary of Foxp3 expression in different cell subsets (G).

Experiments were repeated at least five times and each experiment was performed with n = 5–9 mice. Cumulative data from all experiments are presented. Mean ± SEM. Please also refer to Figure S1.

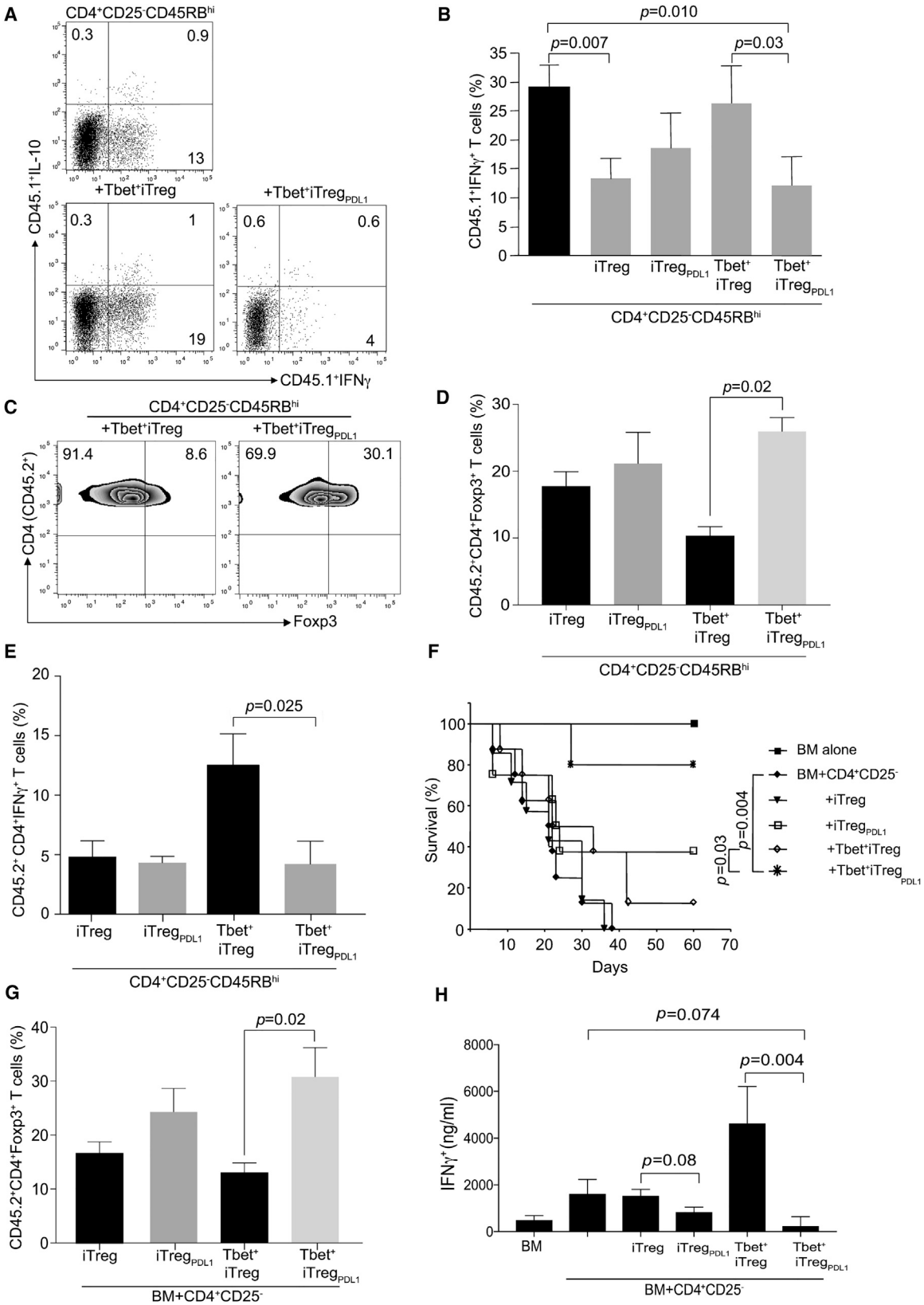

(legend on next page)

Tbet$^+$iTreg$_{PDL1}$ cell-treated cohorts (Figure 2H) was noted. These data indicate that PDL-1 induced a stable regulatory phenotype in Tbet$^+$iTreg$_{PDL1}$ cells.

PD-1 Signaling Downregulates Asparaginyl Endopeptidase in Tbet$^+$iTreg$_{PDL1}$ and iTreg$_{PDL1}$ Cells

In order to identify PD-1-dependent molecular mechanism that was operational in Tbet$^+$iTreg$_{PDL1}$ cells, we first evaluated AKT and mTOR signaling pathway as previously reported in iTreg cells (Francisco et al., 2009). No difference in the phosphorylation of AKT or mTOR pathway was observed (Figure S3A). Therefore, we next evaluated the gene expression profile of Tbet$^+$iTreg and Tbet$^+$iTreg$_{PDL1}$ cells. We found downregulation of a protease, namely asparaginyl endopeptidase (AEP), in Tbet$^+$iTreg$_{PDL1}$ cells using micro-array analysis (Figure S3B). Consistent with our microarray data, AEP protein expression (Figure 3A) and enzyme activity was significantly decreased in Tbet$^+$iTreg$_{PDL1}$ cells compared with Tbet$^+$iTreg cells (Figures S3C and S3D). The active form of AEP was evaluated by using LE28 probe (which emits a fluorescent signal when ligated to the active form of AEP; Figure S3C; Edgington et al., 2013). We next evaluated whether a functional nuclear pool of AEP was available within Tbet$^+$iTreg cells, as previously reported (Dall and Brandstetter, 2016; Haugen et al., 2013; Kosugi et al., 2009), using LE28 by imaging flow cytometry. We found a significant increase in the presence of active nuclear AEP in Tbet$^+$iTreg cells compared with Tbet$^+$iTreg$_{PDL1}$ cells (representative images in Figures 3B and 3C; summary of nuclear activity Figure S3E). In addition, active AEP was expressed in iTreg cells generated in the absence of PDL-1, but not in polarized Th1, Th2, CD4$^+$CD25$^-$, or CD4$^+$CD25$^+$ T cells (Figures 3D and S3F). PDL-1-treated iTreg cell cultures showed relatively diminished AEP activity, which was abrogated in *Pd1*$^{-/-}$ iTreg cells (Figures 3D and S3G). Finally, we evaluated the presence of nuclear AEP by immuno blotting and confocal microscopy. In all cases, we found AEP to be expressed within the nucleus in Tbet$^+$iTreg and iTreg cells (Figures 3E and 3F), which was limited by the addition of PDL-1 (Figure 3F).

Using confocal microscopy and imaging flow cytometry on cells stained with fluorescent markers for Foxp3 protein and active nuclear AEP, we found that Foxp3 and AEP were co-localized in Tbet$^+$iTreg cells and iTreg cells (Figures 3G–3I and S3H–S3O). This result prompted us to examine whether Foxp3 was a specific target of AEP or whether AEP indirectly regulated Foxp3 expression. Co-incubation of activated AEP with Foxp3 protein demonstrated that AEP directly cleaved Foxp3, but not T-bet protein (Figure 3J). In spite of possessing numerous asparaginyl sites, T-bet protein was refractory to AEP cleavage, whereas minimally cleaved Foxp3 bands (band 2 and 3) were noted by immuno blotting. However, band 3 was noted in conditions, which incorporated AEP inhibitor (Figures 3J). When we subjected band 2 and band 3 to high-throughput mass spectrometry, AEP-specific peptide cleavage product was found in band 2 and not band 3. Data from this analysis identified a specific semi-tryptic cleaved peptide within band 2 which was a target for AEP (N155; AEP cleaves after Asn [N]). No other AEP-specific targets were identified within the two bands (Figure 3K and Table S1).

We next evaluated Foxp3 protein turnover within Tbet$^+$iTreg cells in the presence of AEP inhibitor. Significant inhibition of Foxp3 protein degradation was noted in the presence of AEP inhibitor in Tbet$^+$iTreg cells (Figure S4A, top and bottom). To confirm this, we evaluated Foxp3 turnover in WT and *Aep*$^{-/-}$ iTreg cells; again, Foxp3 turnover was lower in *Aep*$^{-/-}$ iTreg cells as compared to WT iTreg cells (Figure S4B, top and bottom).

To further investigate the direct action of AEP on Foxp3, we designed a human Foxp3 mutant 1 (all N mutated to A [alanine]; 12 sites; Figures S4C and S4D). We tested whether the AEP-resistant mutant Foxp3 had enhanced stability in *in vitro* experiments. WT and mutant 1 were transduced into HEK293T cells and then rate of Foxp3 degradation in the presence of AEP and AEP inhibitor was evaluated. AEP specifically degraded WT Foxp3 protein while showing no activity on mutated Foxp3 mutant 1 protein (Figures S4E and S4F). These *in vitro* experiments suggest that AEP may directly act on Foxp3 protein within T cells.

Deletion of AEP-Specific Cleavage Site in Foxp3 Results in Prevention of Alloreactive GvHD

We next evaluated the *in vivo* function of cells that were transduced with WT Foxp3 (mouse and human) or Foxp3 mutant 2 (human) and mouse Foxp3 mutant 1. For these experiments, we first constructed human WT and mutated Foxp3 (N154; Asn site is at 154 in human) as our mass spectrometry data were obtained from human Foxp3 protein. In addition, we also constructed WT and mutated (N153; Asn site is at 153 in mouse) mouse Foxp3. All the constructs were transduced into naive mouse T cells and Foxp3 expression was evaluated (Figure 4A),

Figure 2. *In Vivo* Function of Tbet$^+$iTreg Cells and Tbet$^+$iTreg$_{PDL1}$ Cells

Tbet$^+$iTreg cells and Tbet$^+$iTreg$_{PDL1}$ cells were generated and then utilized for the prevention of autoimmune colitis and alloimmune GvHD. *B6.Rag2*$^{-/-}$ mice were reconstituted with CD45.1$^+$CD4$^+$CD45RB^{hi}CD25$^-$ T cells (4 × 10^5 cells/mouse) either alone or along with CD45.2$^+$iTreg cells, iTreg$_{PDL1}$ cells, Tbet$^+$iTreg cells, and Tbet$^+$iTreg$_{PDL1}$ cells (1 × 10^5 cells/mouse) cells. At day 60 after adoptive transfer, spleens were characterized.

(A) Representative flow plots of intracellular IFN-γ and IL-10 cytokine expression in either cohorts that received CD4$^+$ T effector cells alone, cohorts that received Tbet$^+$iTreg cells in addition to T effector cells, or cohorts that received Tbet$^+$iTreg$_{PDL1}$ cells in addition to T effector cells.

(B) Summary of T cell effector cytokine IFN-γ in the various different cohorts within CD45.1$^+$ cell populations.

(C) Representative flow plot of Foxp3 expression in CD45.2$^+$CD4$^+$Tbet$^+$iTreg cells and Tbet$^+$iTreg$_{PDL1}$ cells.

(D and E) Summary of Foxp3 and IFN-γ expression in iTreg cells, iTreg$_{PDL1}$ cells, Tbet$^+$iTreg cells, and Tbet$^+$iTreg$_{PDL1}$ cells.

(F) Function of Tbet$^+$iTreg cells and Tbet$^+$iTreg$_{PDL1}$ cells were assessed in an experimental model of GvHD. Survival curve of mice that succumbed to GvHD in the various different cohorts.

(G) Summary of Foxp3 expression in iTreg cells, iTreg$_{PDL1}$ cells, Tbet$^+$iTreg cells, and Tbet$^+$iTreg$_{PDL1}$ cells on day 14 after transplant.

(H) Alloreactive IFN-γ was measured using Luminex.

Each experiment had n = 3–5 mice per cohorts. Data shown are cumulative from 2 independent experiments. For survival curve, each cohort consisted of n = 10 mice. Data are presented as mean ± SEM. Please also refer to Figure S2.

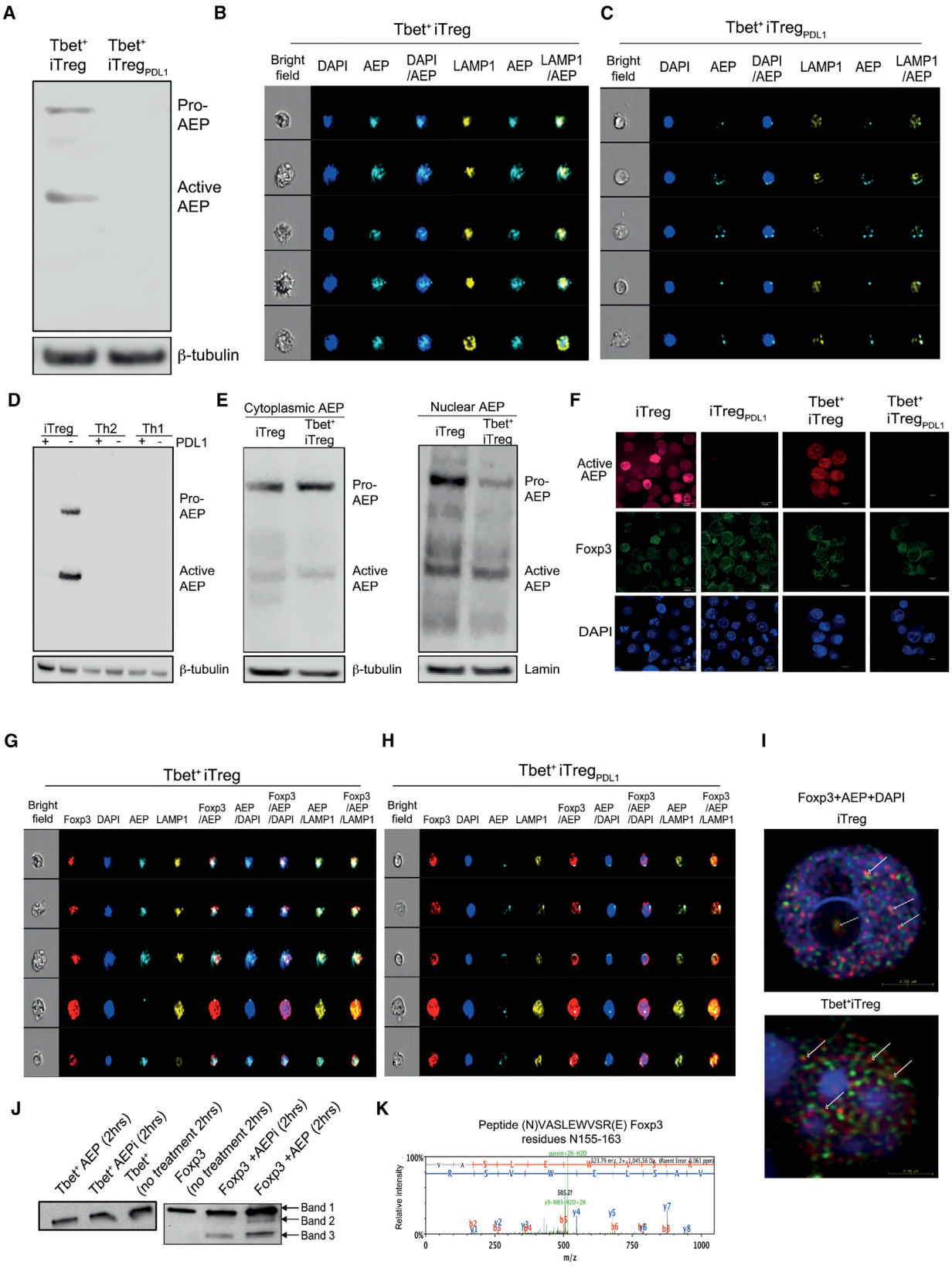

(legend on next page)

and nuclear localization (Figure S5A) for each construct were verified at day 4 after transduction. The transduced WT and mutant forms of Foxp3 were functional as they suppressed the capacity of the transduced cells to produce IFN-γ (IFN-γ being a specific target of Foxp3 *in vitro*) (Figure S5B). The *in vivo* suppressive function of transduced T cells was tested in a murine GvHD model (Laurence et al., 2012). We found that T cells transduced with mutated versions of Foxp3 (both mouse and human) significantly prevented GvHD lethality in murine recipients as compared to WT Foxp3 (Figure 4B).

Inhibiting AEP Activity Maintains Foxp3 Expression in Tbet$^+$iTreg Cells *In Vivo*

We next tested the role of AEP in limiting Foxp3 stability in Tbet$^+$ iTreg cells using an AEP-specific inhibitor (AEPi). First, the *in vitro* efficacy of AEPi was tested in iTreg cell cultures. Naive CD4$^+$ CD25$^-$ T cells from WT mice were expanded under iTreg cell conditions (experimental outline in Figure 1E). Certain culture conditions were supplemented with AEPi. We found that the AEPi cultures had significantly higher Foxp3 expression as compared to the control cultures, whereas no significant difference was noted in *Aep*$^{-/-}$ iTreg cell cultures, thus confirming the specificity of the AEP inhibitor (Figures S5C and S5D). Splenic Tbet$^+$Foxp3$^-$ Th1 cells were expanded into Tbet$^+$iTreg cells in the presence of AEP inhibitor (MV026630, 100 μM) and then Foxp3 stability was tested *in vivo*. Murine recipients were reconstituted with CD4$^+$CD25$^-$ naive T cells (CD45.1$^+$) along with Tbet$^+$iTreg cells (CD45.2$^+$) expanded in the presence of vehicle (DMSO) or AEP inhibitor (MV026630). At day 14 after transplant, the frequency of Foxp3$^+$ cells within the adoptively transferred Tbet$^+$iTreg cells was measured. Tbet$^+$iTreg cells generated in the presence of AEPi exhibited an enhanced frequency of Foxp3$^+$ cells as compared to control Tbet$^+$iTreg cells (Figures 4C and 4D). To further evaluate the role of AEP in Tbet$^+$ iTreg cell function, we overexpressed AEP in Tbet$^+$iTreg$_{PDL1}$ cells using a retro-virus. AEP overexpression and nuclear localization was first confirmed (Figures S5E and S5F) in Tbet$^+$ iTreg$_{PDL1}$ cells. We then tested the function of overexpressed AEP by transducing *Aep*$^{-/-}$ iTreg cells with either empty vector (EV) or AEP RV. At day 7 after expansion, *Aep*$^{-/-}$ iTreg cells were capable of expressing Foxp3, which was completely abrogated when AEP was overexpressed (Figure S5G). We then evaluated the clinical outcome of overexpressing AEP (in Tbet$^+$iTreg$_{PDL1}$ cells) or inhibiting AEP (in Tbet$^+$iTreg cells) in acute GvHD. BALB/c mice that received B6 Tbet$^+$iTreg$_{PDL1}$ cells with forced expression of AEP had a significantly higher mortality compared with those that received control B6 Tbet$^+$iTreg$_{PDL1}$ cells. Similarly, Tbet$^+$iTreg cells expanded with AEP inhibitor showed similar regulatory function to that of Tbet$^+$ iTreg$_{PDL1}$ cells *in vivo* (Figure 4E). To further confirm the role of AEP in Treg cell function *in vivo*, a retroviral small inhibitory RNA (RV-shRNA) for AEP was utilized. AEP silencing in Tbet$^+$iTreg cells was effective (Figures S5H–S5J). Murine recipients reconstituted with Tbet$^+$ iTreg cells transduced with AEP RV-shRNA had a significant delay in the loss of Foxp3 (Figures 4F–4H). Ablating AEP had minimal effect on the expression of Tbet in Tbet$^+$ iTreg cells (Figure 4I). Finally, we mutated the nuclear localization sequence in AEP (AEP NLS mutant) and then evaluated Foxp3 stability. We found that overexpressing AEP NLS mutant in *Aep*$^{-/-}$ iTreg cells maintained Foxp3 expression but this was not the case in cohorts that overexpressed AEP WT protein (Figures S5K–S5M).

AEP Deficiency Modulates *In Vivo* Treg Cell Function by Maintaining Foxp3 Expression

To further assess the role of AEP in Foxp3 regulation, we evaluated the efficacy of iTreg cells from *Aep*$^{-/-}$ mice in an experimental murine model of GvHD. First, we characterized the CD4$^+$ T cell compartment within *Aep*$^{-/-}$ mice. WT and *Aep*$^{-/-}$ mice had a similar phenotype with respect to T cell frequency and activation, but *Aep*$^{-/-}$ mice had higher Treg cell frequency (Figures 5A–5F, S6A, and S6B). By contrast, no significant difference was noted in the cytokine expression by CD4$^+$ T cells from WT and *Aep*$^{-/-}$ mice (Figure S6C). Next, *in vitro* expanded iTreg cells from WT and *Aep*$^{-/-}$ naive CD4$^+$ T cells (Figure S6D) were tested in GvHD. *Aep*$^{-/-}$ iTreg cells were significantly efficient at preventing GvHD compared to WT iTreg cells (Figure 5G). Of note, cohorts treated with *Aep*$^{-/-}$ iTreg cells (CD45.2$^+$) had significantly higher numbers of Foxp3$^+$ cells in the spleen and lymph nodes (Figures 5H, S6E, and S6F) as compared to WT iTreg cell-treated cohorts.

In order to explore the relationship between PD-1 signaling and AEP activation within T cells, we tested the frequency of Treg cells in *Aep*$^{-/-}$ mice under disease conditions in the presence of PDL-1 blocking antibody. A syngeneic B16F10

Figure 3. PDL-1 Exposure Downregulates Asparaginyl Endopeptidase in Tbet$^+$iTreg Cells

(A) Tbet$^+$iTreg cells and Tbet$^+$iTreg$_{PDL1}$ cell lysates were generated at pH 7 and were subjected to immuno blotting. Asparaginyl endopeptidase (AEP; Legumain; LGMN) was measured in the different subsets.

(B and C) Tbet$^+$iTreg cells and Tbet$^+$iTreg$_{PDL1}$ cells were differentiated and then stained with LE28 (measuring active AEP) along with LAMP1 and DAPI and then subjected to Amnis Imaging Cytometry. Representative images of active AEP enzyme expression in the nucleus in Tbet$^+$iTreg cells (B) and Tbet$^+$iTreg$_{PDL1}$ cells (C).

(D) AEP expression in iTreg cells, iTreg$_{PDL1}$ cells, Th1 cells, Th1$_{PDL1}$ cells, Th2 cells, and Th2$_{PDL1}$ cells.

(E) AEP expression was determined in cytoplasmic and nuclear fractions of iTreg cells and Tbet$^+$iTreg cells.

(F) iTreg cells, iTreg$_{PDL1}$ cells, Tbet$^+$iTreg cells, and Tbet$^+$iTreg$_{PDL1}$ cells were stained with DAPI, Foxp3 PE, and AEP cy5. Confocal microscopy showing AEP and Foxp3 expression inside the nucleus (F); red is AEP, green is Foxp3, and blue is DAPI.

(G and H) Foxp3 co-localization with AEP in the nucleus in Tbet$^+$iTreg cells (G) and Tbet$^+$iTreg$_{PDL1}$ cells was shown (H).

(I) Confocal microscopy detecting co-localization of AEP and Foxp3 within the nucleus in iTreg cells and Tbet$^+$iTreg cells; white arrows show AEP co-association with Foxp3 within the nucleus.

(J) Tbet cleavage (left) and Foxp3 cleavage (right) in the presence of AEP or AEP inhibitor.

(K) Spectral analysis of Foxp3 cleavage at N155.

Each experiment was repeated 3–5 times and representative data from one experiment is shown. Data are shown as mean ± SEM. Please also refer to Figures S3 and S4.

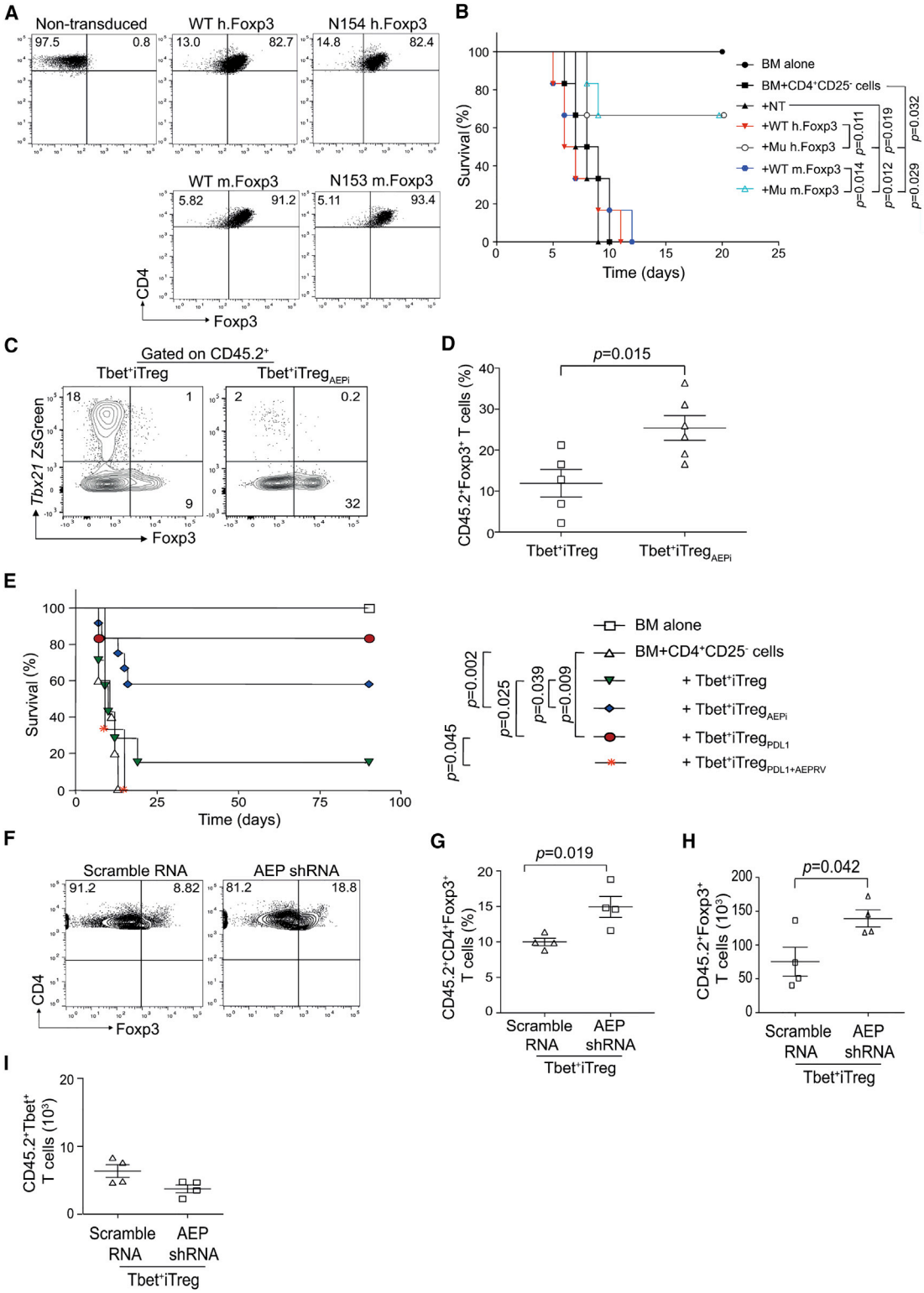

Figure 4. AEP-Specific Foxp3 Mutants and AEP Inhibition Prevents GvHD

(A) Murine $CD4^+CD25^-$ T cells were transduced with WT human Foxp3, mutant (N154) human Foxp3, WT murine Foxp3, or mutant murine Foxp3 (N153). Transduction efficiency at day 4 was measured by flow cytometry.

(B) Host BALB/c mice were subjected to lethal total body irradiation (TBI; 950cGy) and then reconstituted with B6 T depleted bone marrow (BM, 5×10^6 cells) alone, or with $CD4^+CD25^-$ T cells (CD45.1 marked, 0.1×10^6). Certain cohorts were treated with BM plus $CD4^+CD25^-$ T plus non-transduced T cells

(legend continued on next page)

melanoma tumor model was used whereby WT and *Aep*$^{-/-}$ mice were reconstituted with tumor cells and the cohorts were treated with either isotype or PDL-1 antibody. At day 11, tumors were resected and the tumor infiltrating lymphocytes (TILs) were tested for the frequency of Foxp3^{+}Treg cells and Tbet^{+}Foxp3^{+}Treg cells. We found that *Aep*$^{-/-}$ cohorts had a small but significant increase in Foxp3^{+} TILs as compared to WT cohorts (Figures 5I and 5J). In the presence of anti-PDL-1, we saw a decrease in Foxp3^{+} TILs in the tumors of WT cohorts but no change in the *Aep*$^{-/-}$ cohorts (Figures 5I and 5J). When we gated on Tbet^{+} TILs, we found a similar pattern with an elevated proportion of Tbet^{+} TIL's expressing Foxp3 in the *Aep*$^{-/-}$ compared with WT mouse cohorts and the addition of anti-PDL-1 significantly inhibiting Foxp3 expression only in the WT cohorts (Figures 5K and 5L). Collectively, these *in vivo* experiments confirm our *in vitro* data and identified PD-1 as a regulator of Foxp3 through AEP.

Tbet^{+} Th1 Cells Primed during Acute and Chronic Viral Infections Upregulate Foxp3 *Ex Vivo*

We next investigated whether Th1 cells arising during viral infection can also be induced to express Foxp3. First, during acute LCMV infection, a significant percentage of Tbet^{+}Foxp3^{+} cells was observed at day 14 after infection (Figures 6A, 6B, and S7A) and second, Tbet^{+}Foxp3^{-} cells had significant PD-1 expression (Figures S7B and S7C). These virus-primed CD4^{+} Tbet^{+}Foxp3^{-} cells were sorted on day 14 after infection and cultured *in vitro* under iTreg cell conditions with or without PDL-1. In both cases, iTreg cell-polarizing cytokines could induce Foxp3 expression in Th1 cells and this was enhanced to a small but significant extent in the presence of PDL-1 (Figure 6C). Similarly, during chronic LCMV infection, a substantial increase was noted in Tbet^{+}Foxp3^{+} cells at day 14 after infection *in vivo* (Figures 6D, 6E, and S7D) and again, Tbet^{+}Foxp3^{-} cells had significant PD-1 expression (Figures S7E and S7F). These chronic LCMV virus-primed CD4^{+}Tbet^{+}Foxp3^{-} cells were sorted on day 14 after infection and cultured *in vitro* under iTreg cell conditions with or without PDL-1. In both cases, iTreg cell-polarizing cytokines could induce Foxp3 expression in Th1 cells and this was enhanced by a small but significant extent in the presence of PDL-1 (Figures 6F and 6G). In order to confirm that PDL-1 is required for conversion of Tbet^{+} cells into Tbet^{+}pTreg cells during chronic LCMV, we adoptively transferred flow-sorted CD45.2^{+}Tbet^{+}Foxp3^{-} cells into CD45.1^{+} hosts infected with chronic LCMV. Mice were treated with either isotype or anti-PDL-1 antibody. At day 10, frequency of converted Tbet^{+}Foxp3^{+} in the spleen was measured (Figures 6H and 6I). Anti-PDL-1 treatment significantly inhibited the conversion of Tbet^{+} cells into Foxp3^{+} cells and enhanced the proliferation of both total and GP33 specific CD45.1^{+} CD8^{+} T cells *in vivo* (Figures S7G–S7M).

Tbet^{+}pTreg Cells Are Increased in the TILs of Mice Bearing B16F10 Melanoma Tumor

In order to identify the biological context during which Tbet^{+} pTreg cells arise from Tbet^{+}Th1 cells, an animal model of B16F10 melanoma, where PD-1-based therapies play an important role, was used. Adoptive transfer of Tbet^{+}Th1 cells into murine recipients with established tumor was performed (outline of experimental methodology, Figure 7A). The emergence of Tbet^{+} pTreg cells was then evaluated in the spleen and within the TILs. A significant increase in Tbet^{+}pTreg cells was noted within the TILs in the tumor microenvironment (Figures 7B and 7C). We next tested whether PDL-1 contributed to the differentiation of Tbet^{+}Th1 cells into Tbet^{+}iTreg cells in the tumor microenvironment. Stimulation with PDL-1 significantly enhanced Foxp3 expression in sorted Tbet^{+}Th1 cells from tumor-bearing mice in *ex vivo* cultures (Figures 7D and 7E). We subsequently tested *in vivo* Tbet^{+} cell conversion in our tumor model. *Rag2*$^{-/-}$ mice were reconstituted with tumor cells followed by adoptive transfer of sorted Tbet^{+}Foxp3^{-} cells. Cohorts were treated with either isotype control or anti-PDL-1 and then TILs were evaluated for Tbet^{+}Foxp3^{+} cells. The frequency of Tbet^{+}pTreg cells was significantly increased in the isotype-treated cohorts but not in the anti-PDL-1-treated murine recipients (Figures 7F–7H). The experiment was repeated with Tbet^{+}Foxp3^{-} cells that were transduced with either control shRNA RV or AEP shRNA RV. Consistent with our experiments performed using *Aep*$^{-/-}$ mice, AEP silencing rendered Tbet^{+} cells refractory to PDL-1 blockade and resulted in significant conversion toward Tbet^{+} Foxp3^{+} cells within the tumor microenvironment (Figures 7I and 7J). Finally, we evaluated conversion of CD45.2^{+}Tbet^{+} cells in CD45.1^{+} hosts that were reconstituted with B16F10 melanoma tumor. Certain cohorts were treated with either isotype or anti-PDL-1 antibody. In this experimental condition, we again found that Tbet^{+}Foxp3^{-} cells were capable of converting to Tbet^{+}iTreg cells within the tumor microenvironment, which was efficiently blocked in the presence of PDL-1 antibody (Figures 7K and 7L). In all these experiments, CCR4 expression on Tbet^{+} Foxp3^{+} cells within the tumor microenvironment was minimal (data not shown). These results suggest that Tbet^{+} cell conversion can occur *in vivo* within the tumor microenvironment and

(NT, 0.1 × 10^{6}) or T cells transduced with WT human Foxp3 (WT hFoxp3, 0.1 × 10^{6}), or human mutant Foxp3 (Mu hFoxp3, N154; 0.1 × 10^{6}) or murine WT Foxp3 (WT mFoxp3, 0.1 × 10^{6}) or murine mutant Foxp3 (N153; Mu mFoxp3, 0.1 × 10^{6}). GvHD lethality was monitored (n = 6 per cohort).

(C and D) Host BALB/c mice were subjected to TBI and then reconstituted with bone marrow (BM, 10^{7} cells), CD4^{+}CD25^{-} T effector cells (CD45.1 marked; 1 × 10^{6} cells), and either Tbet^{+}iTreg cells (1 × 10^{6} cells) that were expanded with AEP inhibitor or control Tbet^{+}iTreg cells (1 × 10^{6} cells). At day 14 after transplant, splenocytes were harvested and the Foxp3 was measured in the Tbet^{+}iTreg cell populations (marked with CD45.2). Representative flow plots showing Foxp3 expression in the different cell populations (C); frequency of Foxp3 expression (D).

(E) A survival curve experiment was set up to test the efficacy of blocking AEP in preventing GvHD. Animals were conditioned with TBI and then reconstituted with BM alone or plus CD4^{+}CD25^{-} T cells. Cohorts were then treated with Tbet^{+}iTreg cells, Tbet^{+}iTreg cells expanded with AEP inhibitor (AEPi), Tbet^{+}iTreg$_{PDL1}$ cells, or Tbet^{+}iTreg$_{PDL1}$ cells overexpressing AEP.

(F–I) Experiments were repeated with CD45.2^{+} Tbet^{+}iTreg cells that were expanded with AEP shRNA or scramble shRNA and then tested in GvHD. Frequency and absolute numbers of CD45.2^{+}Foxp3^{+} cells in the different cohorts (F–H) and absolute numbers of Tbet^{+} cells at day 14 after transplant in Tbet^{+} iTreg cells (I). Experiments were repeated twice with n = 4–6 mice for immunological studies and n = 6–10 mice for survival curve. Representative data from one experiment are shown as mean ± SEM. Please also refer to Figure S5.

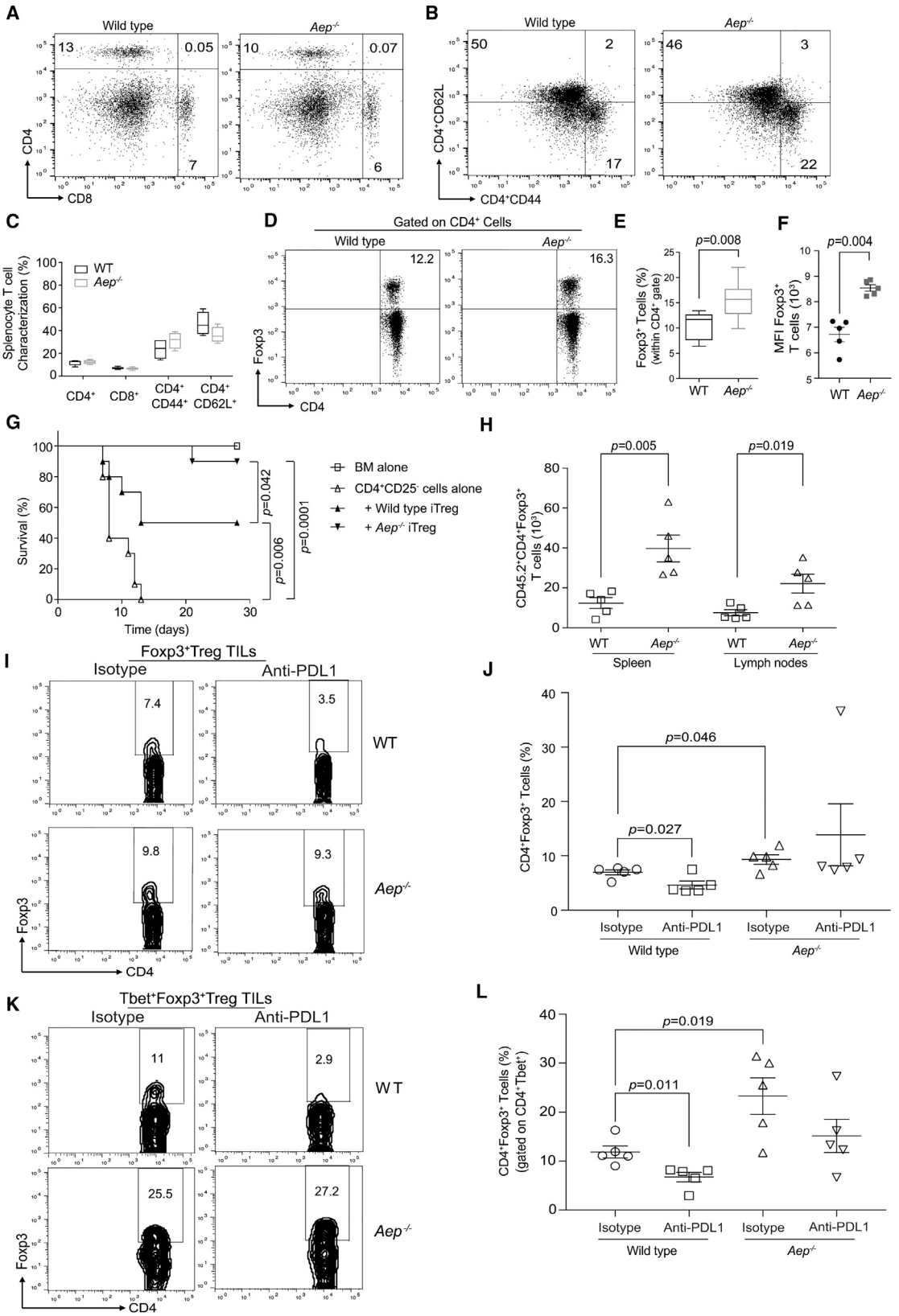

(legend on next page)

PDL-1 blockade reverses the conversion of Tbet$^+$ cells into Tbet$^+$Foxp3$^+$ cells. However, anti-PDL-1 effect in blocking Tbet$^+$ cell conversion to Tbet$^+$Foxp3$^+$ cells is abrogated in the absence of AEP.

DISCUSSION

The regulation of Foxp3 in Treg cells and T helper cell subsets is an active area of investigation and may help in understanding dysregulation of the immune system in disease processes. In this report, we have identified a proteolytic regulation of Foxp3 protein in iTreg cells, Tbet$^+$iTreg cells, and pTbet$^+$Treg cells. We demonstrated that (1) PD-1 signaling maintains Foxp3 protein stability through regulating AEP, (2) AEP directly cleaves Foxp3 and results in Foxp3 instability in iTreg cells and Tbet$^+$iTreg cells, and (3) inhibiting AEP resulted in enhanced Treg cell function. These data elucidate a basic mechanism that is operational in Treg cells and paves a path to the development of translational approaches for developing Treg cell-based cell therapies.

The results outlined in this paper are in agreement with the existence of these Tbet$^+$Foxp3$^+$ T cells *in vivo*. However, reports on Tbet$^+$Treg cells (Hall et al., 2012; Koch et al., 2009, 2012; Levine et al., 2017) propose that tTreg cells are the likely precursors of Tbet$^+$Treg cells. The data presented here extend these observations and clearly demonstrate that an alternate pathway is involved in the upregulation of Foxp3 expression by Tbet$^+$ Foxp3$^-$ T cells.

In vivo cell tracing experiments performed in the long-term colitis model highlights a mechanism by which PDL-1 imparts regulatory function to Tbet$^+$iTreg$_{PDL-1}$ cells. During colitis, Tbet$^+$iTreg$_{PDL-1}$ cells had sustained Foxp3 expression after 60 days in an inflammatory environment unlike their counterpart Tbet$^+$iTreg cells. These data support a regulatory mechanism whereby differentiation of Tbet$^+$ cells in the presence of PDL-1 can result in sustained Foxp3 expression *in vivo* and led us to explore the molecular mechanisms by which PD-1 signaling regulated Foxp3 stability. We found a proteolytic pathway that was operational in maintaining Foxp3 protein stability in iTreg cells and Tbet$^+$iTreg cells involving direct inhibition of the activity of AEP. PD-1 inhibition of AEP was independent of CD28 signaling (Hui et al., 2017; Kamphorst et al., 2017).

The notion that a specific protease can perform an essential specific proteolytic function is controversial as cells express many proteases that exhibit considerable functional redundancy (van Kasteren and Overkleeft, 2014). However, cell type-specific differences in protease function have been previously reported. For example, AEP breaks down self-antigens in DCs (Manoury et al., 2002) and cathepsin G performs this function in B cells (Burster et al., 2004). AEP activity has been reported both in lysosomes and in the nucleus of tumor cells (Haugen et al., 2013). Functionally AEP can induce tumor cell proliferation and migration and process antigens for optimal presentation by DCs (Andrade et al., 2011; Lin et al., 2014; Manoury et al., 1998). In contrast to other lysosomal proteases, AEP is expressed in the cytosol and nucleus and the activity of AEP across both neutral and acidic pH has been previously reported (Haugen et al., 2013). These observations enable a mechanism by which Foxp3 in the nucleus can be targeted by AEP.

The imaging and biochemical data presented here demonstrated that in T cells, AEP played a specific function in cleaving Foxp3 but not Tbet. These results are in accordance with previous AEP studies where it has been shown that AEP substrates in part are not amenable to other protease activity. In addition, AEP is well known for its substrate and cleavage specificity and often AEP-mediated cleavage results in a functional immunological outcome *in vivo* (Manoury et al., 1998, 2002). In T cells, AEP adheres to this phenotype, whereby it specifically targets and cleaves Foxp3 at a single site, which results in the instability of the protein. Therefore, our study implicates the occurrence of a proteolytic-mediated regulation of Foxp3 in iTreg and Tbet$^+$iTreg cells.

The data presented here postulate a post-translational mechanism of Foxp3 protein regulation in addition to the previously described proteosomal pathway that is operational in Foxp3 regulation. However, deleting AEP was sufficient for maintaining Foxp3 protein in iTreg and Tbet$^+$iTreg cells *in vivo*. In contrast to the proteosomal degradation study where an shRNA approach was used (Chen et al., 2013; van Loosdregt et al., 2013; Zhao et al., 2015), we have utilized a genetic loss-of-function model (*Aep*$^{-/-}$ mice) to demonstrate the stability of Foxp3 *in vivo* during acute inflammation. Furthermore, mutating AEP-specific sites in Foxp3 protected mice from GvHD-mediated lethality. Therefore, our data demonstrate that either AEP deficiency or Foxp3 mutated at AEP-specific sites can enhance Treg cell function and is a primary pathway in modulating post-translational stability of Foxp3 protein.

Figure 5. iTreg Cells Deficient in AEP Inhibit GvHD and Maintain Foxp3 Expression *In Vivo*

(A) Splenocytes from WT littermate controls and *Aep*$^{-/-}$ mice were characterized for CD4$^+$ T cells and CD8$^+$ T cells.

(B) T central and effector memory phenotype of CD4$^+$ cells were characterized using CD62L and CD44 markers.

(C) Cumulative data from n = 4 mice on the frequency of CD4, CD8, CD44, and CD62L.

(D) Treg cell frequency was evaluated by intracellular Foxp3 expression.

(E and F) Cumulative data from n = 5 mice of Foxp3 frequency (E) and Foxp3 mean fluorescence intensity (F).

(G) Host BALB/c mice were subjected to TBI and then reconstituted with B6 BM (10^7), CD4$^+$CD25$^-$ T cells (CD45.1 marked; 0.1 × 10^6 cells), and either WT iTreg cells (0.1 × 10^6 cells) or *Aep*$^{-/-}$ iTreg cells (0.1 × 10^6 cells). Survival curve of cohorts that received the various cell populations.

(H) Foxp3$^+$ cells in WT and *Aep*$^{-/-}$ iTreg cells (marked with CD45.2$^+$) at day 14 after transplant.

(I and J) WT and *Aep*$^{-/-}$ mice were reconstituted with 3 × 10^5 B16F10 melanoma cells subcutaneously and cohorts were treated with either isotype control or anti-PDL-1 antibody at day 5, 7, and 9. Mice were euthanized on day 11 and then evaluated for Foxp3$^+$Treg cells and Tbet$^+$Foxp3$^+$Treg cells within the TILs. Representative flow plots of Treg cell frequency within the tumor (I), and summary of Treg cells in the various cohorts (J).

(K and L) TILs were gated on CD4$^+$Tbet$^+$ cells and then Foxp3 expression was evaluated. Representative flow plots of Tbet$^+$Treg cell frequency within the tumor (K), and summary of Tbet$^+$Treg cell in the various cohorts of TILs (L).

Data are shown as mean ± SEM, from one representative experiment. Each experiment was repeated at least twice and had n = 5 mice for immunological studies or n = 10 for survival. Please also refer to Figure S6.

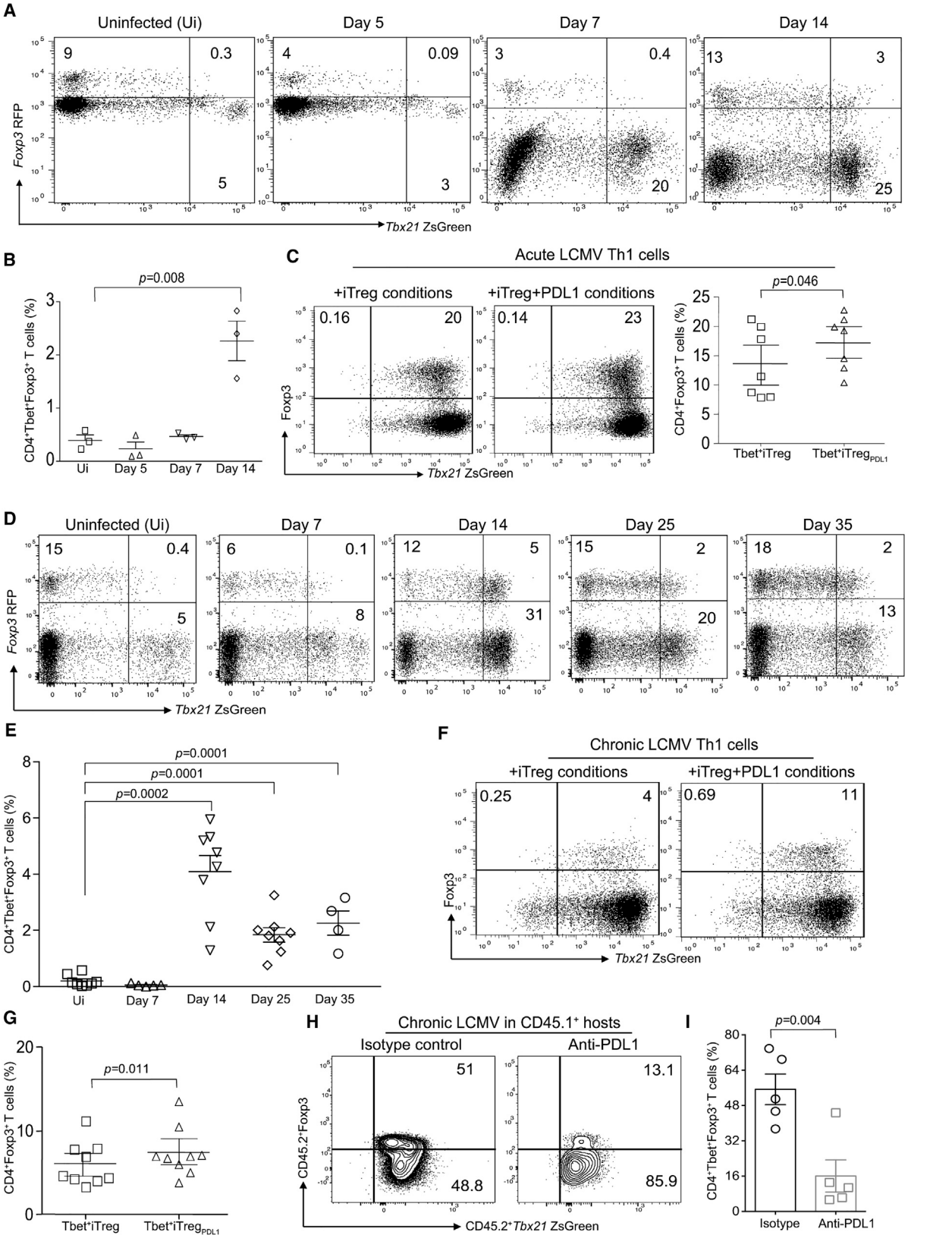

(legend on next page)

Our results suggest that AEP inhibitor can be used to generate large-scale Treg cells that are stable and are functionally robust *in vivo*. The use of PDL-1 to grow Tbet^{+}iTreg cells may be efficacious but a substantial decrease in cell numbers can occur given the role of PD-1 in inhibiting T cell proliferation. Using AEP inhibitors, this hurdle can be overcome in order to generate large numbers of antigen-primed Tbet^{+}iTreg cells that maintain regulatory function *in vivo*. In addition, donor-derived AEP-deficient Treg cells can also be generated for the treatment of GvHD.

Data from the acute and chronic LCMV-infected mice further identified a role for PDL-1 in inducing Foxp3 in primed "antigen-specific" Tbet^{+} Th1 cells. Although insufficient cell numbers prevented us from isolating antigen-specific T cells prior to *ex vivo* iTreg cell culture, the results presented here imply that PDL-1 can be used to generate iTreg cells from previously antigen-primed Tbet^{+}Th1 cells. Consistent with previous studies (Hall et al., 2012; Koch et al., 2009, 2012; Levine et al., 2017), we have also identified a unique population of Tbet^{+}iTreg cells that expands in both acute and chronic LCMV. In summary, these experiments highlight many aspects of Tbet^{+}iTreg cells: (1) primed CD44^{hi}Tbet^{hi}Foxp3^{+} cells can arise during acute and chronic LCMV infection, (2) primed CD4^{+}CD44^{hi}Tbet^{hi}Foxp3^{-} T cells can give rise to Tbet^{+}Foxp3^{+} T cells in *ex vivo* cultures, and finally (3) blocking PDL-1 *in vivo* dampened Tbet^{+}pTreg cell conversion, therefore confirming PDL-1 as a critical mediator of Tbet^{+}pTreg cell generation in chronic viral infection.

In melanoma, Treg cell-mediated tolerance has largely been attributed to the migration of Treg cells from the periphery to the tumor site (Spranger et al., 2013), while Tbet^{+}Th1 cell conversion is largely unexplored. Since the microenvironment in melanoma provides an abundance of PDL-1 that can result in activation of PD-1 signaling on Tbet^{+} TILs, we explored and found that Tbet^{+}Th1 cell conversion indeed occurred. However, this study does not address the contribution of hematopoietic versus non-hematopoietic versus tumor tissue-derived PDL-1 in inducing Treg cell conversion within the tumor microenvironment. The results presented here raise the possibility that the PDL-1-driven Treg cell generation within the TILs is dependent on AEP expression and that individuals who overexpress AEP within their Treg TIL populations may be more responsive to PD-1- and/or PDL-1-based immunotherapeutics.

In conclusion, this report has identified a mechanism by which sustained PD-1 signaling induces robust regulatory function in iTreg cells through post-translational regulation of the Foxp3 protein. Therefore, this study demonstrates an insightful interaction between co-inhibitory receptor signaling and protease activity and has elucidated the importance of these two signaling pathways in maintaining T regulatory phenotype.

STAR★METHODS

Detailed methods are provided in the online version of this paper and include the following:

- KEY RESOURCE TABLE
- CONTACT FOR REAGENT AND RESOURCE SHARING
- EXPERIMENTAL MODEL AND SUBJECT DETAILS
  - Mice
- METHOD DETAILS
  - Cell sorting and Flow cytometry and tetramer staining
  - *In vitro* cell culture
  - *In vitro* Treg suppression assay
  - *In vivo* animal models
  - Histological Analysis
  - Affymetrix Gene Expression Profiling
  - Immuno Blotting
  - AEP enzyme activity
  - Foxp3 co-localization Assays
  - Amnis Imaging Flow cytometry
  - Foxp3 cleavage and Mass Spectrometry
  - Pulse Chase Assays for Foxp3 protein turnover
  - AEP and Foxp3 silencing and mutation assays
- QUANTIFICATION AND STATISTICAL ANALYSIS
- DATA AND SOFTWARE AVAILABILITY

SUPPLEMENTAL INFORMATION

Supplemental Information includes seven figures and one table and can be found with this article online at https://doi.org/10.1016/j.immuni.2018.05.006.

ACKNOWLEDGMENTS

We would like to thank Dr. Tsung-Ping and Dr. Shang-Yi Tsai, National Institute on Drug Abuse, NIH for sharing protocols on pulse chase experiments and

Figure 6. Virus-Primed CD4^{+}Tbet^{+}Foxp3^{-} Cells Upregulate Foxp3 under iTreg and pTreg Cell Conditions

(A) B6.*Tbx21*Zsgreen*Foxp3*RFP mice were infected with LCMV Armstrong (2 × 10^{5} PFU) and then monitored for the presence of CD4^{+}Tbet^{hi}Foxp3^{+} cells. Representative flow plots from three individual experiments showing Tbet^{hi}Foxp3^{+} cells in the CD4 compartment of murine recipients at various time points after infection.

(B) Summary of frequency of Tbet^{hi}Foxp3^{+} T cells at various time points.

(C) Virus-primed Tbet^{hi}Foxp3^{-} cells from acute LCMV-infected mice were flow sorted at day 14 and then expanded under iTreg conditions in the absence or presence of PDL-1fc chimera. The frequency of Foxp3 expression in Tbet^{hi}Foxp3^{-} cell population in the absence or presence of PDL-1 after 7 days of *ex vivo* culture.

(D) B6.*Tbx21*Zsgreen*Foxp3*RFP mice were infected with LCMV clone 13 (2 × 10^{6} PFU) and then monitored for the presence of CD4^{+}Tbet^{hi}Foxp3^{+} cells. Representative flow plots showing Tbet^{hi}Foxp3^{+} cells in the CD4 compartment of murine recipients at various time points after infection.

(E) Summary of frequency of Tbet^{hi}Foxp3^{+} T cells at various time points.

(F) The frequency of Foxp3 expression in Tbet^{hi}Foxp3^{-} cell population in the absence or presence of PDL-1 after 7 days of *ex vivo* culture.

(G) Summary of Tbet^{+}iTreg cell differentiation.

(H and I) CD45.2^{+}Tbet^{+}FoxP3^{-} cells (0.7 × 10^{6} cells) were adoptively transferred into CD45.1^{+} murine hosts that were infected with Clone-13. Cohorts were treated with either isotype control or anti-PDL-1 antibody (200 μg/mouse). Splenocytes were harvested at day 10 and the frequency of CD4^{+}Tbet^{+}Foxp3^{+} pTreg cells were evaluated.

Data are shown as mean ± SEM from a representative of one to three individual experiments involving n = 3–9 mice per cohorts. Please also refer to Figure S7.

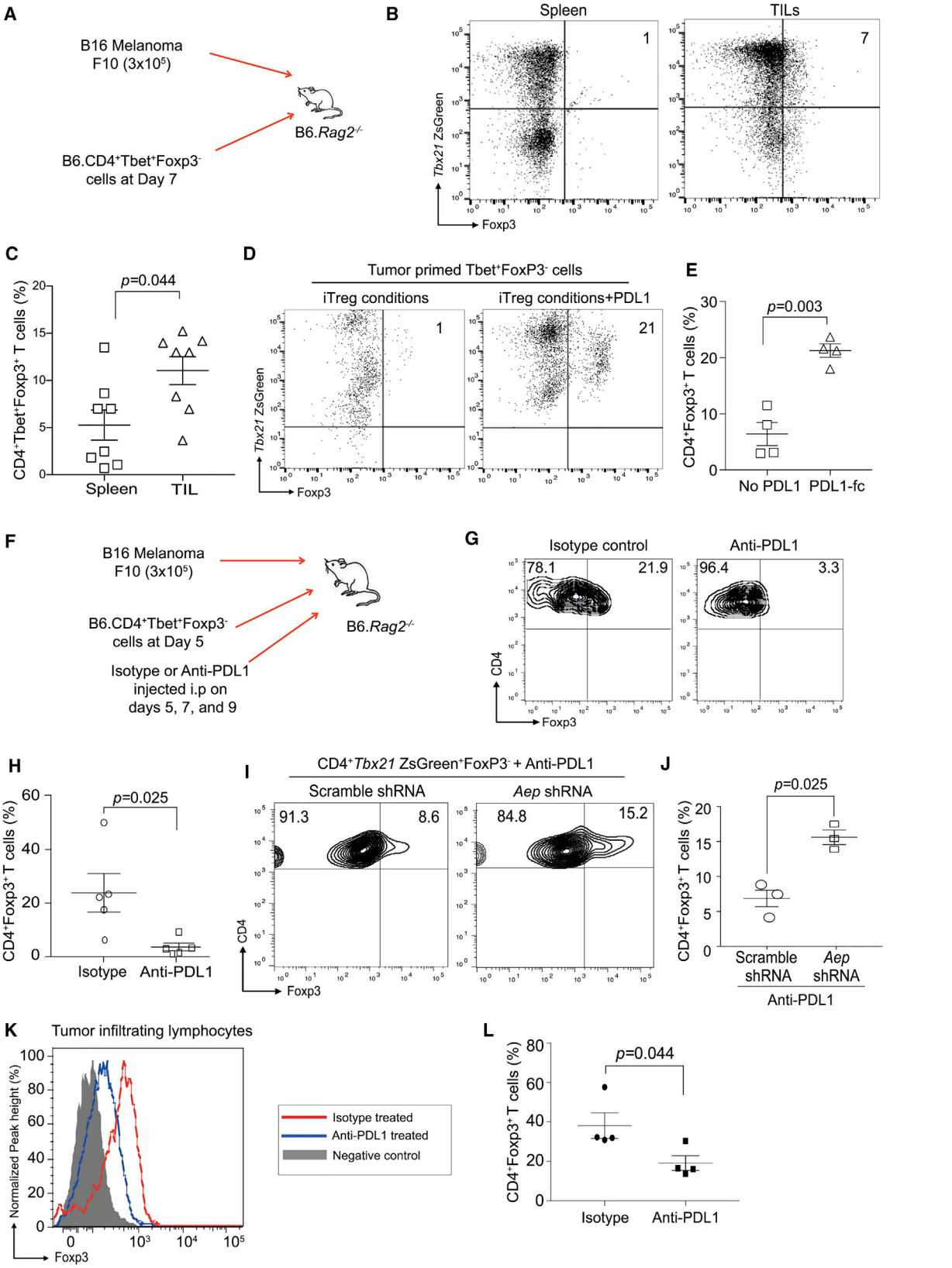

(legend on next page)

analysis. We would like to thank Dr. William G. Telford for his valuable input on Amnis flow cytometry experiments and analysis. We would like to thank Dr. Billur Akkaya, NIAID, for providing us with B6. *Tbx21*ZsGreen*Foxp3*RFP mice for chronic LCMV experiments. We would like to thank Dr. Bishop Hague, NIAID, for his assistance in flow cytometry sorting of virus-infected cells. We would like to thank the core facilities at Newcastle University namely Bioimaging, Comparative Biology Centre, and Flow cytometry. We would also like to thank Mr. Christopher Huggins for his technical expertise. The authors would also like to thank the NIH tetramer core facility for providing the tetramers used in this study. This research was funded by the Division of intramural research program of the NCI and NIAID, NIH, USA, Newcastle University Research Fellowship, Newcastle University, MRC-Newcastle University Single Cell Unit Award and the Academy of Medical Sciences, Springboard Award SBF003\1129; G.M. is supported by MRC-DiMEN Doctoral Training Partnership program; J.M.-F. and C.W. are supported by the Wellcome Trust, S.I.v.K. is supported by an ERC starter grant ER-StG-639005, and A.L. is supported by Crohn's and Colitis Foundation of America.

AUTHOR CONTRIBUTIONS

C.S., G.M., and L.P.L. performed experiments and analyzed data; A.G. performed LCMV experiments, analyzed data, and wrote the paper; D.K. provided intellectual input and performed mass-spectrometry experiments; F.A.F. provided intellectual input, performed gene silencing assays, analyzed data, and wrote the paper; L.A.S. provided intellectual input, performed Amnis experiments, analyzed data, and wrote the paper; T.C.F. and J.M.-F. performed experiments and analyzed data; R.B.-P. provided intellectual input, performed confocal experiments, and analyzed data; L.E.-M. and J.J.Y. engineered LE28 probe; M.A.E. scored histology; M.B., C.W., and S.I.v.K. provided intellectual input on AEP experiments, provided relevant AEP reagents, critically read, and wrote manuscript; E.M.S., A.L., D.H.F., and J.Z. provided intellectual input and reagents and critically read and wrote manuscript; and S.A. conceptualized the project, designed experiments, provided intellectual input, analyzed data, and wrote paper.

DECLARATION OF INTERESTS

The authors declare no competing interests.

Received: February 23, 2017
Revised: April 30, 2018
Accepted: May 17, 2018
Published: July 24, 2018

REFERENCES

Adeeku, E., Gudapati, P., Mendez-Fernandez, Y., Van Kaer, L., and Boothby, M. (2008). Flexibility accompanies commitment of memory CD4 lymphocytes derived from IL-4 locus-activated precursors. Proc. Natl. Acad. Sci. USA *105*, 9307–9312.

Ahmed, R., Byrne, J.A., and Oldstone, M.B. (1984). Virus specificity of cytotoxic T lymphocytes generated during acute lymphocytic choriomeningitis virus infection: role of the H-2 region in determining cross-reactivity for different lymphocytic choriomeningitis virus strains. J. Virol. *51*, 34–41.

Amarnath, S., Mangus, C.W., Wang, J.C., Wei, F., He, A., Kapoor, V., Foley, J.E., Massey, P.R., Felizardo, T.C., Riley, J.L., et al. (2011). The PDL1-PD1 axis converts human TH1 cells into regulatory T cells. Sci. Transl. Med. *3*, 111ra120.

Andrade, V., Guerra, M., Jardim, C., Melo, F., Silva, W., Ortega, J.M., Robert, M., Nathanson, M.H., and Leite, F. (2011). Nucleoplasmic calcium regulates cell proliferation through legumain. J. Hepatol. *55*, 626–635.

Asseman, C., Mauze, S., Leach, M.W., Coffman, R.L., and Powrie, F. (1999). An essential role for interleukin 10 in the function of regulatory T cells that inhibit intestinal inflammation. J. Exp. Med. *190*, 995–1004.

Bailey-Bucktrout, S.L., Martinez-Llordella, M., Zhou, X., Anthony, B., Rosenthal, W., Luche, H., Fehling, H.J., and Bluestone, J.A. (2013). Self-antigen-driven activation induces instability of regulatory T cells during an inflammatory autoimmune response. Immunity *39*, 949–962.

Boniface, K., Blumenschein, W.M., Brovont-Porth, K., McGeachy, M.J., Basham, B., Desai, B., Pierce, R., McClanahan, T.K., Sadekova, S., and de Waal Malefyt, R. (2010). Human Th17 cells comprise heterogeneous subsets including IFN-gamma-producing cells with distinct properties from the Th1 lineage. J. Immunol. *185*, 679–687.

Brown, C.C., Esterhazy, D., Sarde, A., London, M., Pullabhatla, V., Osma-Garcia, I., Al-Bader, R., Ortiz, C., Elgueta, R., Arno, M., et al. (2015). Retinoic acid is essential for Th1 cell lineage stability and prevents transition to a Th17 cell program. Immunity *42*, 499–511.

Burster, T., Beck, A., Tolosa, E., Marin-Esteban, V., Rötzschke, O., Falk, K., Lautwein, A., Reich, M., Brandenburg, J., Schwarz, G., et al. (2004). Cathepsin G, and not the asparagine-specific endoprotease, controls the processing of myelin basic protein in lysosomes from human B lymphocytes. J. Immunol. *172*, 5495–5503.

Chemnitz, J.M., Parry, R.V., Nichols, K.E., June, C.H., and Riley, J.L. (2004). SHP-1 and SHP-2 associate with immunoreceptor tyrosine-based switch motif of programmed death 1 upon primary human T cell stimulation, but only receptor ligation prevents T cell activation. J. Immunol. *173*, 945–954.

Chen, Z., Barbi, J., Bu, S., Yang, H.Y., Li, Z., Gao, Y., Jinasena, D., Fu, J., Lin, F., Chen, C., et al. (2013). The ubiquitin ligase Stub1 negatively modulates regulatory T cell suppressive activity by promoting degradation of the transcription factor Foxp3. Immunity *39*, 272–285.

Dall, E., and Brandstetter, H. (2016). Structure and function of legumain in health and disease. Biochimie *122*, 126–150.

Dunn, K.W., Kamocka, M.M., and McDonald, J.H. (2011). A practical guide to evaluating colocalization in biological microscopy. Am. J. Physiol. Cell Physiol. *300*, C723–C742.

Duraiswamy, J., Freeman, G.J., and Coukos, G. (2013). Therapeutic PD-1 pathway blockade augments with other modalities of immunotherapy T-cell function to prevent immune decline in ovarian cancer. Cancer Res. *73*, 6900–6912.

Figure 7. Tbet$^+$Th1 Cells Upregulate Foxp3 in Tumor Microenvironment

(A) *B6.Rag2*$^{-/-}$ mice were subcutaneously injected with B16F10 melanoma cells. At day 7 after tumor inoculation, adoptive transfer of Tbet$^+$ Th1 cells was performed.

(B) Mice were euthanized on day 14, splenocytes and TILs were isolated, and then Tbet$^+$Foxp3$^+$ cell frequency was determined.

(C) Summary of Foxp3$^+$Tbet$^+$ cells from the spleen and TIL.

(D and E) Tbet$^+$Foxp3$^-$ cells were flow sorted from the spleen and then expanded under iTreg cell conditions or iTreg cell conditions plus PDL-1fc. The upregulation of Foxp3 was then monitored by flow cytometry at day 7 post culture.

(F–H) *B6.Rag2*$^{-/-}$ mice were subcutaneously injected with B16F10 melanoma cells and adoptive transfer of Tbet$^+$Th1 cells was performed at day 5. Cohorts were either treated with isotype control or anti-PDL-1 antibody (250 μg/mouse) at days 5, 7, and 9. Animals were euthanized at day 11. Experimental methodology outlined in (F), and the frequency of Tbet$^+$iTreg cells was monitored within the TILs (G and H).

(I and J) Experiments were performed with Tbet$^+$Foxp3$^-$ cells transduced with either scramble shRNA RV or AEP shRNA RV and then treated with anti-PDL-1 antibody. Frequency of Tbet$^+$iTreg cells within the TILs in the different cohorts.

(K and L) Murine CD45.1$^+$ hosts were reconstituted with B16F10 melanoma tumors and sorted CD45.2$^+$Tbet$^+$Foxp3$^-$ cells. Cohorts were treated with either isotype or anti-PDL-1 antibody. Frequency of Tbet$^+$iTreg cells was measured within the TILs.

Experiments were repeated at least twice and data are shown as mean ± SEM from one to two individual experiments involving n = 3–8 mice per group.

Edgington, L.E., Verdoes, M., Ortega, A., Withana, N.P., Lee, J., Syed, S., Bachmann, M.H., Blum, G., and Bogyo, M. (2013). Functional imaging of legumain in cancer using a new quenched activity-based probe. J. Am. Chem. Soc. *135*, 174–182.

Feng, Y., Arvey, A., Chinen, T., van der Veeken, J., Gasteiger, G., and Rudensky, A.Y. (2014). Control of the inheritance of regulatory T cell identity by a cis element in the Foxp3 locus. Cell *158*, 749–763.

Francisco, L.M., Salinas, V.H., Brown, K.E., Vanguri, V.K., Freeman, G.J., Kuchroo, V.K., and Sharpe, A.H. (2009). PD-L1 regulates the development, maintenance, and function of induced regulatory T cells. J. Exp. Med. *206*, 3015–3029.

Gagliani, N., Amezcua Vesely, M.C., Iseppon, A., Brockmann, L., Xu, H., Palm, N.W., de Zoete, M.R., Licona-Limón, P., Paiva, R.S., Ching, T., et al. (2015). Th17 cells transdifferentiate into regulatory T cells during resolution of inflammation. Nature *523*, 221–225.

Hall, A.O., Beiting, D.P., Tato, C., John, B., Oldenhove, G., Lombana, C.G., Pritchard, G.H., Silver, J.S., Bouladoux, N., Stumhofer, J.S., et al. (2012). The cytokines interleukin 27 and interferon-γ promote distinct Treg cell populations required to limit infection-induced pathology. Immunity *37*, 511–523.

Haugen, M.H., Johansen, H.T., Pettersen, S.J., Solberg, R., Brix, K., Flatmark, K., and Maelandsmo, G.M. (2013). Nuclear legumain activity in colorectal cancer. PLoS ONE *8*, e52980.

Hegazy, A.N., Peine, M., Helmstetter, C., Panse, I., Fröhlich, A., Bergthaler, A., Flatz, L., Pinschewer, D.D., Radbruch, A., and Löhning, M. (2010). Interferons direct Th2 cell reprogramming to generate a stable GATA-3(+) T-bet(+) cell subset with combined Th2 and Th1 cell functions. Immunity *32*, 116–128.

Hui, E., Cheung, J., Zhu, J., Su, X., Taylor, M.J., Wallweber, H.A., Sasmal, D.K., Huang, J., Kim, J.M., Mellman, I., and Vale, R.D. (2017). T cell costimulatory receptor CD28 is a primary target for PD-1-mediated inhibition. Science *355*, 1428–1433.

Jacobs, J.F., Idema, A.J., Bol, K.F., Nierkens, S., Grauer, O.M., Wesseling, P., Grotenhuis, J.A., Hoogerbrugge, P.M., de Vries, I.J., and Adema, G.J. (2009). Regulatory T cells and the PD-L1/PD-1 pathway mediate immune suppression in malignant human brain tumors. Neuro-oncol. *11*, 394–402.

Johansen, H.T., Knight, C.G., and Barrett, A.J. (1999). Colorimetric and fluorimetric microplate assays for legumain and a staining reaction for detection of the enzyme after electrophoresis. Anal. Biochem. *273*, 278–283.

Kamphorst, A.O., Wieland, A., Nasti, T., Yang, S., Zhang, R., Barber, D.L., Konieczny, B.T., Daugherty, C.Z., Koenig, L., Yu, K., et al. (2017). Rescue of exhausted CD8 T cells by PD-1-targeted therapies is CD28-dependent. Science *355*, 1423–1427.

Koch, M.A., Tucker-Heard, G., Perdue, N.R., Killebrew, J.R., Urdahl, K.B., and Campbell, D.J. (2009). The transcription factor T-bet controls regulatory T cell homeostasis and function during type 1 inflammation. Nat. Immunol. *10*, 595–602.

Koch, M.A., Thomas, K.R., Perdue, N.R., Smigiel, K.S., Srivastava, S., and Campbell, D.J. (2012). T-bet(+) Treg cells undergo abortive Th1 cell differentiation due to impaired expression of IL-12 receptor β2. Immunity *37*, 501–510.

Kosugi, S., Hasebe, M., Matsumura, N., Takashima, H., Miyamoto-Sato, E., Tomita, M., and Yanagawa, H. (2009). Six classes of nuclear localization signals specific to different binding grooves of importin alpha. J. Biol. Chem. *284*, 478–485.

Kwon, H.K., Chen, H.M., Mathis, D., and Benoist, C. (2017). Different molecular complexes that mediate transcriptional induction and repression by FoxP3. Nat. Immunol. *18*, 1238–1248.

Laurence, A., Amarnath, S., Mariotti, J., Kim, Y.C., Foley, J., Eckhaus, M., O'Shea, J.J., and Fowler, D.H. (2012). STAT3 transcription factor promotes instability of nTreg cells and limits generation of iTreg cells during acute murine graft-versus-host disease. Immunity *37*, 209–222.

Levine, A.G., Mendoza, A., Hemmers, S., Moltedo, B., Niec, R.E., Schizas, M., Hoyos, B.E., Putintseva, E.V., Chaudhry, A., Dikiy, S., et al. (2017). Stability and function of regulatory T cells expressing the transcription factor T-bet. Nature *546*, 421–425.

Lin, Y., Qiu, Y., Xu, C., Liu, Q., Peng, B., Kaufmann, G.F., Chen, X., Lan, B., Wei, C., Lu, D., et al. (2014). Functional role of asparaginyl endopeptidase ubiquitination by TRAF6 in tumor invasion and metastasis. J. Natl. Cancer Inst. *106*, dju012.

Manoury, B., Hewitt, E.W., Morrice, N., Dando, P.M., Barrett, A.J., and Watts, C. (1998). An asparaginyl endopeptidase processes a microbial antigen for class II MHC presentation. Nature *396*, 695–699.

Manoury, B., Mazzeo, D., Fugger, L., Viner, N., Ponsford, M., Streeter, H., Mazza, G., Wraith, D.C., and Watts, C. (2002). Destructive processing by asparagine endopeptidase limits presentation of a dominant T cell epitope in MBP. Nat. Immunol. *3*, 169–174.

McGeachy, M.J., Bak-Jensen, K.S., Chen, Y., Tato, C.M., Blumenschein, W., McClanahan, T., and Cua, D.J. (2007). TGF-beta and IL-6 drive the production of IL-17 and IL-10 by T cells and restrain T(H)-17 cell-mediated pathology. Nat. Immunol. *8*, 1390–1397.

Miyao, T., Floess, S., Setoguchi, R., Luche, H., Fehling, H.J., Waldmann, H., Huehn, J., and Hori, S. (2012). Plasticity of Foxp3(+) T cells reflects promiscuous Foxp3 expression in conventional T cells but not reprogramming of regulatory T cells. Immunity *36*, 262–275.

Mukasa, R., Balasubramani, A., Lee, Y.K., Whitley, S.K., Weaver, B.T., Shibata, Y., Crawford, G.E., Hatton, R.D., and Weaver, C.T. (2010). Epigenetic instability of cytokine and transcription factor gene loci underlies plasticity of the T helper 17 cell lineage. Immunity *32*, 616–627.

Murphy, K.M., and Stockinger, B. (2010). Effector T cell plasticity: flexibility in the face of changing circumstances. Nat. Immunol. *11*, 674–680.

O'Shea, J.J., and Paul, W.E. (2010). Mechanisms underlying lineage commitment and plasticity of helper CD4+ T cells. Science *327*, 1098–1102.

Peine, M., Rausch, S., Helmstetter, C., Fröhlich, A., Hegazy, A.N., Kühl, A.A., Grevelding, C.G., Höfer, T., Hartmann, S., and Löhning, M. (2013). Stable T-bet(+)GATA-3(+) Th1/Th2 hybrid cells arise in vivo, can develop directly from naive precursors, and limit immunopathologic inflammation. PLoS Biol. *11*, e1001633.

Spranger, S., Spaapen, R.M., Zha, Y., Williams, J., Meng, Y., Ha, T.T., and Gajewski, T.F. (2013). Up-regulation of PD-L1, IDO, and T(regs) in the melanoma tumor microenvironment is driven by CD8(+) T cells. Sci. Transl. Med. *5*, 200ra116.

Taylor, J.J., Mohrs, M., and Pearce, E.J. (2006). Regulatory T cell responses develop in parallel to Th responses and control the magnitude and phenotype of the Th effector population. J. Immunol. *176*, 5839–5847.

Taylor, S., Huang, Y., Mallett, G., Stathopoulou, C., Felizardo, T.C., Sun, M.A., Martin, E.L., Zhu, N., Woodward, E.L., Elias, M.S., et al. (2017). PD-1 regulates KLRG1^{+} group 2 innate lymphoid cells. J. Exp. Med. *214*, 1663–1678.

Thornton, A.M., and Shevach, E.M. (1998). CD4+CD25+ immunoregulatory T cells suppress polyclonal T cell activation in vitro by inhibiting interleukin 2 production. J. Exp. Med. *188*, 287–296.

van Kasteren, S.I., and Overkleeft, H.S. (2014). Endo-lysosomal proteases in antigen presentation. Curr. Opin. Chem. Biol. *23*, 8–15.

van Loosdregt, J., Fleskens, V., Fu, J., Brenkman, A.B., Bekker, C.P., Pals, C.E., Meerding, J., Berkers, C.R., Barbi, J., Gröne, A., et al. (2013). Stabilization of the transcription factor Foxp3 by the deubiquitinase USP7 increases Treg-cell-suppressive capacity. Immunity *39*, 259–271.

Wherry, E.J., Blattman, J.N., Murali-Krishna, K., van der Most, R., and Ahmed, R. (2003). Viral persistence alters CD8 T-cell immunodominance and tissue distribution and results in distinct stages of functional impairment. J. Virol. *77*, 4911–4927.

Wu, Y., Borde, M., Heissmeyer, V., Feuerer, M., Lapan, A.D., Stroud, J.C., Bates, D.L., Guo, L., Han, A., Ziegler, S.F., et al. (2006). FOXP3 controls regulatory T cell function through cooperation with NFAT. Cell *126*, 375–387.

Yang, X.O., Pappu, B.P., Nurieva, R., Akimzhanov, A., Kang, H.S., Chung, Y., Ma, L., Shah, B., Panopoulos, A.D., Schluns, K.S., et al. (2008). T helper 17 lineage differentiation is programmed by orphan nuclear receptors ROR alpha and ROR gamma. Immunity *28*, 29–39.

Zhang, Z., Song, M., Liu, X., Kang, S.S., Kwon, I.S., Duong, D.M., Seyfried, N.T., Hu, W.T., Liu, Z., Wang, J.Z., et al. (2014). Cleavage of tau by asparagine endopeptidase mediates the neurofibrillary pathology in Alzheimer's disease. Nat. Med. *20*, 1254–1262.

Zhao, Y., Guo, H., Qiao, G., Zucker, M., Langdon, W.Y., and Zhang, J. (2015). E3 ubiquitin ligase Cbl-b regulates thymic-derived CD4+CD25+ regulatory T cell development by targeting Foxp3 for ubiquitination. J. Immunol. *194*, 1639–1645.

Zhou, X., Bailey-Bucktrout, S.L., Jeker, L.T., Penaranda, C., Martínez-Llordella, M., Ashby, M., Nakayama, M., Rosenthal, W., and Bluestone, J.A. (2009). Instability of the transcription factor Foxp3 leads to the generation of pathogenic memory T cells in vivo. Nat. Immunol. *10*, 1000–1007.

STAR★METHODS

KEY RESOURCE TABLE

REAGENT or RESOURCE	SOURCE	IDENTIFIER
Antibodies		
CD4 (RM4-4)	BioLegend	Cat#116011
CD8 (53-6.7)	BioLegend	Cat#100759
CXCR3 (CXCR3-173)	BioLegend	Cat#126521
PDL-1 (10F.9G2)	BioLegend	Cat#124319
CD44 (IM7)	BD Biosciences	Cat#553134
CD45.1 (A20)	BD Biosciences	Cat#565813
CD45.2 (104)	BD Biosciences	Cat#740490
CD45RB (C363.16A)	Thermo Fisher Scientific	Cat#17-0455-81
PD-1 (29F.1A12)	BioLegend	Cat#135219
H-2K^{b} (AF6-88.5)	BD Biosciences	Cat#562832
CD62L (MEL-14)	Thermo Fisher Scientific	Cat#15-0621-81
CD8 (53-6.7)	BioLegend	Cat#100737
CCR4 (2G12)	BioLegend	Cat#131217
Neuropilin-1 (3E12)	BioLegend	Cat#145207
Helios (22F6)	BioLegend	Cat#137229
CD25 (PC61)	BioLegend	Cat#102035
CD127 (A7R34)	BioLegend	Cat#135035
LAMP-1 (1D4B)	BioLegend	Cat#121616
Foxp3 (FJK-16 s)	Thermo Fisher Scientific	Cat#12-5773-82
IL-10 (JES5-16E3)	Thermo Fisher Scientific	Cat#17-7101-81
IFN-γ (XMG1.2)	Thermo Fisher Scientific	Cat#25-7311-41
Ki67 (SolA15)	Thermo Fisher Scientific	Cat#25-5698-82
Anti-CD3 (145-2C11)	Thermo Fisher Scientific	Cat#16-0031-82
Anti-CD28 (37.51)	Thermo Fisher Scientific	Cat#16-0281-82
LEAF Purified anti-mouse IL-4 (11B11)	BioLegend	Cat#504115
LEAF Purified anti-mouse IFN-γ (XMG1.2)	BioLegend	Cat#505827
Anti-mouse PDL-1 (10F.9G2)	Bio X Cell	Cat#BP0101
Rat-IgG2b Isotype Control (LTF-2)	Bio X Cell	Cat#BP0090
Mouse Legumain	R&D Systems	Cat#MAB2058
PTEN	Cell Signal	Cat#9188
mTOR	Cell Signal	Cat#2972
Phospho-mTOR	Cell Signal	Cat#2971
AKT	Cell Signal	Cat#4691
Phospho-AKT ser473	Cell Signal	Cat#4060
Phospho-AKT Thr308	Cell Signal	Cat#2965
Foxp3	Cell Signal	Cat#12653
P70S6K	Cell Signal	Cat#2708
Phospho P70S6K (Thr421/Ser424)	Cell Signal	Cat#9204
ERK1/2	Cell Signal	Cat#9102
Phospho-ERK	Cell Signal	Cat#9101
GAPDH	Cell Signal	Cat#5174
β-tubulin	Cell Signal	Cat#5346
β-actin	Cell Signal	Cat#4967
Lamin B1	Cell Signal	Cat#13435

(*Continued on next page*)

Continued

REAGENT or RESOURCE	SOURCE	IDENTIFIER
Rabbit IgG HRP	Cell Signal	Cat#7074
Rat IgG HRP	R&D systems	Cat#HAF005
Bacterial and Virus Strains		
LCMV	Dr. Ethan Shevach Laboratory, NIH, USA	Armstrong Strain
LCMV	Dr. Ethan Shevach Laboratory, NIH, USA	Clone-13 Strain
pENTR hFOXP3 Plasmid	Addgene	Cat#16363
pEV-Th1.1-RV	Dr. Vanja Lazarevic, NIH, USA	N/A
pMIGR-mFoxp3	Addgene	Cat#24067
Chemicals, Peptides, and Recombinant Proteins		
PDL-1 Fc Chimera	R&D Systems	Cat#1019-B7
AEP inhibitor MV026630	Prof. Colin Watts, Dundee, UK	N/A
AEP protein	Prof. Colin Watts, Dundee, UK	N/A
AEP Cy5 probe	Edgington et al.	N/A
rmIL-2	Miltenyi Biotec	Cat#130-098-221
rhTGF-β1	R&D systems	Cat#240-B
Cycloheximide	Sigma-Aldrich	Cat#C104450
MG-132	Sigma-Aldrich	Cat#474787
Leupeptin	Sigma-Aldrich	Cat#EI8
Foxp3 protein	Origene	Cat#TP317580
Tbet protein	Origene	Cat#TP307902
DAPI	BioLegend	Cat#422801
GP33-41 Tetramer	NIH Tetramer Core Facility	H-2D^{b}/Class I GP33-41
Critical Commercial Assays		
Foxp3 Transcription Factor Staining Buffer Kit	Thermo Fisher Scientific	Cat#A25866A
CD90.2 microbeads	Miltenyi Biotec	Cat#130-049-101
Mouse Regulatory T cell isolation kit	Miltenyi Biotec	Cat#130-091-041
CellTrace Violet Cell Proliferation Kit	Thermo Fisher Scientific	Cat#C34557
Deposited Data		
Microarray	This study	GEO:GSE113815
Experimental Models: Cell Lines		
NIH 3T3	Dr. Francis Flomerfelt, NCI, NIH	N/A
293T	Dr. Francis Flomerfelt, NCI, NIH	N/A
B16F10 melanoma	Dr. Pawel Muranski and Dr. Nick Restifo, NCI, NIH	N/A
Experimental Models: Organisms/Strains		
C57BL/6	Charles River	Cat#632
BALB/c	Charles River	Cat#028
C57BL/6 *Rag2*$^{-/-}$	Jax Mice	Cat#008449
C57BL/6 Foxp3RFP	Jax Mice	Cat#008374
C57BL/6 CD45.1	Jax Mice	Cat#002014
C57BL/6 TbetZsgreen	Dr. Jinfang Zhu, NIH, USA	N/A
C57BL6 PDCD1$^{-/-}$	Prof. Tasuku Honjo, Japan	N/A
C57BL/6 AEP$^{-/-}$	Prof. Colin Watts, Dundee, UK	N/A
Oligonucleotides		
Legumain (AEP) Mouse ShRNA	Origene	Cat#TR510967
Scramble Mouse ShRNA	Origene	Cat#TR30012
Recombinant DNA		
AEP cDNA	Prof. Colin Watts	N/A

(*Continued on next page*)

Continued

REAGENT or RESOURCE	SOURCE	IDENTIFIER
Software and Algorithms		
FlowJo software	FlowJo LLC	RRID:SCR_008520
Scaffold Mass spectrometry peptide analysis	Proteome Software.com	RRID:SCR_014345
GraphPad Prism 7	GraphPad Software, Inc.	RRID:SCR_002798

CONTACT FOR REAGENT AND RESOURCE SHARING

Further information and requests for resources and reagents should be directed and will be fulfilled by the Lead Contact, Dr. Shoba Amarnath (shoba.amarnath@newcastle.ac.uk).

EXPERIMENTAL MODEL AND SUBJECT DETAILS

Mice

Female C57BL/6 (B6, H-2K^{b}) and BALB/c (H-2K^{d}) mice 8- to 10- weeks old were obtained from Frederick Cancer Research Facility, USA or Charles River, UK. Female C57BL/6 *Rag2*$^{-/-}$ and C57BL/6 Foxp3RFP mice were purchased from Jackson Laboratories, *Aep*$^{-/-}$ and WT littermate controls were kindly provided by C. Watts. B6.*Tbx21*Zsgreen mice were bred with B6.*Foxp3*RFP mice in a specific pathogen-free facility at the National Institutes of Health, USA and at Newcastle University, UK. B6.*Tbx21*ZsGreen*Foxp3*RFP mice were utilized for all T cell lineage-tracing experiments. The use of animals for this research was approved by the Animal Care and Use Committee, National Cancer Institute, and National Institute of Allergy and Infectious Diseases, NIH, and carried out in accordance with the NIH animal health and safety guidelines. Animal experiments conducted at Newcastle University were approved by the Newcastle Ethical Review committee and performed under a UK home office approved project license. Experimental methodology was in accordance to the NC3R recommendations and data are shown in accordance with ARRIVE guidelines.

METHOD DETAILS

Cell sorting and Flow cytometry and tetramer staining

Unless stated otherwise, ZsGreen fluorescence was used to determine Tbet expression and RFP fluorescence was used to flow sort various cell populations. CD4^{+}Tbet^{+}Foxp3^{-}Th cells were characterized by multi-parameter flow cytometry for surface markers. Cytokine phenotype of day 0 cells was measured by stimulating cells with phorbol-12-myristate 13- acetate (PMA) and ionomycin for four hours along with Golgiplug and Golgistop which was added in the last 2 hr of incubation. Flow cytometry staining antibodies for CD4 (clone: RM4-4), CXCR3 (clone: CXCR3-173), PD-1 (clone: 29F.1A12), PDL-1 (clone: 10F.9G2), CD44 (clone: IM7), CD45.1 (clone: A20), CD45.2 (clone: 104), H-2K^{b} (AF6-88.5), CD62L (clone: MEL-14), CD8 (clone: 53-6.7), CCR4 (clone: 2G12), Neuropilin-1 (clone: 3E12), Helios (clone: 22F6), CD25 (clone: PC61) and CD127 (clone: A7R34) were purchased from BioLegend. Foxp3 (clone: FJK-16 s), IL-10 (clone: JES5-16E3), IFN-γ (clone: XMG1.2) and Ki67 (clone: SolA15) were from Thermo Fisher Scientific. For MHC class I tetramer staining, H-2D^{b} GP33-41 was used at 1:100 dilutions and staining was performed at 4°C for 1 hr. Data were acquired using either an LSR II or Fortessa or FACS CANTO and analyzed using FlowJo software version 9.6.4 or 10.0.6.

In vitro cell culture

CD4^{+}Tbet^{+}Foxp3^{-} T helper cells were flow sorted and stimulated in 24 well cell culture plates coated with anti-CD3 (clone:145-2C11; 5 μg/ml) for 3 days in cell culture media [RPMI, supplemented with 10% FCS, glutamine (2 mM), non-essential amino acids (0.1 mM), 2-mercaptoethanol (50 μM), sodium pyruvate (1 mM), penicillin and streptomycin (100 IU/ml)] along with soluble anti-CD28 (clone:37.51;2 μg/ml), rmIL-2 (80 ng/ml), rhTGF-β1 (2 ng/ml), anti-IL-4 (BioLegend, clone:11B11;20 μg/ml) and anti-IFN-γ (BioLegend, clone:XMG1.2; 20 μg/ml) with or without coated PDL-1fc chimera (5 μg/ml). After 3 days of culture, cells were expanded for an additional four days in the presence of IL-2 (80 ng/ml) and TGF-β1 (2 ng/ml) or with IL-2 alone. Cells were then characterized by intracellular flow cytometry for Foxp3 expression. Both populations were flow sorted for Foxp3^{+} cells and are denoted as Tbet^{+}iTreg and Tbet^{+}iTreg$_{PDL1}$ cells. Post-differentiation Tbet^{+}iTreg and Tbet^{+}iTreg$_{PDL1}$ cells were stimulated overnight with anti-CD3 and anti-CD28 and then supernatants were subjected to a multiplex bead array luminex assay. Control populations of iTregs (iTreg and iTreg$_{PDL1)}$ were generated from CD4^{+}Tbet^{-}Foxp3^{-} subsets, which were similarly cultured and characterized. Subsequently, expanded Foxp3^{+} cells from the various subsets were sorted and utilized in *in vitro* suppression assays and *in vivo* animal models of autoimmunity and alloimmunity. In certain experiments, CD4^{+}Tbet^{+}Foxp3^{-} T helper cells were either cultured with AEP inhibitor MV026630 (100 μM) or AEP ShRNA or Vehicle (DMSO) from day 0 of culture in addition to anti-CD3, anti-CD28, rh-IL-2 and rh-TGF-β1 prior to being used as cellular therapeutics.

In vitro Treg suppression assay

$CD4^+CD25^-$ cells were isolated using the Miltenyi Biotec Treg isolation kit and utilized in a Treg suppression assay as previously described (Thornton and Shevach, 1998). Purified $CD4^+CD25^-$ cells ($5x10^4$) were labeled with CellTrace Violet and then cultured in 96 well round bottom plates in 200 μL complete media along with $2x10^5$ irradiated T cell-depleted spleen cells (3000 cGy) as accessory cells. Anti-CD3 (0.5 μg/ml) was added along with cultured flow sorted $Foxp3^+$iTreg populations (iTreg, $iTreg_{PDL1}$, $Tbet^+$ iTreg and $Tbet^+$ $iTreg_{PDL1}$ cells) at the indicated ratios. Cells were incubated at 37°C for 72 hr and proliferation and suppression was monitored by flow cytometry. Proliferation of responder T cells was evaluated by CellTrace Violet dilution. Percent suppression of CD4 responder T cell was calculated with values representing the ratio of total divided peaks to both divided and non-divided peaks, normalized to the anti-CD3 alone experimental group.

In vivo animal models

Experimental Autoimmune Colitis

B6.Rag2$^{-/-}$ female mice were reconstituted with B6. $CD45.1^+CD4^+CD25^-CD45RB^{hi}$ (T effectors) populations ($4x10^5$) as previously described (Asseman et al., 1999) along with flow sorted $B6.CD45.2^+$iTreg cells ($1x10^5$), $iTreg_{PDL1}$ cells ($1x10^5$), $Tbet^+$iTreg ($1x10^5$), or $Tbet^+$ $iTreg_{PDL1}$ cells ($1x10^5$). Mice were weighed weekly and loss of body weight was used as an indicator of colitis. Immune endpoints were measured in the splenocytes and in LPL. LPL were isolated as previously described (Asseman et al., 1999). Briefly, large intestine was digested using Liberase TL and DNase I followed by percoll gradient centrifugation. LPLs were washed twice with complete media and then used for immunological assays. Both splenocytes and LPL were stimulated with PMA and ionomycin along with GolgiPlug and Golgistop for 4 hr and then effector cytokines were measured by intracellular flow cytometry.

Experimental Allogeneic GVHD

BM was flushed from B6 donor femurs and tibias and T cell depleted (TDBM) using CD90.2 MACS beads (Miltenyi Biotec). Host allogeneic (BALB/c) female mice were conditioned with total body irradiation of 950 cGy in two divided doses three hours apart before being rescued with 10^7 TDBM cells together with $1x10^6$ $CD4^+CD25^-$T cells from WT $CD45.1^+$ B6 donors. In addition, various flow sorted iTreg populations ($CD45.2^+$; $1x10^6$) were adoptively transferred for prevention of GVHD. Survival was monitored as a measure of Treg cell potency. Alloreactive IFN-γ was measured as follows: Single cell suspension of splenocytes ($1x10^6$) was cultured overnight with either syngeneic or allogeneic bone marrow derived dendritic cells DCs ($1x\ 10^5$). Supernatant was harvested at 24 hr and Th1 cytokines were measured by using a multiplex luminex bead array system. Allogenic IFN-γ cytokine in the supernatant was measured by subtracting the amount of IFN-γ present in the syngeneic controls.

LCMV

Six to eight weeks old B6.*Tbx21*ZsGreen*Foxp3*RFP mice were infected with Armstrong ($2x10^5$ PFU, i.p) or Clone-13 virus ($2x10^6$ PFU, i.v) as previously described (Wherry et al., 2003). Titers of virus were determined by plaque assay on Vero cells as previously described (Ahmed et al., 1984). At indicated time points, spleens were harvested and the frequency of $Tbet^+Foxp3^+$ T cells was characterized by flow cytometry. In certain experiments, primed $CD4^+Tbet^+Foxp3^-$ T cells were flow sorted on day 14 post-infection and then differentiated under iTreg conditions with or without PDL-1 followed by Foxp3 characterization using flow cytometry. $B6.CD45.1^+$ murine recipients were injected with anti-CD4 (500 μg/mouse; day −7) infected with Clone-13 virus along with adoptive transfer of $CD45.2^+Tbet^+Foxp3^-$ cells ($0.7x10^6$). Cohorts were treated with either isotype or anti-PDL-1 antibody (200 μg/mouse) at day 1, 5 and 9. On day 10 $Tbet^+Foxp3^+$ cells were analyzed in spleens of the infected mice.

B16F10 melanoma

B6.Rag2$^{-/-}$mice, WT mice, CD45.1 and *Aep*$^{-/-}$ mice were reconstituted with $3x10^5$ B16F10 melanoma cells (kindly provided by Dr. Pawel Muranski and Prof. Nick Restifo, NCI,NIH) and the tumor was allowed to progress for 7 days. At day 7, murine recipients were reconstituted with $2x10^5$ $Tbet^+Foxp3^-$T effectors from B6.*Tbx21*ZsGreen*Foxp3*RFP mice. At day 14 post-tumor inoculation, mice were euthanized, spleen and TILs were isolated and analyzed for the presence of $Tbet^{hi}Foxp3^+$ cells. In certain experiments, cohorts were treated with either isotype or anti-PDL-1 antibody (250 μg/mouse) at days 5, 7 and 9. For shRNA experiments, *Rag2*$^{-/-}$ mice were reconstituted with tumor at day 0 along with flow sorted $CD4^+Tbet^+Foxp3^-$ T cells transduced with either scramble or AEP shRNA. Murine recipients were then treated with anti-PDL-1 antibody at days 5, 7 and 9. Host $CD45.1^+$ murine hosts were reconstituted with tumor at day 0 along with flow sorted $CD4^+Tbet^+Foxp3^-$ T cells and then treated with antibodies at days 5, 7 and 9. Splenocytes and tumors were harvested at day 11 and the frequencies of $Foxp3^+$ cells were evaluated.

Histological Analysis

Representative samples of liver, intestine and colon were obtained from the mice that underwent GvHD and fixed in 10% phosphate buffered formalin. Samples were embedded in paraffin, sectioned and stained with hematoxylin and eosin. All slides were coded and read by an external pathologist (Dr. Michael Eckhaus) in a blinded fashion. A four-point scale of GvHD severity was used to score the samples.

Affymetrix Gene Expression Profiling

Total RNA was isolated with RNAeasy kit from QIAGEN. RNA quality was checked on Agilent Bioanalyzer. All samples used for microarray analysis had high quality score (RIN > 9). 100 ng of RNA was reverse transcribed and amplified using Ambion WT expression kit following manufacturer's suggested protocol. Sense strand cDNA was fragmented and labeled using Affymetrix WT terminal labeling kit. Four replicates of each group were hybridized to Affymetrix mouse Gene ST 2.0 GeneChip in Affymetrix hybridization oven at

45°C, 60RPM for 16 hr. Wash and stain were performed on Affymetrix Fluidics Station 450 and scanned on Affymetrix GeneChip scanner 3000. Data were collected using Affymetrix AGCC software. Statistical and clustering analysis was performed with Partek Genomics Suite software using RMA normalization algorithm. Differentially expressed genes were identified with ANOVA analysis. Genes that are up- or downregulated more than 2 fold and with a $p < 0.001$ were considered significant.

Immuno Blotting

Protein lysates were obtained from Tbet$^+$ iTreg, and Tbet$^+$ iTreg$_{PDL1}$ cells. Lysates were run on 10%–20% SDS-PAGE gels and transferred onto nitrocellulose membrane. Membranes were blocked with 5% milk in TBST buffer (20mmol/L TrisHCl, 500 mmol/L NaCl, and 0.01% Tweeen-20) and incubated overnight at 4°C with primary antibodies (Ab) in TBST containing either 5% milk or BSA. Immune reactivity was detected by sequential incubation with HRP-conjugated secondary Ab and enzymatic chemiluminescence (Cell Signaling Technology). Primary Abs to mouse PTEN, mTOR, phospho-mTOR, Akt, phospho-AKT (Ser473 and Thr 308), Foxp3, P70S6K, phospho-p70S6K, ERK, phospho-ERK, GAPDH, β-tubulin, β-actin were procured from Cell Signaling. AEP (Legumain) was obtained from R&D systems. Images were acquired using a LiCOR FcOdyssey system or Wes Simple Protein system.

AEP enzyme activity

AEP activity in cell lysates was measured in triplicates by cleavage of the substrate z-Ala-Ala-Asn-AMC (Bachem) as previously described (Haugen et al., 2013; Johansen et al., 1999). Briefly, cell lysate (20 μl) was added to black 96-well microplates. After the addition of 100 μL buffer and 50 μL substrate solution (final concentration is 10 μM) at pH 5.8, a kinetic measurement based on increase in fluorescence over 10 min was performed at 30°C in a plate reader and presented as enzyme units where one unit of activity was defined as the amount of enzyme releasing 1.0 μmol of product/min under the standard conditions described. Enzyme activity was then normalized to the enzyme activity of DCs. DC enzyme activity was set to 100% and then the % enzyme activity of Tbet$^+$ iTreg and Tbet$^+$ iTreg$_{PDL1}$ cells was calculated. Enzyme activity was also measured by using imaging flow cytometry using the AEP probe LE28 (Edgington et al., 2013). LE28 specifically binds to active AEP enzyme. Briefly, Tbet$^+$ iTreg and Tbet$^+$ iTreg$_{PDL1}$ cells were incubated with the AEP probe LE28 cy5 for 1 hr at 37°C, washed and then AEP activity was measured using flow cytometry.

Foxp3 co-localization Assays

The co-localization of Foxp3 in the nucleus was measured using imaging flow cytometry on the Amnis Image stream MKII. For this, cells were fixed and then stained with DAPI, Foxp3 APC and LAMP-1 APC-Cy7 (BioLegend, clone 1D4B). For co-localization experiments with AEP cells were stained with DAPI, Foxp3 PE, LAMP-1 APC-Cy7, and LE28 Cy5.

Amnis Imaging Flow cytometry

Sample Acquisition: Samples were run on an Image StreamX MKII using INSPIRE data acquisition software (Amnis EMD-Millipore) at a concentration of approximately $1x10^6$ cells in 50 μL of PBS. The system was outfitted with 2 cameras, 12 channels, 405, 488, 561, 642, and 785nm lasers, and an extended depth of field element (EDF). Brightfield was collected in channels 1 and 9, SSC was collected in channel 6 at a 785nm power of 2mW, DAPI was detected in channel 7 (430-505nm filter) at a 405nm laser power of 10mW, TbetZsgreen was detected in channel 2 (480-560nm filter) at a 488 laser power of 20mW, Foxp3 PE was detected in channel 3 (560-595 filter) at a 561nm laser power of 200mW, and LE28 Cy5 were detected in channel 11 (660-745nm filter) and LAMP1 APC-Cy7 was detected in channel 12 (745-800nm filter) respectively, at a 642nm laser power of 150mW. Acquisition gates in INSPIRE were set as follows: a single cell gate was set on a Brightfield Area versus Brightfield Aspect Ratio plot to encompass single cells and eliminate debris and aggregates, a Brightfield Gradient RMS plot was used to gate single cells which were in focus, and gates were set in Raw Max Pixel plots to eliminate events saturating the camera in each fluorescent channel used. 20,000 single, focused, non-saturating events were acquired at 60X magnification, using the EDF element.

Data Analysis: Data analyses were performed in IDEAS 6.0 software (Amnis EMD-Millipore). A compensation matrix was created utilizing single color controls acquired with Brightfield and the 785 laser turned off, and all others laser powers set to the powers listed above. In IDEAS, single, focused, and nucleated (DAPI$^+$) cells were gated and used for downstream analysis.

Determination of Foxp3 in the nucleus: A series of masks was created which enabled the determination of the amount of Foxp3 in the nucleus. First, a tight mask was created on the nuclear image by eroding the default mask in one pixel (Erode (M07, 1). Next, a mask was created which identified Foxp3 staining (Intensity (M11, 11_Foxp3, 100-4095)). Lastly, a mask was created to identify pixels which contained DAPI staining and Foxp3 staining by combining the aforementioned masks with an AND operator ((Erode (M07, 1) And Intensity(M11, 11_Foxp3, 100-4095)). The area of Foxp3 inside the nucleus was determined by creating an Area feature on the combined DAPI:Foxp3 mask and gating the Area plot on DAPI$^+$Foxp3$^+$ cells.

Determination of Foxp3 and AEP co-localization in the nucleus: A series of masks was created which enabled the determination of the co-localization of Foxp3 and AEP in the nucleus. First, a mask was created which identified Foxp3 staining (Intensity (M03, 3_Foxp3, 300-4095). Next, a mask was created which identified AEP staining (Intensity (M11, 11_Legumain/AEP, 362-4095). The DAPI mask used is as described in the section above. Lastly, a mask was created to identify pixels which contained DAPI, Foxp3, and AEP staining by combining the aforementioned masks with an AND operator (Intensity (M03, 3_Foxp3, 300-4095) AND (Erode (M07, 1) AND Intensity (M11, 11_Legumain). The area of the pixels containing DAPI, Foxp3, and AEP staining was determined by creating an Area feature on the combined DAPI:Foxp3:AEP mask and gating the Area plot on DAPI$^+$Foxp3$^+$AEP$^+$ cells.

Confocal Microscopy

Flow sorted iTregs, iTreg$_{PDL1}$, Tbet^{+}iTreg and Tbet^{+}iTreg$_{PDL1}$ were first stained with AEP Cy5 followed by fixation and permeabilization. Cells were washed with permeabilization buffer and then stained with Foxp3 PE and DAPI. Images were acquired on a Leica SP8 point scanning confocal microscopy with white light super continuum lasers. Colocalization analysis were performed as previously described (Dunn et al., 2011). A comprehensive explanations of the confocal analysis is provided below:

Orthogonal projection view to enhance visualization of protein spatial location: An orthogonal projection of the image allows identification of the spatial location of a protein within the cell. It is a three-dimensional view of the cell but in a two-dimensional figure. A quadrant was drawn on a particular point in the nucleus, if all three fluorophores are present together in this 3D view, then the analysis shows this on merging the three images.

Deconvolution of the images to enhance signal to noise ratio in an orthogonal projection: Deconvolving is a recognized image processing technique to digitally reassign out of focus light to its originating focal plane. Deconvolution corrects optical aberration and provide higher resolution which enhances signal to noise ratio therefore minimizing false positive analysis. Combining deconvolution and orthogonal projection enhances understanding of the spatial location and co-localization of proteins within a cell.

Particle Analysis: Particle analysis was performed with the deconvolved images as recently shown (Kwon et al., 2017). Using this technique, we measured the number of Foxp3 and AEP particles within the nucleus. We next performed a quantitative analysis of the particles and plotted the values as follows: Each data point depicts the number of particles within the nucleus and the y axis denotes the relative volume of Foxp3 within the nucleus and similarly the relative volume of AEP within the nucleus. If cytosolic contamination occurs, it will be represented in this analysis as follows. 100% on y axis denotes that the entire particle is within the nucleus whereas 20% denotes a particle that does not explicitly localize in the nucleus.

We next quantitatively measured AEP and Foxp3 co-localization. Each data point depicts the number of particles within the nucleus that is colocalized and the y axis denotes the value which is the sum of the intensity of all voxels that colocalize with each other.

Foxp3 cleavage and Mass Spectrometry

Human Foxp3 protein and Tbet protein was purchased from Origene and then used in the cleavage assay in the presence of purified AEP protein (kindly provided by Dr. Colin Watts). Briefly, 1 μg of human AEP protein was incubated in 200 μL of activation buffer (0.1M NaCl, 0.1M NaOAc, pH 4.5) in 96 well round bottom plates for 30 mins at 37°C. In certain conditions, the AEP inhibitor was added (100 μM). Post AEP activation, either Foxp3 protein (5 μg) or Tbet protein (5 μg) was added to the wells with only activation buffer or activation buffer plus AEP or activation buffer plus AEP plus inhibitor. The plate was then incubated for 2 hr at 37°C. Samples were then reduced with LDS sample buffer and then subjected to immuno blotting. Once the proteins were run on a gel, they were transferred to a membrane and blotted for Foxp3 and Tbet. In separate experiments, gels were stained with Coomassie blue (Gel Code Blue reagent; Thermo Fisher Scientific) and then bands were cut out and subjected to mass spectrometry as previously described (Zhang et al., 2014). Briefly, bands were dehydrated using acetonitrile followed by vacuum centrifugation, reduced with 10 mM dithiothreitol and alkylated with 55 mM iodoacetamide. Gel pieces were then washed alternately with 25 mM ammonium bicarbonate followed by acetonitrile. Samples were digested with trypsin overnight at 37°C. Digested samples were analyzed by LC-MS/MS using an UltiMate® 3000 Rapid Separation LC (RSLC, Dionex Corporation, Sunnyvale, CA) coupled to an Orbitrap Elite (Thermo Fisher Scientific, Waltham, MA) mass spectrometer. Peptide mixtures were separated using a gradient from 92% A (0.1% FA in water) and 8% B (0.1% FA in acetonitrile) to 33% B, in 44 min at 300 nL min^{-1}, using a 75 mm x 250 μm i.d. 1.7 mM CSH C18, analytical column (Waters). Peptides were selected for fragmentation automatically by data dependent analysis. Data produced were searched using Mascot (Matrix Science UK), against the SWISSPROT database. Data were validated using Scaffold (Proteome Software, Portland, OR). Additional Foxp3 degradation experiments were performed with WT or mutated Foxp3 expressing 293 cells. The WT Foxp3 cDNA was isolated from a BamH1 + Xho1 digest of plasmid purchased from Addgene. The Mu Foxp3 containing alanine substituted for asparagine was synthesized by Integrated DNA Technologies custom gene synthesis service. The construct contained BamH1 and Xho1. These sites were used to clone both WT and mutant Foxp3 cDNAs into pCDNA3.1 and pEV Thy1.1 RV. The mutant Foxp3 construct also included a Not1 site to identify recombinant plasmids. The Foxp3 mutant cDNA was fully sequenced prior to use in experiments.

Pulse Chase Assays for Foxp3 protein turnover

Tbet^{+}iTreg and Tbet^{+} iTreg$_{PDL1}$ cells were washed and then aliquoted into 24 well tissue culture plates at 3x10^{6}/ml. In certain experiments, WT or *Aep*$^{-/-}$ iTregs were plated into 24 well plates at 1x10^{6}/ml. Cells were treated with cycloheximide (150 μg/ml) for the indicated time points and lysates were used to measure Foxp3 and Tbet protein degradation by immuno blotting. In order to block proteosomal degradation of Foxp3 and Tbet, MG132 (0.5 μM, Sigma-Aldrich) was added to certain culture conditions. AEP inhibitor MV026630 (100 μM, kindly provided by Prof. Colin Watts and Dr. Sander I. van Kasteren) was added to cultures to block specific AEP mediated degradation of Foxp3.

AEP and Foxp3 silencing and mutation assays

AEP specific shRNAs were obtained from Origene. On confirming efficient silencing of AEP in NIH 3T3 cells, the most efficient shRNA was chosen for further analysis. Single-stranded oligonucleotides containing shRNA targeted to AEP or scrambled sequence, 20 bp complementary to the sequence flanking a Xho1 site within with the expression vector pEV Thy1.1 RV (gift from Dr. Vanja Lazarevic, NCI, NIH), and a Not1 site were purchased from IDT and annealed in buffer containing 1 mM Tris pH 8.0, 50 mM NaCl

and 1 mM EDTA. The vector pEV Thy1.1 RV was digested with Xho1. The vector and the double stranded oligos were combined and a Gibson reaction (New England Biolabs) was performed. Recombinant clones were identified by Not1 restriction analysis. The integrity of the insert sequence and orientation was confirmed by DNA sequencing. Silencing of AEP was further confirmed in 3T3 cells and then was used to silencing AEP in primary murine Tbet^{+}iTreg cells. pENTR Foxp3 was a gift from Prof. Anjana Rao [Addgene plasmid # 16363 (Wu et al., 2006)] containing WT human Foxp3 cDNA that was cloned into pEV-Thy1.1-RV using BglII and Xho1. The AEP resistant human Foxp3 was synthesized as a mini-gene (IDT) and cloned into the BglII and Xho1 sites of pEV-Thy1.1-RV. The N154A human Foxp3 mutant was created by inserting a 240 bp G-Block DNA fragment (IDT) between the Bcl1 and BstB1 sites using the Gibson reaction (New England Biolabs). AEP cDNA was obtained from Prof. Colin Watts and cloned into pEV-Thy1.1-RV using Xho1. For NLS experiments AEP NLS site was mutated whereby KRK was replaced to AAA at site 318-320. pMIGR-mFoxp3 was a gift from Prof. Dan Littman (Addgene plasmid # 24067, unpublished). The N153A mutant was created by inserting a 182 bp G-Block DNA fragment (IDT) between the Bcl1 and BamH1 sites using the Gibson reaction (New England Biolabs). All modified constructs were verified by sequencing before use.

Retroviral transductions of Tbet^{+}iTreg cells were performed as follows. Briefly, cells were stimulated for 24 hr and then washed once. Cells ($0.5x10^{6}$) were spin inoculated with 1ml of virus supernatant in the presence of polybrene (4 μg/ml) consisting of scramble or AEP shRNA for 50 mins at 3000RPM. The cells were then placed at 37°C for 2 hr after which an additional 2ml of complete RPMI media was added. Infection was monitored after 4 days as the percent of CD90.1 and AEP cy5 expression by flow cytometry. CD90.1^{+}Foxp3^{+}Tbet^{+} iTreg cells were flow sorted and then adoptively transferred in to a murine model of allogeneic GVHD and *in vivo* stability of Foxp3 in Tbet^{+} iTreg cells was monitored.

QUANTIFICATION AND STATISTICAL ANALYSIS

Statistical analysis was determined using GraphPad Prism 7 software. For experiments where two groups were compared, a two-tailed Student's t test was performed. For comparison of three or more groups, a one-way ANOVA was performed followed by appropriate multiple comparison tests. For survival curve analysis, Kaplan-Meier survival curve analysis followed by a log rank test was performed. Unless stated otherwise, histogram columns represent the mean values for each experiment and error bars indicate the standard error of the mean. Data presented were considered significant if p value was ≤ 0.05.

DATA AND SOFTWARE AVAILABILITY

The microarray data reported in this paper have been deposited in the NCBI Gene Expression Omnibus (GEO) database under accession number GEO:GSE113815.

Immunity, Volume *49*

Supplemental Information

PD-1 Inhibitory Receptor Downregulates Asparaginyl Endopeptidase and Maintains Foxp3 Transcription Factor Stability in Induced Regulatory T Cells

Chaido Stathopoulou, Arunakumar Gangaplara, Grace Mallett, Francis A. Flomerfelt, Lukasz P. Liniany, David Knight, Leigh A. Samsel, Rolando Berlinguer-Palmini, Joshua J. Yim, Tania C. Felizardo, Michael A. Eckhaus, Laura Edgington-Mitchell, Jonathan Martinez-Fabregas, Jinfang Zhu, Daniel H. Fowler, Sander I. van Kasteren, Arian Laurence, Matthew Bogyo, Colin Watts, Ethan M. Shevach, and Shoba Amarnath

Supplementary Figure 1 (related to Figure 1)

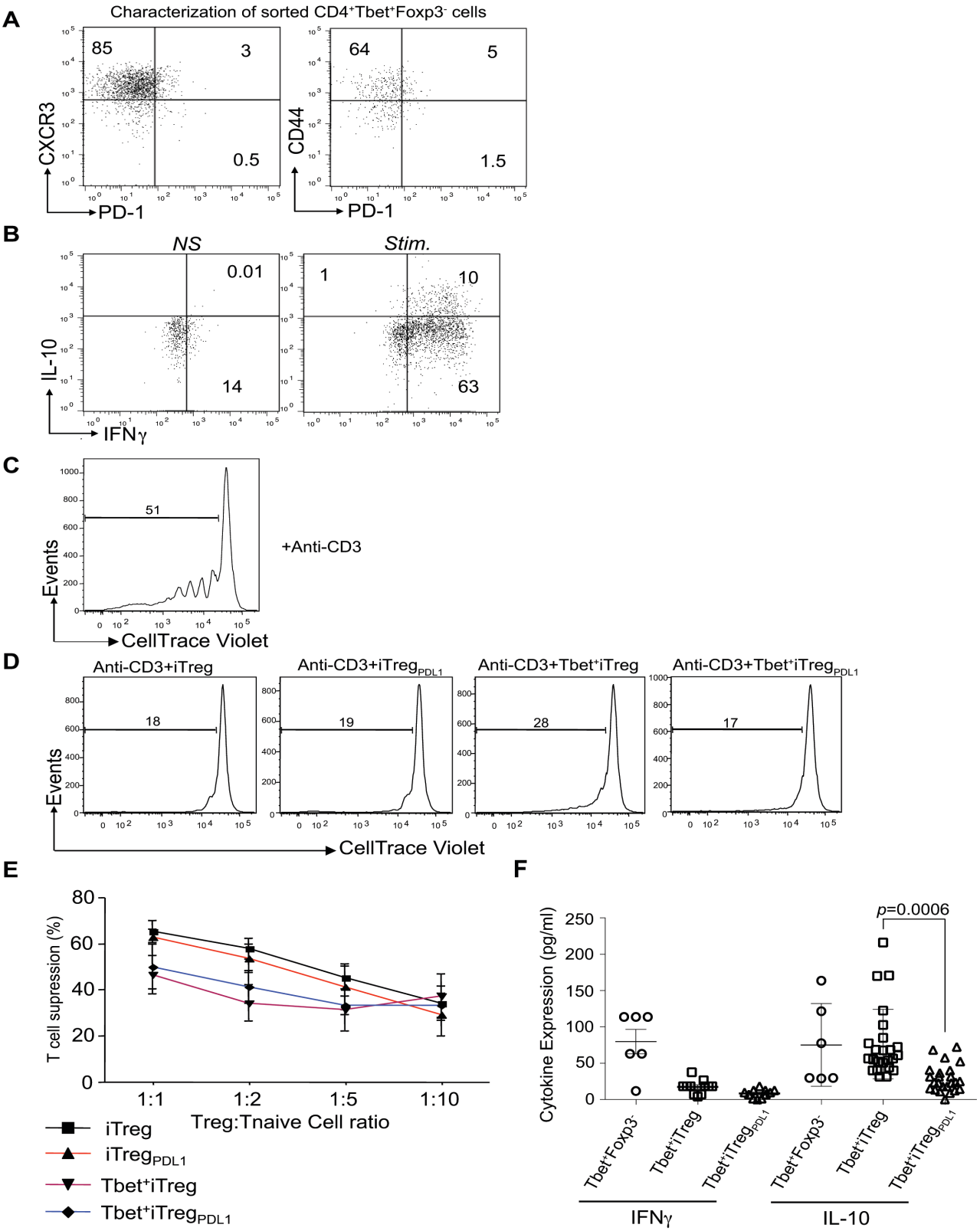

***In vitro* function of Tbet$^+$ iTreg cells and Tbet$^+$ iTreg$_{PDL1}$ cells**

Characterization of flow sorted CD4$^+$Tbet$^+$Foxp3$^-$ cells was performed prior to cell culture. Sorted cells had Th1 cell phenotype and expressed CXCR3, CD44 and PD-1 (**A**). Flow sorted cells also

expressed Th1 cytokines IFN-γ and IL-10, which was measured by intracellular flow cytometry (**B**). $Tbet^+$ iTreg cells and $Tbet^+$ $iTreg_{PDL1}$ cells were generated from the flow sorted $Tbet^+Foxp3^-$ cells and then utilized in an *in vitro* suppression assay. Responders were labeled with CellTrace Violet followed by stimulation with irradiated splenocytes and anti-CD3 and proliferation was measured by flow cytometry (**C**). Various Treg cell populations were added at different ratios and proliferation was measured (**D**). Summary data for three experiments was shown (**E**). Cytokine profile was obtained using Luminex from $Tbet^+$iTreg cells and $Tbet^+iTreg_{PDL1}$cells from at least 6 experiments (**F**). Experiments were repeated at least 5 times and each experiment was performed with n=3-5 mice and are presented as Mean±SEM.

Supplementary Figure 2 (related to Figure 2)

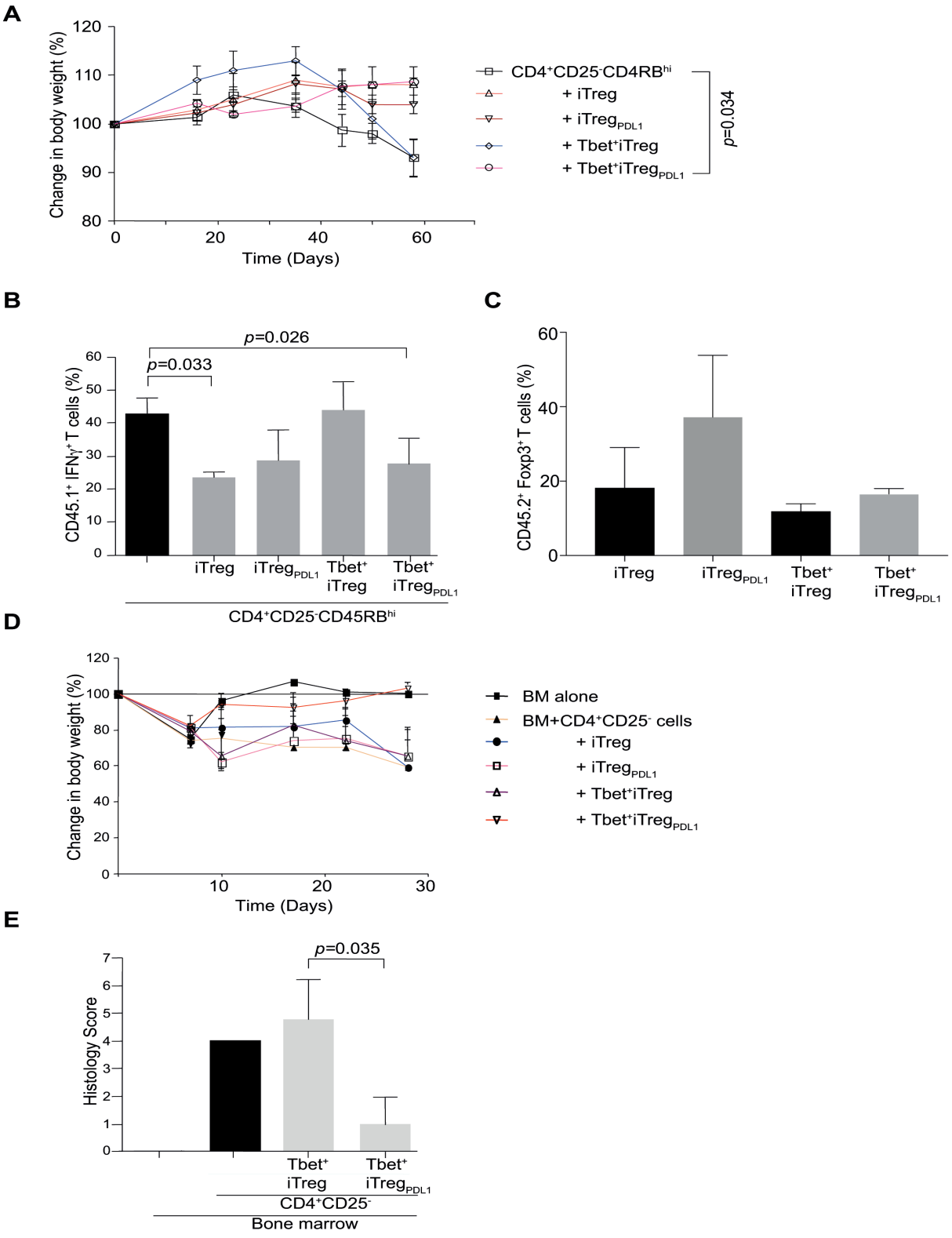

Tbet^{+} iTreg$_{PDL1}$ cells have regulatory function *in vivo*

Tbet^{+}iTreg cells and Tbet^{+}iTreg$_{PDL1}$ cells were generated and then utilized for the prevention of autoimmune colitis and alloimmune GvHD. B6.*Rag2*$^{-/-}$ mice were reconstituted with 4x10^{5}

$CD45.1^+CD4^+CD45RB^{hi}CD25^-$ T cells alone (T effectors) or along with $CD45.2^+$ iTreg cells, $iTreg_{PDL1}$ cells, $Tbet^+$ iTreg cells and $Tbet^+$ $iTreg_{PDL1}$ cells ($1x10^5$ cells/mouse). Weight loss was monitored in various cohorts (**A**). LPL were harvested for measuring immunological endpoints. Summary of T cell effector cytokine IFN-γ in various different cohorts was shown (**B**). Summary of Foxp3 ($CD45.2^+$) expression in iTreg cells, $iTreg_{PDL1}$ cells, $Tbet^+$ iTreg cells and $Tbet^+$ $iTreg_{PDL1}$ cells in LPL (**C**). Function of $Tbet^+$iTreg cells and $Tbet^+$ $iTreg_{PDL1}$ cells were assessed in an experimental model of GvHD. Host BALB/c mice were subjected to lethal total body irradiation (950cGy) and then reconstituted with B6 T depleted bone marrow (BM) cells alone. All cohorts received $CD4^+CD25^-$ T cells in addition to BM. Certain cohorts received additional cell populations as indicated. Weight loss of mice that succumbed to GvHD over a period of 30 days in the various different cohorts (**D**). Histology of mice that received either $Tbet^+$ iTreg cells and $Tbet^+$ $iTreg_{PDL1}$ cells was evaluated (**E**). For weight loss, each cohort consisted of n=10 mice. For histology, n=5 mice per cohorts were used. Cumulative data from 2 independent experiments are presented as Mean±SEM.

Supplementary Figure 3 (related to Figure 3)

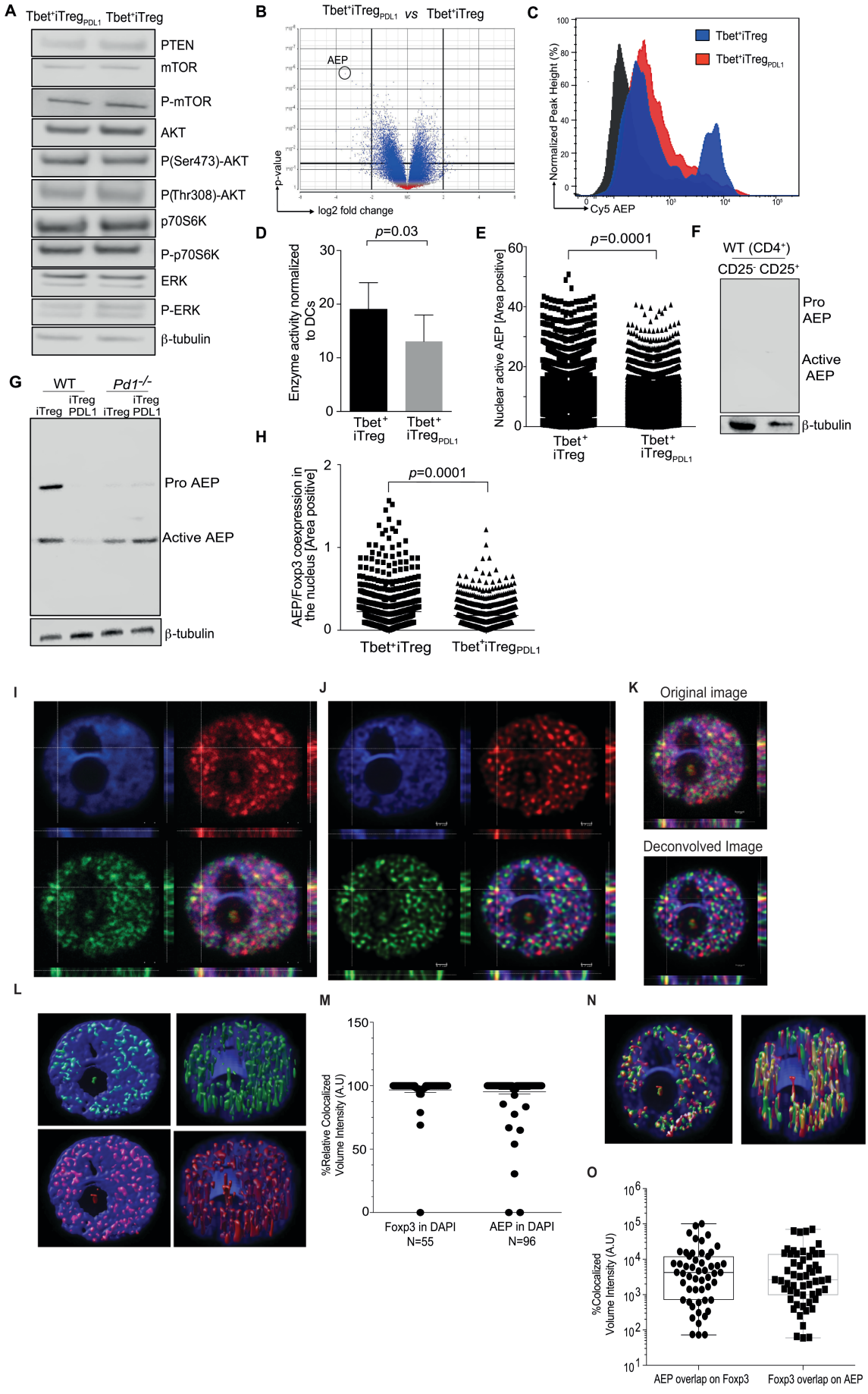

PD-1 signaling downregulates AEP on Tbet^{+} iTreg$_{PDL1}$ cells and iTreg$_{PDL1}$ cells

$Tbet^{+}$iTreg cells and $Tbet^{+}$ $iTreg_{PDL1}$ cell lysates were subjected to immuno blotting analysis to measure AKT and mTOR signaling pathway proteins (**A**). Volcano plot showing log2 fold change versus p value in gene expression between $Tbet^{+}$iTreg cells and $Tbet^{+}iTreg_{PDL1}$ cells (**B**). Expression of active AEP in $Tbet^{+}$iTreg cells and $Tbet^{+}$ $iTreg_{PDL1}$ cells was measured by flow cytometry using the LE28 AEP Cy5 probe (**C**). AEP enzyme activity in $Tbet^{+}$iTreg cells and $Tbet^{+}iTreg_{PDL1}$ cells (**D**). Summary plot showing AEP nuclear activity in $Tbet^{+}$iTreg cells and $Tbet^{+}iTreg_{PDL1}$ cells (**E**). Naïve $CD4^{+}CD25^{-}$ T cells and $CD4^{+}CD25^{+}$ T cells were isolated from WT mice and lysates were tested for AEP by immuno blotting (**F**). Splenocytes were harvested from WT and *Pd1*$^{-/-}$ mice, and then naïve cells were isolated, differentiated under iTreg conditions alone or in the presence of PDL-1 fc. AEP expression was analyzed in *in vitro* induced WT and *Pd1*$^{-/-}$ iTreg cells (**G**). Summary plot showing AEP nuclear co-expression with Foxp3 in $Tbet^{+}$iTreg cells and $Tbet^{+}iTreg_{PDL1}$ cells (**H**). Orthogonal projection view on confocal imaging data is shown in iTreg cells (**I**). The nucleus stained with DAPI and is depicted as blue, active AEP stained with activity probe AEP Cy5 is depicted as red and Foxp3 stained with Foxp3 PE is depicted as green. A quadrant is drawn on a particular point in the nucleus (blue image; top left panel) and then pasted on to AEP (top right panel) and Foxp3 staining (bottom left panel). If all three fluorophores are present together in this 3D view, then the analysis shows this on merging the three images (denoted as yellow in bottom right panel). The yellow is surrounded by blue in the x, y and z axis further suggesting the presence of active AEP and Foxp3 within the nucleus. Orthogonal projection view on deconvolved images (**J**). Deconvolution will correct optical aberration and provide higher resolution which enhances signal to noise ratio therefore minimizing false positive analysis. Combining deconvolution and orthogonal projection enhances our understanding of the spatial location and co-localization of proteins within a cell. Images processed by orthogonal projection and deconvolving is depicted on the top and bottom panels (**K**). Particle analysis of Foxp3(**L**; top panels) and AEP (**L**; bottom panels) within the nucleus (**L**; left panels showing image of the cell at normal view and right panels at 60^{0}) and quantitative analysis (**M**) is shown. Similarly, colocalization of AEP and Foxp3 within the nucleus is depicted (**N**; left panel and 60^{0} view right panel**)** and quantitative analysis (**O**) is shown. Experiments were repeated 3 times and representative immuno blots are shown. Cumulative data are shown as Mean±SEM.

Supplementary Figure 4 (related to Figure 3)

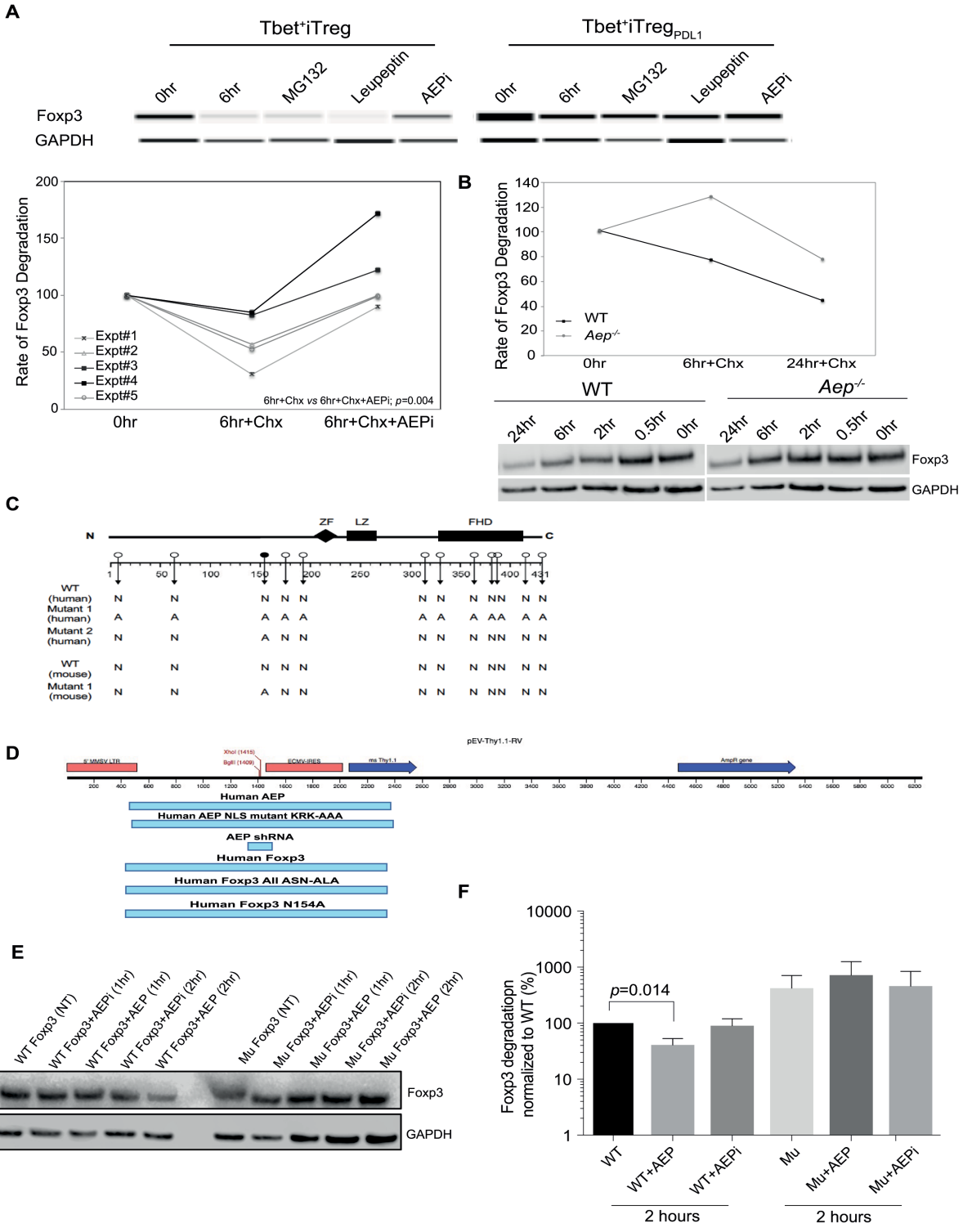

AEP inhibition prevents Foxp3 protein turnover in Tbet$^+$iTreg cells and iTreg cells

Protein turnover was measured using standardized cycloheximide assays. Tbet$^+$iTreg cells and Tbet$^+$ iTreg$_{PDL1}$ cells were tested for the rate of Foxp3 turnover. Tbet$^+$ iTreg cells and Tbet$^+$ iTreg$_{PDL1}$ cells were differentiated and then treated with cycloheximide (150 μg/ml) at different time points. Certain conditions were supplemented with AEP inhibitor (AEPi; MV026630; 100 μM), or leupeptin (1 mM)

or MG132 (0.5 μM). Cell lysates were then subjected to immunoblotting (**top panel**). Foxp3 was normalized to the internal control GAPDH, and time 0 hr was set as 100% then percent Foxp3 degraded is shown (**bottom panel**). Data is shown from 5 independent experiments (**A**). WT and *Aep*$^{-/-}$ $CD4^{+}CD25^{-}$ T cells were differentiated under iTreg conditions and then Foxp3 turnover was measured in the presence of cycloheximide (**B**). Map showing AEP specific sites within the Foxp3 protein. The symbol N denotes Asparagine and A denotes alanine. Human mutant 1 was mutated at all N sites with A; human mutant 2 was mutated at N154 to alanine. Mouse mutant 1 was mutated at N153 to alanine (**C**). Plasmid map and the cloning sites of the various WT and mutant Foxp3, AEP shRNA, human AEP protein and mutant AEP protein were shown (**D**). Immuno blot of HEK293T cells transduced with human WT and mutant 1 human Foxp3. Cell lysates were subjected to AEP degradation assay and then WT and mutant human Foxp3 was determined (**E**). Relative amounts of WT versus mutant Foxp3 protein normalized to 0 hr WT and 0 hr mutant were shown (**F**). Experiments were repeated 3 times and data shown are from one independent experiment. Summary plots are depicted as Mean±SEM.

Supplementary Figure 5 (related to Figure 4)

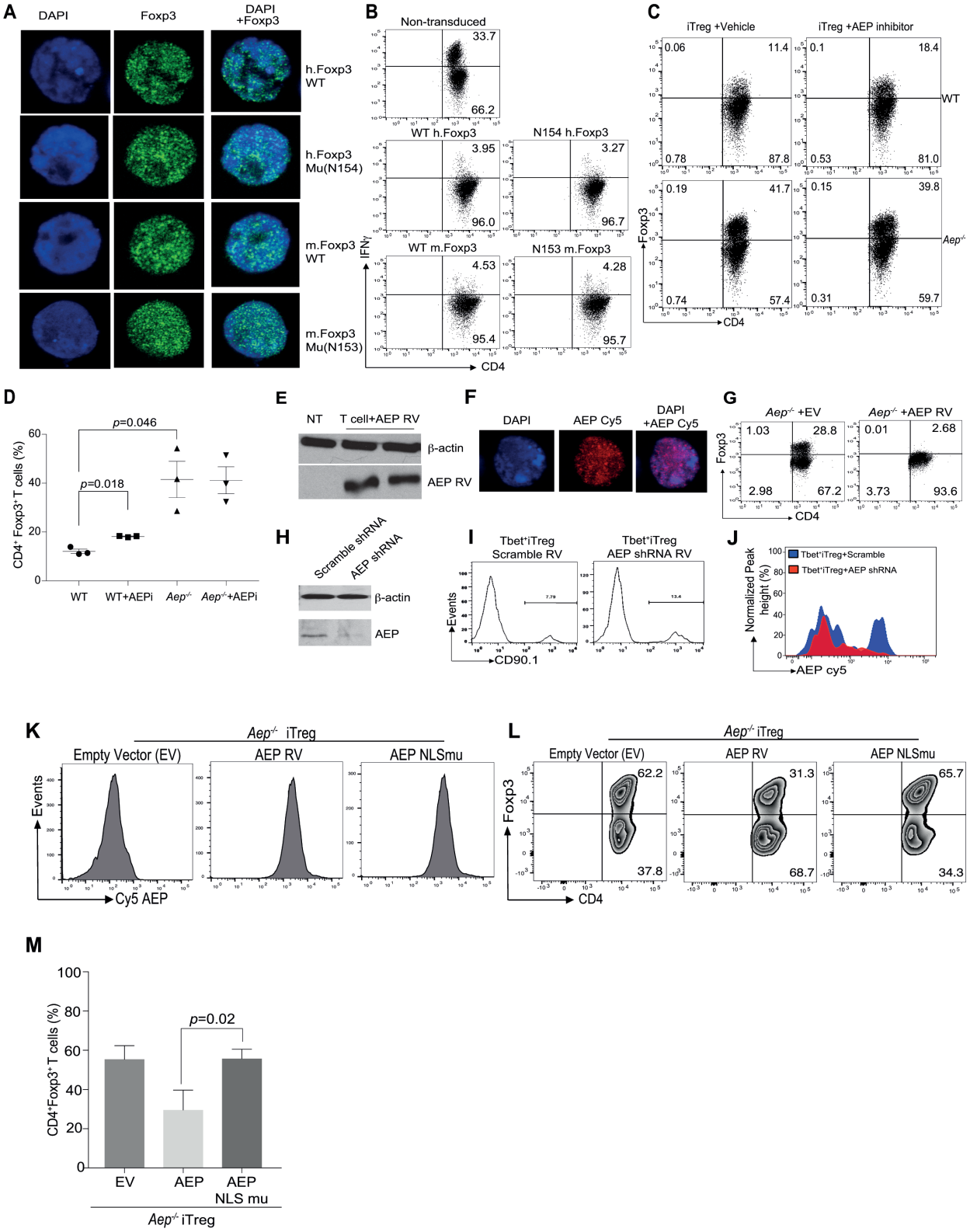

AEP specific Foxp3 mutation or AEP downregulation or AEP NLS mutation regulates Foxp3 protein stability.

$CD4^+CD25^-$ T cells from WT mice were activated with anti-CD3, anti-CD28 and IL-2 for 24 hrs and then transduced with human WT or mutant 2 human Foxp3 or mouse WT or mutant 1 mFoxp3. At day 4, cells were stained with DAPI and either human or mouse Foxp3 and then subjected to confocal microscopy (**A**). The ability of Foxp3 transduced cells to produce IFN-γ was tested by stimulating

the cells with PMA plus ionomycin for 4 hrs and golgistop and golgiplug were included during the last 2hrs of stimulation. Cells were then subjected to intracellular flow cytometry (**B**). $CD4^+CD25^-$ cells were isolated from WT and *Aep*$^{-/-}$ mice and then differentiated in the presence of anti-CD3, anti-CD28, IL-2 and TGF-β1 in the absence or presence of AEP inhibitor for 3 days followed by expansion in IL-2 alone for another four days. At day 7, Foxp3 expression was measured by intracellular flow cytometry (**C**). Summary of Foxp3 expression in the various cohorts was shown (**D**). $Tbet^+iTreg_{PDL1}$ cells were activated with anti-CD3, anti-CD28, IL-2 and TGF-β1 for 24 hrs and then transduced with human AEP RV. At day 4, cell lysates were measured for human AEP protein expression (**E**). Transduced cells were stained with DAPI and AEP LE28 Cy5 probe and then subjected to confocal microscopy (**F**). *Aep*$^{-/-}$ iTreg cells were transduced with empty vector or AEP over-expressing RV and then Foxp3 stability was tested at day 7 post expansion (**G**). $Tbet^+$iTreg cells from WT mice were activated with anti-CD3, anti-CD28, IL-2 and TGF-β1 for 24 hrs and then transduced with mouse control (scramble) shRNA or AEP shRNA. At day 4, AEP expression was measured by immunoblot analysis (**H**), expression of Thy1.1 in the transduced cells (**I**), and active AEP was measured by flow cytometry (**J**). AEP was mutated at the nuclear localization sequence and then cloned into a Thy1.1 vector. $CD4^+CD25^-$ T cells were isolated from *Aep*$^{-/-}$ mice and then stimulated under iTreg conditions. During the stimulation, cells were infected with retrovirus containing either empty vector (EV), AEP overexpressing vector (AEP RV) or AEP NLSmu (KRK-AAA mutation, site 318-320). Successful infection was measured by flow cytometry in the various cohorts using the AEP Cy5 probe (**K**). At day 7, Foxp3 expression was measured by flow cytometry in the listed cohorts (**L-M**). Experiments were repeated three times and data shown are Mean±SEM.

Supplementary Figure 6 (related to Figure 5)

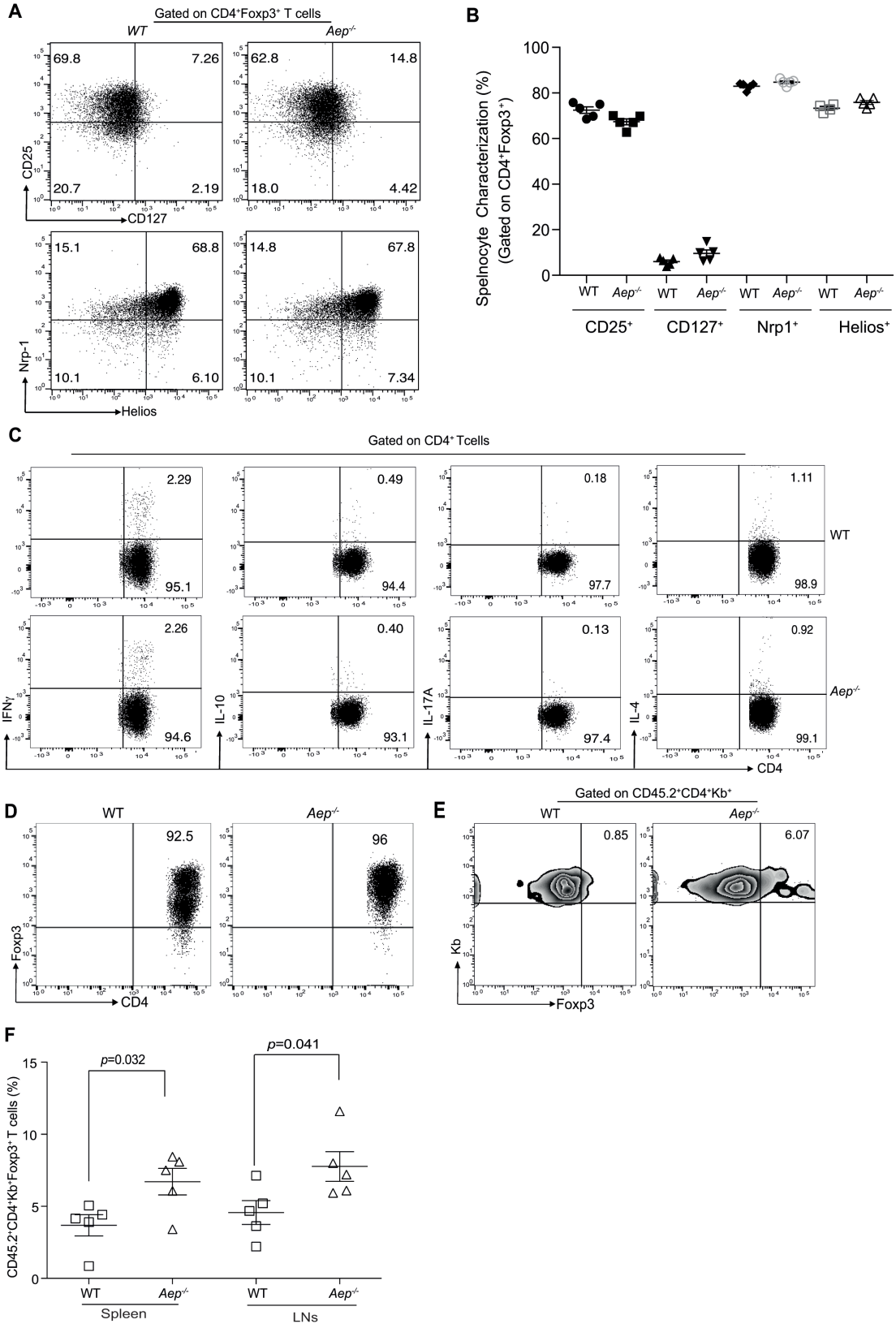

AEP deficiency delays loss of Foxp3 *in vivo*

Splenocytes were harvested from WT and *Aep*$^{-/-}$ mice, and then CD4^{+}Foxp3^{+} T cells were characterized for Treg markers namely CD25, CD127, Neuropilin-1 and Helios (**A-B**). Splenocytes were stimulated for 4 hrs in the presence of PMA plus ionomycin and then treated with golgiplug and golgistop for the last 2 hrs of stimulation. Cells were then stained for Th1 cell, Th2 cell, Th17 cell

specific cytokines and subjected to intracellular cytometry (**C**). Naïve T cells from WT and *Aep*$^{-/-}$ mice were isolated, differentiated under iTreg conditions for 3 days. Foxp3 expression was analyzed in *in vitro* induced WT and *Aep*$^{-/-}$ Treg cells (**D**). Balb/c mice were subjected to total body irradiation, followed by reconstitution with CD45.1^{+} bone marrow cells plus CD45.1^{+}CD4^{+}CD25^{-} T cells. Certain cohorts received CD45.2^{+} WT or *Aep*$^{-/-}$ iTreg cells in addition to bone marrow cells and CD45.1^{+}CD4^{+}CD25^{-} T cells. Foxp3 expression within the WT and *Aep*$^{-/-}$ iTreg cells at day 14 post-transplant (**E**). Frequency of CD45.2^{+}Foxp3^{+} cells in the spleen and lymph nodes of the various cohorts (**F**). Experiments were repeated twice and each cohort had n=4-5 mice. Data are shown as Mean±SEM.

Supplementary Figure 7 (related to Figure 6)

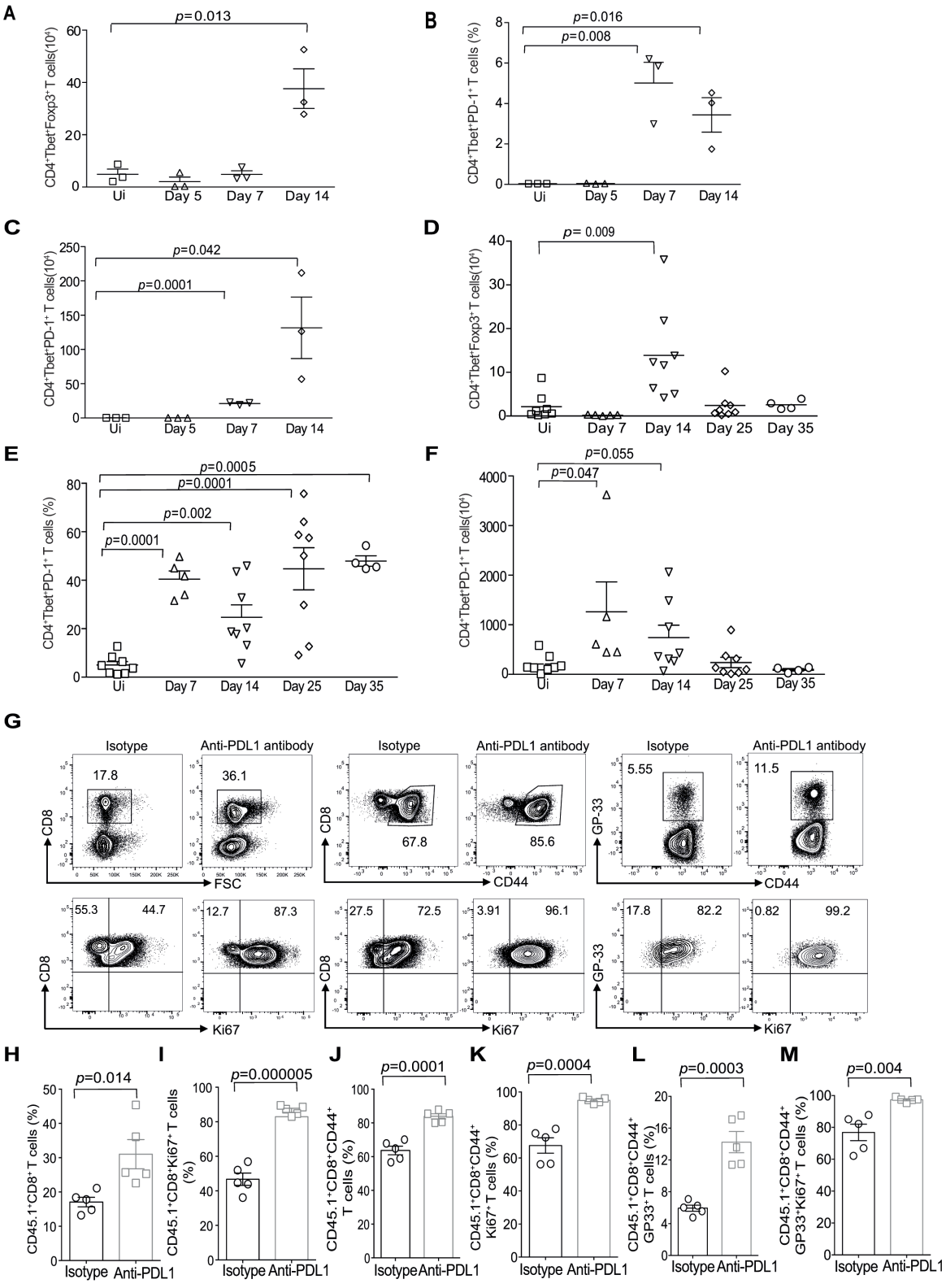

Tbet^{hi} cells express PD-1 during acute and chronic LCMV infection

B6.*Tbx21*Zsgreen*Foxp3*RFP mice were infected with LCMV Armstrong (2x10^5 PFU) and then monitored for CD4$^+$Tbet^{hi}FoxP3$^+$ cells and CD4$^+$Tbet^{hi}PD-1$^+$ cell kinetics. Absolute numbers of CD4$^+$Tbet^{hi}FoxP3$^+$ cells (**A**), frequency of PD-1 expressing cells at different time points (**B**), and absolute numbers of PD-1 expressing cells at different time points were shown (**C**).

B6.*Tbx21Z*sgreen*Foxp3*RFP mice were infected with LCMV Clone-13 ($2x10^6$ PFU) and then monitored for $CD4^+Tbet^{hi}FoxP3^+$ cells and $CD4^+Tbet^{hi}PD\text{-}1^+$ cells kinetics. Absolute numbers of $CD4^+Tbet^{hi}FoxP3^+$ cells (**D**), frequency of PD-1 expressing cells at different time points (**E**), and absolute numbers of PD-1 expressing cells at different time points were shown (**F**). $CD45.1^+$ hosts were infected with Clone 13 and reconstituted with $CD45.2^+CD4^+Tbet^+FoxP3^-$ cells. Cohorts were treated with isotype or anti-PDL1 antibody (200μg/mouse). At day 10, splenocytes were harvested and the frequency of $CD45.1^+CD8^+$ T cells (**G**, left two top panels; **H**), that were $Ki67^+$ (**G**, left two bottom panels; **I**) were determined. The frequency of $CD8^+CD44^+$ cells (**G**, top middle panels; **J**), that were $Ki67^+$ cells (**G**, bottom middle panels; **K**) is shown. The frequency of GP33 specific $CD8^+$ T cells (**G**, top right two panels; **L**), and that were $Ki67^+$ (**G**, bottom right two panels; **M**) were measured. Experiments were repeated twice and each cohort had n=3-8 mice. Representative data from one experiment is shown as Mean±SEM.

Supplementary Table 1: AEP-specific semi-tryptic cleavage in Foxp3 bands 2 and band 3 (related to Figure 3)

Sequence-Band 2- AEP cleavage site	Start	Stop
(R)PGKPSAPSLALGPSPGASPSWR(A)	6	27
(K)ASDLLGAR(G)	32	39
(N)VASLEWVSR(E)	**155**	**163**
(R)KDSTLSAVPQSSYPLLANGVcK(W)	179	200
(K)VFEEPEDFLK(H)	207	216
(R)EmVQSLEQQLVLEK(E)	237	250
(R)EMVQSLEQQLVLEK(E)	237	250
(R)EmVQSLEQQLVLEK(E)	237	250
(L)SAmQAHLAGK(M)	254	263
(K)GSccIVAAGSQGPVVPAWSGPR(E)	278	299
(R)EAPDSLFAVRR(H)	300	310
(R)WAILEAPEK(Q)	348	356
(R)WAILEAPEKQR(T)	348	358
(K)cFVRVESEK(G)	394	402
(K)GAVWTVDELEFRK(K)	403	415
Sequence-Band 3- Additional degraded band		
(R)PGKPSAPSLALGPSPGASPSWR(A)	6	27
(K)ASDLLGAR(G)	32	39
(R)GPGGTFQGR(D)	40	48
(R)GGAHASSSSLNPmPPSQLQLPTLPLVmVAPSGAR(L)	52	85
(R)KDSTLSAVPQSSYPLLANGVcK(W)	179	200
(R)EmVQSLEQQLVLEK(E)	237	250
(R)EMVQSLEQQLVLEK(E)	237	250
(R)EmVQSLEQQLVLEK(E)	237	250
(R)EMVQSLEQQLVLEKEK(L)	237	252
(L)SAmQAHLAGK(M)	254	263
(R)WAILEAPEK(Q)	348	356